SEISMIC STRENGTHENING OF PRECAST RC WALL PANELS USING FRP COMPOSITES

Teză destinată obţinerii
titlului ştiinţific de doctor inginer
la
Universitatea Politehnica Timişoara
în domeniul INGINERIE CIVILĂ
de către

Ing. Carla Toduț

Conducător ştiinţific:	prof.univ.dr.ing. Valeriu Stoian
Referenţi ştiinţifici:	prof.univ.dr.ing. Nicolae Țăranu
	prof.univ.dr.ing. Zoltán Kiss
	prof.univ.dr.ing. Daniel Dan

Ziua susţinerii tezei: 06.03.2015

Seriile Teze de doctorat ale UPT sunt:

1. Automatică
2. Chimie
3. Energetică
4. Ingineria Chimică
5. Inginerie Civilă
6. Inginerie Electrică
7. Inginerie Electronică şi Telecomunicaţii
8. Inginerie Industrială
9. Inginerie Mecanică
10. Ştiinţa Calculatoarelor
11. Ştiinţa şi Ingineria Materialelor
12. Ingineria sistemelor
13. Inginerie energetică
14. Calculatoare şi tehnologia informaţiei
15. Ingineria materialelor
16. Inginerie şi Management

Universitatea Politehnica Timişoara a iniţiat seriile de mai sus în scopul diseminării expertizei, cunoştinţelor şi rezultatelor cercetărilor întreprinse în cadrul şcolii doctorale a universităţii. Seriile conţin, potrivit H.B.Ex.S Nr. 14 / 14.07.2006, tezele de doctorat susţinute în universitate începând cu 1 octombrie 2006.

România, 300159 Timişoara, Bd. Republicii 9,
Tel./fax 0256 403823
e-mail: editura@edipol.upt.ro

Preface

The current doctoral thesis presents the work carried out between October 2011 and November 2014, at the Department of Civil Engineering, Faculty of Civil Engineering, Politehnica University Timișoara. As a PhD Student, I received the task to continue the research work started and investigated by Dr. István Demeter on the seismic response of precast reinforced concrete wall panels weakened by cut-out openings and retrofitted by FRP composites.

During my doctoral studies, I had the pleasure to investigate on the theme, perform the experimental tests on six precast reinforced concrete walls with openings and opening enlargements, investigate and test various strengthening techniques for the rehabilitation or retrofitting of the specimens, perform numerical simulations using dedicated software, make analytical investigations on the shear strength of the specimens using design code provisions, assess the weakening effect using also design code expressions, and evaluate the strengthening costs.

The first experimental test was carried out in April 2012 while the last one in April 2013. During this time the author was phisically involved in every experimental testing operation and preparatory works, such as fixing the specimens in the test set-up, instrumentation application, surface preparation for strengthening, strengthening procedure and testing. Dr. István Demeter, Dr. Tamás Nagy-György, Dr. Dan Diaconu, PhD Student Mihai Fofiu, PhD Student Andrei Bîndean, MSc Bianca Pasc and other colleagues from the Department were also involved in the logistics. Technical staff members Mr. Nicoale Albu and Mr. Ionel Mihalache also helped during the set-up and strengthening of the specimens.

After the experimental tests were performed, followed a nearly two year period of data processing, literature survey and the elaboration of the thesis. During this time the author received valuable guiding from Prof. Stoian, Prof. Dan, Assoc.Prof. Nagy-György. The final draft of the thesis was reviewed by Prof. Nicolae Țăranu from Technical University "Gheorghe Asachi" Iasi, Prof. Zoltán Kiss from Technical University of Cluj-Napoca, Prof. Daniel Dan and Prof. Valeriu Stoian.

I would like to thank my supervisor Prof. Valeriu Stoian for believing in me and guiding me in research and also real life. As a coordinator professor he made financial efforts to support the current research and was involved in the progress of the research. I am also grateful to Assoc.Prof. Ștefan Iosip-Moț for guiding me as a student to make choices in research and real life.

I want to thank Prof. Daniel Dan for his guidance, colaboration on my most valuable results and received advice. I must also acknowledge my colleagues for their help and advices given during my research.

Special thanks go to Mapei Corporation Romania, Eng. Cristian Cartaș and his team who sponsored my research with strengthening materials and also helped at their application. I am also grateful to Prof. Viorel Ungureanu for his financial support and implication in my research program. I am grateful for everything I learned during my doctoral studies, for all the help and guidance I received from my colleagues and I am also looking forward to further collaboration. I also want to thank my parents who raised me, supported me and guided me in life.

The author expresses his grateful acknowledgement for all who were involved in this work.

Timişoara, march 2015 Carla Toduț

„This work was partially supported by the strategic grant POSDRU/159/1.5/S/ 137070 (2014) of the Ministry of National Education, Romania, co-financed by the European Social Fund – Investing in People, within the Sectoral Operational Programme Human Resources Development 2007-2013".

TODUȚ, Carla

Seismic strengthening of precast RC wall panels using FRP composites

Teze de doctorat ale UPT, Seria 5, Nr. 129, Editura Politehnica, 2015, 283 pagini, 110 figuri, 47 tabele.

ISSN: 1842-581X
ISBN: 978-606-554-919-7

Cuvinte cheie: reinforced concrete, precast, wall, wall opening, cut-out opening, earthquake, FRP, cyclic test, seismic performance

Rezumat

The research work investigated addresses the seismic behaviour of precast reinforced concrete wall panels. Among the objectives of the study were the investigation of the seismic performance of the wall specimens, as built openings and cut-out opening effects on the response characteristics, FRP strengthening using various methods in order to establish the most convenient solutions, shear strength estimations using design code provisions and numerical analysis. The experimental program consisted in eleven quasi-static cyclic tests on near-full scale wall specimens. The experimental variables considered in the current research refer to the opening type and dimensions, and the strengthening considerations. The cut-out opening effect on the shear strength, stiffness and energy dissipation rate was found to be significant, whereas the experimental results show an equal to or higher performance of the strengthened specimens compared to the reference ones in terms of load bearing capacity, stiffness and energy dissipation capacity.

TABLE OF CONTENTS

Preface.....3
Abstract.....4
Table of contents.....5
Symbols and abbreviations.....7
List of figures.....10
List of tables.....14
1. Introduction.....**17**
1.1. Context.....17
1.2. Motivation.....17
1.3. Objectives.....17
1.4. Overview of the thesis.....18
1.5. Similar research in literature.....19
1.6. Precast RC large panel buildings in Romania.....43
2. Experimental program.....49
2.1. Experimental specimens and test set-up.....50
2.2. Material considerations.....57
2.3. Experimental test set-up.....60
2.4. Testing procedure.....63
2.5. Boundary conditions.....63
2.6.Instrumentation.....64
2.7. Behaviour of the reference specimens.....67
2.8. Repair and strengthening of the specimens.....74
2.8.1. Rehabilitation of PRCWP (7-E1-T/R) specimen using EBR-CFRP.....74
2.8.2. Rehabilitation of PRCWP (8-E3-T/R) specimen using EBR-CFRP.....75
2.8.3. Strengthening of PRCWP (9-E1/E3-R/T) specimen using EBR-CFRP combined with NSM-CFRP.....75
2.8.4. Rehabilitation of PRCWP (10-L1/L3-T/R) using TRM.....76
2.8.5. Strengthening of PRCWP (11-L1-T/R) using TRM.....76
2.8.6. Strengthening of PRCWP (12-E1-T/R) using NSM-CFRP combined with EBR-CFRP.....77
3. Results.....105
3.1. General behaviour and failure modes of FRP strengthened specimens.....105
3.2. Force–drift ratio response and observations.....122
3.2.1. Force-drift ratio hysteresis loops.....125
3.2.2. Force-drift ratio cyclic envelopes.....127
3.2.3. Force-drift ratio monotonic envelopes.....130
3.2.4. Force-drift ratio backbone envelope.....133
3.2.5. Strength analysis.....138
3.2.6. Displacement analysis.....139
3.2.7. Comparison.....141
3.3. Energy dissipation.....143
3.4. Ductility coeeficient.....153
3.5. Strain analysis.....156
3.6. Stiffness degradation.....159
3.7. Numerical analysis for the prediction of the shear response.....161
3.8. Theoretical study on the shear resistance of the specimens.....170
3.8.1. Evaluation of the shear strength using design code provisions.....170
3.8.2. Evaluation of the plastic mechanism model.....171

3.9. Weakening assessments.....171
3.10. Cracking pattern.....175
4. Conclusions..... **179**
5. Personal contributions..... **181**
6. Recommendations for further research..... **184**
Bibliography..... **185**
Appendices..... **195**
A Behaviour of the specimens at each cycle peak..... 195
B Sensor list of the specimens..... 229
C Strengthening cost evaluation.....253

Symbols and abbreviations

SYMBOLS

Latin lower case letters

b_w	thickness of the web
f_c	concrete compressive strength
f_{ck}	characteristic cylinder compressive strength of concrete
f_{cm}	mean value of concrete cylinder compressive strength
$f_{cm,cube}$	mean concrete compressive cube strength of concrete
f_y	yield strength of steel reinforcement
f_{yk}	characteristic yield strength of steel reinforcement
f_t	tensile strength of steel reinforcement
f	flexural (sheets)
sh	shear (sheets)
c	confinement (sheets)
s	spacing between reinforcement
z	lever arm of internal forces
dN	distance between the axial force position and the centroid of the compressed reinforcement
d1,2	distance between the reinforcement centroid position and the tensioned/ compressed fibre of the section (on x-axis)
x	neutral axis depth
k_{nn}	normal stiffness
k_{tt}	tangential stiffness
c	cohesion

Latin upper case letters

A	in-plane area
A_o	in-plane area of the opening
A_w	in-plane area of the web-panel
A_c	cross sectional area of concrete
A_s	cross sectional area of reinforcement
A_{sw}	cross-sectional area of the shear reinforcement
C	class of concrete
CD_j	Cumulative Drift corresponding to a point "j" on the load-displacement curve
CED_j	Cumulative Energy Dissipated corresponding to a point "j" on the response
CED_{max}	maximum cumulative energy which could be theoretically dissipated during the load-displacement response
CR_j	cumulative drif ratio corresponding to a point "j" on the load-displacement curve
E_s	modulus of elasticity of steel reinforcement
ED_{max}	the maximum energy which could be theoretically dissipated during a load-displacement cycle
K	stiffness

K_{sec}	secant stiffness
$K_{sec,Ri}$	denotes the secant stiffness corresponding to the δi displacement amplitude (Ri drift ratio) on the monotonic load-displacement envelope
K_0	initial stiffness (at 0.1% drift ratio)
M	bending moment
N	axial load
N_1, N_2	axial loads acting above pier#1 and pier#2, respectively
R	drift angle (drift ratio)
$(R)_{sound}$	response characteristic of the sound (solid, as-built) member in terms of shear resistance, initial stiffness or energy dissipation rate
$(R)_{weak}$	response characteristic of the weakened member in terms of shear resistance, initial stiffness or energy dissipation rate
R_r	response ratio
V	lateral load; shear force
V_{th}	theoretical shear force
N_c	constant axial force
N_v	variable axial force
$V_{R,max}$	maximum shear force, which can be sustained by the member, limited by crushing of the compression struts
$V_{R,s}$	the shear force which can be sustained by the yielding shear reinforcement
$V_{exp,max}$	maximum experimental shear force
H_w	height of the wall
H_p	height of the wall pier
L_p	length of the wall pier
P	peripheral ratio
S	steel grade

Greek lower case letters

α_p	performance ratio
α_s	aspect ratio
δ	displacement
δ_i	drift at the i-th displacement level
δ_j	drift corresponding to a point "j" on the load-displacement curve
δ_u	ultimate displacement
δ_y	yield displacement
ε	unit strain
η	opening ratio
θ	inclination angle of the concrete strut to the vertical direction
μ	ductility factor
$\mu_{0.85}$	ductility measured at 0.85 pre- and 0.80 post-peak shear strength
Φ	diameter of reinforcing bar
α_{cw}	coefficient taking account of the state of the stress in the compression chord
ν_1	strength reduction factor for concrete cracked in shear
φ	friction coefficient

ABBREVIATIONS

A	type A test set-up
B	former Romanian designation of concrete quality
C	Cyclic; Cycle
C1, C2	first and the second load-displacement cycle on a displacement level
CD	Cumulative Drift
CCD	Cyclic Cumulative Drift
CED	Cumulative Energy Dissipated
CF	carbon fibre
GF	glass fibre
FRP	fibre reinforced polymer
CFRP	Carbon FRP
GRP	Glass FRP
CR	Cumulative drift ratio
D	Displacement; displacement transducer
E	Energy
E	opening
E1	narrow door opening
E3	wide door opening
E1/E3	narrow door opening enlarged to a wide door opening
L1	small window opening
L1/L3	small window opening enlarged to a wide window opening
EBR	Externally Bonded Reinforcement
NSM	Near Surface Mounted
TRM	Textile Reinforced Mortar
ED	Energy Dissipated
G	Strain Gauge
P	Pressure transducer
M	Monotonic
M	average (mean)
M1	monotonic envelope
M2	average cyclic envelope
OB	Romanian smooth (plain) reinforcing bar
PRCLP	Precast Reinforced Concrete Large Panel
PRCWP	Precast Reinforced Concrete Wall Panel
PC	Romanian ribbed reinforcing bar
QSC	quasi-static cyclic loading
R	retrofit
R/T	prior-to-damage strengthening (Retrofitted and Tested)
RC	Reinforced Concrete
RR	restrained rotation (boundary condition)
STNB	Romanian smooth wire reinforcement
STPB	Cold-drawn ribbed welded fabric
T	test
T/R	post-damage strengthening (Tested and Retrofitted)
DCM	medium ductility class
$I_{54\text{-}2a}$	interior wall (Project type 770-81)
$E_{36\text{-}7}$	exterior wall (Project type 770-81)
$I_{36\text{-}1}$	interior wall (Project type 770-81)
7,8,9,10,11,12	number of specimens

LIST OF FIGURES

Figure 1.1. Front view of the building.....43
Figure 1.2. Lateral view.....44
Figure 1.3. Vertical section.....44
Figure 1.4. Ground floor plan.....44
Figure 1.5. Execution details.....45
Figure 1.6. Investigated prototype wall panels.....46
Figure 1.7. Precast RC buildings in Timișoara.....47
Figure 2.1. Testing time-line of the specimens.....50
Figure 2.2. General view of the experimental specimens.....51
Figure 2.3. Parts of the manufacturing process.....53
Figure 2.4. Experimental specimens manufacturing on site.....54
Figure 2.5. The schematics and reinforcement details of the specimens.....55
Figure 2.6. Deisgnation of wall specimen's components.....56
Figure 2.7. Shear key detail.....56
Figure 2.8. Wall - foundation anchorage detail.....56
Figure 2.9. Experimental wall - foundation anchorage.....57
Figure 2.10. FRP reinforcement used in the experimental program.....60
Figure 2.11. Test set-up configuration.....61
Figure 2.12. Detail of reaction beams.....61
Figure 2.13. Reaction beams details.....62
Figure 2.14. Hydraulic cylinders.....62
Figure 2.15. Electric and hand pumps used.....62
Figure 2.16. Axial loading procedure.....63
Figure 2.17. Monitoring system.....65
Figure 2.18. Instrumentation layout of the tested specimens.....66
Figure 2.19. Data acquisition system used.....67
Figure 2.20. Observation grid details.....67
Figure 2.21. PRCWP (7-E1-T) failure details.....69
Figure 2.22. PRCWP (8-E3-T) failure details.....71
Figure 2.23. PRCWP (10-L1/L3-T) failure details.....71
Figure 2.24. PRCWP (11-L1-T) failure details.....72
Figure 2.25. PRCWP (12-E1-T) failure details.....73
Figure 2.26. FRP strengthening layout for PRCWP (7-E1-T/R).....78

Figure 2.27. FRP strengthening details..... 79
Figure 2.28. FRP strengthening layout for PRCWP (8-E3-T/R)..... 80
Figure 2.29. FRP strengthening details..... 81
Figure 2.30. FRP strengthening layout for PRCWP (9-E1/E3-R/T)..... 82
Figure 2.31. NSM-FRP application details..... 83
Figure 2.32. Double disc grinder used for the NSM channel cut..... 83
Figure 2.33. FRP strengthening details..... 86
Figure 2.34. TRM strengthening details..... 87
Figure 2.35. FRP strengthening layout for PRCWP (10-L1/L3-T/R)..... 89
Figure 2.36. FRP strengthening details..... 92
Figure 2.37. TRM strengthening details..... 93
Figure 2.38. FRP strengthening layout for PRCWP (11-L1-T/R)..... 95
Figure 2.39. FRP strengthening details..... ..100
Figure 2.40. NSM-FRP application details..... ..101
Figure 2.41. FRP strengthening layout for PRCWP (12-E1-T/R)..... ..102
Figure 2.42. FRP strengthening details..... ..104
Figure 3.1. Failure details of the PRCWP (7-E1-T/R) specimen..... ..109
Figure 3.2. Failure details of the PRCWP (8-E3-T/R) specimen..... ..111
Figure 3.3. Failure details of the PRCWP (9-E1/E3-R/T) specimen.....113
Figure 3.4. Failure details of the PRCWP (10-L1/L3-T/R) specimen..... ..117
Figure 3.5. Failure details of the PRCWP (11-L1-T/R) specimen.....120
Figure 3.6. Failure details of the PRCWP (12-E1-T/R) specimen.....122
Figure 3.7. Load-drift ratio hysteresis loops of the reference specimens..... ..125
Figure 3.8. Load-drift ratio hysteresis loops of the strengthened specimens..126
Figure 3.9. Comparison of the load-drift ratio hysteresis loops for the tested walls..... ..127
Figure 3.10. Load-drift ratio cyclic envelopes of the reference specimens..... ..128
Figure 3.11. Load-drift ratio cyclic envelopes of the strengthened specimens..129
Figure 3.12. Comparison of the load-drift ratio cyclic envelopes for the tested specimens..... ..130
Figure 3.13. Load-drift ratio monotonic envelopes of the reference..131 specimens.....
Figure 3.14. Load-drift ratio monotonic envelopes of the strengthened specimens..... ..132
Figure 3.15. Comparison of the load-drift ratio monotonic envelopes for the tested specimens..... ..132
Figure 3.16. Tri-linear backbone (type 1) curves of the reference specimens..134
Figure 3.17. Tri-linear backbone (type 1) curves of the strengthened specimens..... ..134
Figure 3.18. Comparison of the tri-linear backbone (type 1) curves of the tested walls..... ..135
Figure 3.19. Tri-linear backbone (type 2) curves of the reference specimens..... ..136

Figure 3.20. Tri-linear backbone (type 2) curves of the strengthened specimens.....137
Figure 3.21. Comparison of the tri-linear backbone (type 2) curves of the tested walls.....137
Figure 3.22. The shear strength of the unstrengthened specimens.....138
Figure 3.23. The shear strength of the stregthened specimens.....139
Figure 3.24. The shear strength of the tested wall specimens.....139
Figure 3.25. The drift at failure of the unstrengthened wall specimens.....140
Figure 3.26. The drift at failure of the strengthened wall specimens.....140
Figure 3.27. The drift at failure of the tested wall specimens.....140
Figure 3.28. Comparison of the M2 envelopes.....141
Figure 3.29. Comparison of the M1 envelopes.....141
Figure 3.30. Comparison of envelopes for the tested specimens.....141
Figure 3.31. Comparison of backbone (type 1) curves.....142
Figure 3.32. Comparison of backbone (type 2) curves.....142
Figure 3.33. Comparison of backbone curves.....142
Figure 3.34. Cumulative energy vs. drift ratio of the reference specimens.....144
Figure 3.35. Cumulative energy vs. drift ratio of the strengthened specimens.....145
Figure 3.36. Cumulative energy vs. cumulative drift of the reference specimens.....146
Figure 3.37. Cumulative energy vs. cumulative drift of the strengthened specimens.....146
Figure 3.38. Energy dissipation – reference specimens.....147
Figure 3.39. Energy dissipation – strengthened specimens.....148
Figure 3.40. Cumulative energy dissipation (per half-cycle) – reference specimens.....149
Figure 3.41. Cumulative energy dissipation (per half-cycle) – strengthened specimens.....149
Figure 3.42. Cumulative energy dissipation (per cycle) – reference specimens.....150
Figure 3.43. Cumulative energy dissipation (per cycle) – strengthened specimens.....151
Figure 3.44. The ductility coefficient of the tested specimens.....154
Figure 3.45. Comparison of the ductility coefficients.....155
Figure 3.46. Comparison of the ductility coefficients.....155
Figure 3.47. Comparison of the ductility coefficients for the tested specimens.....155
Figure 3.48. Steel strain (ε) versus drift ratio of the tested specimens.....158
Figure 3.49. Comparison of the stiffness degradation.....160
Figure 3.50. The stiffness versus drift ratio diagram of the specimens.....160
Figure 3.51. Initial stiffness of the tested specimens.....160
Figure 3.52. The stiffness versus drift ratio diagram of the specimens.....161

Figure 3.53. Stress-strain and failure laws for materials..... ..162
Figure 3.54. The layout and meshes of the numerical specimens..... ..164
Figure 3.55. Experimental versus numerical load-drift ratio curves.....168
Figure 3.56. Experimental versus numerical failure details 169
Figure 3.57. Plastic mechanism considerations..... ..171
Figure 3.58. Investigated wall specimen’s layout..... ..172
Figure 3.59. Load – drift ratio curves..... ..173
Figure 3.60. The weakening effect of the cut-outs on the seismic response.. ..174
Figure 3.61. The final cracking pattern of the tested specimens..... ..178

LIST OF TABLES

Table 2.1. Overview of the experimental program.....49
Table 2.2. Variables of the experimental program.....52
Table 2.3. Properties of the concrete in the web-panel.....58
Table 2.4. Measured properties of the steel reinforcement.....58
Table 2.5. Geometrical and mechanical properties of the CF fabric and plates.....58
Table 2.6. Geometrical and mechanical properties of the grid used in TRM 59
Table 2.7. Properties of the repair mortar.....59
Table 3.1. Primary results of the tested wall specimens.....123
Table 3.2. Load bearing capacity and failure drift results.....124
Table 3.3 Results depending on the peak force attained by (11-12) strengthened walls.....124
Table 3.4. Cumulative energy dissipation at each cycle.....151
Table 3.5. Material properties of concrete-concrete interface (10 cm surface contact).....162
Table 3.6a. Comparison of the analytical and experimental results.....165
Table 3.6b. Comparison of the analytical and experimental results.....166
Table 3.7. Shear resistance of the reference walls evaluated using design code expressions.....170
Table 3.8. Investigated wall specimens opening data.....172
Table 3.9. Basic results of the investigated specimens.....173
Table 3.10. Response characteristic in terms of shear resistance.....174
Table A.1. Grid observations for PRCWP (7-E1-T) 196
Table A.2. Grid observations for PRCWP (8-E3-T) 199
Table A.3. Grid observations for PRCWP (10-L1/L3-T) 203
Table A.4. Grid observations for PRCWP (11-L1-T) 206
Table A.5. Grid observations for PRCWP (12-E1-T) 209
Table A.6. Grid observations for PRCWP (7-E1-T/R) 212
Table A.7. Grid observations for PRCWP (8-E3-T/R) 215
Table A.8. Grid observations for PRCWP (9-E1/E3-R/T) 219
Table A.9. Grid observations for PRCWP (10-L1/L3-T/R) 222
Table A.10. Grid observations for PRCWP (11-L1-T/R) 225

Table A.11. Grid observations for PRCWP (12-E1-T/R) 227
Table B.1. Sensor list for PRCWP (7-E1-T) specimen..... ..230
Table B.2. Sensor list for PRCWP (8-E3-T) specimen..... ..232
Table B.3. Sensor list for PRCWP (10-L1/L3-T) specimen..... ..234
Table B.4. Sensor list for PRCWP (11-L1-T) specimen..... ..236
Table B.5. Sensor list for PRCWP (12-E1-T) specimen..... ..238
Table B.6. Sensor list for PRCWP (7-E1-T/R) specimen..... ..240
Table B.7. Sensor list for PRCWP (8-E3-T/R) specimen..... ..242
Table B.8. Sensor list for PRCWP (9-E1/E3-R/T) specimen..... ..244
Table B.9. Sensor list for PRCWP (10-L1/L3-T/R) specimen..... ..246
Table B.10. Sensor list for PRCWP (11-L1-T/R) specimen..... ..248
Table B.11. Sensor list for PRCWP (12-E1-T/R) specimen..... ..250
Table C.1. Repair and strengthening costs for PRCWP (7-E1-T/R) specimen..... ..254
Table C.2. Repair and strengthening costs for PRCWP (8-E3-T/R) specimen..... ..258
Table C.3. Strengthening costs for PRCWP (9-E1/E3-R/T) specimen..... ..262
Table C.4. Repair and strengthening costs for PRCWP (10-L1/L3-T/R) specimen..... ..267
Table C.5. Repair and strengthening costs for PRCWP (11-L1-T/R) specimen..... ..271
Table C.6. Repair and strengthening costs for PRCWP (12-E1-T/R) specimen..... ..276
Table C.7. Economical evaluation summary..... ..281

1. INTRODUCTION

1.1. Context

Post-earthquake reconnaissance missions report good seismic behaviour of precast reinforced concrete shear wall buildings, but due to both 50 years of existence and actual comfort requirements of buildings, the use of such a structural system requires upgrading. In this context, experimental studies that are required not only provide an evaluation on the seismic performance and investigation on the weakening produced in structural walls due to cut-outs, but also intend to improve the ductile behaviour of the walls and provide solutions for a better seismic performance of buildings. Based on initial architectural considerations, openings in walls should be limited as number, as small as possible in dimension and as symmetric as possible. However, actual comfort requirements, architectural reasons and access necessities, led to cut-out interventions to be performed in walls. Compared to other structural elements, the existing literature lacks information concerning reinforced concrete walls (RC) retrofitted by FRP composites. Having a large variety of strengthening materials and strengthening techniques, research is strongly encouraged in order to reduce the vulnerability of the existing buildings and to improve the seismic risk.

1.2. Motivation

The seismic evaluation of precast reinforced concrete large panel buildings requires appropriate tools to identify critical regions and to consider strengthening resources where there is a need for intervention. Therefore, the research focuses on nearly full-scale precast reinforced concrete shear walls. The investigated wall specimens have as-built openings and/or opening enlargements, and meet the requirements of Eurocode 8 for walls designed to DCM (medium ductility) as large, lightly reinforced walls. Due to the fact that the lightly reinforced shear walls generally exhibit a brittle to low ductile behaviour, the strength and deformation estimations are conservative in the seismic evaluation.

1.3. Objectives

The research focuses on both experimental, numerical and theoretical investigations on the behaviour of precast reinforced concrete shear wall panels subjected to reversed cyclic loading. The seismic performance is characterized by failure modes, the force-displacement relationship, energy dissipation, stiffness degradation and ductility. In order to evaluate the seismic performance of the walls, the current research aims to provide progress related to the following questions:

- What is the influence of cyclic reversed shear loading on failure modes?
- How does the type of the opening or weakening influence the structural response?

• What type of strengthening technique suits best for the rehabilitation or retrofitting of such elements?
• What is the ductility of the shear walls having various openings?
• In what regions of the wall is the strain activity higher?
• Are the simple numerical models sufficient for the estimation of the shear strength?
• How accurate are the design code provisions for the estimation of the shear strength?
• Is it possible to make good assessments on the weakening induced in walls based on code provisions and numerical simulations?
• Are the obtained results in agreement with other available in literature?

Research into these questions will improve knowledge for the seismic evaluation of precast reinforced concrete walls, and also of precast reinforced concrete large panel buildings.

1.4. Overview of the thesis

The thesis is composed of five chapters and appendices totalising over 200 pages. The research is based on eleven quasi-static cyclic tests on near-full scale strengthened and reference precast reinforced concrete wall panels.

The first chapter emphasizes the frame of reference of the current research, presenting the objectives and a short overview of the thesis. During the performed study, the author searched for latest documentation available in literature with similar directions, like precast constructions, investigations on reinforced concrete walls with/without openings, ductility considerations, numerical analysis and strengthening using similar methods such as externally bonded reinforcement, near-surface mounted reinforcement and textile reinforced mortar. A brief presentation of the precast reinforced concrete large panel buildings in Romania is also presented, showing architectural details of the chosen project building type and the selected prototype walls from which the whole investigation started.

Chapter 2 contains a detailed description of the experimental program. The chapter commences with the presentation of the experimental specimens, followed by material considerations, test set-up, testing procedure and instrumentation. Considering established the testing procedure, the general behaviour of the reference specimens is presented. The chapter ends with a detailed description of the repair and strengthening strategy of the specimens.

Chapter 3 summarizes all the investigated and analysed results of the specimens. The following analysis types were undertaken: failure modes of FRP strengthened specimens, force-drift ratio response observations, strength analysis, displacement analysis, energy dissipation, ductility, strain and stiffness analysis. In addition to the measured response analyses, the author performed numerical analysis for the prediction of the shear response, theoretical study on the shear resistance of the specimens using design code provisions and plastic mechanism model and weakening assessment using a design code. The chapter ends with the computation of the final cracking pattern of the investigated specimens based on an assembled photo-maps.

In Chapter 4 the conclusions are drawn with respect to the response characteristics of the specimens, in terms of general behaviour, seismic

performance, weakening effect, strengthening using FRPs, reliability of numerical models and shear strength estimations using design code provisions.

Chapter 5 contains the personal contributions of the author, a list of selected papers and contributions to research projects.

Chapter 6 gives further recommendations for research.

A number of three appendices were considered important to be provided in the thesis, for supplementary information. Appendix A gives a tabulated presentation on the observation grid marked on the front face of the wall specimens. The occurrence of cracks and other failure details are depicted here, at each cycle peak. Appendix B gives a detailed description of the used instrumentation for each specimen. Appendix C provides an important aspect, related to the repair and strengthening costs performed in the case of all the investigated specimens.

1.5. Similar research in literature

Considering the behaviour during and after major earthquakes of the precast reinforced concrete large panel buildings, and their ability to support gravity loads and provide lateral resistance, together with the benefits of prefabrication, this type of structural system could be an excellent choice for designing earthquake resistant buildings. Fintel, author of "Performance of Buildings with Structural Walls in Earthquakes of the Last Thirty Years" [1] and "Shear Walls – An answer for seismic resistance" [2] has investigated and reported on many earthquakes between 1960 and 1990, in which reinforced concrete structures were involved.

Among the first observations were from the Chilean earthquake of 1960, where instances of cracking of shear walls were observed, but which did not affect the overall performance of the buildings and the walls continued to function after damage had occurred. Then from the earthquake in Skopje, Macedonia (1963) the author reported on a 14-story building having a structural system for lateral resistance composed of a shear wall frame interaction, where the three unreinforced concrete cores interacted with the frame of two-way slabs resisting on beams. It was observed that the building swayed during the earthquake, but however withstood without damage. In 1967, during the Caracas, Venezuela earthquake of 7.0 magnitude on Richter scale, it was reported that the buildings containing shear walls performed considerably better than buildings with flexible frames. After the 1972 earthquake in Managua, Nicaragua, measuring 6.0 on Richter scale, an 18-story buildings having concrete walls was reported with no significant structural and non-structural damage, except from one coupling beam that failed in shear, caused by over reinforcing in flexure of the short coupling beam with a large duct opening. In 1977, located at 130 miles north of Bucharest, Romania an earthquake of 7.2 magnitude on Richter scale occurred, causing the collapse of 35 buildings. It was found that hundreds of buildings consisting in concrete wall systems withstood the earthquake, the majority with no damage. In 1985, earthquakes of 8.1 and 7.5 magnitude on Richter scale caused 280 buildings to collapse in Mexico City. The Armenia 1988 earthquake, 6.9 magnitude on Richter scale, caused the collapse of 79 buildings and severe damage of 149 buildings, and it was reported that none of these buildings contained structural walls, whereas a number of 21 buildings containing shear walls were found to have experienced the earthquake undamaged.

Alfred A. Yee [3] investigated on structural and economic benefits of precast /prestressed concrete construction. The structural system of precast concrete elements were highly appreciated by architects and engineers due to the fact that

the products could be fabricated in a large variety of shapes and sizes, whereas by prestressing, longer spans could be achieved compared to the conventional in situ methods of construction. Fabrication of precast concrete products could be made with good precision on dimensions and had consistency in finishes and textures. However, it was observed that higher material consumptions were necessary, heavier precast units were expensive to handle, transport and erect, whereas they also required more expensive foundations and columns to support them. The connection of precast elements in order to form a structural frame was made by extending the reinforcing steel from the precast units into the in situ reinforced concrete. The author stated that according to past research and testing of precast joinery, multi-story precast buildings frames can be designed and constructed to resist severe seismic forces, as they performed successfully in both low and high rise buildings subjected to severe seismic forces over the past four decades. The author states that the precast elements can be integrated vertically and horizontally in building frames that behave in a monolithic manner with enough strength, stiffness and ductility to resist seismic forces. Concluding upon the investigation, the author considers the structures can be built with speed and economy, achieving efficiency in labor, and high level of material quality. Thomas and Sritharan [4] performed an evaluation of seismic design guidelines proposed for precast jointed wall systems. The authors also present in their paper the limitations of precast concrete in seismic regions, which apparently led designers consider this structural system inferior compared to the cast-in-place concrete. Some of the limitations were based on the poor performance of the precast framed structures during past seismic events, which was due to deficient connection details, ineffective load paths in buildings and poor construction practices [5,6,7]. The authors consider also a lack of design procedures and engineers with design experience in precast concrete, giving as example de 1999 edition of the ACI 318 standard, which did not include seismic design provisions for precast concrete, but contained design of precast structures equivalent to monolithic concrete structures. Also according to past earthquakes, it was observed that under large lateral displacements, significant damage occurred in precast concrete structures designed using cast-in-place concrete emulation. Demeter [8] investigated the seismic retrofit of precast reinforced concrete wall panels (PRCWP) by externally bonded CFRP composites. The aim of the research was to investigate the seismic performance of the PRCWP, evaluate the weakening effects caused by cut-outs and the effects of the seismic retrofit using EBR-CFRP. A number of seven quasi-static cyclic tests were performed in the experimental program, on near-full scale PRCWP. The considered design of the test set-up and loading procedure for the modeling of the outrigger effect induced a shear behaviour instead of a flexural one. The parameters of the study were the opening and the strengthening condition. The strengthening strategies intended to counterbalance the weakening incurred by a solid wall as a result of a door cut-out, and it was based on the behaviour and failure mode observed during the experimental tests performed on the bare specimens. Among the observed behaviour aspects reported by the author, were the flexural cracking at the joints between the spandrel beams and wall piers, shear cracking of the piers, and concrete spalling and crushing at the beam-pier joints and at the piers' bottom corners near the cut-out opening. Therefore, the strengthening scheme was designed to offer flexural capacity along the vertical and horizontal edges of the cut-out opening, increase the shear capacity of the wall piers, and provide confinement effect at the cut-out opening corners. Based on the obtained results, the author concluded that the influence of the cut-out opening on the shear strength, stiffness

and energy dissipation rate was significant, whereas the used CFRP-EBR retrofitting strategies revealed an improved behaviour in terms of energy dissipation, load and displacement capacity. The author stated that according to the test results in which the outrigger effect was taken into account, the cyclic response and the failure mode of the shear wall specimens was governed by diagonal compression.

Reinforced concrete walls were investigated by several other researchers, among which Dan et al. [9], who conducted a theoretical and experimental study on composite steel–concrete shear walls with vertical steel encased profiles. The experimental program was performed on six 1:3 scale elements, tested under quasi-static reversed cyclic horizontal loads. The obtained results revealed that the composite steel–concrete shear walls with encased profiles were more ductile in terms of displacement ductility compared to the common reinforced concrete walls. The researchers stated that the shear failure of CSRCW can be avoided by taking into account in the design process the bending and shear at the associated shear force of the capable bending moment. Authors recommend the use of connectors at the ends of profiles in order to avoid the splitting of concrete and to assure the anchorage of steel profiles, and a high class of concrete for a more dissipative behaviour of CSRCW. Greifenhagen and Lestuzzi [10] performed static cyclic tests on lightly reinforced concrete shear walls. The test series comprised four specimens based on the shear dominated response of the walls that were not designed for earthquake conditions. The authors investigated the deformation capacity of the specimens under reversed static cyclic loading in order to contribute to a more realistic seismic evaluation of existing shear wall buildings that were built prior to the introduction of earthquake-resistant design recommendations in building codes. The experimental tests revealed that the flexural capacity of the specimens limited the maximum observed base shear whereas shear related failure modes such as sliding, diagonal compression, and diagonal tension restricted the deformation capacity of the elements. Concrete compressive strength and axial force ratio variations lead to crack patterns that are substantially different. Damage due to reversed static cyclic loading accumulates near the base of the wall thereby degrading the concrete in sliding, compression, and tensile straining. Parulekar et al. [11] investigated a simulation on reinforced concrete short shear wall subjected to cyclic loading. The authors present experimental and analytical results of the behaviour of reinforced concrete stiff squat shear walls subjected to reversed cyclic loading conditions. Three-dimensional and two-dimensional finite element programs were used for analytical simulations and the results for the FE analysis and experiments were found in good agreement. Among the stated observations, the authors claim that the two-dimensional analysis predicted fairly accurate the load-deformation of structures, but it failed to capture some important three-dimensional effects such as the out-of-plane confinement. Thomson et al. [12] developed a simplified model for damage in squat RC shear walls. In order to validate the model, tests were carried out on specimens subjected to cyclic lateral loading of increasing amplitude and zero axial force. The model was based on concepts and methods of damage and fracture mechanics, allowing a representation of stiffness and strength degradation due to diagonal cracking of the concrete, plastic deformations due to yielding of the horizontal reinforcement and sliding shear across diagonal cracks. Permanent deformations due to flexural effects were neglected and only plastic deformations due the shear effects were considered. A good correlation between experiment and model was found by the authors. The model does not account for the combined damage due to shear and bending, as in tall shear walls, where cracking due to bending may be more significant than cracking due to shear.

Sánchez-Alejandre and Alcocer [13] investigated the shear strength of squat reinforced concrete walls subjected to earthquake loading. In order to assess a model for predicting the wall shear strength, a database with relevant information from tests was constructed by the authors. Data from 372 tests available in the literature was gathered, revised and organized, among which eighty rectangular walls that exhibited failures controlled by shear (diagonal tension) were selected for further analysis. The authors showed that for walls with M=VL < 0:5, the calculated shear strengths obtained through applying the code equations (such as Chapter 21 of ACI 318-08) were smaller than those measured in tests. A robust, yet simple shear strength model was developed and calibrated, consistent with the well-accepted formulation in design that shear strength may be considered as the addition of the concrete and steel contributions. However, the model departs from typical code equations, by considering the effects of drift demand on both the concrete and steel contributions, as well as the extent of plasticity in web reinforcement. Authors state that the axial load and the amount of vertical web reinforcement in the model increase the wall shear strength. Comparing the measured strengths in tests and calculated strengths using the proposed model, it was shown that the model was reliable. Pavese and Bournas [14] performed an experimental assessment of the seismic performance for a prefabricated concrete structural wall system. Seismic tests were performed on single full-scale walls with or without openings tested as cantilevers or with fixed ends. Among the obtained results, it was shown that the increase of the walls' length resulted in an increase of walls' shear resistance, regardless of the level of axial load, whereas the deformation capacity at failure was not affected. The axial load increase resulted in an increase in strength for most tested elements. The authors state that the strength of the walls with windows and doors decreased on the average by 28% and 48%, respectively, but on the other hand, the presence of openings in the prefabricated walls resulted in substantial increases of the deformation capacity. Jiang and Kurama [15] conducted an analytical investigation on the seismic retrofit of older medium-rise reinforced concrete shear walls under lateral loads. A number of three ASCE 41-06 retrofit methods (reduction of flexural reinforcement, addition of concrete confinement at the wall boundaries, and increased shear strength) were evaluated by comparing the behaviour of walls with different properties and simulating the intended effect for each retrofit method. Among the conclusions of the research, authors claim that concrete confinement provided in the end regions of a wall may not improve the behaviour of the element, since crushing can shift to the adjacent unconfined web concrete. The increase in the wall web thickness with added transverse reinforcement can be an effective retrofit method, but for walls with no confinement, the increase in transverse reinforcement does not result in a significant increase in the wall lateral displacement capacity. The combination of different retrofit methods can result in significantly improved results. Ganesan et al. [16] investigated the ultimate strength of reinforced concrete wall panels. The authors tested a number of 8 reinforced concrete wall panels, reviewed the studies available in the literature on the strength and behaviour of RC wall panels under one-way action and found that the model proposed by Pillai and Parthasarathy gives the better comparison with the experimental results compared to other models. Kara and Dundar [17] performed a prediction of deflection for reinforced concrete shear walls. The proposed model was tested by comparing theoretical with experimental results of the deflections of reinforced concrete shear walls. It was shown that the analytical procedure predicts with good accuracy the flexural and total deflection of shear walls to a value of load equal to approximately 85% of the

ultimate load, while the percentage of shear deflections in the total deflection increases with decreasing the aspect ratio of shear walls. Orakcal et al [18] investigated the shear strength of lightly reinforced wall piers and spandrels. The experimental program involved testing of six wall pier and eight wall spandrel, 3/4-scale elements. The authors assembled a database of test results available in the literature and compared the results with ACI 318-05 [19] provisions and FEMA 356 [20] recommendations on wall nominal shear strength. Among the conclusions, it was stated that the use of the FEMA nominal shear strength calculation for walls with a single curtain of web reinforcement is appropriate, if the wall thickness does not exceed approximately 300 mm, the longitudinal reinforcement is continuous, the transverse web reinforcement is sufficiently anchored with 180-degree hooks, and a moderate amount of boundary reinforcement is provided at the wall boundaries. The conducted experimental results were not in agreement with the ACI 318-05 provisions related to the shear strength of existing wall segments with one curtain of web reinforcement which cannot be taken larger than the nominal shear strength of concrete alone. The FEMA provisions for calculating nominal shear strength underestimates the shear strength of the wall piers subjected to relatively low axial load levels, regardless of the amount of boundary reinforcement provided and the anchorage conditions of transverse reinforcement.

The presence of openings in reinforced concrete walls attracted the interest of several researchers, among which Guan et al. [21] performed an ultimate strength analysis of normal and high strength concrete wall panels with varying opening configurations. After analysing twenty wall models in three parametric studies the authors concluded that by increasing the height and length of the opening in equal proportion, significantly decreases the axial strength ratio. Increasing only the length of the opening, decreases the axial strength ratio, while increasing only the height of the opening, little effect was found on the ultimate carrying capacity and the deflection. The combined effects of increasing the opening height together with the opening length were included in the proposed opening parameter in order to ensure a safe design, and a new ultimate load formula was proposed for walls with openings, acting in both one-way and two-way. Mosoarca [22] investigated the seismic behaviour of reinforced concrete shear walls with regular and staggered openings after the strong earthquakes between 2009 and 2011. The experimental program comprised five wall experimental specimens, among which a number of three had staggered openings walls, one was with regular openings and one was a solid wall. The author concluded that the walls with staggered openings were more rigid for the same value of the seismic action, and that they record smaller top horizontal displacement compared to the walls with regular openings. The wall specimens having staggered openings record cracks for smaller values of the relative displacement compared to those with regular openings. Considering the same amount of reinforcement and reinforcing layout, the walls with staggered openings developed a ductile failure, whereas the ones with regular openings developed a brittle failure. The walls having staggered openings failed at higher seismic forces than the ones with regular openings. The inclined cracks from shear occurred between two consecutive openings for the walls with staggered openings, but for a ductile failure it is recommended that this zone be reinforced with inclined rebars or have a higher percentage of horizontal reinforcement which should not reach the yielding limit. Wang et al. [23] developed a macro model for reinforced concrete structural walls having various opening ratios. The analytical study used three test specimens, which were 40% scale models of concrete structural walls with eccentric openings. Among the objectives of

the study was to establish the influence of openings on the shear capacity of a structural wall, as the specimens were designed to fail in shear, not in flexure. Specimens were tested under cyclic horizontal loading, whereas vertical axial loads were also applied. The modified multiple macro model was established by the authors, modifying the original model proposed by Tekehara et al. [24], in order to obtain more accurate load-deformation relationships in the case of multi-story walls with eccentric openings. Comparing the analytical and experimental results, it was shown that the modified multiple macro model was applicable to the structural walls even for the case of the opening ratio exceeding 0.4. The modified multiple macro model can predict well the behaviour of a wall with an eccentric opening, which is different depending on the loading direction. Hara and Doh [25] performed a finite element investigation of R/C wall panels, simply supported on two edges and on four edges with openings. Some considerations adopted in the numerical analysis refer to the use of the degenerate shell element, the geometric and material nonlinearities, the use of displacement incremental scheme, the yield condition of concrete was defined as the Dracker-Prager type (concrete yields when the equivalent stress based on mean stress and second deviatoric stress invariants reaches uniaxial compressive strength), the crushing condition was controlled by strains, the ultimate compressive strain of concrete was assumed as 0.003 by Kupfer's experiment (Kupfer 1969). The obtained numerical results showed a 0 up to 30% higher values than the ultimate strength of R/C panel obtained experimentally. The cracking pattern obtained numerically simulates well the experimental results. Li and Chen [26] investigated the initial stiffness of reinforced concrete structural walls with irregular openings. Six wall specimens with irregular openings were analysed using the proposed numerical approach. A total of 288 case studies were considered in the study. The lateral force was used to determine the initial stiffness of the walls with irregular openings. The initial stiffness was obtained by dividing the lateral load with the displacement at the top of the wall. The analytical stiffness of six test walls with irregular openings using the proposed approach was compared with the experimental results and a good agreement between them was found, whereas the parametric study comprising 288 case studies showed that the axial load ratio, opening ratio and aspect ratio can have a significant influence on the effective stiffness of walls with irregular openings. Fragomeni et al. [27] studied the behaviour of axially loaded concrete wall panels with openings. A total of forty seven reinforced concrete walls with openings in one and two-way action were investigated. A static loading regime was adopted for testing the specimens. The obtained test results indicated that the failure loads and crack patterns depend on the opening configuration and support conditions. The failure loads of two-way panels with openings were about 2 to 4 times those of similar one-way panels with openings. The failure loads decreased when the number of openings was increased from one to two. The axial strength ratio for one-way panels decreased when slenderness ratios were increased from 30 to 40. The Australian Standard (AS3600-2009) wall design equation was found to be inadequate in predicting failure load for walls with openings, but the derived prediction equation for normal strength concrete walls with openings by Doh and Fragomeni (2006) was found to give good prediction of failure loads for the walls tested and can be extended for use for normal and high strength concrete walls with one or two openings and high slenderness. The authors state that the equation tends to slightly over-estimate failure load in some cases where openings are not symmetrical about the wall axes, and therefore refinement may be necessary. Carrillo and Alcocer [28] investigated the degradation properties of reinforced

concrete walls with openings. Four isolated walls with openings were studied in the experimental program, two full-scale prototypes tested under QSC loading and two 1:1.25 scaled models tested under shaking table excitation. Considering the size of the models, similar to the prototypes, the models were built with the same material as the prototype and only the dimensions of the models were altered. The models were subjected to three earthquake hazard levels using both natural and artificial acceleration records. The authors showed that the loading history of the QSC testing ignored the principal dynamic effects observed in structures subjected to earthquake loads, mainly, the parameter associated with the strain rate and the number of cycles. Comparison between the dynamic and the QSC responses showed that stiffness and strength degradation properties were clearly dependent upon the loading rate, the strength mechanisms associated to the failure modes (crushing of concrete or plastic yielding of reinforcement), the number of cycles, as well as the cumulative parameters such as ductility demand and energy dissipated. According to the computed measures the proposed empirical models can be used suitably to predict the stiffness and strength degradation properties for RC walls with openings. Wang et al. [29] studied the behaviour of reinforced concrete structural walls with various opening locations. The used analytical objects were two specimens, 40% scale models of concrete structural walls with eccentric openings or central openings, tested under cyclic horizontal loading, whereas vertical axial loads were also applied. The authors proposed an M-M model by modifying an original macro model to obtain more accurate load-deformation relationships and behaviours in the case of multi-story walls with various large opening locations. It was concluded that the behaviour of a structural wall with eccentric openings becomes different depending on the loading direction, whereas the ultimate strength becomes different depending on the opening locations. But the opening locations and/or loading direction were not taken into account in the considered design code, and even if the specimens were designed according to the current design code, the shear slip failure in the first story wall with eccentric openings still occurred at the final stage. Comparing the analytical results and the experimental results, it was shown that the M-M model could predict the different behaviours of the structural walls with various opening locations and different loading directions well, and that the M-M model is applicable to structural walls even in the case of the opening ratio exceeding 0.4. The comparison of strength, stiffness, lateral load-drift angle relationship between M-M model and the O-M model indicated that the M-M model was more adequate.

Various estimations on the evaluation of the ductility of the elements have been performed during time, e.g., Park (1988) [30], Priestley (2000) [31], and Salonikios et al. (2000) [32]. Carrillo et al. [33] investigated on the displacement ductility for seismic design of RC walls for low-rise housing. The authors proposed values of the displacement ductility ratio, based on experimental results obtained from 39 concrete wall specimens, tested under quasi-static reversed-cyclic lateral loads and shaking table excitations. Variables included in the experimental program were the height-to-length ratio and wall with openings, concrete type, web steel ratio and type of web reinforcement. The results showed that displacement ductility ratios between 1.63 and 2.92 can be achieved for walls with web shear reinforcement composed of deformed bars, and between 1.39 and 2.71 for walls with welded wire mesh. Greifenhagen [34] investigated on the seismic behaviour of lightly reinforced concrete squat shear walls. The test series included four specimens that were not designed for earthquake actions. The author investigated on the deformation capacity of lightly reinforced concrete shear walls under reversed static-cyclic loading. The concrete compressive strength, amount of horizontal

reinforcement, and axial force ratio were the parameters of the experimental program. It was shown that the shear intensity (the shear stress at nominal flexural strength normalized to the square root of concrete compressive strength) governs both the crack pattern and the failure modes of lightly reinforced shear walls. The study revealed that low to moderate ductility can be expected for such walls. According to Priestley & Kowalsky (1998), the ductility is based on the level of straining of vertical rebars, whereas this approach can also be applied on lightly reinforced shear walls, stated the author since it is applied on reinforced columns too (Kowalsky & Priestley 2000), (Sezen & Moehle 2004). Neglecting the contribution of axial force to shear capacity, the revised UCSD model can be a robust tool to predict the ductility supply of walls susceptible to shear failure. Christidis et al. [35] performed a seismic assessment of existing RC shear walls non-compliant with current code provisions. In the experimental program, six shear walls were designed and tested under static cyclic loading. Lower levels of ductility seemed to develop for walls without seismic detailing. Significant reduction of the ductility level was found for walls with low shear reinforcement ratio, which developed a brittle failure mode. The presence of confined boundary elements in wall appeared to improve on the deformation capacity. The variation of axial compressive load was observed to have a negative influence on the wall behaviour, leading to a brittle failure mode and a lower deformation capacity. Kuang and Ho [36] investigated on the enhancement of ductility for non-seismically designed RC shear walls. Six large-scale, RC squat shear wall specimens were tested under reversed cyclic loading. The experimental investigation revealed that the inherent displacement ductility factor of 2.5 to 3 may be achieved for the shear walls with non-seismic reinforcement detailing. The authors concluded that ordinary shear walls designed and detailed without seismic consideration may not sufficiently satisfy the ductility demand for shear-wall building structures in low to moderate earthquake regions. The displacement ductility factor of 4 to 5 can be achieved by modifying the current non-seismic design practice of reinforcement details, by introducing the boundary-confinement zones at the ends of the wall panel and providing secondary links in the confinement zone and cross-tie sets throughout the cross-section. Among the special seismic compliant reinforcement details for shear walls with nonseismic design for the enhancement of the ductility and energy dissipation capacity, safety and moderate seismic events, were proposed as follows: a boundary-confinement zone should be provided with a width of 1.5 to 2 times the wall thickness at the side boundaries of the wall, in the boundary-confinement zone the secondary closed links should be provided and arranged between the main transverse reinforcement, cross-ties should be provided throughout the wall panel, in addition to use of the secondary links in the boundary-confinement zones.

Fiber reinforced polymer (FRP) materials continue to show great promise for use in strengthening reinforced concrete structural elements. FRP materials are an excellent option for use, having different available application techniques such as externally bonded, near-surface mounted or integrated in textile reinforced mortar. Bashar et al. [37] studied one way RC wall panels with openings strengthened with CFRP. A number of sixteen 1/3 scale RC walls with openings consisting in four identical series of four specimens were used in the experimental program, among which series 3 and 4 were tested with CFRP. The strengthening was applied in the vicinity of the openings. The objectives of the study were to investigate the influences of the opening sizes on the strength and the structural behaviour of one-way RC walls, while the reinforcement ratios were kept constant for all specimens. The author cited Enochsson et al. (2006) who introduced a simplified method to

estimate the amount of CFRP required for strengthening the openings in two-way RC slabs, which can also be used for strengthening openings of one-way RC slabs and RC walls. In order to compute the failure load of RC walls with openings strengthened with CFRP for different range of limitation, the authors introduced new constants to existing Saheb and Desayi [38] equation. The strengthening using CFRP improved the load bearing capacity of the RC walls with by which reducing the principal stresses acting on the upper corners of the openings. Altin et al. [39] investigated the hysteretic behaviour of RC shear walls strengthened with CFRP strips. A number of five, ½ scaled RC wall specimens were used in the experimental program in order to investigate the influence of shear strengthening using CFRP on the hysteretic response of structural walls. The specimens were tested under cyclic lateral loading, whereas no axial load was applied. A number of four strengthening configurations using CFRP strips were used, namely the lateral strip, Xshaped diagonal strips, X-shaped diagonal and lateral strip combination, X-shaped parallel strips. The authors concluded that the strengthening of shear deficient reinforced concrete walls using CFRP strips was effective by improving the hysteretic behaviour of the walls under the cyclic lateral loading. The best performance for lateral displacement capacity and lateral strength of shear walls was obtained from the strengthening with lateral strips. The configuration using X-shaped strips increased the wall shear strength, but they were not enough to reach the flexural capacity. The strengthened wall specimens dissipated much more energy compared to the reference specimen. The maximum measured strains on CFRP strips were 0.008–0.009 mm/mm. ACI-440 code [40] was used for strengthening design. Antoniades et al. [41] performed cyclic tests on seismically damaged reinforced concrete walls strengthened using fiber-reinforced polymer reinforcement. The authors claim that the study was the first one to address the retrofit with FRP jackets in combination with FRP strips intended for flexural strengthening of squat RC walls that have sustained heavy seismic damage. Testing a specimen as reference one, that was repaired by replacing of damaged concrete with high-strength mortar and lap-welding of fractured reinforcement in the plastic hinge region, revealed that the strength was almost fully restored. In the case of the FRP-strengthened walls, strength increased compared to the repair-only one with 2% (where early failure of the anchorage system of the CFRP strips occurred) and 32% for the case where a steel plate was used and improved the anchorage conditions of the strips. The full restoration of energy dissipation capacity of the original walls could not be achieved, no matter the efficiency of the retrofitting scheme used. Li and Lim [42] conducted tests on seismically damaged reinforced concrete structural walls repaired using fibre-reinforced polymers. A number of four low-rise and medium-rise wall specimens were used in the experimental program, tested under in-plane horizontal loading, with cycles of quasi-static cyclical loading. Based on the failure of the original specimens, the walls were repaired, and FRP strips were externally bonded to the wall in the horizontal and vertical directions in order to increase the member size and shift the failure of the wall toward a ductile behaviour. Cracks at the base of the specimens were injected with epoxy and a crack sealer made of epoxy was used to seal the remaining parts of the cracks during epoxy injection. GFRP anchors were placed at various locations along the length of the sheets, whereas the splay out roving of the fibre extend for a minimum of about 100-mm diameter on the surface of the wall specimen. The authors concluded that the flexural strength and stiffness can be increased by the use of GFRP and CFRP sheets, generally the dissipated energy of the repaired specimens is significantly larger than those of the original counterparts, the increase in anchorage length along with plates or angles

help in preventing early peeling. Dan [43] performed experimental tests on seismically damaged composite steel concrete walls retrofitted with CFRP composites. The experimental program included six 1:3 scale elements, namely composite shear walls with steel encased profiles (CSRCW). The specimens were damaged under cyclic lateral loads and thereafter retrofitted and retested. Retrofitting of the specimen was performed by externally bonded carbon fibre reinforced polymer reinforcement, applied symmetrically on both faces of the wall, in order to restore the initial load bearing capacity of the reference elements. Unidirectional carbon fibre sheets and plates were used in the strengthening. The author concluded that the strengthening solutions were efficient in terms of the load bearing capacity, the anchorages provided for CFRP strips and plates were efficient and no weakening being observed during the tests, the initial stiffness of the retrofitted elements was up to 80% of the initial stiffness of the reference specimens, whereas the dissipated energy of the strengthened walls was slightly smaller compared to the reference elements. Kheyroddin et al. [44] made a hysteretic evaluation on the seismic behaviour of RC shear walls strengthened with FRP sheets. The tests of eight scaled, low-rise shear walls with boundary elements were used in order to investigate the effect of externally bonded FRP sheets on the behaviour of shear walls. A number of three different models with different configurations of FRP layers were considered and developed, namely strengthening with one vertical ply of carbon fibre sheets, strengthening with two vertical plies of carbon fibres, and strengthening with two vertical plies of carbon fibres and one in the horizontal direction. According to the obtained results, the application of externally bonded carbon fibre sheets was an effective seismic strengthening procedure for RC shear walls. CFRP sheets wrapped around the plastic hinge range of RC wall provides enough shear strength, resulting in a ductile flexure failure mode, whereas confinement of concrete in the plastic hinge leads to an increase in the ductility of the RC wall. Meftah et al. [45] Seismic behaviour of RC coupled shear walls repaired with CFRP laminates having variable fibres spacing. The authors proposed a seismic analysis method for RC coupled shear walls structures strengthened with thin composites plates having variable fibres spacing using the mixed finite element method. A typical 20-storey RC strengthened coupled shear walls was analysed under three different earthquakes. According to the obtained results, significant improvement in the seismic deflections was observed when the fibres were clustering near the wall edges. Demeter et al. [46] analysed the seismic retrofit of cut-out weakened precast RC walls by externally bonded CFRP composites. The experimental program included seven quasi-static cyclic tests on near-full scale (1:1.2) precast reinforced concrete wall panels, having as variables the opening and the strengthening condition. The author also investigated on the response characteristic of the weakened structural member in terms of shear resistance, initial stiffness or energy dissipation rate, using equations from the AIJ recommendation (AIJ 1999 [47], quoted in Warashina et al. 2008 [48]), but also checking on two peripheral ratios greater than the upper limit given in the AIJ document, namely for 0.48 and 0.73, and it was generalised also for the dissipation rate response characteristic. Good agreement was found for the weakening effect of the cut-out opening using the predictions provided by the AIJ equation. Related to the strengthening used, an increased energy dissipation capacity of the retrofitted walls was obtained. The author claims that the improved seismic behaviour of the walls should be attributed to the confinement and shear component of the strengthening system, because the flexural FRPs were found to be susceptible to premature failure. Ghobarah and Khalil [49] investigated on the seismic

rehabilitation of reinforced concrete walls using fibre composites. For the experimental program an innovative test setup that provides the possibility of controlling the ratio of the shear force to both bending moment and axial load was used. For one specimen the rehabilitation strategies had to include both a shear strengthening scheme and a ductility improvement scheme, as the control wall was deficient in shear and ductility. The shear capacity improvement involved wrapping the wall with two layers of Tyfo BCC fabrics, whereas the ductility improvement scheme involved the confinement of two end column elements of the wall. For the second specimen, the shear strengthening scheme was identical to the previous one with small but significant difference, while the ductility enhancement procedure consisted of two components similar to the first rehabilitation scheme, namely U-shaped FRP sheets attached to the two end elements of the wall similar to the first wall, and steel anchors used to close the confinement hoop and generate two confined columns on both sides of the wall. The authors concluded that the proposed rehabilitation strategies using CFRP sheets and carbon or steel anchors proved to be effective in enhancing the shear strength and ductility for structural walls, the increase in confinement of the end elements delayed the concrete crushing in compression up to very high compression strains and allowed the full utilization of the longitudinal steel in tension due to the increased strength of concrete, the steel anchors through the wall proved a better confinement compared to the FRP anchors, and both the experimental and the analysis results showed that a plastic hinge was developed at the base of the wall in the case of the rehabilitated specimens which was effective in the dissipation of energy. Antoniades et al. [50] performed an evaluation of hysteretic response and strength of repaired R/C walls strengthened with FRPs. The study presents the results from the post-processing of experimental data that were recorded during the testing of eleven R/C wall specimens, initially tested to failure and then repaired and strengthened using FRP reinforcement. The objectives of the strengthening were to increase both the flexural and shear strength. The specimens were strengthened using FRP sheets and strips, with a view to increasing flexural as well as shear strength and ductility. A detailed description of the strengthening techniques used and the behaviour of the specimens under cyclic loading to failure was provided. According to the obtained results, the displacement capacity of the FRP-strengthened walls was found to be generally inferior to that of the virgin ones, the rate of stiffness degradation during cyclic loading was found to be similar in both the virgin and the strengthened walls, it was noted in the tests that FRP-strengthening of R/C walls was effective in preventing development of unfavourable failure mechanisms, like those dominated by shear. Failure of all strengthened specimens was predominantly flexural, which eventually led to an anchorage failure of FRP reinforcement in many walls, after inelastic flexural deformations developed at the critical crack (wall base). Floruţ et al. [51] performed tests on reinforced concrete slabs with cut-out openings strengthened with fibre-reinforced polymers. In the experimental program, a number of eight tests were carried out on four two-way slabs, with and without cut-out openings. The authors report that the elements replicate two-way single span simply-supported slabs, designed according to EN1992-1-1 [52]. Related to the strengthening scheme, the CFRP components were bonded to the soffit of the slabs in two directions. NSM technique was applied for the CFRP components parallel to the short edge of the specimens and EB application for those on the direction parallel to the long edge of the slabs. Based on the obtained results, the authors concluded that the load capacity of slabs with cut-out openings is not directly proportional to the reduction in their area, whereas by using a quantity of FRP

equivalent to the steel reinforcement removed by sawing the cut-out, the capacity of the slab can be restored fully, even when damaged prior to strengthening. Due to their superior mechanical properties compared to steel reinforcement, the FRPs allowed for better stress redistribution and a more uniform cracking distribution.

Several advantages were reported in literature for the near-surface mounted FRP reinforcement in comparison with the externally bonded technique, such as the development of higher strain in the FRP before debonding, protection from fire /other environmental influences, and also a minimal impact on the aesthetics of the structure [53]. Konthesingha et al. [54] evaluated experimentally the static cyclic in-plane shear response of damaged masonry walls retrofitted with NSM FRP strips. Three different retrofitting schemes were considered using unidirectional pultruded CFRP strips, namely horizontal FRP strips inserted into the mortar bed joints for aesthetics, reinforcement on both faces of the wall because it is more efficient compared to the single side reinforcement and eccentricity is avoided, and the trial of the use of vertical FRP strips in order to increase the strength and ductility. In all the strengthening strategies, slots were cut into the surface of the panels using a brick cutting saw and the FRP strips were glued into the slots using a two-part epoxy adhesive. The authors concluded that the retrofitting performed was efficient by obtaining increased displacement capacities for the walls, the maximum load was not significantly improved after retrofitting the damaged specimens, greater energy dissipation was obtained for the retrofitted walls compared with URM walls. The combination of horizontal and vertical reinforcement retrofitting scheme showed the best performance in terms of its ability to enhance the ultimate load capacity, displacement capacity and energy dissipation for the tested walls. Sakar et al. [55] investigated the nonlinear behaviour of shear deficient RC beams strengthened with near surface mounted glass fibre reinforcement under cyclic loading. A number of five rectangular RC cantilever beams were casted without stirrups to fail in a shear mode. According to the obtained results, the tested NSM GRRP shear strengthening system has significantly improved the cyclic load carrying capacity of the tested specimens, the NSM shear strengthening system with GRRP rods has also improved significantly the ductility of the beam by increasing the displacement, the displacements at failure (ductility) of the strengthened specimens were larger than for the control unstrengthened specimen, whereas the load carrying capacity has been slightly improved when increasing the GFRP bar size from 6 mm to 10 mm and reducing the spacing from 160 mm to 120 mm. Griffith et al. [56] investigated on the flexural displacement response of NSM FRP retrofitted masonry walls. In the experimental program a number of fifteen walls were tested in vertical one-way bending, having as variables the reverse cyclic loading, the axial pre-compression, the FRP strip spacing, and the reinforcement ratio. The FRP strips were aligned vertically along the brick units avoiding the perpend joints (one exception) in order to increase the ultimate capacity. The retrofitting strategy was designed according to the full interaction theory so that IC debonding was the failure mode, rather than tensile rupture of the FRP or crushing of the masonry. All wall specimens were reinforced on both faces with vertical NSM CFRP strips, placed along the centre-line of the flexural face, hence for one specimen the strip alternately penetrated brick units and perpend joints in adjacent courses, while for the others the strip ran through the brick units. The authors concluded that the NSM retrofitting technique was efficient in terms of vertical bending capacity, multiple strips with smaller spacing produced stronger walls with increased displacement capacities for the same reinforcement ratio, the increase in reinforcement ratio resulted in an increase in strength but also in a reduction in displacement capacity, applied axial load was

observed to increase the flexural stiffness of the walls but with a small effect on the strength and displacement capacity of walls. The authors recommend that for an efficient use of FRP, to choose optimal strip spacing rather than increasing the reinforcement ratio in order to achieve better results for the overall behaviour of wall. Lee and Cheng [57] studied the bond of NSM systems in concrete strengthening by examining design issues of strength, groove detailing and bond-dependent coefficient. A comparison between experimental data and predictions on the bond strength were made using five analytical and semi-empirical bond models. It was found that the capability to accurately predict the average bond strength is still limited using the existing analytical and semi-empirical models. The bond performance was found to be significantly affected by the groove dimensions. According to Lee et al. [58] who examined ten different types of NSM FRP rods in order to investigate the effect of groove size on bond strength, it was found that the bond strength increased as the groove dimensions increased. In the existing design guide [59] are suggested only the minimum dimensions of grooves for circular or rectangular NSM rods. In order to determine the optimum groove size for each type of NSM reinforcement, the authors used a simple method based on the concept of Classification and Regression Trees [60, 61] and the results were summarized in the paper. Bianco et al. [62] investigated a three dimensional mechanical model for simulating the NSM FRP strips shear strength contribution to RC beams. The authors developed a numerical model for simulating the NSM shear strength contribution in order to provide an explanation for the failure mode affecting the behaviour, at ultimate, of RC beam strengthened in shear by the NSM technique. T cross-section RC beams were used in the experimental program. The numerical modeling strategy herein proposed also lets parametric studies be carried out in order to assess the influence of all of the involved parameters on the NSM shear strength contribution. Good agreement was found between the numerical predictions and the experimental measurements, considering that the proposed model neglects aspects such as the softening behaviour of concrete in tension and the high scatter affecting concrete tensile strength. Ali et al [63] studied the interfacial stress transfer of near surface-mounted FRP-to-concrete joints. The analytical models were developed and used to predict the load/slip characteristics of a NSM CFRP plate. In order to validate the accuracy of the developed models, the analytical models using both unilinear and bilinear interfacial bond characteristics were compared to the results from a series of NSM pull-push tests. Good precision at all levels of loads, especially at failure was found comparing the analytical models with the experimental data. The authors claim to have developed fundamental equations that govern the behaviour of an NSM plate in a pull-test from the initial application of load to complete plate debonding, and that the models are applicable within the bounds of the variables in the experimental data used. The considered approach can be simplified by taking into account only the falling branch of the interface bond characteristics which leads to a closed form solution for the IC debonding resistance for plates that are fully anchored and which agrees well with test results. De Lorenzis et al. [64] performed a numerical and experimental investigation on the anchorage length of near-surface mounted fibre reinforced polymer bars for concrete strengthening. The specimen used for this investigation were C-shaped concrete blocks with a square groove in the middle for embedment of the NSM bar. The test variables considered in the study were the groove-filling material, the bonded length, the groove size and the surface configuration of the bar (spirally wound and ribbed). A total number of 34 specimens were used. The authors concluded that the epoxy offers superior mechanical performance as groove filler with respect to the cement paste, the most

suitable types of bar for NSM applications were CFRP ribbed and CFRP spirally wound bars, a groove size-to-bar diameter equal to 2.0 should be the optimal one, and a smooth groove surface, although it yields slightly lower local bond strengths, results in a more ductile bond-slip behaviour. A finite element model was also developed in order to study the bond of NSM FRP reinforcement in concrete and it was found to be able to capture the change in failure mode corresponding to increasing groove depth and the experimental failure load and load versus displacement behaviour of the specimens. Li et al [65] performed an analysis on unreinforced masonry concrete walls strengthened with GFRP bars. The specimens investigated in the experimental program were made using concrete masonry blocks and were built by qualified masons to eliminate differences in handwork and mortar workability. Different strengthening strategies and material systems were used, namely: small-dimension glass FRP (GFRP) and stainless steel bars inserted in the joints, and GFRP laminates and internal steel wire-ladders. An equal amount of reinforcement was provided by GFRP laminates and GFRP bars in terms of axial stiffness EA. According to the obtained results, the FRP strengthening technique proved to be effective by increasing the in-plane strength and ductility of URM walls. The strengthened walls exhibited a better pseudo-ductility and were more stable after failure, reducing the risk of partial or total collapse. The specimens with FRP reinforcement applied only on one side tilted toward the direction of the strengthened face, while the ones having symmetrical distribution of reinforcement on two faces had an improved overall stability and exhibited the largest pseudo-ductility. Sas [66] investigated in his doctoral thesis the FRP Shear Strengthening of RC Beams, where he included an article where he was one of the authors, named "Flexural-shear failure of a full scale tested RC bridge strengthened with NSM CFRP", where it was described the full-scale failure test of a bridge strengthened in flexure with NSM CFRP reinforcement. The strengthening applied was found to increase the flexural capacity of the bridge by about 30%. The authors also investigated the recommendations given in three codes for the prediction of the shear force capacity of the bridge after the strengthening. Among the conclusions it was stated that according to the Eurocode, the VAT model predicts the crack inclination angle well but it gives the most conservative estimates of the shear capacity. The ACI model was found to be a fixed model that does not take into account the flexural shear interaction, while the CSA model captures the flexural shear interaction, but in a conservative manner compared to the Eurocode.

The FRP retrofitting technique has its disadvantages too, such as the poor behaviour at high temperatures, high costs, inapplicability on wet surfaces and difficulty to conduct post-earthquake assessment behind FRP jackets, which are mainly attributed to the organic resins used to bind the fibres. Textile-Reinforced Mortars are an interesting alternative to FRP materials, comprising textiles impregnated with inorganic binders, such as cement-based mortars [67]. Ombres [68] performed a debonding analysis of reinforced concrete beams strengthened with fibre reinforced cementitious mortar. A total of six long beams were used in the experimental program. The bottom surface of the beams was sandblasted to remove the loose cement layer, cleaned with water and left for some days to dry out in order to ensure a good bonding. The first mortar layer was then applied on the concrete surface, than the first layer of PBO (short of Polypara-phenylene-benzo-bisthiazole) mesh was applied and pressed slightly into the mortar, followed by the next mortar layer, and the operation was repeated until all PBO layers were applied and covered by mortar. The authors investigated the debonding of RC beams strengthened with an externally bonded Fibre Reinforced Cementitious Mortar made

by fabric meshes of high strength PBO fibres embedded into a cement based mortar, and according to the experimental and theoretical results it was concluded that in absence of transversal ends anchorages, the intermediate crack debonding was the predominant failure mode of PBO-FRCM strengthened beams. In the presence of an effective bonded length, the debonding propagation was gradual and an increase of the flexural capacity was observed after the beginning of the debonding. For all the tested specimens the debonding occurred after the yielding of tensile steel rebars. Papanicolaou et al. [69] investigated externally bonded grids as strengthening and seismic retrofitting materials of masonry panels. The experimental program consisted in five types of medium-scale, single-wythe, fired clay brick and stone block wallettes composed of running bond courses, namely shear walls (1300 mm x 800 mm), beam-columns (1300 mm x 400 mm), beams (400 mm x 1300 mm), shear walls (1200 mm x 1120 mm), beams (400 mm x 1500) mm. The main parameter investigated was the number of grid layers used to form the jackets, but the authors considered the effect of other parameters too, such as the type of bonding agent, the type of grid and the axial compressive load level exerted on the walls simultaneously with the in-plane load applied in the transverse direction. According to the test plan the elements were subjected to out-of-plane flexure perpendicular to the bed joints (beam-column), out-of-plane flexure parallel to the bed joints (beams), in-plane flexure combined with axial force (beam-column), in-plane flexure/shear (beams – 400 mm x 1300 mm) and in-plane shear with axial force (shear walls). A number of five different commercial textiles with equal quantity of fibres in two orthogonal directions were used in the study and were made of high-strength carbon, bitumen-coated E-glass, bitumen-coated polyester, polypropylene and basalt. A stepwise presentation of the TRM application procedure was given in the paper. According to the obtained results the authors concluded that for the beam-column type walls and beam type walls subjected to cyclic out-of-plane or in-plane loading, the TRM overlays provide a substantial gain in strength and deformation capacity, whereas for the out-of-plane loading TRM overlays outperform their FRP counterparts on the basis of maximum load and displacement at failure, provided that tensile fracture of the textile reinforcement does not occur. The authors claim that even the weakest TRM configurations when adequately anchored resulted in more than 400% increase in strength and 130% in deformability. Bernat-Maso et al. [70] performed an experimental assessment of textile reinforced sprayed mortar strengthening system for brickwork wallettes. Three experimental groups were investigated, namely a group consisting in three masonry specimens that were used as control samples for comparison, a group made of nine specimens strengthened with Textile Reinforced Mortar (TRM) and a third group of samples strengthened with Textile Reinforced Sprayed Mortar (TRSM). The parameters investigated in the study were the type of textile grid, the number of layers of reinforcement and the number of reinforced sides. The most relevant conclusions given by the authors were: the spraying technique has no noticeable drawbacks in comparison with the hand application when compared under the same conditions, but by spraying the mortar led to time saving in comparison with hand application. A greater amount of strengthening fibres inside the TRSM layer was found to lead higher load-bearing capacity, but the influence of the additional mortar thickness has to be taken into account. TRSM applied on both sides of the samples did not improve the performance in comparison with the cases where the TRSM was applied only on the tensile side. The application procedure of TRSM in comparison with the TRM system was found to use a larger amount of mortar, whereas it was observed a poor finishing of the strengthened surface. Urban

and Stempniewski [71] investigated the evolution of a strengthening system for masonry buildings from prototype to practical implementation "RÖFIX Sisma Calce". The paper presents the scientific history on the development of a strengthening system for masonry buildings vulnerable to earthquakes. The developed strengthening system consisted in fibre (made of polypropylene and alkali resistant glass and were woven into a multi-axial hybrid fabric) reinforcement embedded in a fresh cement based mortar. Also a two-story masonry building was tested on a shaking table. The building was made of natural stones, and it was first tested unreinforced, then it was repaired, strengthened and shacked again until the limit of the used shaking table was reached. A number of two additional tests were performed on new two-story brick buildings in unreinforced and reinforced condition using very soft masonry. The authors used small tension samples to evaluate the bonding efficiency of several mortars in connection with the used hybrid textile and a calculation method was developed for the usage within commercial finite element programs. Beginning with a high performance epoxy based mortar, the development lead to a more breathable material with only one component and together with an optimized bond behaviour Röfix Sisma Calce+. Bernat et al. [72] performed an experimental and analytical study of TRM strengthened brickwork walls under eccentric compressive loading. In order to investigate on the effectiveness of the TRM strengthening, two unreinforced walls and nine TRM strengthened walls were experimentally tested. The parameters chosen in the program were the type of fibre grids, the number of installed grids, the type of mortar and the possible connectors used between the TRM and the masonry. Based on the obtained results the authors concluded that all the tested mortars reached the necessary bonding strength for the adherence of the TRM to masonry, making unnecessary the use of connectors for the walls tested under compressive loads. A stiffer behaviour of the walls was found due to the use of TRM strengthening, in both in- and out-of-plane direction. No failure due to TRM debonding was observed in the experimental tests. The authors concluded that the TRM strengthening obviously prevents the masonry walls from failing due to pure mechanism formation, limiting the second order effects and enlarging the load bearing capacity under eccentric axial load. Papanicolaou et al. [73] investigated the textile reinforced mortar (TRM) versus FRP as strengthening material of URM walls under out-of-plane cyclic loading. The experimental program was composed of two series of medium-scale, single-wythe, fired clay brick wallettes comprising running bond courses. The first series of specimens measured 1300 mm in height and 400 mm in width and were tested out-of-plane, while the second series of specimens measured 400 mm in height and 1300 mm in width and were tested out-of-plane. The major parameters investigated were the use of inorganic mortar versus resin-based matrix material for the textile reinforcement and the number of textile layers. The strengthened specimens were subjected to cyclic out-of-plane loading using a stiff steel frame, while the walls were laid in horizontal position and were loaded in three-point bending. The authors concluded upon the obtained results that the textile-reinforced mortar overlays provide a substantial gain in strength and deformability. The gain was found to be higher as the number of layers increased. Based on the condition that the failure is controlled by damage in the masonry, the TRM overlays outperform their FRP counterparts in terms of maximum load and displacement at failure, whereas if the failure mechanism involved tensile fracture of the textile reinforcement the effectiveness of TRM versus FRP was slightly reduced. Corradi et al. [74] investigated the shear strengthening of wall panels through jacketing with cement mortar reinforced by GFRP grids. The authors classify the tested strengthening technique as near surface

mounted (NSM) reinforcement. Instead of metal bars, a GFRP grid, made up of alkali resistant glass fibre with a zirconium content equal to or greater than 16% pre-impregnated with thermosetting epoxy vinyl ester resin was inserted into a low cement content mortar jacketing. Connectors were also used in the strengthening scheme of the panels, composed of two unidirectional fiberglass L shaped bars joined together by injecting epoxy paste into the hole. The authors obtained a significant increase in strength by using GFRP grids, while the problem of wall leaves connection was dealt through the use of composite bars inserted in holes in the masonry and connected to the GFRP grid applied to the surface of the panels. Triantafillou et al. [75] investigated the concrete confinement with textile-reinforced mortar jackets. The experimental program was performed on cylindrical specimens with a diameter of 150 mm and a height of 300 mm and short column-type specimens with a rectangular cross section of 250 x 250 mm and a height of 700 mm. The considered parameters for the cylindrical specimens were the use of inorganic mortar versus resin-based matrix material for the textile reinforcement, the strength of the inorganic mortar and the number of textile layers, while for the rectangular prisms the parameters were the inorganic mortar versus resin-based matrix for the textile reinforcement, number of textile layers and effectiveness of bonded versus unbonded confining systems. Based on the obtained response of the confined cylinders, it resulted that the textile-mortar confining jackets provide substantial gain in compressive strength and deformability, and in comparison with their resin-impregnated counterparts, mortar-impregnated textiles may result in reduced effectiveness for strength and ultimate strain. It was also found that the failure of mortar-impregnated textile jackets was less abrupt compared with that of their resin-impregnated counterparts. According to the response of the rectangular columns, it was concluded that mortar-impregnated textile jackets were effective in confining columns of rectangular cross sections for strength and axial deformability, while compared to their epoxy-based counterparts, mortar-impregnated textile jackets gave approximately the same effectiveness in terms of strength and slightly inferior for the ultimate strain. San-José et al. [76] investigated experimentally the FRP and TRM strengthening systems on stone masonry walls. The paper presents an international experimental program focused on the study of mortars and stone components for full scale wall elements tested under static loading process. The combination of FRP and TRM strengthening solution with heritage structures attracted the researches interest. For the nine wall structures considered, a TRM based on BFRP textile, embedded in a poor lime mortar, was applied in one and two layers and with BFRP anchorage devices (25 per wall) plus 7 GFRP bars, sewing the two external leafs. The specimens were not tested at the moment the article was written, but the authors considered a vertical in-plane loading process, under static conditions for the elements. Two types of anchor systems for the transmission of stress and deformation from the structure substrate to the reinforcement layer were tested, namely unidirectional glass and basalt fibres used as embedded anchors, and an expansion insulation fastener, entirely made of plastic with a plastic expansion pin was used as mechanical anchor. The anchorage systems were tested with the TRM for the evaluation of bond strength by two experimental approaches, namely pull-off test and shear test, performed on concrete cube specimens. The specimens subjected to pull-out test failed by rupture of the FRP anchors, the fibres of the anchors were severed, while the textile and the adhesive joints was still intact with the concrete substrate. The specimens subjected to shear test failed by fracture of the adhesive joint at different load levels, or rupture of the FRP textiles. The authors consider the FRPs in its different forms a reasonable solution for the

reinforcement of masonry structures, whereas the anchorage solution depends on the substrate material nature, its conservation status, the load history and the aesthetic requirements. The application of a TRM solution was also taken into account having as advantage the fact that it does not increase significantly the original weight and it does not modify the external appearance. Thomas Blanksvärd [77] in his licentiate thesis investigated the strengthening of concrete structures by the use of mineral based composites and presents the experimental tests for flexural strengthening and shear strengthening using CFRP grids and polymer modified mortar as bonding agent. A number of 21 concrete beams with and without shear strengthening subjected to four-point bending were evaluated, having as parameters were the concrete strength, shear reinforcement design, mortar properties, grid design and the addition of flexural strengthening using near surface mounted reinforcement. According to the obtained experimental results of the shear capacity using MBC on beams with no shear reinforcement it was found that strengthening concrete structures with the MBC system, it reached 97% of the ultimate load achieved by a strengthening system with vertically applied epoxy bonded carbon fibre sheets. Good anchorage was provided by the mineral based bonding agent such that fibre rupture in the utilized CFRP grid was achieved. The author concluded that by using a CFRP grid with smaller tow distance generated a higher load for the occurrence of the first inclined crack, whereas the ultimate shear failure load increases if the fibre amount in the CFRP grid is increased. Mineral based bonding agent (mortar) with low modulus of elasticity leads to premature cracking in the MBC strengthening system. Steel reinforced beams with MBC and without NSMR, were found to have a more ductile failure compared to the beams without the MBC system.

Various anchorage systems for strengthening strategies were investigated by researchers. The anchorage systems provide the connection between the strengthening material and substrate, ensure the transmission of stresses and hence improve the performance under different solicitations the element is subjected to. Eshwar et al. [78] investigated the performance of two anchor systems of externally bonded fibre-reinforced polymer laminates. The paper presents two different types of anchors for wet layup systems, namely end anchor and spike anchor. For the evaluation of end anchors a number of sixteen plain concrete T-beams were cast and externally strengthened using CFRP wet layup laminate, whereas for the spike anchors, tests were conducted to determine the shear load, which the spike anchors could resist prior to pull-out or rupture of the laminate. The considered parameters of the study were the location of the anchors, groove size and depth, diameter of FRP bar for the one-end anchor system, and depth of the anchors for the two-spike anchor system. Based on the obtained results, the authors concluded that by providing an adequate end anchorage for the externally bonded CFRP, the performance can be improved considerably. When using an anchor after re-entrant corner, compared to an anchor system before the re-entrant corner, the capacity of the specimens is significantly increased. The minimum groove size should range between 1.5 to 2.5 times the bar anchor diameter, whereas a minimum radius of 13 mm should be maintained at the corners of the groove in order to limit the stress concentration and to prevent the premature peeling. Improved performance of the externally bonded CFRP can be achieved when sufficient anchorage is provided by means of spike anchors. It is suggested for the application of spike anchors into the concrete substrate a minimum of 10 mm diameter with a minimum embedment depth of 50 mm, whereas by using multiple spike anchors significantly increases the ultimate capacity. Zhang et al. [79] studied

on the optimisation of carbon and glass FRP anchor design. The experimental investigation included 27 FRP-to-concrete single shear joint tests in which three joints were unanchored and 24 joints anchored with a single anchor. The parameters of the study were the fibre type (i.e. glass or carbon), anchor fibre content and the method of anchor construction (dry or impregnated anchor). Therefore, a number of three tests series were established, namely control series, glass series and carbon series. The authors concluded upon the obtained results that the addition of a single anchor can increase significantly the strength capacity of the joint above the unanchored control joint. An anchor can also increase the slip capacity of the joint. According to the experimental results, impregnated carbon anchors constructed from 200 mm wide fibre sheets were found to be optimal based on the range of variables considered. It is evident that the load and slip characteristics of an anchored joint can be adjusted by varying the amount of fibre in the anchor and the method of anchor construction. Smith et al [80] investigated FRP-strengthened RC slabs anchored with FRP anchors. In the experimental program, eight simply supported one-way spanning RC slab tests were considered, where a number of two were tested as control slabs. The parameters of the study were the type and positioning of the FRP anchorage. The aim of the study was to study the effectiveness of FRP anchors for the increase of strength and deflection of FRP flexurally strengthened RC slabs. The authors found that the anchorage of the FRP strengthening plate with FRP anchors can build robustness into the member, whereas the positioning of the anchors in the shear span were the most effective. A closer spacing of the anchors reduced the rate of debonding crack propagation and also enabled higher deflections. A far spacing of the anchors led to gains in deflection capacity but limited the gains in strength. A greater fibre content used for anchors that were positioned closer to the peak bending moment region compared to anchors having lesser fibre content but spaced close together near the free ends of the FRP plate produced the greatest enhancement in strength with significant deflection capacity. Khalifa et al. [81] investigated on the anchorage of surface mounted FRP reinforcement. For the purpose of their research, authors developed an innovative anchor system in order to allow for a better exploitation. The developed U-anchor system was found to provide effective behaviour for the cases where the bonded length of FRP composites was not sufficient to develop its full capacity or where anchorage to adjacent members was required. The utilization of U-anchor can be made on FRP sheets and pre-cured laminates that are unbonded or fully bonded to concrete, the anchorage being compatible with the FRP strengthening system and avoiding high stress concentrations and durability concerns. The authors stated that for a beam strengthened with CFRP without U anchor, the shear capacity increased but failure was governed by debonding of the CFRP, but when anchors were used in the specimen, the shear capacity of the member further increased and no FRP debonding was observed at ultimate. Huang and Chen [82] investigated on the bonding and anchoring characterization between FRP sheets, concrete and viscoelastic layers under static and dynamic loading. In order to test the bond strength, five specimens were designed with CFRP sheets and two Sorbothane VE/rubber layers, which were sandwiched between three FRP sheets. For anchorage testing, concrete blocks and an FRP sheet that was anchored though a groove into one side of the concrete block by varying depths were used. The construction of the FRP anchorage was performed by pouring MBrace Saturant resin to fill half of the groove, then an FRP sheet was pushed into the groove with an FRP rod and finally, additional MBrace Saturant resin was poured on top of the FRP rod to fill up the groove. Effective bonding mechanism between VE layers and

FRP sheets with Mbrace saturant epoxy was found. The authors sustain that the strength of the mechanical bond between FRP sheets and VE layers increases under dynamic loading while the strain range at failure decreases. The tested specimens were able to withstand a maximum strain of over 300% before VE layers were torn apart or at the end of each test. The anchorage mechanism of FRP sheets into concrete by a FRP rod was found effective in transferring the damping forces from column through VE layers and FRP anchoring sheets to column footing. The authors also developed a simple design equation based on the shear rupture of concrete along two surfaces between FRP and concrete, which can predict the anchorage strength that agrees very well with experimental results. Ko et al. [83] studied the development of a simplified bond stress–slip model for bonded FRP–concrete interfaces. A number of 18 double-shear bond tests have been conducted to evaluate the bond characteristics of externally bonded FRP reinforcement. New simplified equations for the assessment of existing bond stress–slip relationships were proposed, applicable to the fib Model Code 2013 bi-linear bond stress–slip model for externally bonded FRP reinforcement. Based on the obtained results, the authors concluded that the elements failed mostly due to debonding in the concrete adjacent to the adhesive–concrete interface. The main factors affecting the bond stress–slip model were the concrete compressive strength, FRP stiffness and fracture energy. According to the 11 existing bond stress–slip models analysed, it was found that the models proposed by Lu et al. appeared the most accurate with respect to the 18 experiments conducted. The advantage of the proposed model is its simplicity of expression and that parameters like maximum bond stress, corresponding slip, and maximum slip can be determined by concrete compressive strength. Kotynia R. [84] investigated the bond between FRP and concrete in reinforced concrete beams strengthened with near surface mounted and externally bonded reinforcement. The experimental program comprised fifty single-span, modified simply supported RC beams. One series was strengthened with CFRP strips/sheets externally bonded on the tension surface of the beams and the other one was strengthened with CFRP strips mounted inside the longitudinal grooves made in the concrete cover of the beams. Among the findings of the study the author stated that the increase in the concrete strength delays the CFRP debonding and increases the debonding CFRP strain; the concrete strength does not influence much on the ultimate load of the strengthened beams; the externally strengthened beams with the wet lay-up sheets indicate the greater CFRP bond strain than those strengthened with the prefabricated strips; the location of the CFRP bond length affects its debonding strain; the increase in the composite reinforcement ratio results in the decrease of the CFRP bond strain; the internal steel reinforcement has the crucial effect on the FRP-concrete bond behaviour. The presence of the internal steel bars moves the concrete failure plane from the trapezoidal (in the clear concrete specimens) to almost horizontal, along or slightly below the longitudinal steel reinforcement (in the reinforced concrete elements).

In order to understand the behaviour of different structural elements, there are necessary investigations in terms of experimental testing, but also parametric studies using numerical modeling. Several numerical models have been developed by researchers for the behaviour prediction of elements having various parameters, in order to save time and especially costs. Kazaz et al. [85] performed a benchmark study on the numerical simulation for dynamic shear wall tests. According to the numerical results it was found that the global structural behaviour, such as displacements, forces, and moments can be calculated rather accurately, but interpretation of local behaviour requires more elaborate and refined FE modeling.

The simulation of test conditions such as load application, boundary conditions, member sizes and material properties were the key elements of the considered modeling. The effective experimental measurements predictions using numerical models depends also on the value assigned to shear transfer coefficients for open and closed cracks. Belmouden and Lestuzzi [86] investigated an analytical model for predicting nonlinear reversed cyclic behaviour of reinforced concrete structural walls. The aim of the study was the development of a simplified structural engineering model in order to investigate the inelastic performance predictions of RC structural walls as equivalent frame elements and for seismic vulnerability assessment of reinforced concrete existing frame-wall buildings. The finite element model used was an inelastic one-dimensional finite element for seismic two-dimensional frame analysis, which had two nodes and three degrees of freedom at each node. The finite element presented was based on the force method of structural analysis. The element was decomposed into a multilayer beam element, having two connection fibre hinges used as interface fibre sub-elements at the beam ends. Good agreement was found by the authors between analytical predictions and experimental results, whereas the proposed model proved to be reliable for the inelastic seismic performance prediction of reinforced concrete structural walls and also for code calibration. The model is able to provide optimal structural design solutions in order to have sufficient energy dissipation capacity and resistance to seismic actions, by considering design parameters such as the reinforcement mechanical properties, confinement effects and gravity load. Jalali and Dashti [87] investigated the nonlinear behaviour of reinforced concrete shear walls using macroscopic and microscopic models. The used macroscopic model was found to be capable of simulating the nonlinear behaviour of the tested specimens at different stages of loading to a very good degree of accuracy. The model gives the predicted flexural response directly to uniaxial material behaviour without incorporating any other empirical relations. By comparing the results of the finite element model, using microscopic models with the test results of the specimens, a good prediction for the lateral load versus top displacement response of RC shear walls was found. The finite element model can simulate important aspects of wall behaviour such as the interaction between the shear and flexural response components and the distribution of cracks and stresses, and the mode of failure of the specimens, especially the out-of-plane deformations of the compression column observed in the experimental behaviour of the rectangular wall. However, microscopic model was found to be relatively sensitive to mesh refinement. The authors concluded that considering the CPU time, simplicity, and parametric sensitivity, the observed agreement among three lateral load-displacement diagrams of the experimental measurements, the macroscopic and the microscopic models of tested specimens indicated the efficiency of the investigated macroscopic model in simulating the overall wall lateral load versus top displacement. Bilotta et al. [88] performed an experimental calibration of a capacity model for the FRP-to-concrete interface debonding. The SST test results on 18 sheets and 16 plates were reported and compared by the authors to highlight the main differences derived by the reinforcement type on the debonding load. An experimental database was considered in order to refine the experimental coefficient in the fracture energy calibration which controls the FRP shear strengthening design (end-debonding). It was also analysed the influence on the prediction of the debonding load of the coefficient of variation (CV) related to concrete and FRP. Comparing the experimental results with the theoretical expression provided by CNR-DT200/2004 [89] to compute debonding load showed that the sheets reinforcement debonding

load was underestimated and that related to plates was overestimated, whereas design equations provided by the main international codes (i.e. fib bulletin 14 [90], ACI 440-2R-08 [91] and CNR-DT200/2004 [89]) to predict the effective bond length were found to be in good agreement with the experimental results for sheets and more conservative for plates. The authors joined the results of the 34 original experimental tests to an extensive database developed by selecting experimental tests available in literature so that the results of 139 SST were collected (87 related to sheets and 52 related to plates) and a new calibration of the coefficient kG was performed by means of two methods. Biscaia et al. [92] investigated a nonlinear numerical analysis of the debonding failure process for FRP-to-concrete interfaces. Considering a nonlinear bond–slip law, particularly the Popovics' formula, the used numerical model enables the full definition of the FRP-to-concrete debonding process, i.e., up to the complete debonding of the FRP plate from the concrete surface. After the identification of the debonding process the definition of the effective bond length of the FRP-to-concrete interfaces could be performed, and when the bonded length was shorter than the effective bond length it also enabled a parameter to be defined that affects the maximum load transmitted to the FRP plate. The authors sustain that the used method allows for accurate calculations of some important parameters of the FRP-to-concrete interface, such as the maximum load transmittable to the FRP or effective bond length, the slip distribution. It was suggested that the step used in the numerical method must be small in order to approximate the bond and longitudinal stresses' distribution along the interface to the exact solution. It was also stated that the equations available in literature show a consistent dependency on the FRP stiffness and some include the concrete strength as well. Nguyen et al. [93] performed a pushover experiment and numerical analyses on CFRP-retrofit concrete shear walls with different aspect ratios. The authors investigated the behaviour of lightly RC walls with two different aspect ratios, 2.5 and 0.6 for the slender and short walls, respectively, first without CFRP and secondly with CFRP retrofitting. The objectives of the study were to reproduce the experimental behaviour by considering reliable models of RC walls un-retrofitted and retrofitted by CFRP strips. A number of two numerical approaches were considered, namely a classical smeared fixed crack approach for the concrete material with a regularization technique based on the fracture energy, and a coupled elasto-plastic damage model which was tested using a local approach. Three bars having the equivalent section of the real section of the CFRP strip were used in the model, whereas a perfect bond between the steels and the concrete was assumed as well as between the bars representing the CFRP strips and the concrete. According to the obtained results, the authors concluded that both numerical approaches were successful for reproducing the behaviour of the slender walls, with or without the strengthening by CFRP strips. Good agreement was also found for the pushover curves obtained in terms of load–displacement predicted by both numerical approaches compared to the experimental results. Gebreyohaness et al. [94] performed a finite element modeling for non-ductile RC walls. A three-dimensional numerical model was developed by the authors, in order to undertake a study on the behaviour of non-ductile RC walls when subjected to earthquake induced lateral forces. Good agreement for the peak strengths was obtained between the predicted numerical model and the experimental results. The numerical model was able to capture the initial stiffness, the lateral force resisting capacity and the stiffness and strength degradation properties of the tested specimens. The authors reported that simulations of the specimens under cyclic loading were unsuccessful, as buckling of the longitudinal reinforcement was not accounted for in

the numerical model, as at the time of analyses, methods on how to incorporate the effects of buckling using the FE package employed were not available in the literature. Sas et al. [95] performed a numerical optimization of strengthening disturbed regions of dapped-end beams using NSM and EBR CFRP. The authors studied a parametric investigation, based on non-linear finite element modeling, in order to identify the most effective configuration of CFRP for strengthening reinforced concrete dapped-end beams. A number of 24 externally bonded (EBR) and near surface mounted reinforcement (NSMR) configurations on yield strain in steel and the capacity and failure mode of dapped-end beams were investigated, having as parameters the mechanical properties of the CFRP, the strengthening procedure and the inclination of the fibres with respect to the longitudinal axis. Good agreement was obtained between the numerical modeling and the experimental test data. The modeling applied intended to combine CFRPs with different mechanical properties and shapes but similar alignments to tested specimens. The obtained results showed that mechanically anchoring the CFRP could have increased the beams' capacity compared to the reference one, by up to 36%. Simulation of debonding was investigated by monitoring the strains and the characteristic bond length in the FRP, and it was found that in some cases the debonding load was close to the rupture load of the FRP.

Several assessments were also performed by researchers for RC buildings placed in seismic areas, comprising numerical simulations and recommendations from design codes. Gonzales and López-Almansa [96] investigated the seismic performance of buildings with thin RC bearing walls. Seven existing buildings were selected by the authors to represent the vast majority of the buildings with thin walls in Peru. A numerical seismic assessment of seven existing representative thin shear–wall and mid-height buildings located in Peru was performed in both static and dynamic nonlinear analyses. Based on the obtained results, the authors concluded that the seismic strengths of the analysed buildings were insufficient. Five of the seven analysed buildings exhibit inadequate behaviour, at least in one direction for the immediate occupancy performance level, whereas for the Life Safety (LS) and Collapse Prevention (CP) levels, the numbers of buildings that behave unacceptably were seven and four. Better performances in terms of the ratios between the target drifts and the corresponding damage limit states were found on the strong directions, with highest densities of walls. The damage limit states for immediate occupancy, life safety and collapse prevention were achieved first in the coupling beams, followed by the failure mode corresponding to the flexure of the walls. Tjhin et al. [97] studied on the yield displacement-based seismic design of RC wall buildings. The authors determined the required base shear strength using the yield point spectra based on an "equivalent" single-degree-of-freedom system representation of the wall system. The single base shear force of the walls established based on one or more performance objectives, where each performance level was expressed in terms of roof drift and plastic hinge rotation at the base of the wall. A six-story building with the hazard represented by either smoothed design spectra or recorded ground motions was used in the analysis. The results obtained from the nonlinear dynamic analyses showed that the design method was sufficiently accurate for use in a design environment. Bardakis and Dritsos [98] evaluated assumptions for the seismic assessment of existing buildings, and used the assumptions of the American pre-standard and the European Codes via pushover analyses and experimental results from a four-storeyed building. Performance-based evaluations were made for two levels of seismic action, namely the serviceability earthquake (low-level excitation) and the maximum design

earthquake (high-level excitation). Based on the obtained results, the authors concluded that the assumptions for effective yield point rigidities using FEMA 356 [99] were about three times greater than those of the GRECO [100] procedure for columns and were about five times greater for beams. The assumptions using FEMA 356 [99] were close to the pre-yield characteristics of structural systems and may be rationalised for low-level earthquakes, whereas the predictions of storey drift displacements for such earthquakes appeared to be more consistent with experimental measurements. The FEMA 356 [99] procedure for high-level earthquakes was found to overestimate rigidities and underestimate demand deformations. However, for the investigated building, the GRECO [100] procedure predicted higher deformations compared to the FEMA [99] procedure for high and low levels of excitation. By using the design spectrum of EC 8 [15], the GRECO [100] procedure was found to predict more plastic hinges and greater rotations, whereas the plastic mechanism and the local performance levels would be closer to the FEMA [99] model. Therefore, the GRECO [100] procedure gave better predictions for displacements at high levels of excitation, while the FEMA [99] procedure gave better predictions for displacements at low levels of excitation, when the EC 8 [101] design spectrum was used instead of the test pseudo-acceleration spectrum. Martinelli and Filippou [102] performed a numerical simulation of the shaking table test for a seven-story shear wall building. In the analysis, the shear wall building was subjected to four consecutive table motions with increasing maximum acceleration from 0.15 to 0.93g, representative of low, medium, and high levels of excitation. Good agreement was found between the measured earthquake response of the R/C shear wall specimen and the prediction results, in terms of the time histories of floor displacements and base shear force, and the envelopes of floor displacement, interstory drift, floor acceleration, story shear, and overturning moment over the height of the structure. The maximum strain values obtained from the model were similar to the isolated measurements of steel and concrete strains at the base of the wall. However, the lack of a bond-slip model with pull-out capability did not allow to capture the lap splice failure of the specimen during EQ4. Therefore, it was concluded that the existing software was able to represent the hysteretic response of the complex structural system, but more sophisticated analyses and integrated experimental–analytical studies are necessary in order to develop a better understanding of the complex interplay between the different components of the specimen. Thermou and Pantazopoulou [103] investigated on the assessment indices for the seismic vulnerability of existing RC buildings. The used method is suitable for cases where only estimates of member details are known due to the lack of design drawings, for countries with high seismicity and large inventory of substandard construction, in order to single out potentially dangerous buildings that need further evaluation. In the analysis is estimated first the interstorey drift demand posed by the design earthquake from the structural period. Using its relation to structural stiffness, it was shown to depend on the area ratio of the vertical elements in the critical storey of the structure, and on the number of floors. Then, it was evaluated the potential for premature shear failure (prior to flexural yielding), using information on the arrangement of stirrups in the columns. The interstorey drift capacity was calculated from the drift at yielding scaled down to the ratio of shear strength divided by the flexural yield strength of the critical floor. Comparing the estimated interstorey drift demand and drift capacity, revealed that higher area ratios of the vertical elements in the critical floor lead to reduced drift demands and the design charts shown can be used to guide rehabilitation.

1.6. Precast RC large panel buildings in Romania

The construction period between 1950s and 1970s is characterized by a wide use of large panel structures, but then after followed the decay period until the 1990s, which also marked the end in Romania. The structural system composed of precast reinforced concrete panels is known to be able to provide a good seismic performance of buildings. However, after 50 years of existence and interventions some of the buildings were subjected to, detailed investigation is strongly needed.

The Romanian Project Type 770-81 was chosen in the current research for the analysis of precast reinforced concrete wall panels. The main function of the studied building is multi-family housing. Architectural plans of the chosen building type are represented in Figure 1.1 – front view, Figure 1.2 – lateral view, Figure 1.3 – vertical section, Figure 1.4 – ground floor plan, and Figure 1.5 – execution details (vertical and horizontal). As observed in Figure 1.4, the load-bearing wall panels were laid in two principal directions and were made of B250 concrete – which corresponds to C16/20 class of concrete. Depending on the location within the building, the connection of the panels are vertical or horizontal joints. The vertical joints connect the vertical faces of adjoining wall panels and primarily resist vertical seismic shear forces, whereas the horizontal joints connect the horizontal faces of the adjoining wall and floor panels and resist both gravity and seismic loads. The wet type of joints were constructed with cast-in-place concrete poured between the panels. In order to ensure the structural continuity, protruding reinforcing bars from

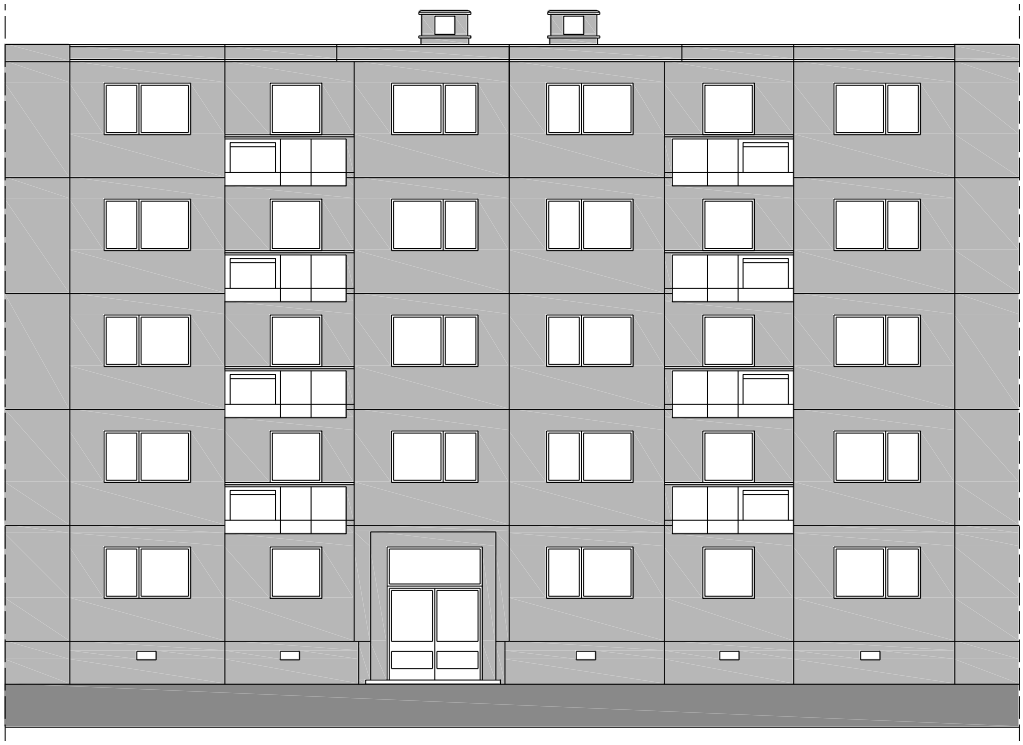

Figure 1.1 – Front view of the building

the panels were welded, looped, or otherwise connected in the joint region before the concrete was placed. The connection of the wall panels was realised by means of splice bars welded to the transverse reinforcement of the adjacent panels.

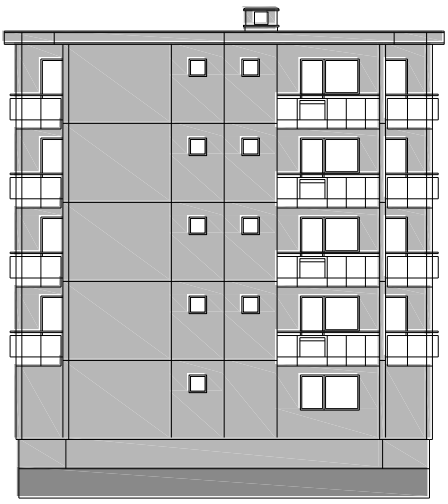

Figure 1.2 – Lateral view

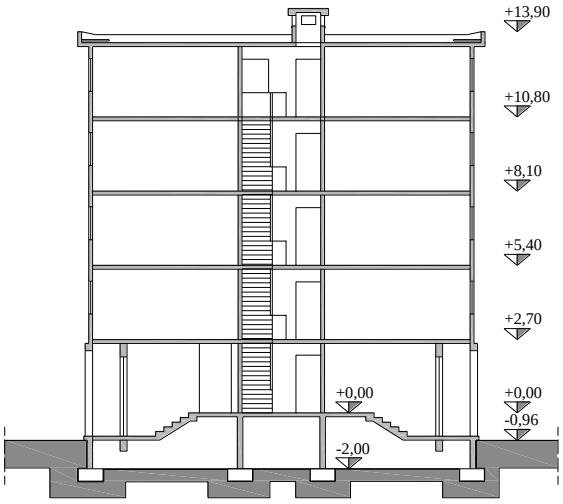

Figure 1.3 – Vertical section

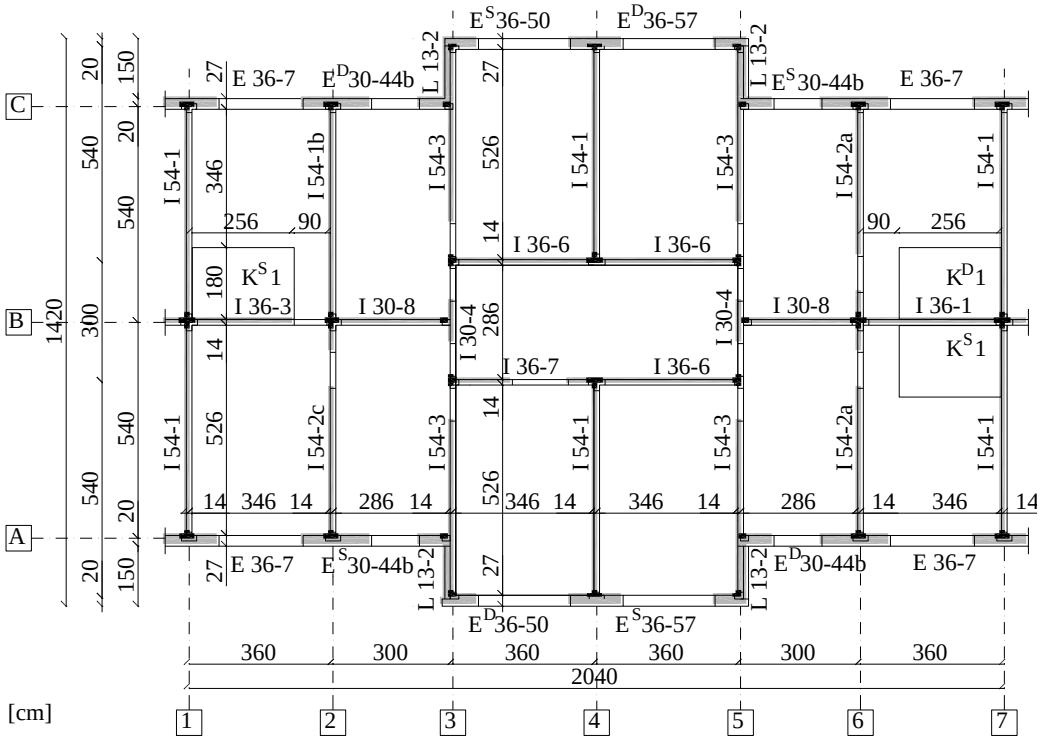

Figure 1.4 – Ground floor plan

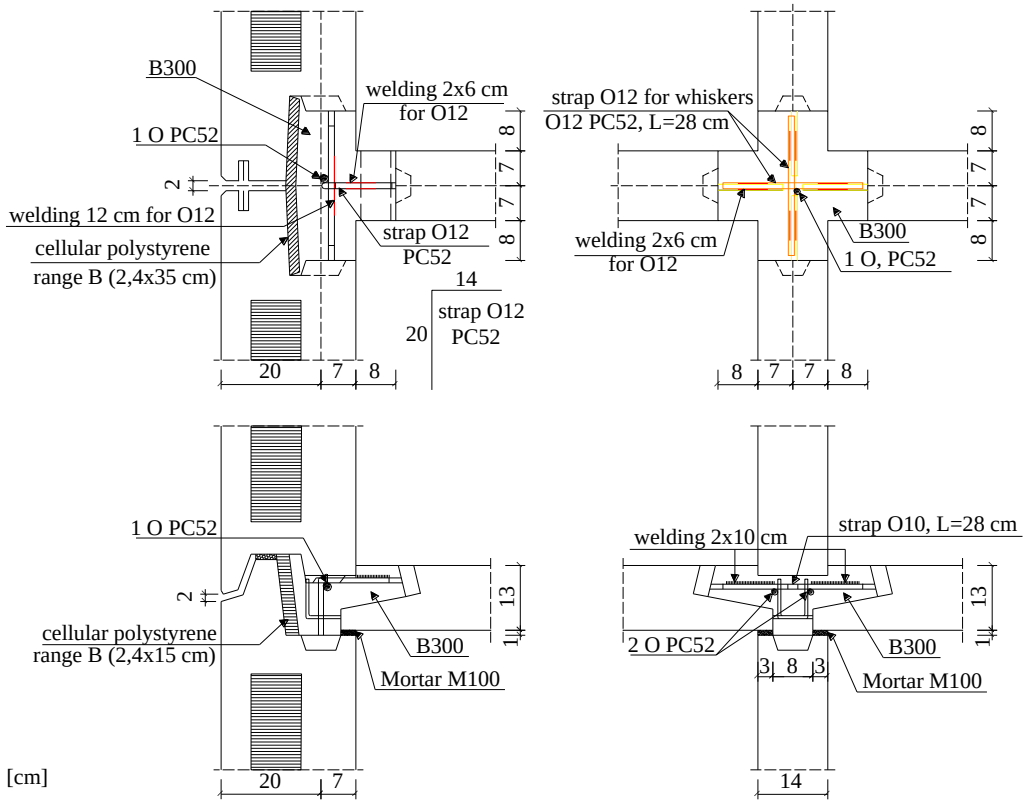

Figure 1.5 – Execution details

The precast reinforced concrete panel buildings were first addressed by the P100-81 code of the country. The prototype wall panels chosen for the experimental program were interior wall panel denoted I54-2a (see Figure 1.6 a) and exterior longitudinal panel denoted E 36-7 (see Figure 1.6 b). Starting from these two prototype wall panels and another one investigated by Demeter [8] (I36-1 – interior wall panel) an experimental program was developed at the Politehnica University Timișoara, Civil Engineering Department.

The experimental program comprises a number of 15 specimens so far, with/without openings or cut-outs. The main research interests are to determine the seismic performance of precast reinforced concrete wall panels, evaluate the effect of openings and cut-outs made in walls, investigate on the reliability of the numerical and analytical analysis, perform structural rehabilitation using FRPs and establish the most convenient strengthening solutions.

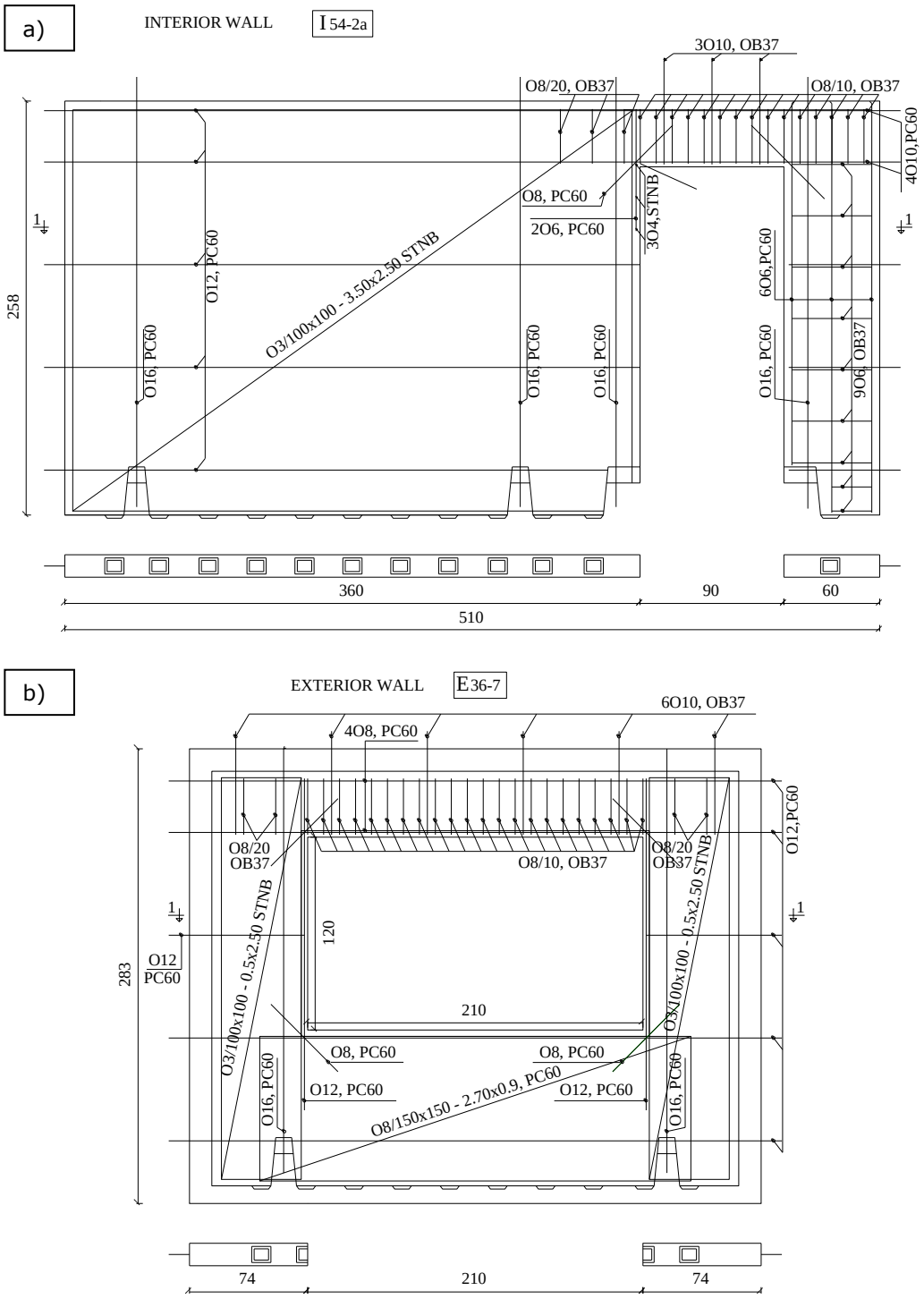

Figure 1.6 – Investigated prototype wall panels

Figure 1.7 – Precast RC buildings in Timișoara

2. EXPERIMENTAL PROGRAM

The main objectives of the experimental research were to investigate the seismic performance of the precast reinforced concrete wall panels, evaluate the weakening induced by cut-outs made in walls and perform rehabilitation and retrofitting strategies using FRP composites. Besides the laboratory part, several analytical and numerical modelings were performed, strengthenings costs were evaluated, and further research needs were highlighted. The overview of the experimental program is presented in Table 2.1. The experimental tests were carried out in the Reinforced Concrete Structures Laboratory of the Civil Engineering Department, Construction Faculty, Politehnica University of Timisoaa, Romania, starting on April, 2012 until April, 2013 (see Fig. 2.1). The tested specimens were fixed to the floor through a foundation beam and were loaded at the top through a loading beam (arrangement type A [8]). The experimental research program presented here continued a previous phase, where six specimens known as PRCWP (1-6) were investigated and presented by Demeter [8]. The specimens tested in the previous phase comprise solid walls with/without narrow/wide door cut-outs, whereas the specimens with cut-outs were repaired and post-damage strengthened with EBR-CFRP or prior-to-damage strengthened with EBR-CFRP.

Table 2.1 - Overview of the experimental program

Program ID	Laboratory	Reinforced Concrete Structures Civil Engineering Department Construction Faculty Politehnica University Timisoara
	Country	Romania
	Year	2012-2013
Specimen	Designation	PRCWP
	Construction type	civil
	Specimen type	wall element
	Concrete technology	precast
	Opening	door; window; door cut-out; window cut-out
	Strengthening	non; EBR-CFRP; NSM-CFRP; TRM
	No. of specimens	6
	Scale	0.83
Boundary conditions	Set-up	A-type
	Loading	quasi-static cyclic
	Boundary condition	restrained rotation

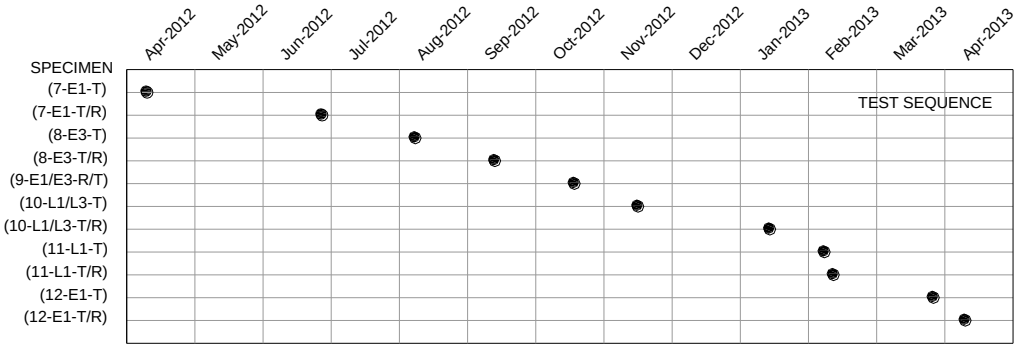

Figure 2.1 – Testing time-line of the specimens

2.1. Experimental specimens and test set-up

The specimens analysed in the experimental program are depicted in Figure 2.2, and the variables of the experimental program are given in Table 2.2. The experimental specimens were designed and casted according to a Romanian Project Type 770-81 [104], [105]. The prototype wall panels chosen for the experimental program were interior wall panel denoted I54-2a and exterior longitudinal panel denoted E 36-7, see Figure 1.6. The dimensions of the prototype walls were 5100 mm length, 2580 mm height and 140 mm thickness (for I54-2a), and 3580 mm length, 2830 mm height and 270 mm thickness (for E 36-7).

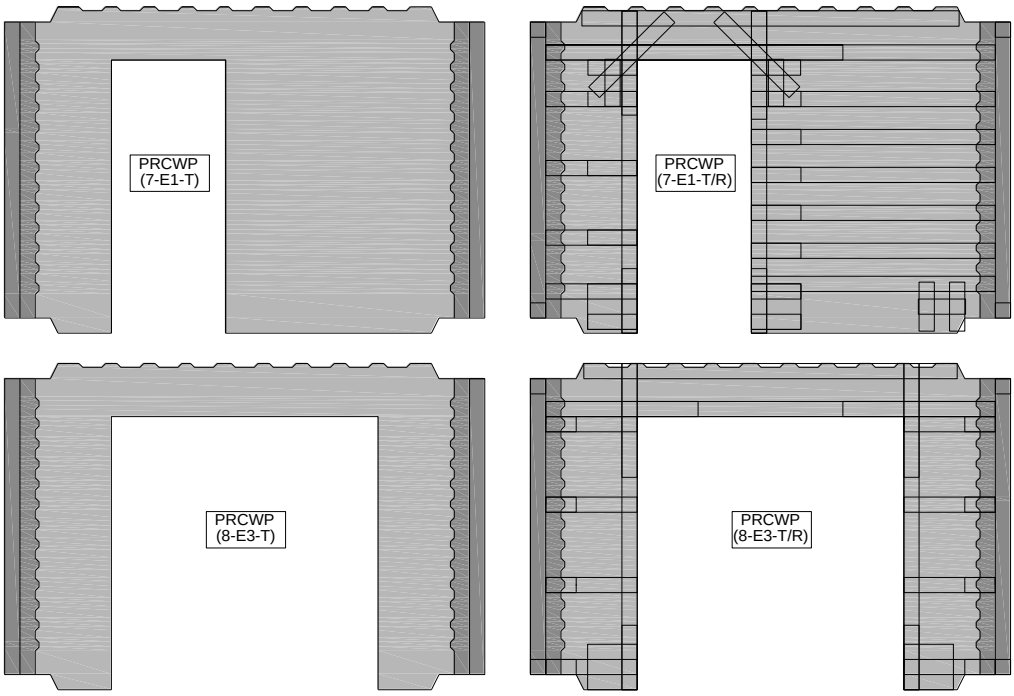

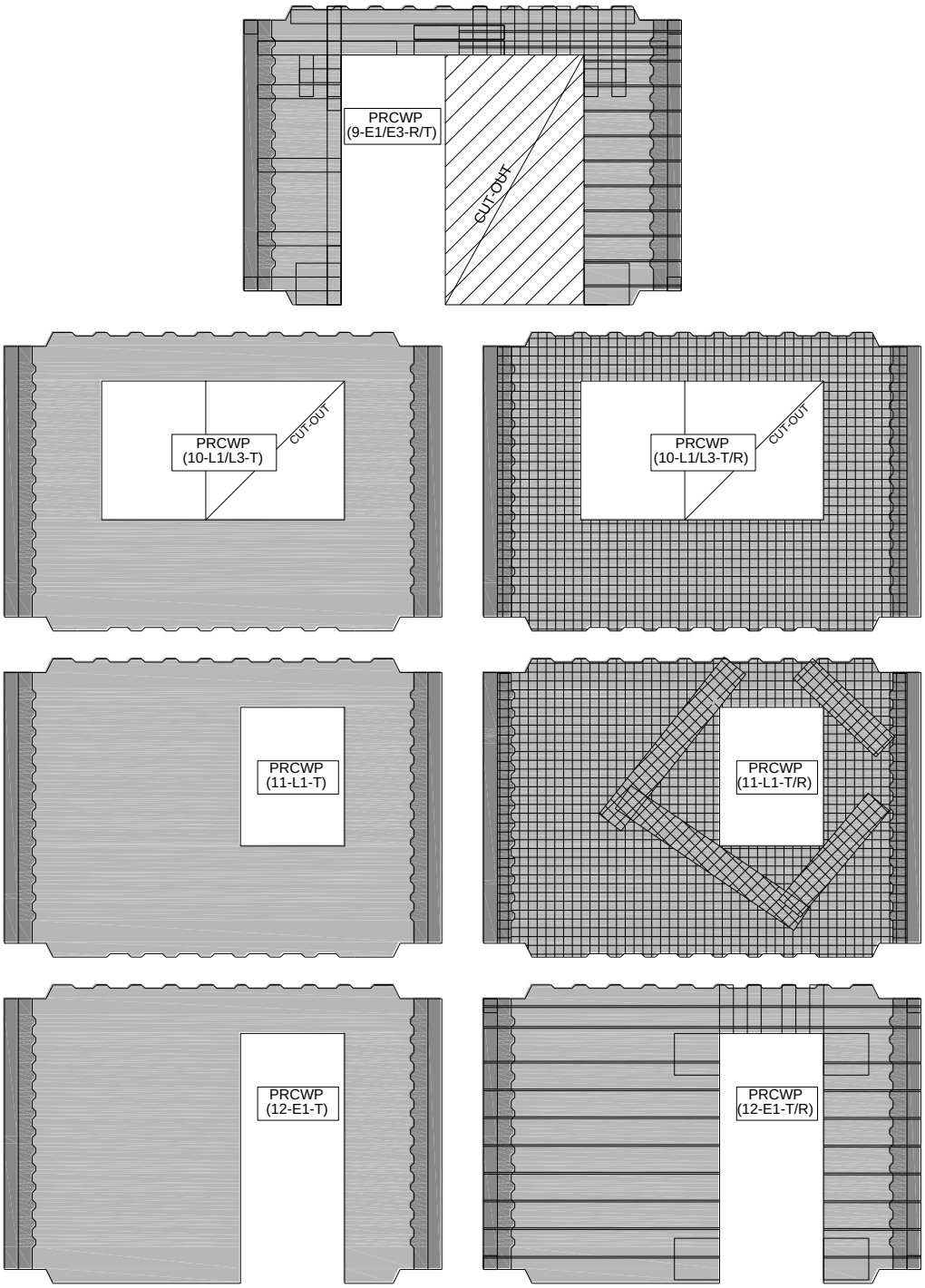

Figure 2.2 – General view of the experimental specimens

Table 2.2 Variables of the experimental program

Element designation	As-built / cut-out opening type	Strengthening condition
PRCWP (7-E1-T)	Narrow door (E1)	Unstrengthened (T)
PRCWP (8-E3-T)	Wide door (E3)	Unstrengthened (T)
PRCWP (10-L1/L3-T)	Small window / wide window (L1/L3)	Unstrengthened (T)
PRCWP (11-L1-T)	Small window (L1)	Unstrengthened (T)
PRCWP (12-E1-T)	Narrow door (E1)	Unstrengthened (T)
PRCWP (7-E1-T/R)	Narrow door (E1)	Post-damage strengthened (T/R)
PRCWP (8-E3-T/R)	Wide door (E3)	Post-damage strengthened (T/R)
PRCWP (9-E1/E3-R/T)	Narrow door / wide door (E1/E3)	Prior-to-damage strengthened (R/T)
PRCWP (10-L1/L3-T/R)	Small window / wide window (L1/L3)	Post-damage strengthened (T/R)
PRCWP (11-L1-T/R)	Small window (L1)	Post-damage strengthened (T/R)
PRCWP (12-E1-T/R)	Narrow door (E1)	Post-damage strengthened (T/R)

The tested specimens were 1:1,2 scaled elements due to the capacity of the testing facility available in the laboratory. All specimens were composed of a web-panel and two boundary elements called wings. The wing elements were considered in order to prevent the out-of-plane displacements during the in-plane lateral loading and also to simulate the vertical connection joints. The specimens were manufactured in Timisoara, on a constructional site, where the timber formwork was assembled and the steel reinforcement bars were shaped, see Figure 2.3.

The concrete was cast in two phases, as reported by Demeter [8], in horizontal position and vibrated in the formwork for the web panel, and after a few days of curing, the timber formwork was removed, the wing reinforcement cages were mounted in the wing formwork and the wings were poured, see Figure 2.4. The completed specimens were stacked at the constructional site and then transported to the laboratory, where they were placed in horizontal position one over the other.

As the experimental program involved testing of the unstrengthened specimens first, and thereafter their repair, strengthening and retesting, the elements were named using specific notations, namely by adding the suffix T/R to elements initially tested prior to failure, thereafter rehabilitated and retested; R/T for the elements strengthened initially on undamaged elements and tested; and the reference elements tested initially have the suffix (T). Therefore, a brief mention of the investigated specimens denotes PRCWP (7-E1-T), (7-E1-T/R), (12-E1-T) and (12-E1-T/R) as specimens with a narrow door opening (E1), PRCWP (8-E3-T) and (8-E3-T/R) as specimens with a large door opening (E3), PRCWP (9-E1/E3-R/T) specimen with an initial narrow door opening that was enlarged to a wide door opening (E1/E3), PRCWP (10-L1/L3-T) and (10-L1/L3-T/R) with an initial narrow window opening that was enlarged to a wide window opening (L1/L3) and PRCWP (11-L1-T) and (11-L1-T/R) specimen having a small window opening (L1).

The concrete outlines and reinforcing details of the tested specimens are presented in Figure 2.5. The web-panel dimensions were 2750 mm length, 2150 mm height and 100 mm thickness. The dimensions of the openings were: 1800 mm height and 750 mm length for the narrow door opening; 1800 mm height and 1750 mm length for the wide door opening; 1000 mm height and 750 mm length for the small window opening; and 1000 mm height and 1750 mm length for the wide window opening. The wing elements were composed of a short in-plane connection zone and a flange perpendicular to the wall plane.

The steel reinforcement details are given in Figure 2.5 and are described and listed for each type of specimen as follows: the specimen having an as-built narrow door opening (E1) - the web-panel reinforcement had horizontal and vertical steel rebars, welded wire mesh in the right pier, a spatial steel reinforcement cage on the entire height of the left pier, spatial steel reinforcement cage in the coupling

Figure 2.3 – Parts of the manufacturing process

Figure 2.4 – Experimental specimens manufacturing on site

beam, vertical continuity steel bars in the coupling beam, a plain steel reinforcement cage at the top right corner of the narrow door opening, and two inclined bars at the top corners of the opening. The specimen having a large door opening (E3) had horizontal and vertical steel rebars, a spatial steel reinforcement cage on the entire height of the left and right piers, a spatial steel reinforcement cage in the coupling beam, vertical continuity bars in the coupling beam, and two inclined bars at the top corners of the opening. The specimen having a small window opening (L1) had horizontal and vertical steel rebars, welded wire mesh in the left and right piers, a spatial steel reinforcement cage in the coupling beam, four

inclined bars at the corners of the window opening, a vertical steel bar each side of the opening on its height, and a wire mesh in the parapet. The specimen having an initial narrow window opening that was enlarged to a wide window opening (L1/L3) has the reinforcement corresponding to the narrow window opening (L1), but reduced according to the wider window opening dimensions, because it is not an as-built opening but a cut-out. The same situation refers also to the specimen having

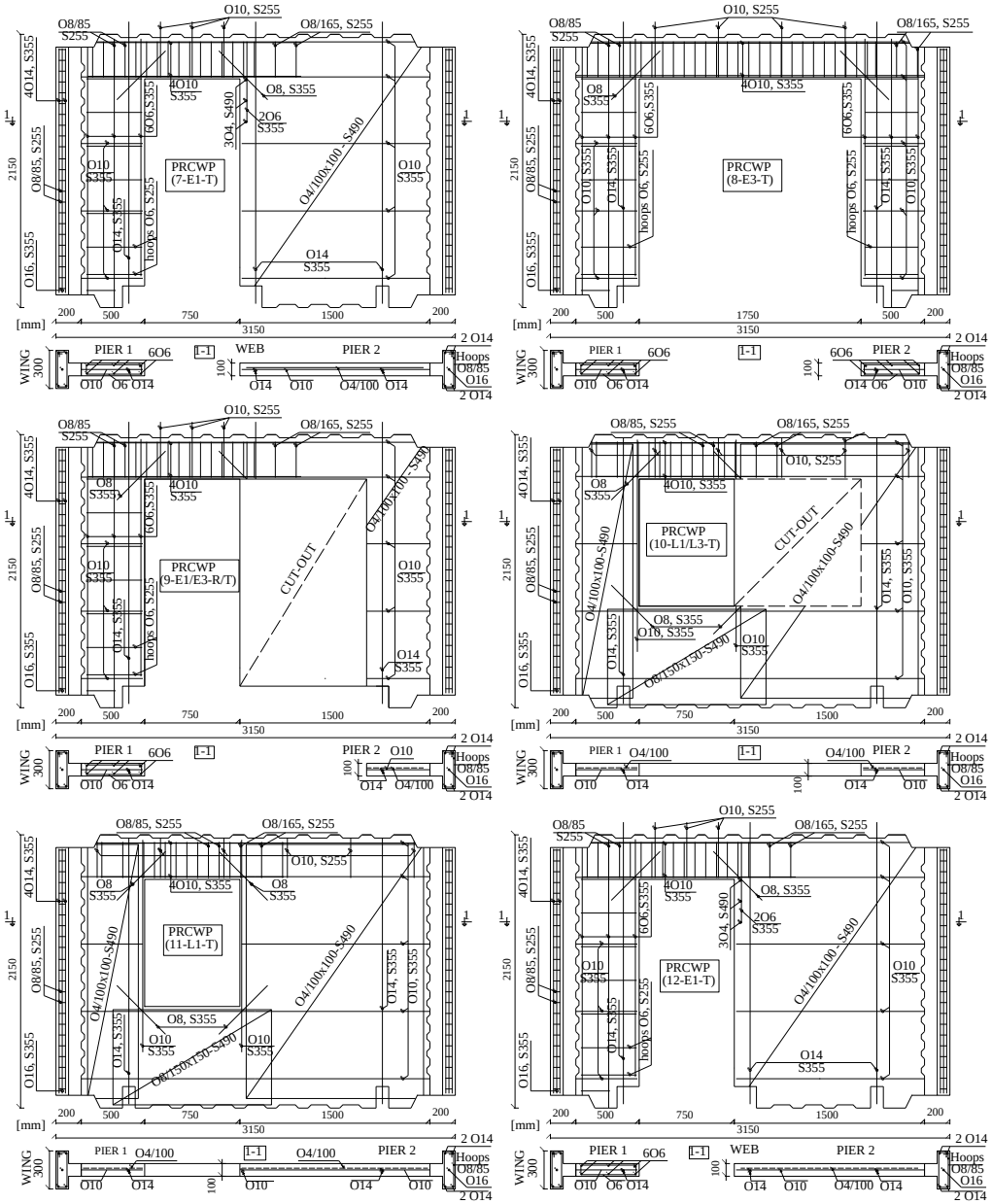

Figure 2.5 – The schematics and reinforcement details of the specimens

an initial narrow door opening that was enlarged to a wide door opening (E1/E3). The two specimens which involved cut-outs were casted with cut-out opening instead of cutting out after the opening enlargement, see Figure 2.5. The designation of the wall panel components, which comprise piers, spandrel and in some cases the parapet, are presented in Figure 2.6.

Flange dimensions were 300 mm width and 100 mm thickness. Following the original large panels, shear keys were considered along the edges of the web-panel and larger set-backs were formed at the corners of the panel in order to improve the sliding shear resistance, see details in Figure 2.7. The flanges of the end-wings were reinforced by steel spatial cages made of vertical steel rebars and plain steel transverse hoops and a vertical continuity steel rebar. The connection between the web panel and the wings was realised by anchoring the horizontal steel rebars into the confined core of the flange.

The anchorage between the wall panel and the foundation beam was realised by lap-welding of the 4 or 5 vertical continuity rebars (depending on the opening type) to the starter bars of the foundation and also to the steel L channels in the span (namely, except the ends of the wing walls) which were fixed to the foundation beam, see Figure 2.8 and Figure 2.9.

Cast-in-place high strength mortar was applied at the regions between the web-panel and the reaction beams.

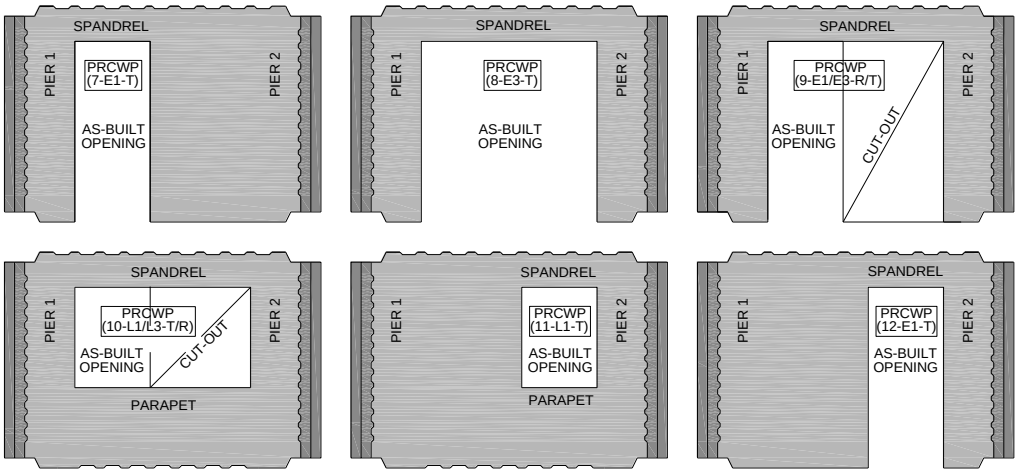

Figure 2.6 – Designation of wall specimen's components

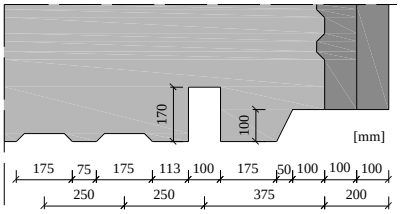

Figure 2.7 – Shear key detail

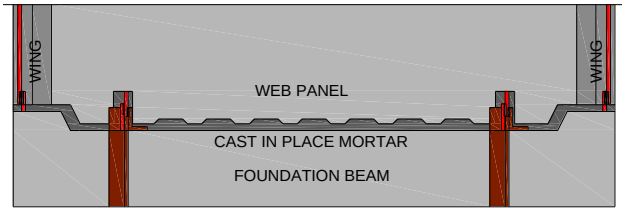

Figure 2.8 – Wall - foundation anchorage detail

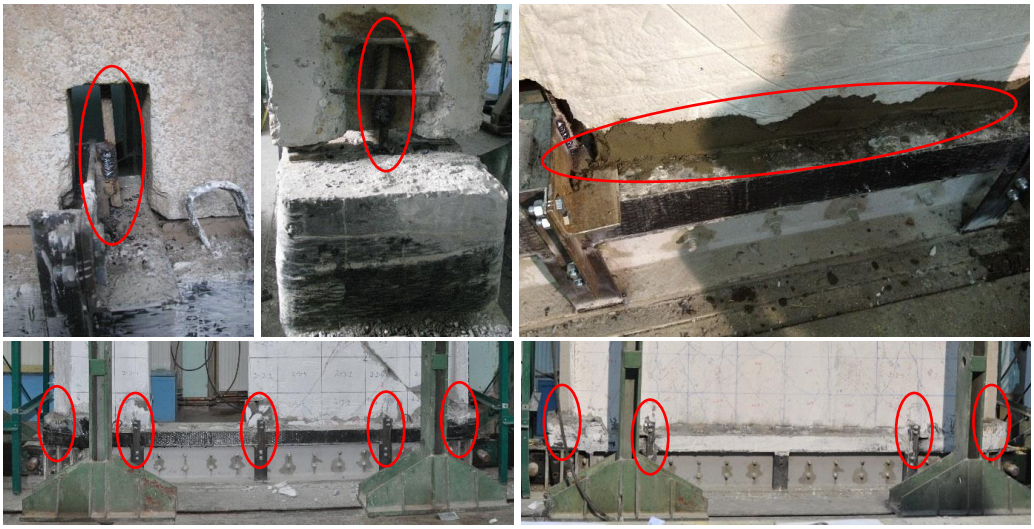

Figure 2.9 – Experimental wall - foundation anchorage

2.2. Material considerations

The structural materials used for the experimental specimens were concrete, steel reinforcement, FRP reinforcement and repair mortar. Material tests were performed on concrete and steel by Demeter [8], while the properties of the FRP composites and the repair mortar were specified by the producer in the product technical data sheet. The compression test results obtained on cube samples are given in Table 2.3. Different concrete classes were obtained for the analysed specimens, and for some elements it differs from the intended class C16/20 of the prototype walls. The author accepted this compromise and turned it into a variation parameter of the experimental program, considering that such differences may occur frequently in the constructional process. Tensile tests were performed on the steel rebars samples, namely, smooth (OB37), ribbed (PC52) hot-rolled bars and cold-drawn ribbed welded fabric (STPB) using the Universal Testing Machine of the Steel Structures Laboratory, Politehnica University of Timisoara. The measured steel reinforcement properties are presented in Table 2.4.

The FRP composites used in the current experimental program were unidirectional carbon fibre fabrics (applied externally bonded) from Sika (Fig. 2.10a) and from Mapei (Fig. 2.10b), carbon fibre plates (near-surface mounted) from Sika (Fig. 2.10c) and from Mapei (Fig. 2.10d), glass fibre grid (in textile reinforced mortar) from Sika (Fig. 2.10e) and carbon fibre grid (also in textile reinforced mortar) from Mapei (Fig. 2.10f). The geometrical and mechanical properties of the CF fabric and CF plates are summarized in Table 2.5, while the properties of the glass fibre and CF grid used are given in Table 2.6. Different types of component mortars were used in the textile reinforced mortar system (mixed with water and mixed with latex), and also two different types of anchorages (punctual type and surface type) for the connection between the wall panel and the TRM strengthening system were investigated and presented in detail in Section 2.5. The presented FRP characteristics are based on the manufacturer's data.

Table 2.3 - Properties of the concrete in the web-panel

Experimental specimen	$f_{cm,cube}$ (N/mm^2)	f_{ck} (N/mm^2)	Class of concrete
PRCWP (7-E1-T)	45,48	30,17	C 30/37
PRCWP (8-E3-T)	17,48	12,28	C 12/15
PRCWP (9-E1/E3-R/T)	44,50	29,58	C 25/30
PRCWP (10-L1/L3-T)	27,26	18,78	C 16/20
PRCWP (11-L1-T)	27,26	18,78	C 16/20
PRCWP (12-E1-T)	44,74	29,73	C 25/30

Table 2.4 – Measured properties of the steel reinforcement

Re-bar type	Production / surface	Φ (mm)	f_y (MPa)	f_t (MPa)	f_t / f_y	E_s (N/mm^2)
OB	hot-rolled / smooth bar	6	400	550	1,38	207
		8	425	507	1,19	205
PC	hot rolled / ribbed bar	8	424	553	1,30	208
		10	450	564	1,25	210
		14	395	584	1,48	206
		16	385	613	1,59	210
STPB	cold-drawn / ribbed wire	4	618	667	1,08	208

Table 2.5 - Geometrical and mechanical properties of the CF fabric and plates [me]

Component	carbon fibre fabric	carbon fibre plate	carbon fibre fabric	carbon fibre plate
Product name	SikaWrap 230C	Sika CarboDur S512	MapeWrap C UNI-AX	Carboplate E170/100/1.4
Thickness [mm]	0,131	1,2	0,166	1,4
Areal weight [g/m^2]	230	96 g/ml	300	225 g/ml
Tensile strength [MPa]	4300	3100	4830	3100
Tensile modulus [GPa]	238	165	230	170
Elongation at break [%]	1,8	1,7	2,0	2,0

Table 2.6 - Geometrical and mechanical properties of the grid used in the TRM system

Component	Areal weight [g/m^2]	Opening size [mm x mm]	Tensile stregth [MPa]	Tensile modulus [GPa]	Elongation at break [%]	Component mortar
SikaWrap 350G grid	280	15.7 x 10.1	3400	73	3,5	Sika MonoTop 722 Mur
Mapegrid C170	170	5 x 5	4800	230	2,0	Planitop HDM

Table 2.7 – Properties of the repair mortar

Component	Compressive strength at 28 days [N/mm^2]	Modulus of elasticity [GPa]	Specific consumption [kg/sqm] for 1cm thickness
Sika MooTop 614	55-60	24	19-20
Mapegrout Easy Flow GF	>60	27	18,5

The repair mortar used to replace the heavily damaged concrete and as tie to cast in place between the wall panel and the beams, was Sika MonoTop 614 for PRCWP (7, 8, 10) and Mapegrout Easy Flow GF for PRCWP (11-12). According to the product technical data sheet, the used mortars had a compressive strength of about 60 N/mm^2 at 28 days (see Table 2.7). Besides the conventional repair type using high strength mortar, in one case the cracks were injected with a fluid epoxy resin using mechanical injection packers and a hand pump.

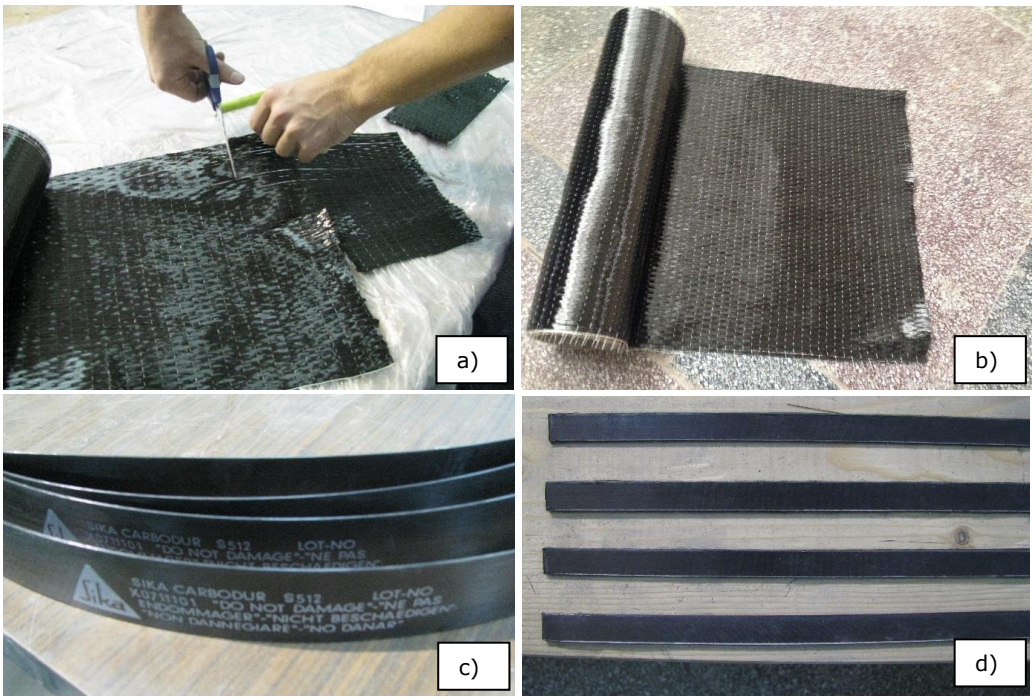

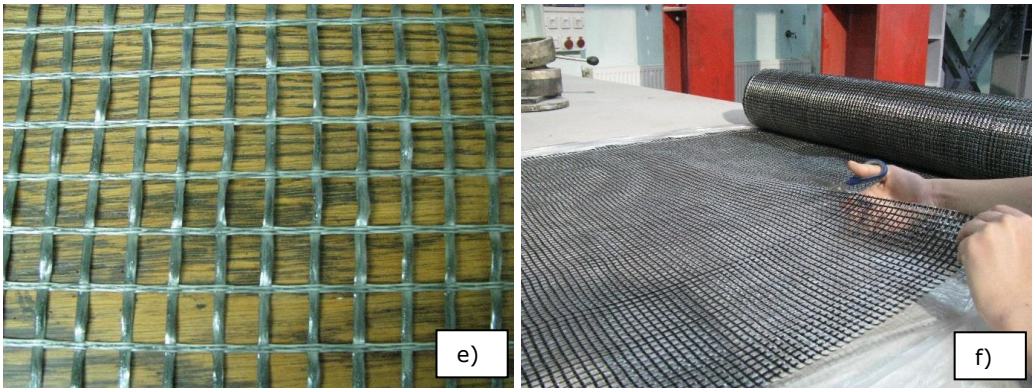

Figure 2.10 – FRP reinforcement used in the experimental program

2.3 Experimental test set-up

As the experimental research program presented here continued a previous phase, investigated and reported by Demeter [8], the same test set-up was used for the current specimens too. The test set-up configuration was composed of the wall specimen which was set between two reaction beams, four vertical steel reaction frames and two lateral steel reaction frames anchored in the floor channels, and the hydraulic loading equipment composed of electric pumps and hand pumps, jacks, cylinders and hoses. A general view of the test set-up is presented in Figure 2.11. The two reaction beams the wall specimen was set between, were reinforced steel concrete composite beams, one serving as a loading beam at the top of the specimen and one as a base beam, serving as the foundation. As the two reaction beams were reused in all the experimental tests performed, this aspect was considered in the design by Demeter, see Figure 2.12 [8], using two U300 steel channels and a reinforced concrete T-beam, connected by ϕ20 mm threaded tie rods. Shear keys were also provided for the beams, as for the web panel horizontal edges and at the beam ends shear steps were formed (see Figure 2.13a and b). The extremities of the base beam were fixed to the lateral steel reaction frames (see Figure 2.13c). For anchorage between the wall specimens and the foundation beam, lap-welding of the 4 or 5 vertical continuity rebars (depending on the opening type) to the starter bars of the foundation was used in the initial experimental program, and in the current one this anchorage was improved by lap-welding of the vertical rebars also to the steel L channels which were fixed to the foundation beam (see Figure 2.13d). Cast-in-place high strength mortar was provided in the space between the wall panel and the reaction beams.

The four hydraulic cylinders (see Figure 2.14) which were used in order to impose the seismic loadings, were placed two horizontal for the lateral loads acting on the ends of the top beam, actuated by a single electric pump (see Figure 2.15a), and two vertical for axial loads, actuated by two hand pumps (see Figure 2.15b). Each loading device had the capacity to generate a nominal 1000 kN force. As seen in Figure 2.11, according to the loading type, ±V notation was used for the horizontal ones and N1 and N2 for the vertical ones (the considered axial, vertical loads were composed of a constant part and an alternating part, and are presented

in detail in Section 2.4.). The presented configuration was maintained the same throughout the entire experimental program for all the investigated wall specimens.

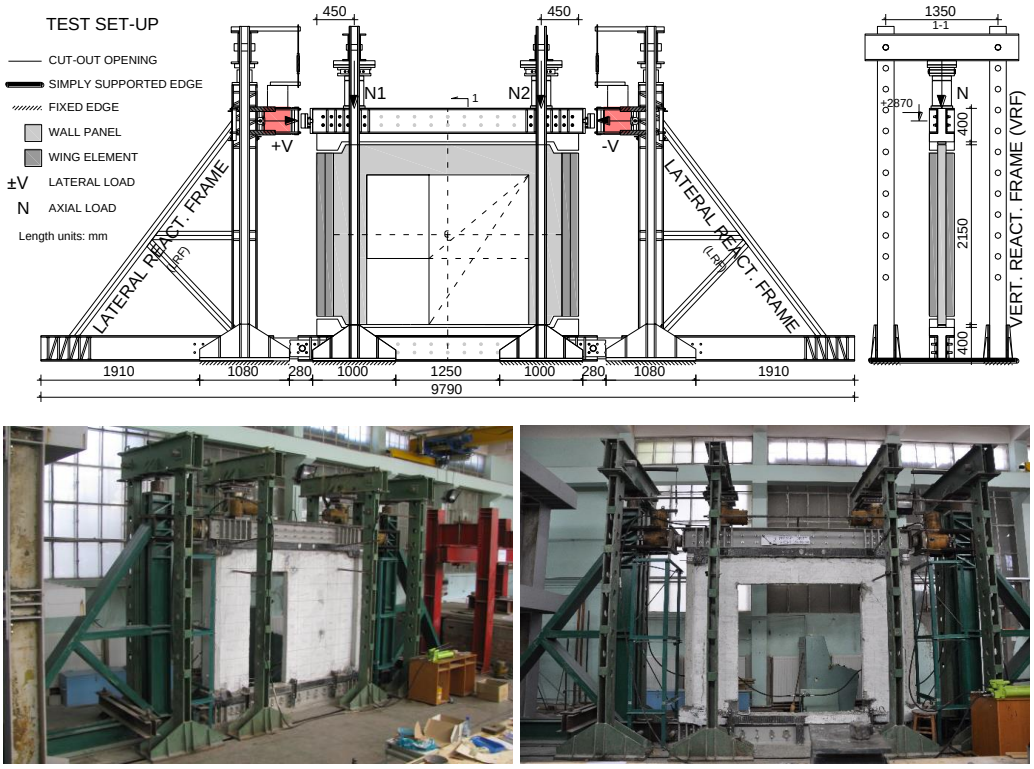

Figure 2.11 – Test set-up configuration

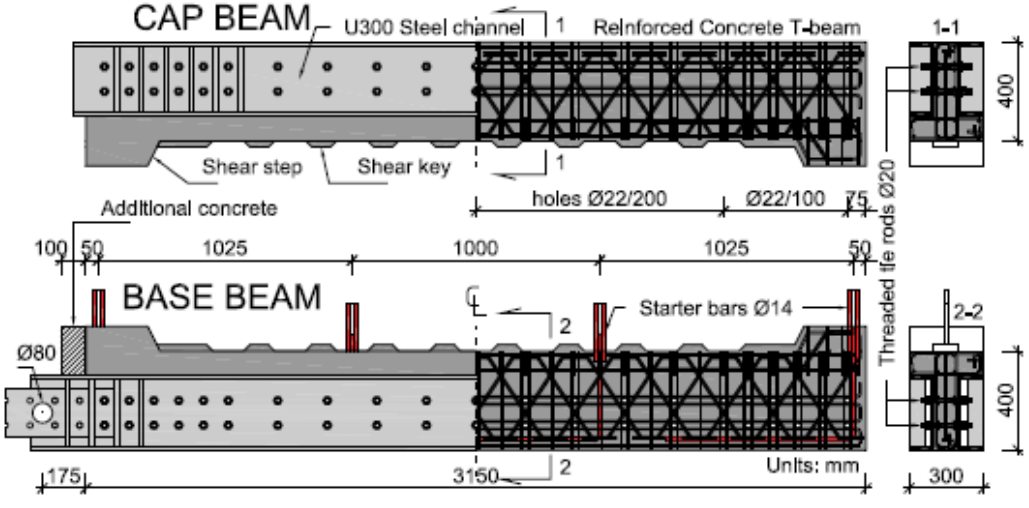

Figure 2.12 – Detail of reaction beams [8]

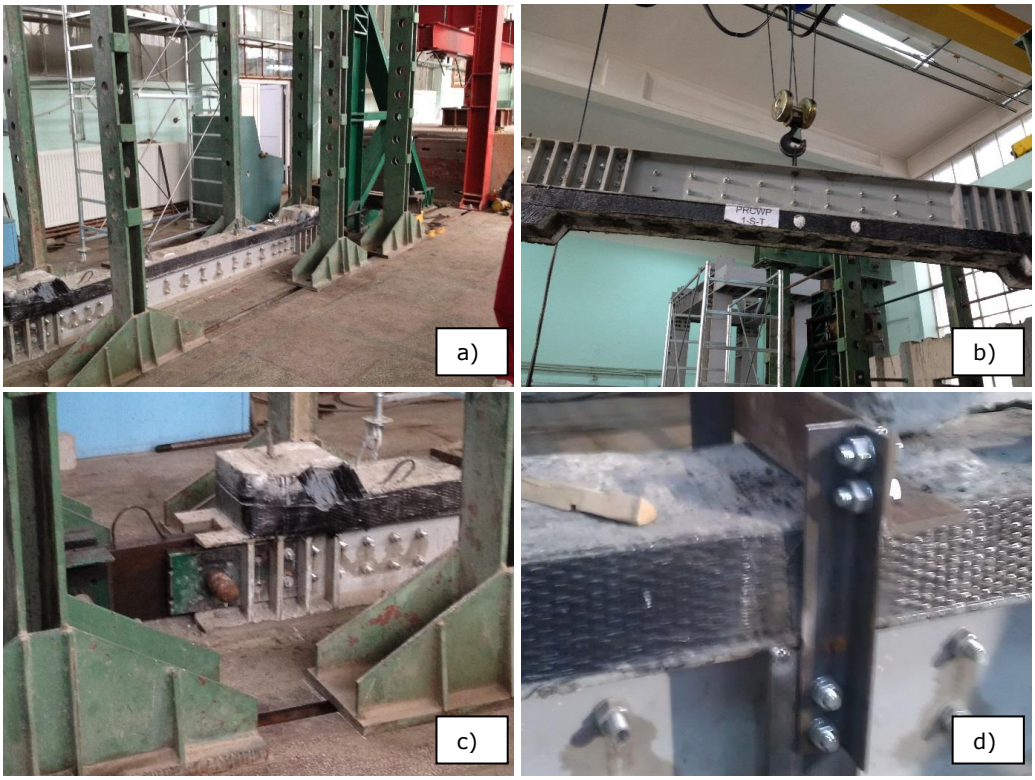

Figure 2.13 – Reaction beams details

Figure 2.14 – Hydraulic cylinders

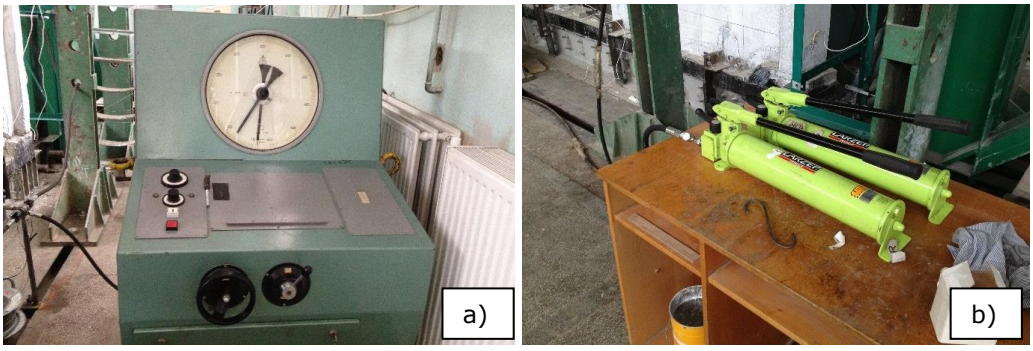

Figure 2.15 – Electric and hand pumps used

2.4 Testing procedure

The testing procedure for the specimens consisted of quasi-static in-plane reversed cyclic horizontal loads and alternating vertical loads. The adopted procedure was used in the previous research program and it is based on a literature survey published by Demeter et al. in [106, 107]. The experimental specimens were laterally loaded, reversed cyclic - displacement controlled using two horizontal hydraulic cylinders acting on the ends of the top beam, to generate the shear forces, and they were also vertically loaded using two horizontal hydraulic cylinders, to generate the axial loads. As the height of the wall specimen was 2150 mm, 21.5 mm corresponds to a 1 % drift ratio. The displacement control was considered a drift ratio of 0.1 %, namely 2.15 mm. Two cycles per drift were performed. During the experimental tests, before the displacement reached 1 mm the specimens were also subjected to one load controlled cycles of 10, 50, 100, 150 kN. No or minor cracks were observed under the force controlled cycles of the specimens, and are presented in detail in Appendix A.

The considered axial loads (see Figure 2.16) were composed of a constant part, which was used to simulate the gravity loading condition at the base of the wall panel, and an alternating part, which was used for restraining the rocking rotation of the specimens. The value of the constant axial load was calculated considering the concrete compressive strength and the compressed area of each wall specimen. Because of the resulted differences in the concrete properties of the experimental specimens, a value of 0.051 for the normalised axial load was adopted. The alternating axial loads were imposed by applying an incremental force of 100 kN each time the wall specimen lifted 1 mm.

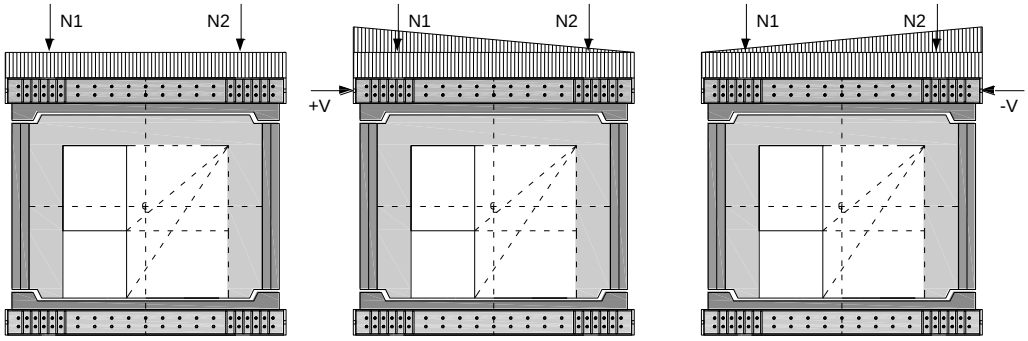

Figure 2.16 – Axial loading procedure

2.5 Boundary conditions

The boundary conditions in the present and previous experimental program consisted in restrained rotation for the wall specimens, imposing the shear behaviour. By applying additional alternating axial loads, the development of the moments was limited.

In the present research program the sliding-dowel failure was avoided by considering the shear keys, the diagonal tension mechanism through the lack of vertical reinforcement anchored to the loading beam and by the variable compression axial loads. Therefore, the only mechanism that was allowed was the diagonal compression shear transfer.

2.6 Instrumentation

The investigated specimens were monitored during the experimental tests by pressure transducers (P), displacement transducers (D) and strain gauges placed onto the steel and FRP reinforcement bars (G) (see Figure 2.17).

The instrumentation of the tested wall specimens is presented in Figure 2.18. The displacement transducer position was the same for all of the elements. The instrumentation layout of the specimens was also presented in [108, 109]. As seen in Figure 2.18, for the strengthened specimens, strain gauges were mounted on externally bonded CFRP fabric, near-surface mounted CFRP plates, and also on carbon fibre and glass fibre grid.

Linear potentiometers (Almemo FWA100TR, FWA025TR and Almemo FA150T) were used to measure the displacements, and during testing they were fixed on independent steel frames or directly on the specimens. The displacement schematics considered four displacement measurements in order to control the loading of the walls (D1, D2, D7, D8), two horizontal displacement measurements (D3, D4), two diagonal measurements between the opposite corners (D9, D10), and two out-of-plane horizontal displacements at each end of the loading beam (D11, D12). A detailed list of the instrumentation for each test is given in Appendix B. Almemo 5990 system was used for the data acquisition, see Figure 2.19.

Electric resistance strain gauges (HBM 1-LY18-6/120 and HBM 1-LY11-1.5/120) were used to measure the unit strains of the internal steel rebars and FRP reinforcements. The strain gauges were applied on vertical, horizontal and inclined reinforcement, in various locations considered critical. A total of 78 strain gauges were used in the present experimental program.

Piezo-resistive transducers were used to measure the pressure in three hoses of the hydraulic cylinders, namely one for the lateral loads and two for the axial loads. The resulted loads were obtained by multiplying the measured pressure with the piston area of the cylinders.

The cracking pattern on the front face of the wall at each cycle peak was observed and marked. An orthogonal reference grid was drawn on the wall face, which divided the web-panel area in 64 rectangles (see Figure 2.20). After each test the rectangles were photographed and a photo-map was assembled in order to obtain the final cracking pattern. Detailed data related to the observation grid are indicated in Section 3.10 and Appendix A.

Figure 2.17 – Monitoring system

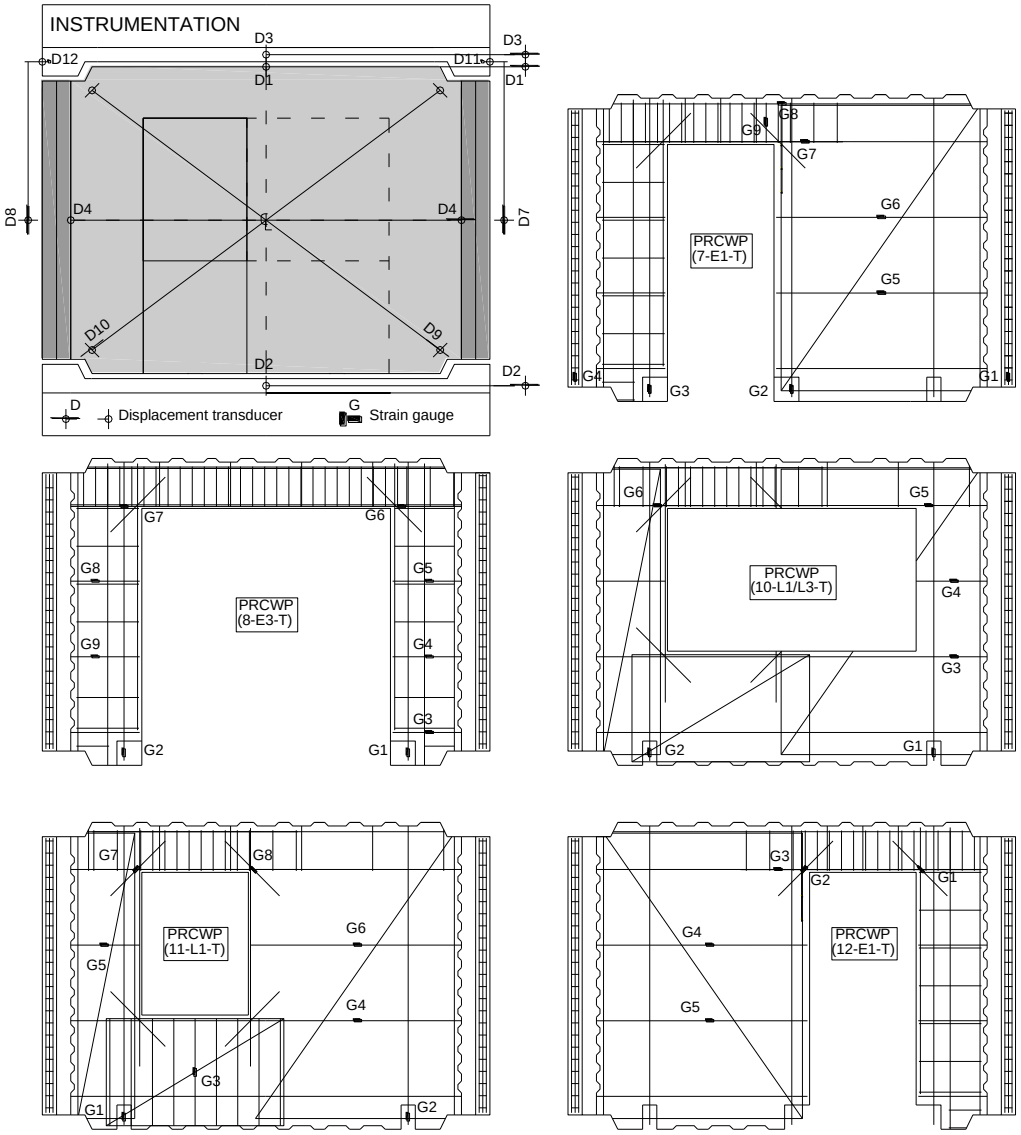

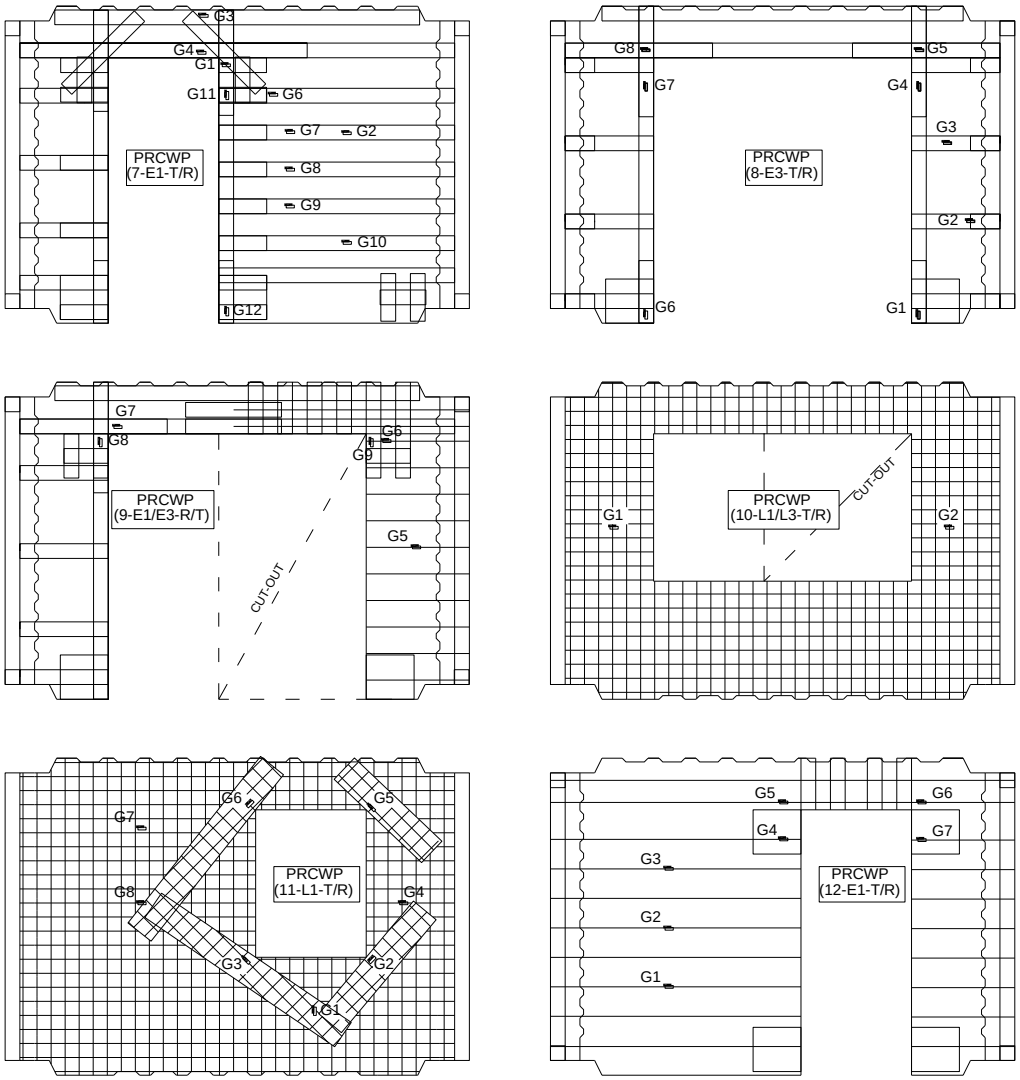

Figure 2.18 – Instrumentation layout of the tested specimens

Figure 2.19 – Data acquisition system used

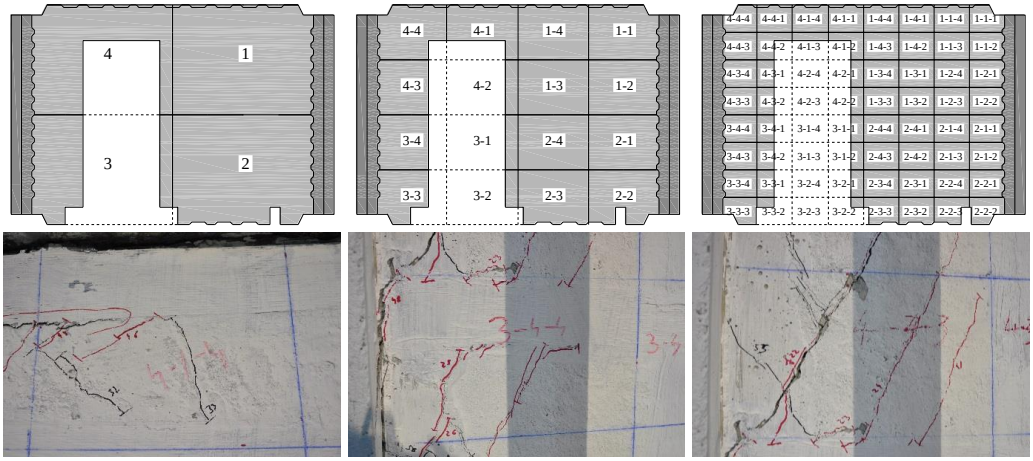

Figure 2.20 – Observation grid details

2.7 Behaviour of the reference specimens

General behavioural aspects that were observed in the case of the unstrengthened, reference specimens during the experimental tests consist in a significant number of cracks which appeared in all the regions of the panel, concrete crushing and reinforcement yielding and reinforcement tearing in one case. Detailed data related to the failure mode of each specimen is presented below. Reinforcement yielding aspects are given in Section 3.5 and the behaviour at each cycle peak is presented in Appendix A.

PRCWP (7-E1-T) specimen developed cracks in the spandrel, piers, wing, spandrel – pier connection regions, bottom extremities of the piers (near the opening) and cast-in-place mortar. The first inclined crack appeared in the right pier at 0.5 % drift ratio (10.75 mm), first cycle, and loaded from the left. Concrete crushing was observed at the bottom right corner of the wall panel, the spandrel – right pier connection region and the cast-in-place mortar at the bottom right corner of the opening. Among steel reinforcement failure aspects it was observed a dowel

effect for the vertical steel rebars of the welded wire mesh along the inclined crack in the right pier, and tearing of the horizontal steel rebars of the welded wire mesh along the inclined crack in the right pier at 0.8 % drift ratio (17.2 mm). The formation of a necking phenomenon in some horizontal steel reinforcing bars was also observed. All of these failure aspects led to a sudden failure of the specimen under an uncontrolled reduction in the load bearing capacity of 74%. The presented failure aspects resulted in a sudden failure for the PRCWP (7-E1-T) specimen (see Figure 2.21).

PRCWP (8-E3-T) specimen exhibited cracks in the spandrel, piers, wings, spandrel – pier connection regions, bottom extremities of the piers (near the opening), bottom right corner region of the panel, and cast-in-place mortar. The first inclined crack was observed in the right pier and it appeared at 0.5 % drift ratio (10.75 mm), first cycle, and loaded from the right. Sliding shear was observed in the left pier through a horizontal crack, and a vertical crack between the web panel and the wing appeared in the right pier. Concrete crushing took place at the spandrel – pier connection regions (near the opening) and in the cast-in-place mortar. Related to steel reinforcement failure aspects, the vertical rebars of the steel spatial reinforcement cage in the right pier was observed to be bent (see Figure 2.22).

PRCWP (10-L1/L3-T) specimen also developed cracks in the spandrel, piers, wings, spandrel – pier connection regions, parapet – pier connection regions, bottom right corner region of the panel, cast-in-place mortar and most of the parapet. The first inclined crack was observed in the left pier at 0.2 % drift ratio (4.3 mm), first cycle and loaded from the right; while in the right pier the first inclined crack appeared at 0.3 % drift ratio (6.45 mm), first cycle, and loaded from the right. Concrete crushing was observed in the spandrel-left pier connection region and parapet – left pier connection region (see Figure 2.23).

PRCWP (11-L1-T) exhibited cracks in the spandrel, piers, parapet, wings, spandrel – pier connection region (near the opening), parapet – pier connection regions and cast-in-place mortar. The first inclined crack was observed in the right pier at 0.3 % drift ratio (6.45 mm), first cycle, and loaded from the right. Concrete crushing took place at the parapet – left pier connection region, parapet and in the right wing (see Figure 2.24).

PRCWP (12-E1-T) developed cracks in the spandrel, piers, wings, spandrel – pier connection region (near the opening), bottom extremities of the piers (near the opening) and cast-in-place mortar. The first inclined crack appeared in the right pier at 0.2 % drift ratio (4.3 mm), first cycle, and loaded from the left. Concrete crushing was observed in the spandrel – right pier connection region and the cast-in-place mortar at the bottom extremities of the wall piers, near the opening (see Figure 2.25).

Failure details of the tested unstrengthened specimens were also partly discussed and presented in [108-116], whereas for the strengthened specimens are presented in Section 3.1.

Figure 2.21 – PRCWP (7-E1-T) failure details [108-110, 112, 115]

Figure 2.22 – PRCWP (8-E3-T) failure details [108-109, 112, 115]

Figure 2.23 – PRCWP (10-L1/L3-T) failure details [108-109, 111-112, 116]

Figure 2.24 – PRCWP (11-L1-T) failure details [108-109, 113-114, 116]

Figure 2.25 – PRCWP (12-E1-T) failure details [108-109]

2.8 Repair and strengthening of the specimens

After the experimental testing of the unstrengthened specimens, the repair process started by removing the crushed concrete and replacing it with non-shrink, high-strength repair mortar, while the observed cracks were cleaned and filled superficially with epoxy resin. In the case of one specimen only, namely for PRCWP (11-L1-T/R) the cracks were injected with a fluid epoxy resin. When the repair process ended, the surface of the wall was prepared for the corresponding strengthening strategy used in each case. The strengthening systems used in the present experimental program included Carbon Fiber Reinforced Polymers (CFRP) and Glass Fibre Reinforced Polymers (GFRP) using various application techniques like Externally Bonded Reinforcement (EBR), Near Surface Mounted Reinforcement (NSM) and Textile Reinforced Mortar (TRM). The main objectives of the strengthening were to re-establish or increase the seismic performance of the damaged wall panels or affected by cut-out interventions.

The adopted strengthening strategies presented herein were based on the behaviour and failure mode of the reference, unstrengthened specimens, focused mostly on the critical regions. The identified failure modes for the reference specimens were flexural cracking at the pier – spandrel connection joint, shear cracking of the piers, concrete crushing at the spandrel - pier connection joint and at the bottom extremities of the piers. Therefore, the main considered aspects in the strengthening strategy were to increase the flexural capacity along the vertical and horizontal edges of the opening or cut-out opening, to enhance the shear capacity of the piers, and to provide confinement effect at the opening corners and at the ends of the wing walls. In the following subsections, the repair and strengthening process for each specimen is presented in detail. The considered strengthening strategies of the specimens were also partly discussed and presented in [108-120]. The material properties were given in Section 2.2.

2.8.1 Rehabilitation of PRCWP (7-E1-T/R) specimen using EBR-CFRP

The damaged specimen was repaired before the rehabilitation process, by replacing the crushed concrete with high-strength repair mortar. Using a special grinder, the surface of the wall was polished in order to achieve a fully smooth surface for the application of CF strips, and the concrete edges of the specimen were rounded at a radius of about 20 mm for the effectiveness of the confining solution. Local ϕ10 mm holes were drilled in the wall panel for the FRP anchorage of the strengthening system, and then the surface of the wall was vacuum cleaned.

In order to re-establish the seismic performance of the tested specimen, a design strengthening strategy was performed, based on EBR-CFRP (see Figure 2.26). For this, SikaWrap 230C unidirectional carbon fibre sheets of 100 mm width were applied symmetrically on both faces of the wall. The sheets were designated as flexural (f), shear (sh) and confinement (c) sheets, according to the strengthening objectives. In the application process, the CFRP sheets were placed parallel to the tension forces for flexural strengthening, parallel to the shear forces for shear strengthening and perpendicular to the compression forces for confinement.

The flexural strengthening of the panel comprised vertical CF sheets, placed along the opening (f3) and horizontally along the spandrel (f1, f2). Additional shorter sheets were applied inclined at the top corners of the opening (f7),

horizontally (f4) and vertically (f5) in the spandrel region. Short CFRP tows were used to anchor the bottom vertical sheets (f3, f6) to the foundation beam. Horizontal CF sheets (sh1, sh2) were applied on both piers, anchored at their ends by overlapping sheets on the door opening side (sh3) and by short CFRP tows at the wing-side end. Confinement was provided by CF sheets at the corners of the opening, namely the pier – spandrel connection region and bottom extremities of the piers on the opening side (c1, c2, c4), in the right pier (c3, c4) and at the ends of the wing walls (c5). The strengthening application details are given in Fig. 2.27. According to the adopted design philosophy, a more ductile behaviour for the rehabilitated specimen is expected instead of the brittle failure of the reference element.

Detailed data related to the repair and strengthening material consumption and cost evaluation for all the specimens are given in Appendix C.

2.8.2 Rehabilitation of PRCWP (8-E3-T/R) using EBR-CFRP

Following the idea in the previous rehabilitation strategy, similar design was performed for the specimen with as-built wide door opening (see Figure 2.28). Unidirectional carbon fibre sheets (SikaWrap 230C) were applied vertical along the door opening (f3) and horizontally along the spandrel (f1, f6). Additional shorter sheets were applied horizontally (f2) and vertically (f4) in the spandrel region. Short CFRP tows were used to anchor the bottom vertical sheets (f3, f5) to the foundation beam. Horizontal CF sheets (sh1) were applied on both piers, wrapping from one face to the other, anchored by short CFRP tows at the wing-side end. Confinement was provided by CF sheets at the bottom corners of the opening, namely the bottom extremities of the piers on the opening side (c1), and at the ends of the wing walls (c2). Considering the vertical crack that appeared between the right pier and the wing during the experimental test of the unstrengthened specimen, c3 confinement was provided. C3 sheet was used to tie back the connection between the web panel and the wing, wrapping from one face of the pier, through the wing, to the other face of the pier. The strengthening details are given in Figure 2.29.

2.8.3 Strengthening of PRCWP (9-E1/E3-T/R) using EBR-CFRP combined with NSM-CFRP

The experimental specimen simulating a door opening enlargement was the only case not tested initially unstrengthened. Therefore, the specimen was first strengthened and thereafter tested, as it was assumed to be weakened due to the cut-out intervention. Taking into account the reinforcement of the specimen having a narrow door opening (E1), in which the left pier was provided besides horizontal and vertical bars with a spatial steel reinforcement cage on the entire height, while the right pier was provided with a welded wire mesh besides the horizontal and vertical steel rebars, the NSM-CFRP (Sika CarboDur S512) was applied in the right pier, whereas the EBR-CFRP (SikaWrap 230C) in the left pier (see Figure 2.30). According to the strengthening strategy, unidirectional CF sheets were applied vertically along the left side of the opening (f3) and horizontally in the spandrel (f1, f2). Additional shorter sheets were applied horizontally (f6) and vertically (f4) in the spandrel region. The bottom vertical sheets (f3, f5) were anchored to the foundation beam by short CFRP tows. Horizontal CF sheets (sh1) were wrapped on the left pier, from one face to the other, anchored at the wing-side end by CFRP tows.

Confinement was provided at the corners of the opening (c1, Hst, Hdr) and at the ends of the wing walls (c2). The NSM-CFRP plates (12 mm x 1.2 mm) were applied horizontally along the entire height of the right pier at 180 mm centres, whereas the last two from the top were extended until the middle of the spandrel. All CFRP plates were anchored in the wing element using epoxy resin (see Fig. 2.31).

Due to the fact that the double disc grinder (Figure 2.32) used to cut the channels for the near-surface mounted reinforcement application had the thickness of 3 mm for one disc, it was not possible to obtain a smaller thickness than 6 mm for the groove. Additional horizontal strips (f7) were provided to assure the left anchorage of the top CFRP plates. Additionally, vertical strips were wrapped from one face of the spandrel to the other (hoops), taking into account the lack of the spatial steel reinforcement cage in the spandrel region corresponding to the cut-out. The strengthening details are given in Figure 2.33.

2.8.4 Rehabilitation of PRCWP (10-L1/L3-T/R) using TRM

After repairing the damaged specimen by replacing the crushed concrete with high-strength mortar, the surface of the wall was polished and the concrete edges of the specimen were rounded at a radius of about 20 mm. Local holes were drilled in the wall panel for the mechanical anchorage system, and then the surface of the wall was vacuum cleaned.

The mechanical anchorage system was composed of threaded rods (6 cm length) which were fixed in the wall using resin in order to ensure the connection between the precast panel and the TRM system. The mechanical anchorage was a punctual type, being composed besides threaded rods, of nuts and washers. The TRM system used a glass fibre grid. Patching mortar Sika Monotop 910 N was applied on the surface of the wall to provide a bonding bridge for the concrete. The first layer of mortar (Sika Monotop 722 Mur) was then applied on the surface of the wall, followed by the glass fibre grid (SikaWrap 350G) which was fixed with a nut and washer and then the second layer of mortar was applied (see Figure 2.34). The strengthening system was applied symmetrically, on both faces of the wall (see Figure 2.35).

According to the design strategy, the grid pieces marked 4 on figure were first applied on each side of the parapet, followed by the number 5 grid pieces, which were also wrapped around the parapet. The grid pieces number 2 were applied on each side of the piers, followed by the number 3 grid pieces wrapping the piers on the opening side. Then, the grid piece marked 1 was wrapped around the coupling beam. The strengthening details are given in Figure 2.36.

2.8.5 Strengthening of PRCWP (11-L1-T/R) using TRM

The damaged specimen was repaired by replacing the crushed concrete with high-strength mortar, the surface of the wall was polished and the concrete edges of the specimen were rounded at a radius of about 20 mm. Local holes were drilled in the wall panel for the surface anchorage system, and then the surface of the wall was vacuum cleaned. Another set of holes were drilled in the panel for the mechanical packers fixing. Only for this specimen, the cracks were injected with a very fluid resin (Epojet) using a hand pump.

Considering inefficient the previous used punctual anchorage, a surface type of anchorage was selected this time by using a high-strength steel fibre cord

(MapeWrap S Fiocco). The steel fibre cord, cut in 25 cm and 35 cm in length pieces, was impregnated with resin a day before fixing in the wall, using epoxy resin.
No bonding bridge was neccessary for the TRM system usd in this case, as the component mortar (Planitop HDM) was a two-component material, a high-strength, cement based mortar blended with latex. The first layer of the component mortar was then applied on the wall, followed by the fresh impregnated CF grid (Mapegrid C170) and the second layer of mortar. The strengthening procedure was applied symmetrically on both faces of the wall (see Figure 2.37). Figure 2.38 shows the strengthening layout for the specimen and the order of grid application, namely the grid pieces marked 4 were applied on each side of the parapet, followed by the number 9 pieces which were wrapped around the parapet. The number 2 and 2" pieces were fixed on each side of the pier, followed by the number 3 grid piece, wrapped around the right pier on the opening side. The number 1 grid piece was wrapped around the copuling beam, whereas the number 5, 8, 6, and 7 pieces were fixed inclined in the corners of the opening. Finally, the steel surface anchorage ends were unfolded, and a washer with a concrete nail was fixed in the resin to realize the surface anchorage. The strengthening details are given in Figure 2.39.

2.8.6 Strengthening of PRCWP (12-E1-T/R) using NSM-CFRP combined with EBR-CFRP

After the damaged specimen was repaired by replacing the crushed concrete with high-strength mortar, the surface of the wall was polished locally and the concrete edges of the specimen were rounded locally at a radius of about 20 mm. Holes were drilled in the wall panel for the FRP anchorage system, and then the surface of the wall was vacuum cleaned. In the strengthening process, NSM-CFRP plates (Carboplate E170/100/1.4) of 10 mm x 1.4 mm were fixed horizontally in the piers and in the spandrel on each side of the wall, at 200 mm centres, using epoxy resin (see Figure 2.40). All CFRP plates were anchored in the wing element. CFRP confinement strips (MapeWrap C UNI-Ax) were applied in the corners of the opening and vertical, wrapping from one face to the other of the spandrel, and at the ends of the wing walls (see Figure 2.41). The strengthening details are given in Figure 2.42.

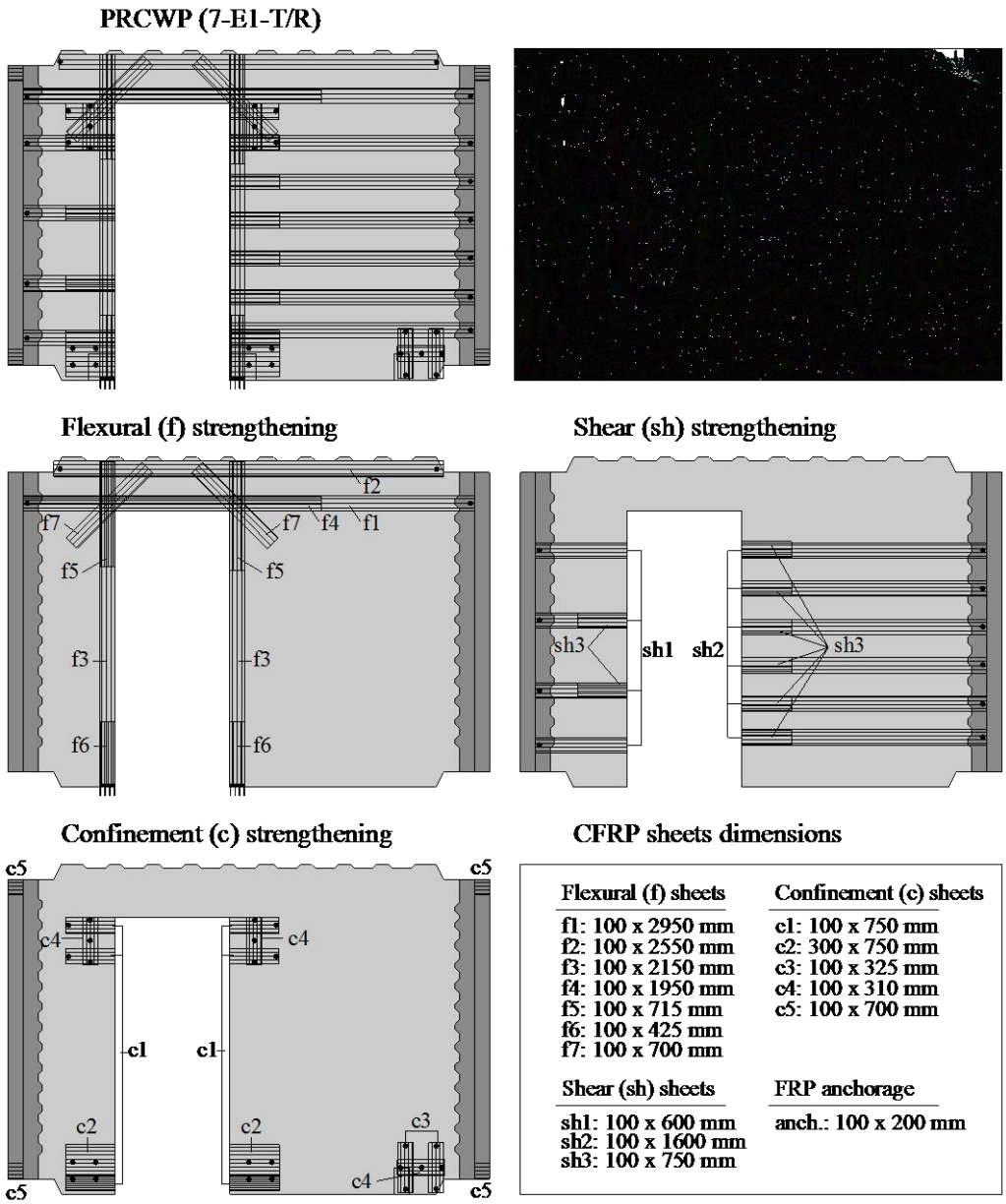

Figure 2.26 – FRP strengthening layout for PRCWP (7-E1-T/R)

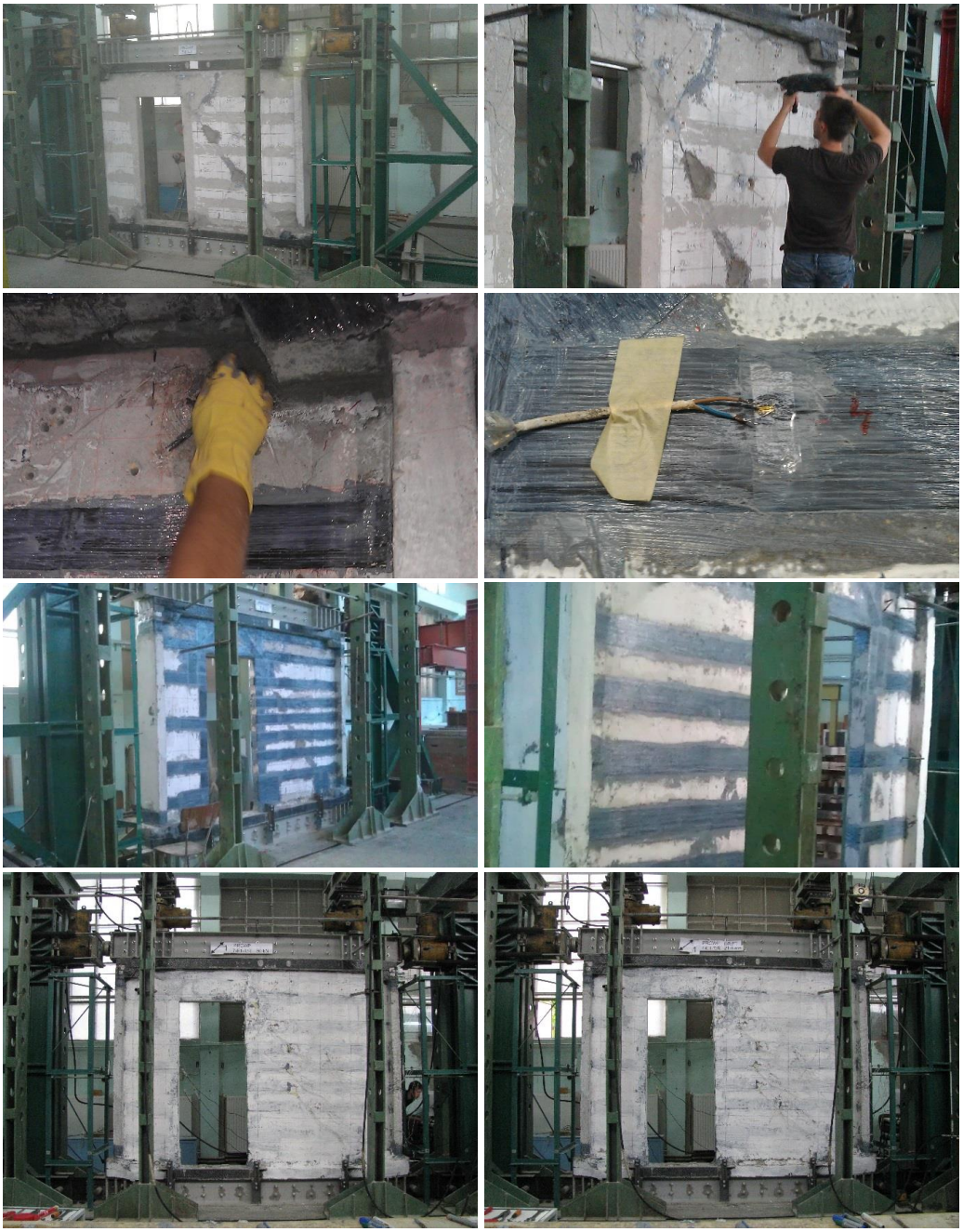

Figure 2.27 – FRP strengthening details

PRCWP (8-E3-T/R)

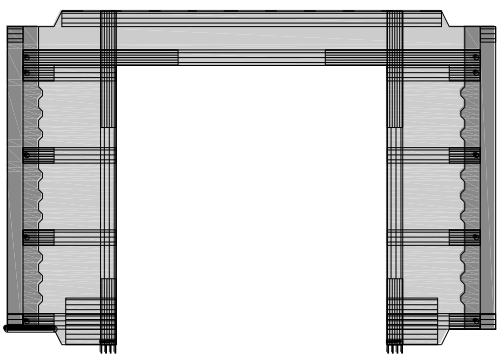

Flexural (f) strengthening

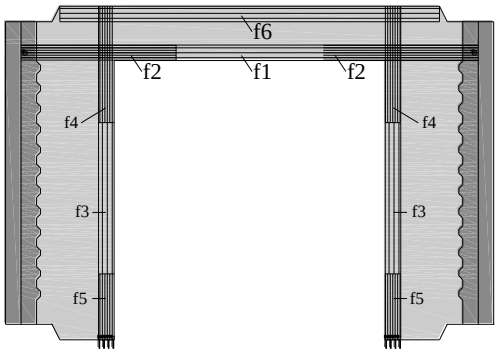

Shear (sh) strengthening

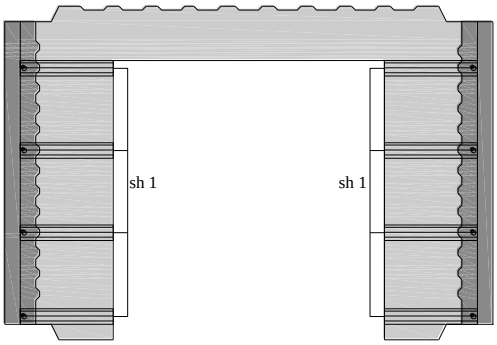

Confinement (c) strengthening

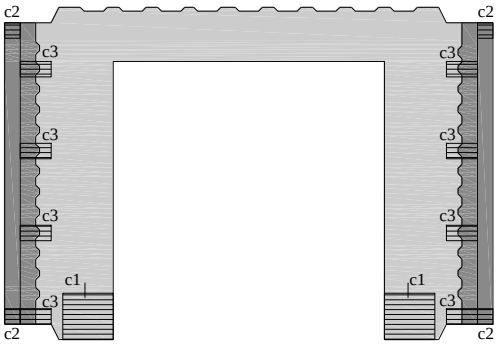

CFRP sheets dimensions

Flexural (f) sheets	Confinement (c) sheets
f1: 100 x 2950 mm	c1: 300 x 750 mm
f2: 100 x 1000 mm	c2: 100 x 700 mm
f3: 100 x 2150 mm	c3: 100 x 700 mm
f4: 100 x 750 mm	
f5: 100 x 425 mm	
f6: 100 x 2550 mm	

Shear (sh) sheets	FRP anchorage
sh1: 100 x 1300 mm	anch.: 100 x 200 mm

Figure 2.28 – FRP strengthening layout for PRCWP (8-E3-T/R)

Figure 2.29 – FRP strengthening details

PRCWP (9-E1/E3-R/T)

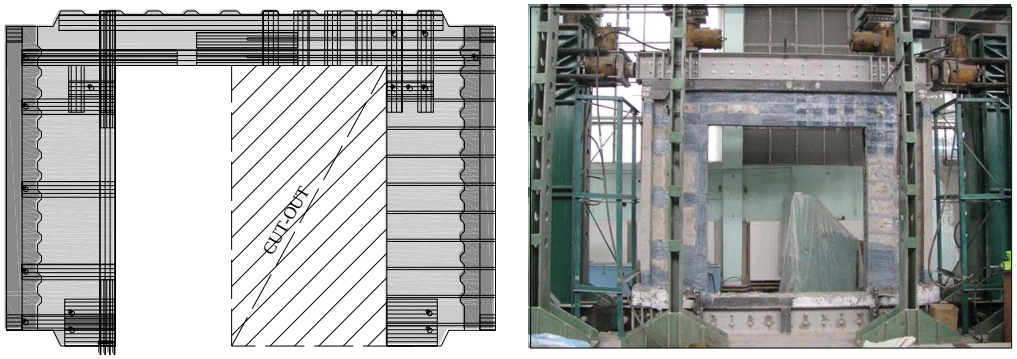

Flexural (f) strengthening

Shear (sh) strengthening

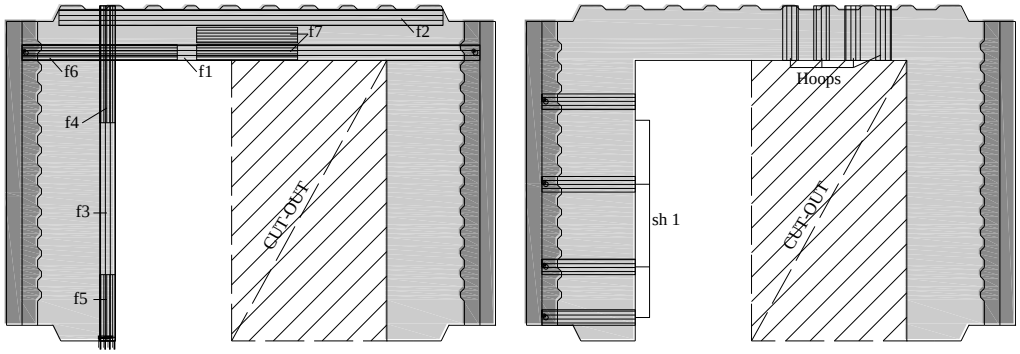

Confinement (c) strengthening

NSM-CFRP shear strengthening

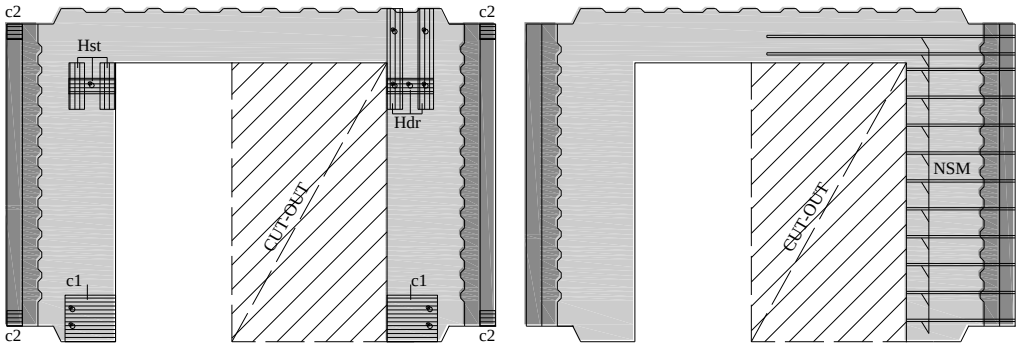

CFRP sheets dimensions

Flexural (f) sheets	Confinement (c) sheets	Shear (sh) sheets	NSM plates
f1: 100 x 2950 mm	c1: 300 x 750 mm	sh1: 100 x 1300 mm	12 x 1.2 x 700 mm
f2: 100 x 2550 mm	c2: 100 x 700 mm	hoops: 100 x 800 mm	12 x 1.2 x 1600 mm
f3: 100 x 2150 mm	Hst: 3 x 100 x 300 mm		
f4: 100 x 750 mm	Hdr: 100 x 300 mm +	FRP anchorage	
f5: 100 x 425 mm	2 x 100 x 650 mm	anch.: 100 x 200 mm	
f6: 100 x 1000 mm			
f7: 100 x 650 mm			

Figure 2.30 – FRP strengthening layout for PRCWP (9-E1/E3-R/T)

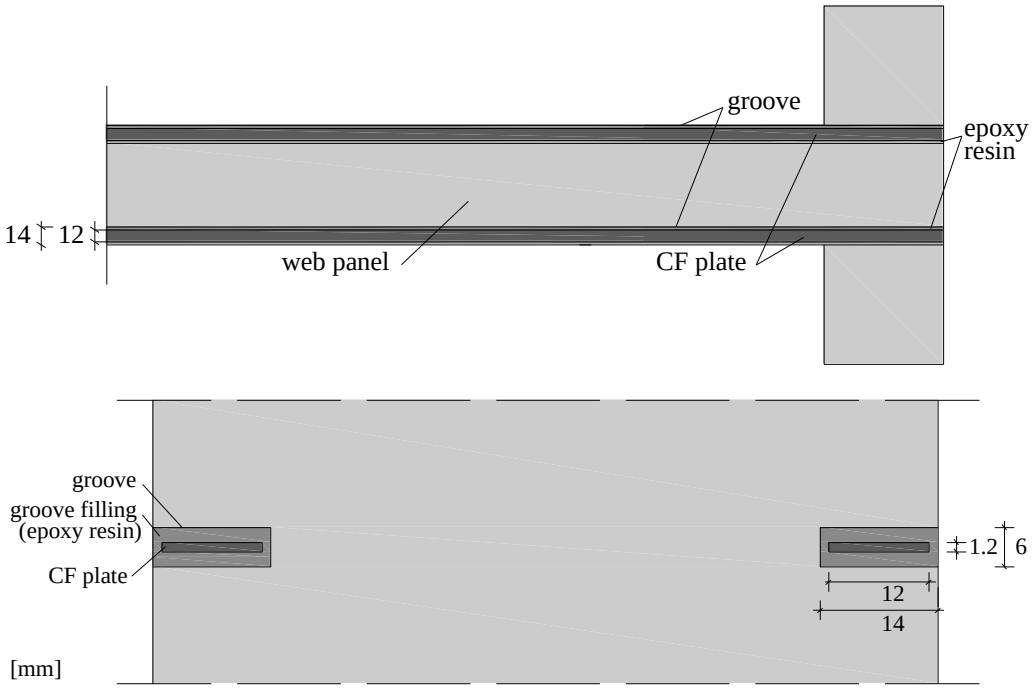

Figure 2.31 – NSM-CFRP application details

Figure 2.32 – Double disc grinder used for the NSM channel cut

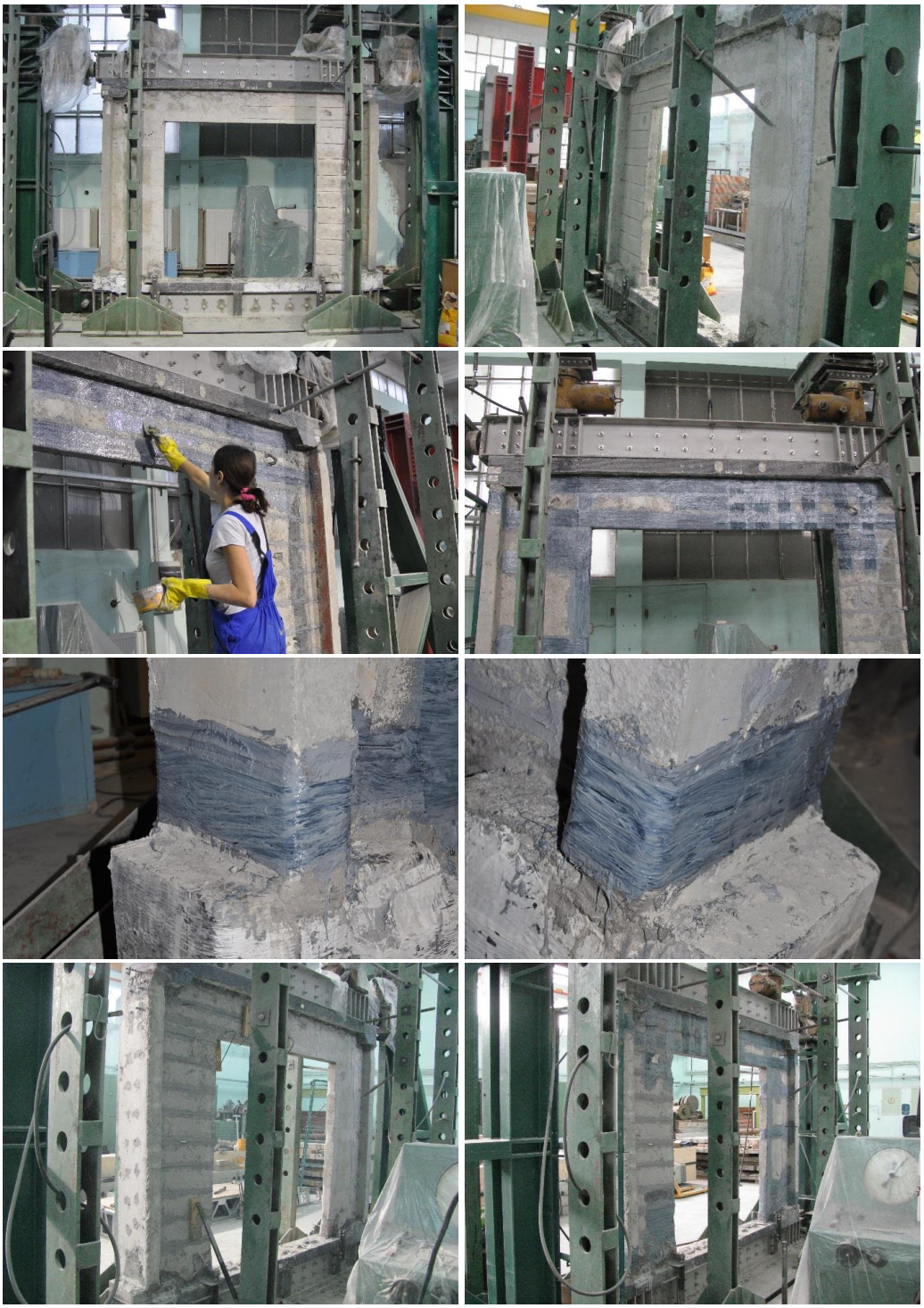

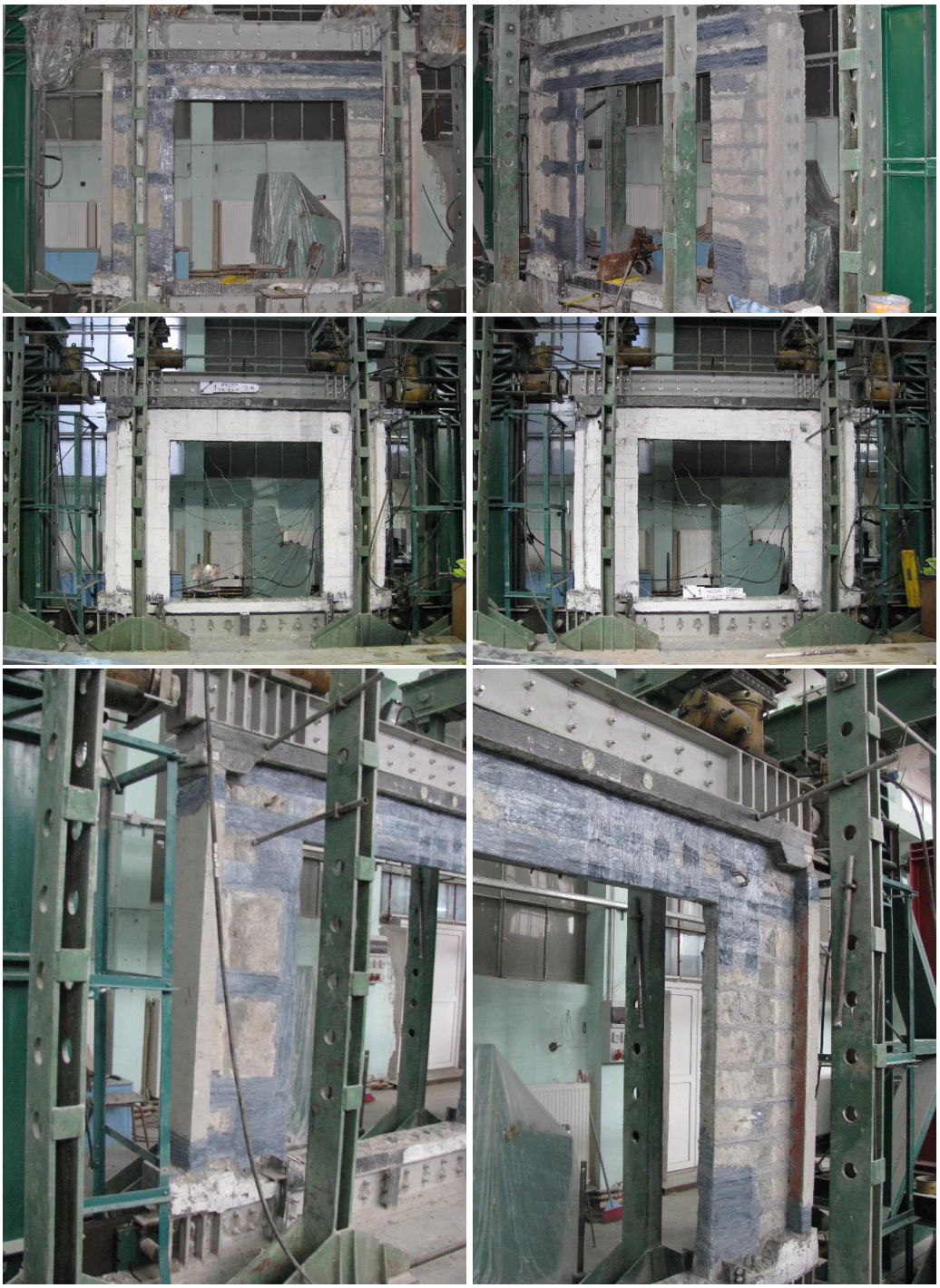

Figure 2.33 – FRP strengthening details

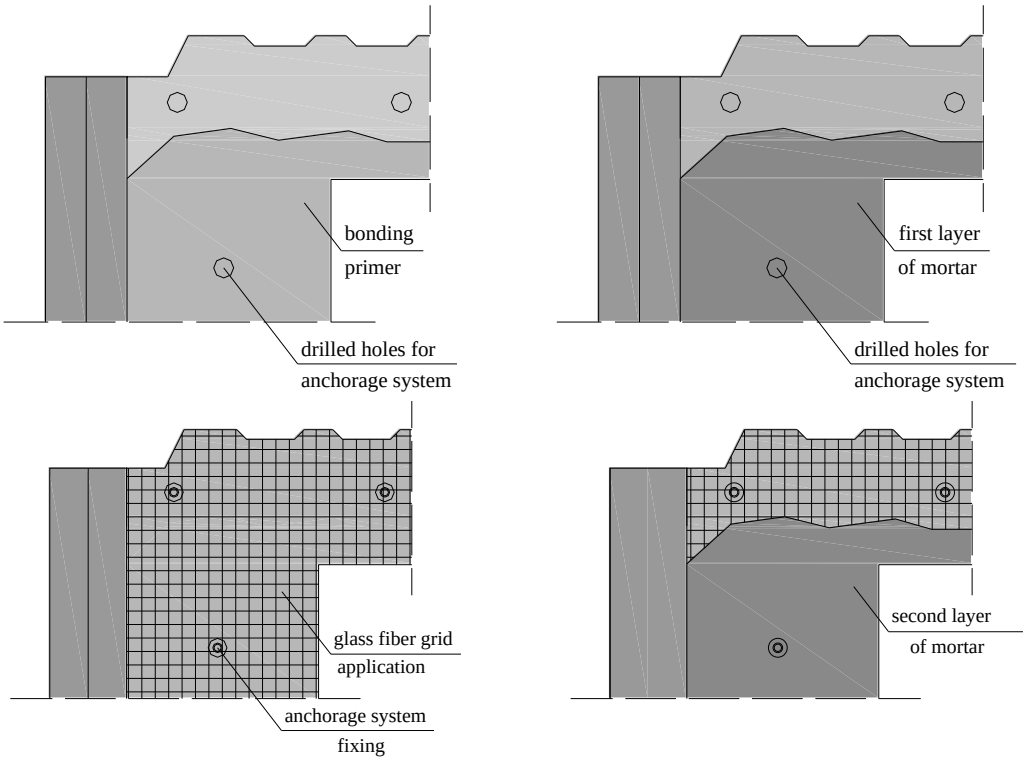

Figure 2.34 – TRM strengthening details

PRCWP (10-L1/L3-T/R)

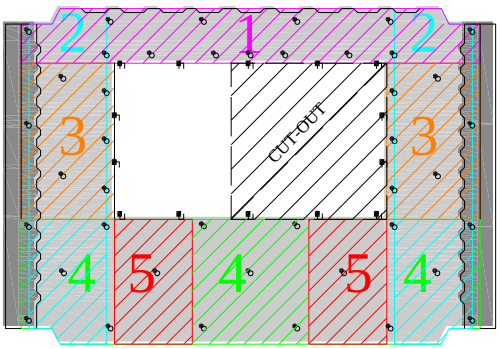

Parapet strengthening

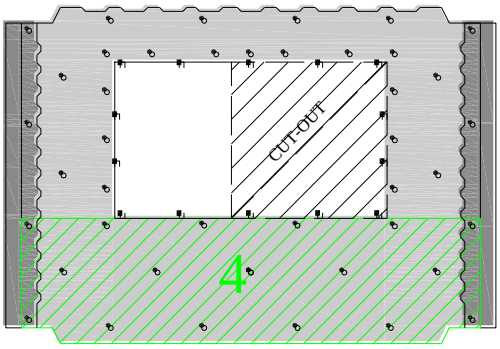

Parapet strengthening

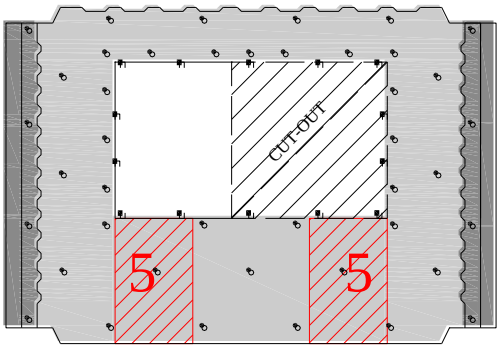

Pier strengthening

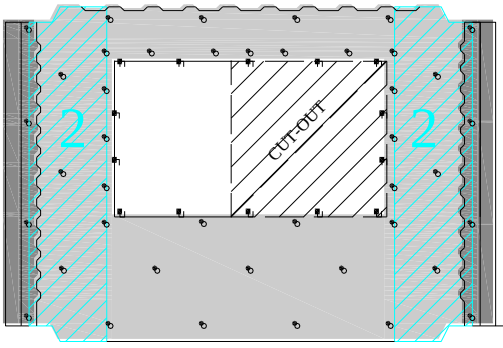

Pier strengthening

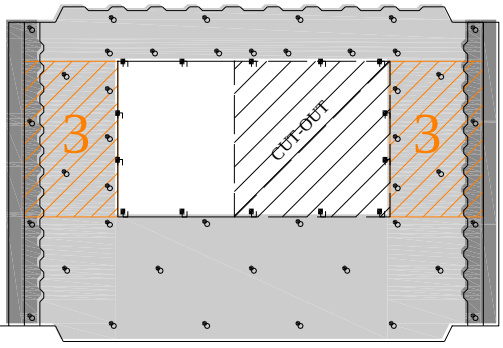

Spandrel strengthening

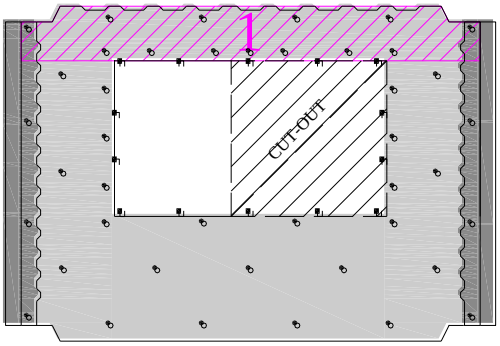

Mechanical anchorage position

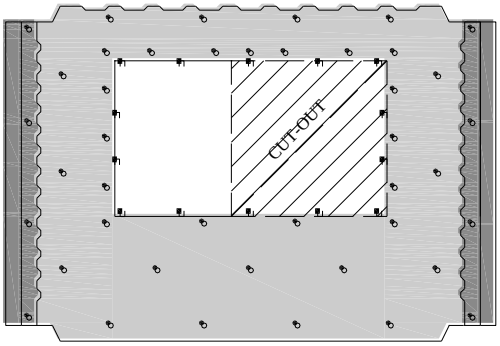

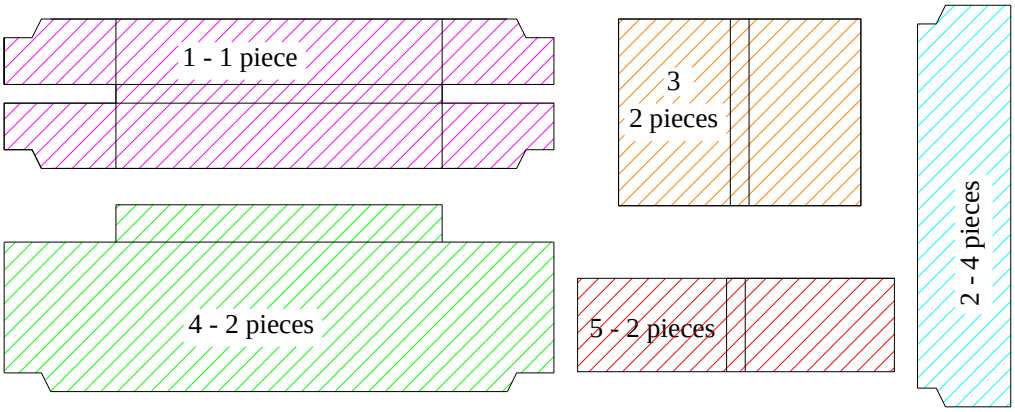

Figure 2.35 – FRP strengthening layout for PRCWP (10-L1/L3-T/R)

Figure 2.36 – FRP strengthening details

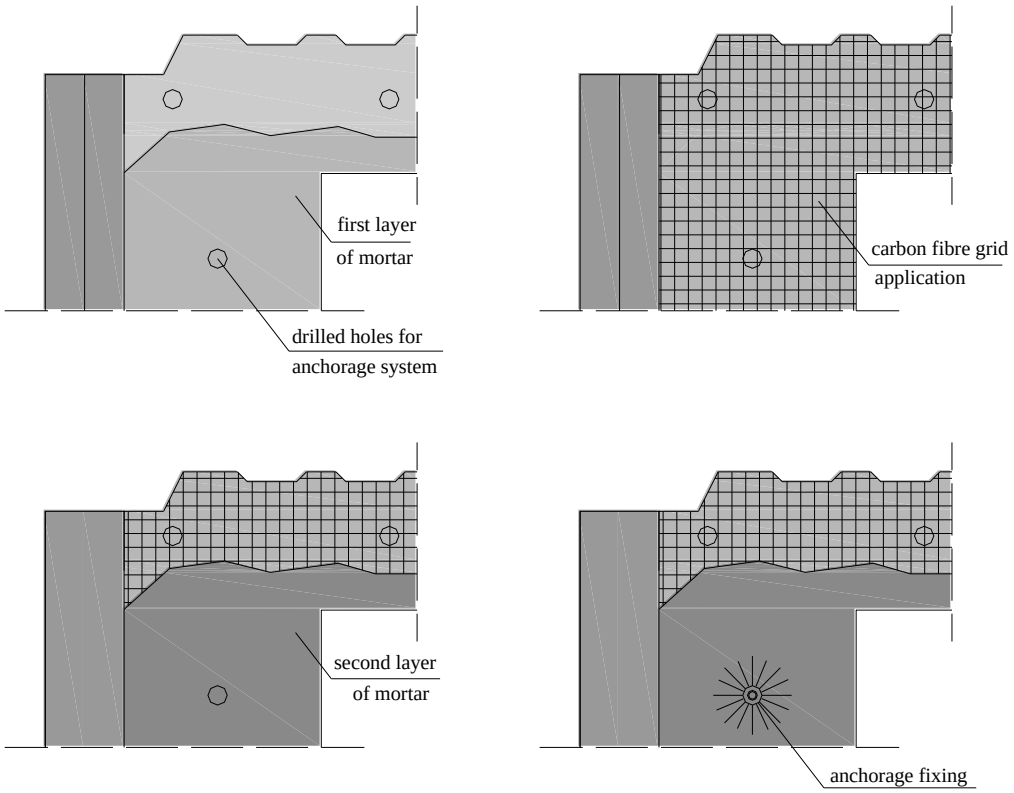

Figure 2.37 – TRM strengthening details

PRCWP (11-L1-T/R)

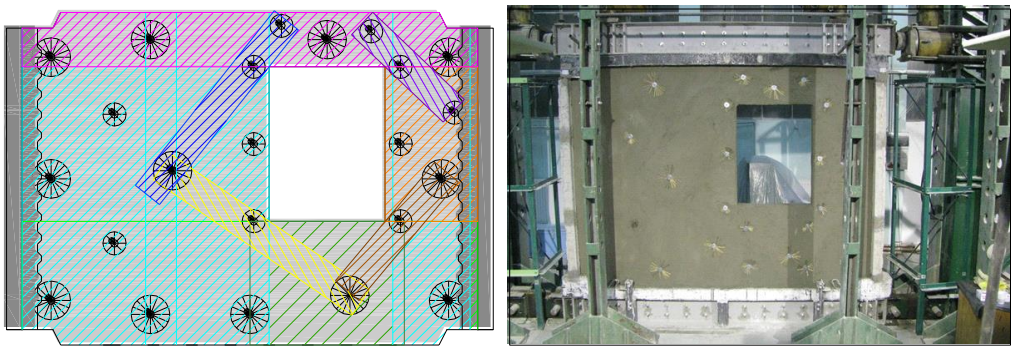

Parapet strengthening

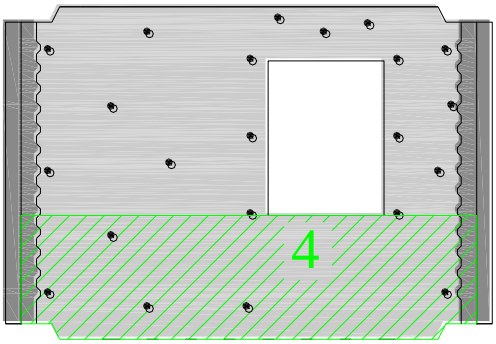

Parapet strengthening

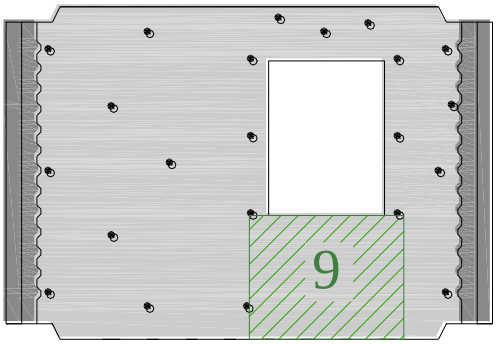

Pier strengthening

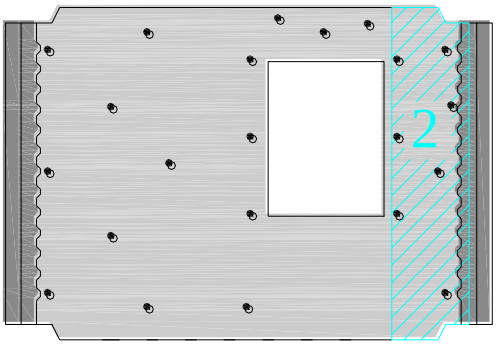

Pier strengthening

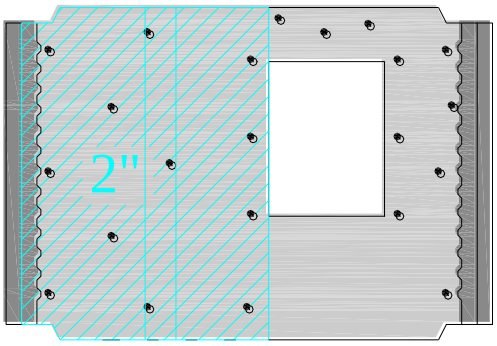

Pier strengthening

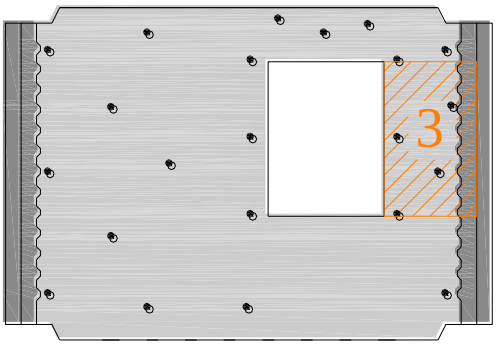

Spandrel strengthening

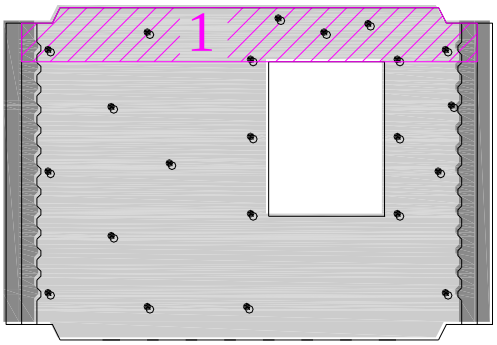

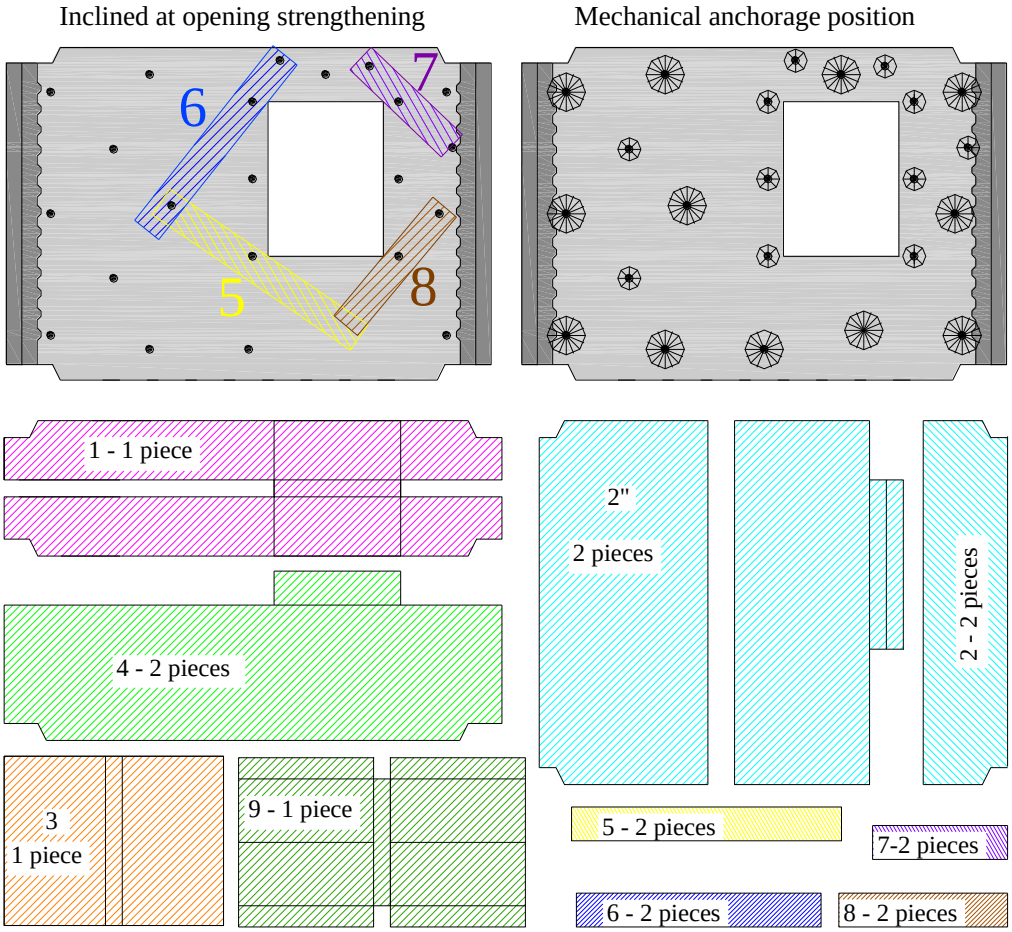

Figure 2.38 – FRP strengthening layout for PRCWP (11-L1-T/R)

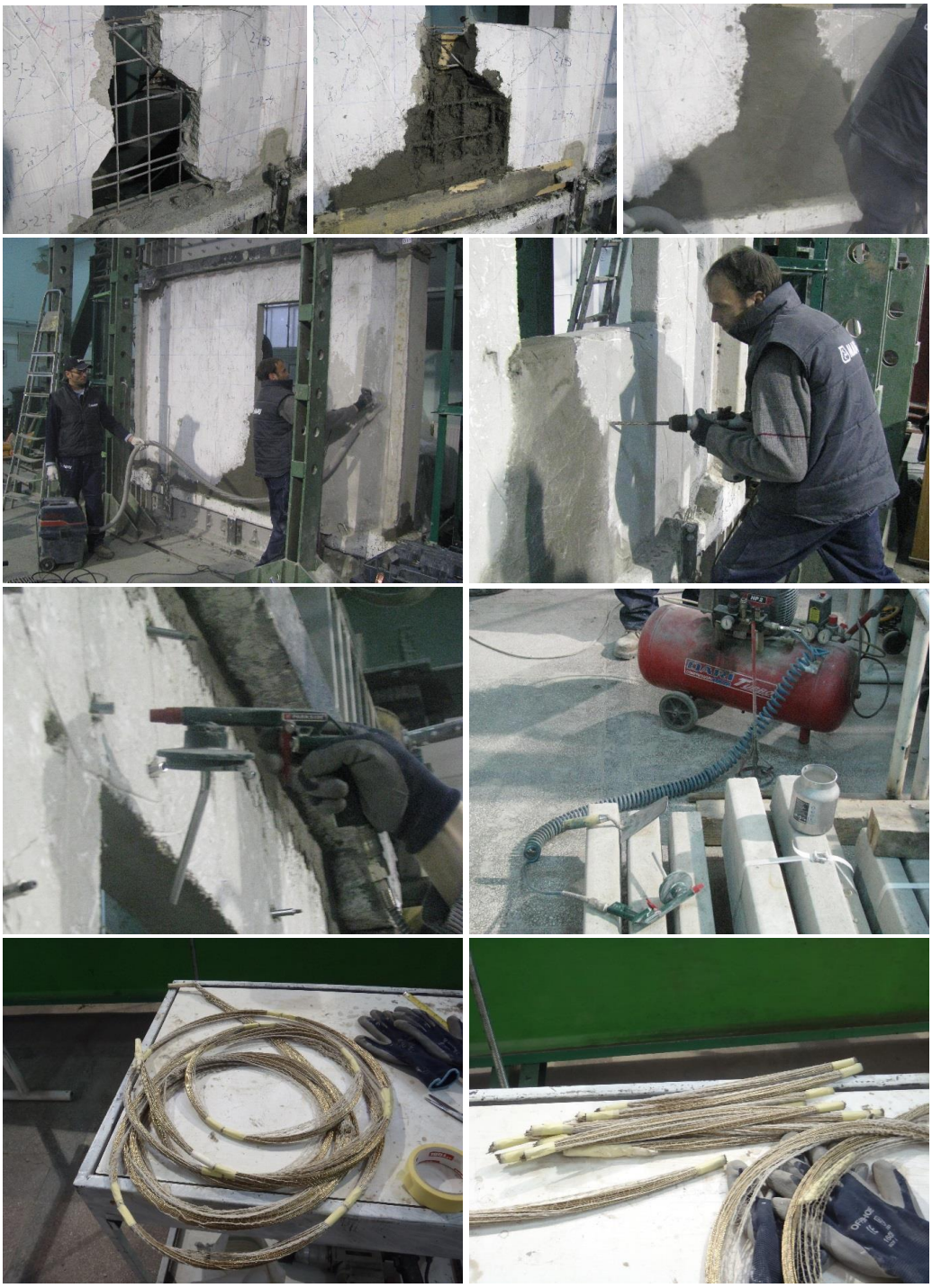

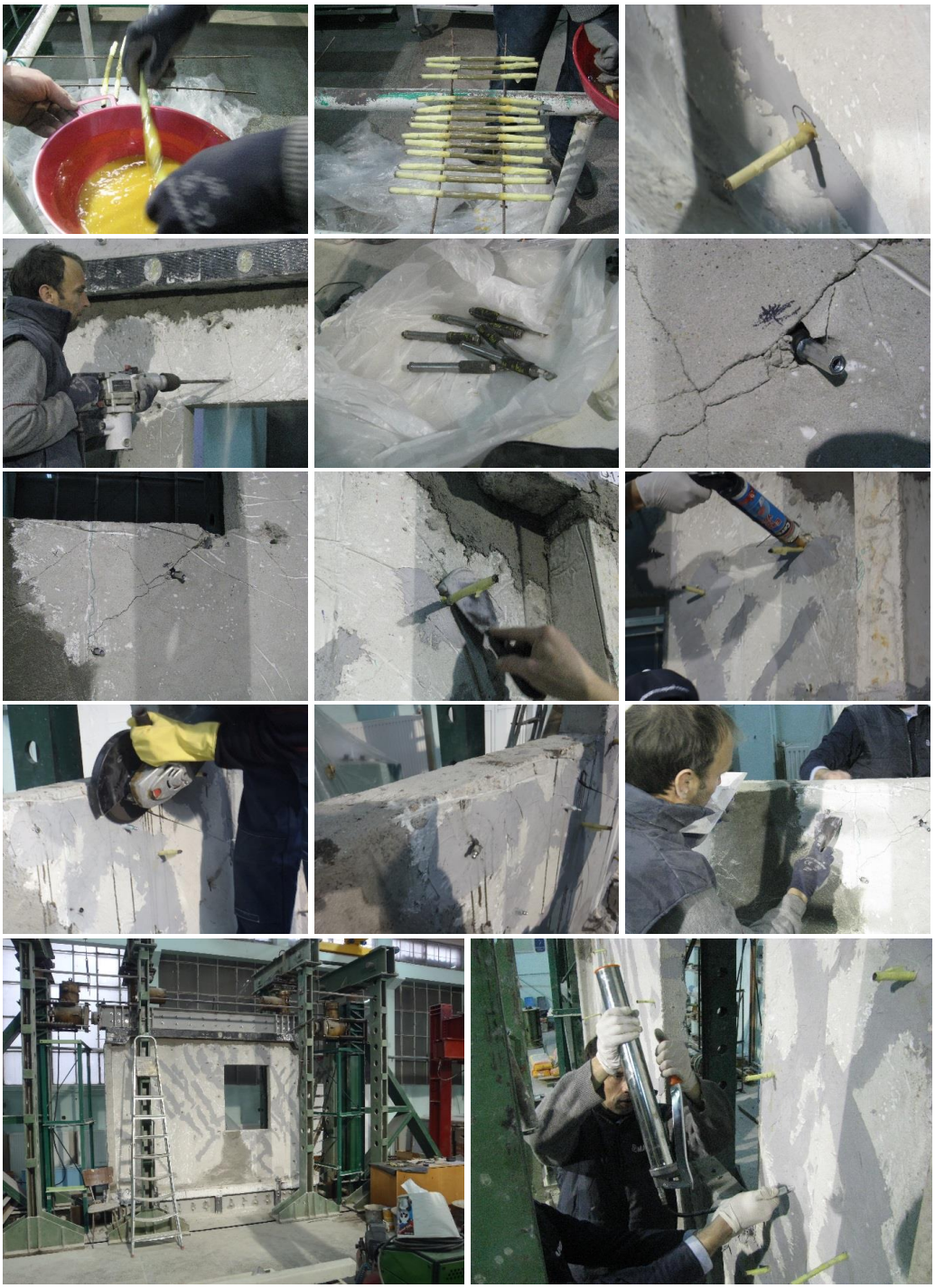

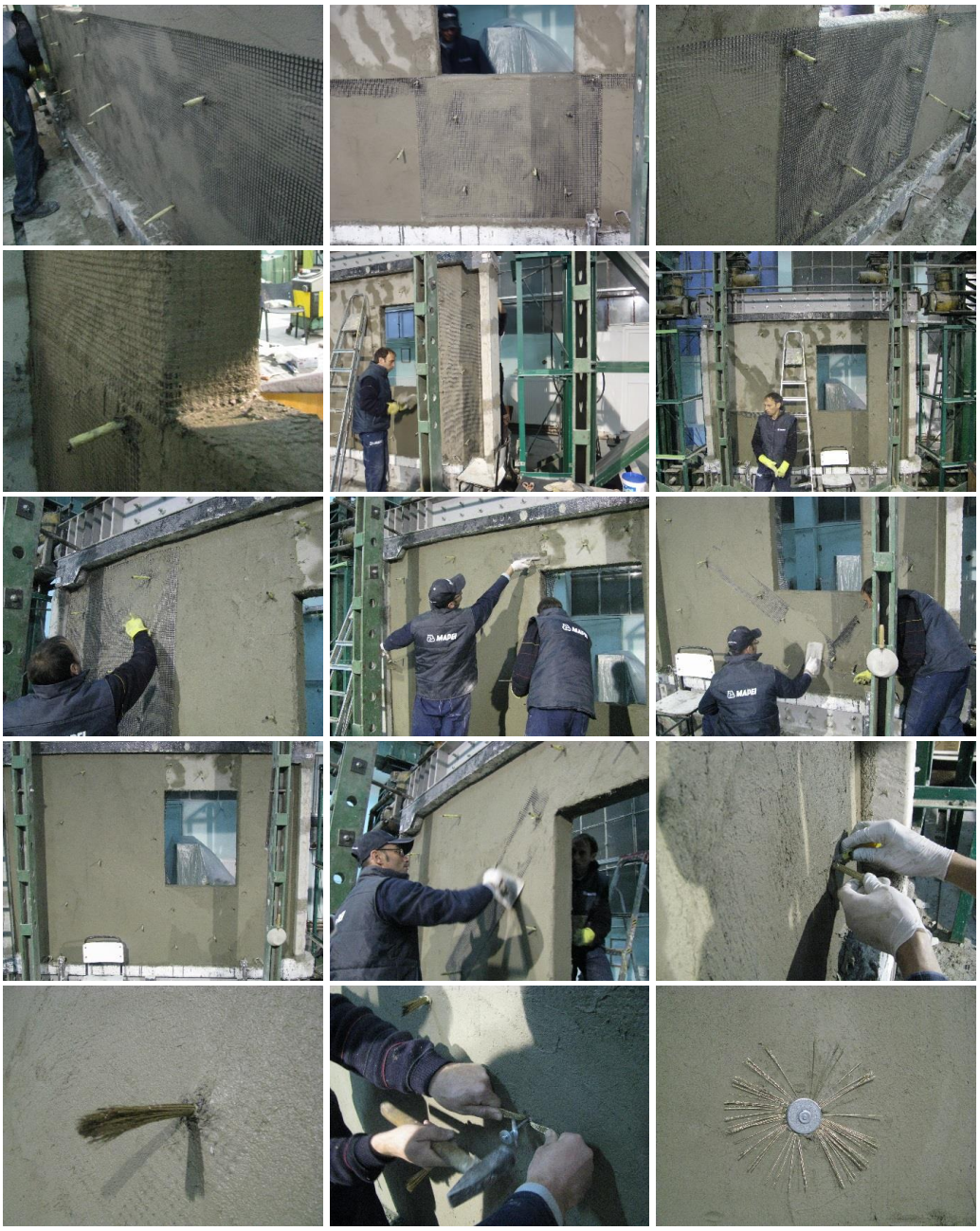

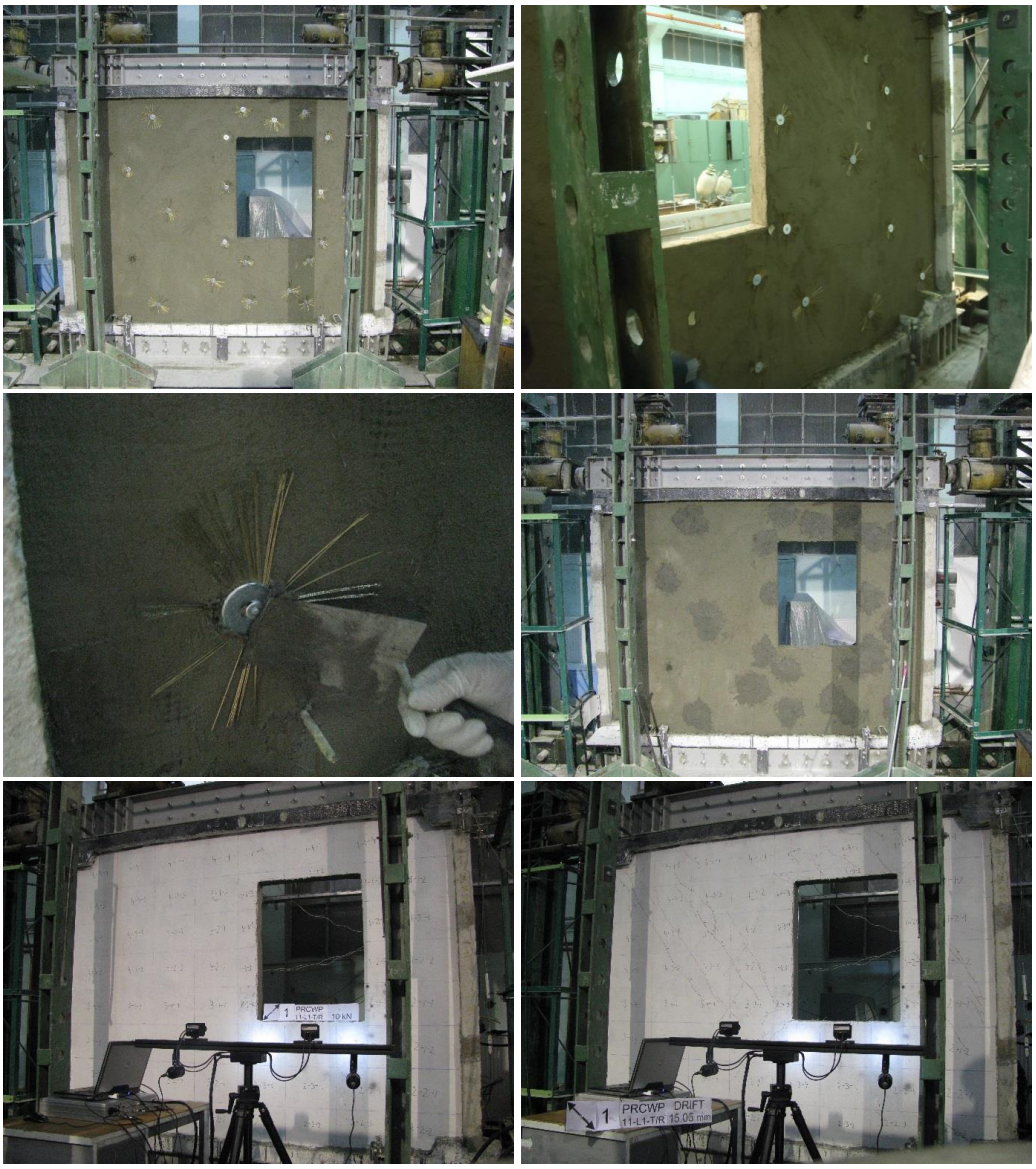

Figure 2.39 – FRP strengthening details [114]

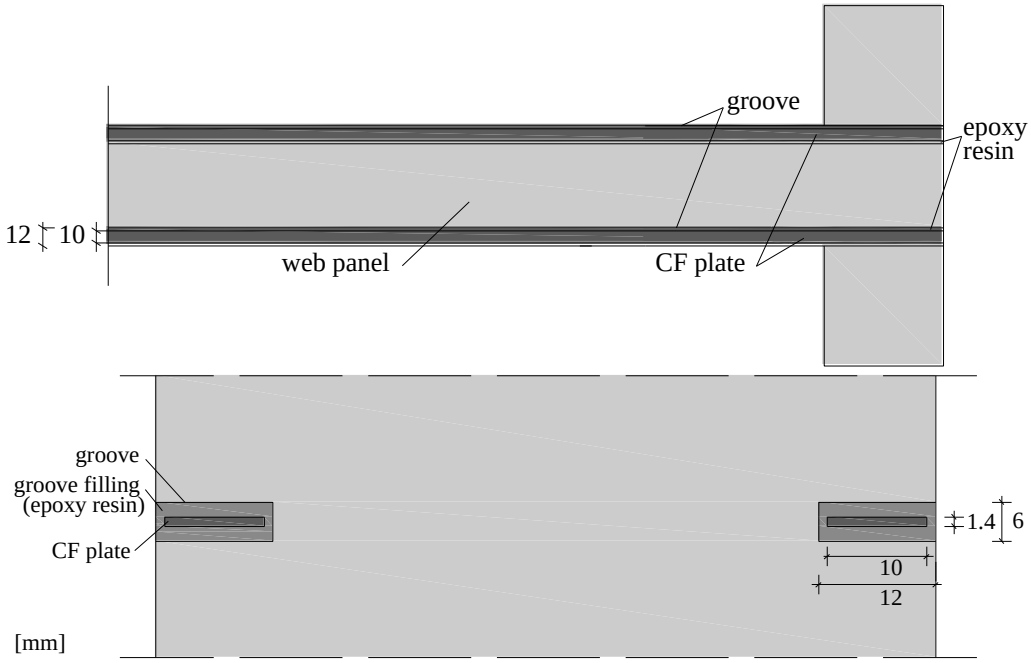

Figure 2.40 – NSM-CFRP application details

PRCWP (12-E1-T/R)

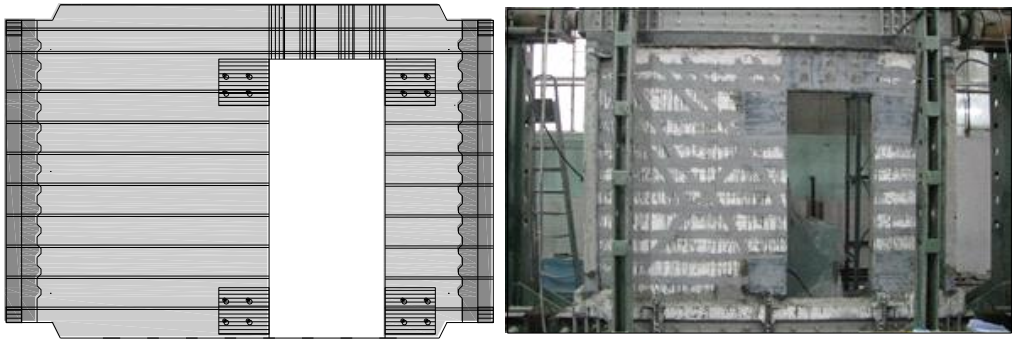

NSM shear (sh) strengthening

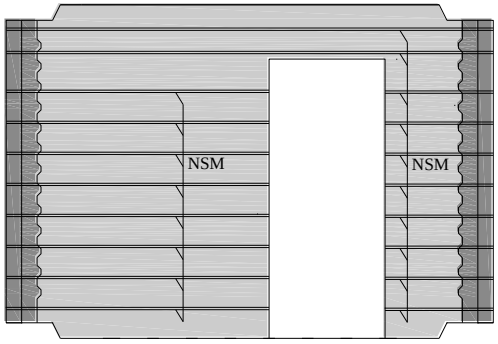

Confinement (c) strengthening

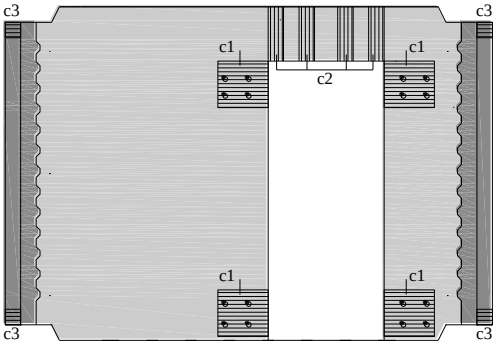

CFRP sheets and strips dimensions

Confinement (c) sheets	FRP anchorage	NSM plates
c1: 300 x 750 mm c2: 100 x 800 mm c3: 100 x 700 mm	anch.: 100 x 200 mm	10 x 1.4 x 700 mm 10 x 1.4 x 1700 mm 10 x 1.4 x 3150 mm

Figure 2.41 – FRP strengthening layout for PRCWP (12-E1-T/R)

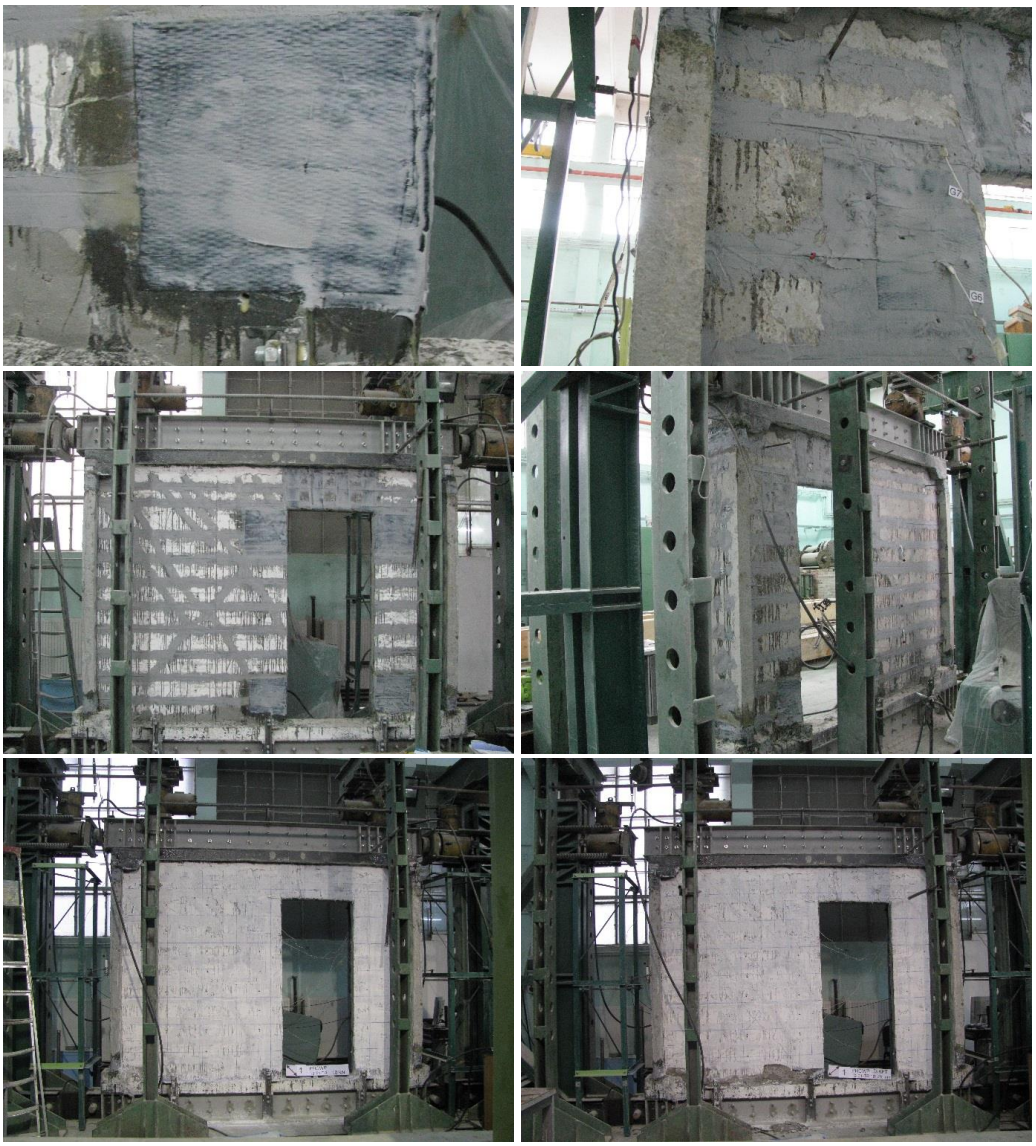

Figure 2.42 – FRP strengthening details

3. RESULTS

In order to determine the response characteristics of the investigated specimens, all the recorded data was analysed and processed, giving as a result an evaluation of the following important aspects: the general observed behaviour of the walls during the experimental tests, the force-drift ratio analysis, the dissipated energy, the ductility of the specimens, the strain analysis, the stiffness degradation of the walls, numerical analysis, evaluation of the shear strength using design code provisions and plastic mechanism model, weakening assessment using design code provisions, and computation of the final cracking pattern. In the below sub-sections are presented in detail all the investigated response characteristics.

3.1. General behaviour and failure modes of FRP strengthened specimens

Generally, the behaviour of the wall specimens was in accordance with the testing procedure and the rehabilitation or retrofitting strategy. General behavioural aspects that were observed in the case of the strengthened specimens during the experimental tests consist in a significant number of cracks which appeared in all the regions of the panel, concrete crushing, FRP debonding, FRP fracture, TRM debonding. However, no failure for the FRP plates was observed during the experimental tests. Reinforcement yielding aspects are given in Section 3.5 and the behaviour at each cycle peak is presented in Appendix A. Among the failure details observed in the experimental tests of the strengthened specimens, the followings were noted:

- PRCWP (7-E1-T/R): during the first loading cycles, diagonal cracks from the previous experimental test of the unstrengthened specimen, reopened now, whereas new cracks appeared mostly in the spandrel and in the right pier. Among the first FRP failure details, the c1 confinement sheets applied in the spandrel-right pier connection region started debonding. Then, the bottom shear sheet in the right pier started debonding. New cracks continued to appear in the spandrel and in the right pier, until on the rear face of the wall panel, the bottom four shear sheets in the right pier were observed to debond. The concrete and cast-in-place mortar crushed at the bottom right wing side end, whereas the corresponding c5 confinement strip fractured. A crack due to sliding shear was observed on the rear face of the wall, between the two bottom shear strips. Failure details of the PRCWP (7-E1-T/R) specimen are given in Figure 3.1.
- PRCWP (8-E3-T/R): Several cracks appeared in the spandrel and in the piers during the first loading cycles, whereas snapping sounds of the FRP sheets were heard. The second shear sheet (sh1) from the top in the right pier was the first to start debonding, followed by the bottom shear sheet (sh1) in the right pier, and a diagonal crack reopening in the right pier. Then, the flexural (f3, f4) sheets from the spandrel – right pier connection region started swelling, as the bottom shear sheet (sh1) in the left pier started debonding. New cracks continued to appear in all the regions of the wall panel, whereas the above mentioned FRP sheets continued to debond, and the concrete in the spandrel – right pier connection region crushed. A

vertical crack between the left pier and the wing was observed. The second shear sheet (sh1) from the bottom, in the left pier was also observed to debond, before the failure of the specimen was attained. Failure details of the PRCWP (8-E3-T/R) specimen are given in Figure 3.2.
- PRCWP (9-E1/E3-R/T): Snapping sounds of the FRP sheets were heard during the first loading cycles, whereas cracks appeared in the spandrel and in the piers. Then, the flexural (f2) sheet started debonding. The cast-in-place mortar at the bottom left wing-side end crushed. Then, the flexural (f1, f4) sheets in the spandrel – left pier connection region started debonding, followed by the (Hdr) confinement sheet debonding, at the spandrel – right pier connection region. The cast-in-place mortar at the bottom right corner of the opening crushed, whereas the concrete in the spandrel – left pier connection region, also crushed. The (Hst) confinement sheet debonded, whereas the first shear strip (sh1) in the left pier debonded. The concrete and cast-in-place mortar at the bottom right wing-side end crushed, as the (c2) confinement sheet fractured. However, no failure of the CFRP plates was observed. Failure details of the PRCWP (9-E1/E3-R/T) specimen are given in Figure 3.3.
- PRCWP (10-L1-/L3-T/R): Snapping sounds in the TRM system were heard from the first loading cycles, whereas cracks appeared in the spandrel, piers and parapet. Cracks were observed in the spandrel – piers and parapet – piers connection regions also. Among the first TRM system debonding regions observed, were in the left pier. The TRM mortar component exfoliated and crushed at the parapet – left pier connection region. Then, the TRM system continued debonding in the spandrel – right pier connection region also. Most of the cracks were observed in the parapet during testing, which makes the element important in preventing other failure details of the specimen, such as the concrete crushing in the corresponding connection regions. Before the failure of the specimen was attained, severe TRM debondings were observed in the left pier, whereas measuring the TRM system detachment distance from the panel surface, up to 2.5 cm were found. It was concluded that the TRM system could not work at its high level of capacity due to the inefficient distribution of the anchorage. A denser distribution of the mechanical anchorage would have ensured a better connection between the TRM system and the wall panel. At the end of the experimental test, the TRM system was detached from the piers, and severe inclined cracks were found, together with concrete crushing and vertical reinforcement bending. However, the TRM system did not debond together with concrete surface, in the detached pieces only the glass fiber grid, some anchorage pieces, TRM mortar component and patching mortar were observed. Failure details of the PRCWP (10-L1/L3-T/R) specimen are given in Figure 3.4.
- PRCWP (11-L1-T/R): Several cracks in the piers, spandrel, spandrel – piers and parapet – piers connection region were observed during the first loading cycles of the specimen, followed by snapping sounds in the TRM system. At 0.4 % drift ratio, the maximum capacity of the testing facility was attained. TRM component mortar crushing was observed at the parapet – left pier and spandrel – left pier connection region, together with local debonding. Due to the fact that the failure of the specimen was not attained in the experimental test, another testing facility with a higher capacity was provided and the test continued. Further cracks and debondings occurred in the spandrel – piers and parapet – piers connection regions, spandrel and piers, whereas the concrete and cast-in-place mortar at the top left wing-side end, crushed. Based on the cracking pattern observed, namely cracks which were overpassing the small opening, the behaviour of the specimen was considered

similar with the behaviour of the solid wall specimen [3]. Failure details of the PRCWP (11-L1-T/R) specimen are given in Figure 3.5.

- PRCWP (12-E1-T/R): Cracks appeared in the piers, spandrel and spandrel – piers connection regions. Cast-in-place mortar crushed between the left pier and the foundation beam. C1 confinement sheet debonded and fractured at the bottom left corner of the opening. However, no failure of the CFRP plates was observed. The failure of the specimen was not attained during the experimental test due to the available capacity of the testing facility. Failure details of the PRCWP (12-E1-T/R) specimen are given in Figure 3.6.

Failure details of the tested strengthened specimens were also partly discussed and presented in [109-116, 118, 120].


G10

Figure 3.1 - Failure details of the PRCWP (7-E1-T/R) specimen [109-110, 112, 115]

Figure 3.2 - Failure details of the PRCWP (8-E3-T/R) specimen [109, 112, 115]


D1-1
D1-1

Figure 3.3 - Failure details of the PRCWP (9-E1/E3-R/T) specimen [109, 112, 118]

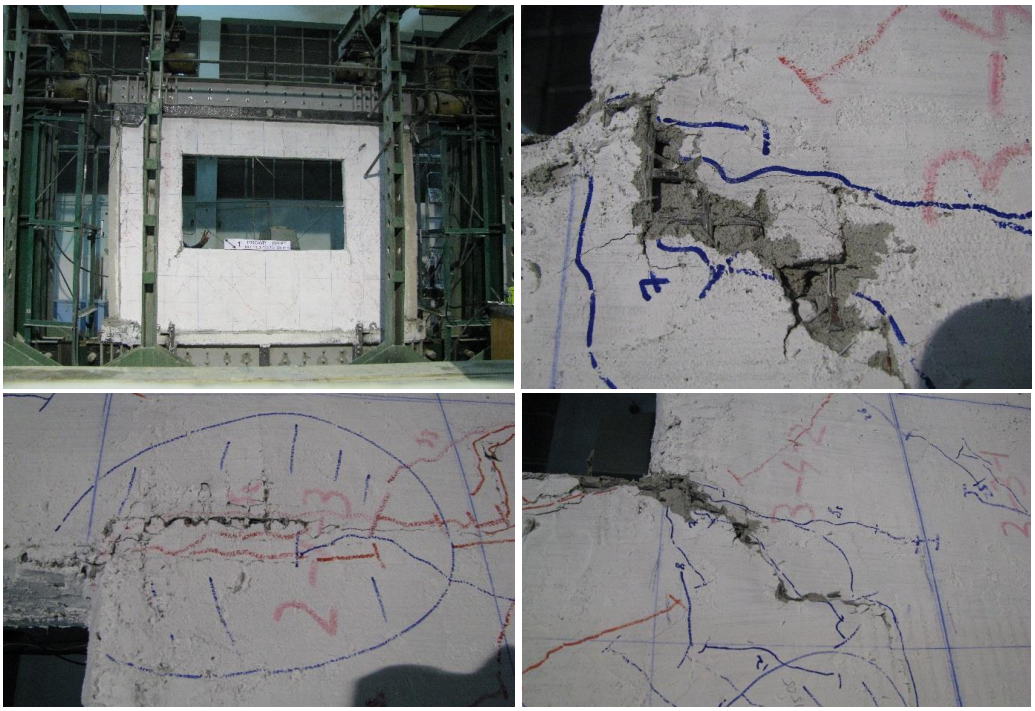

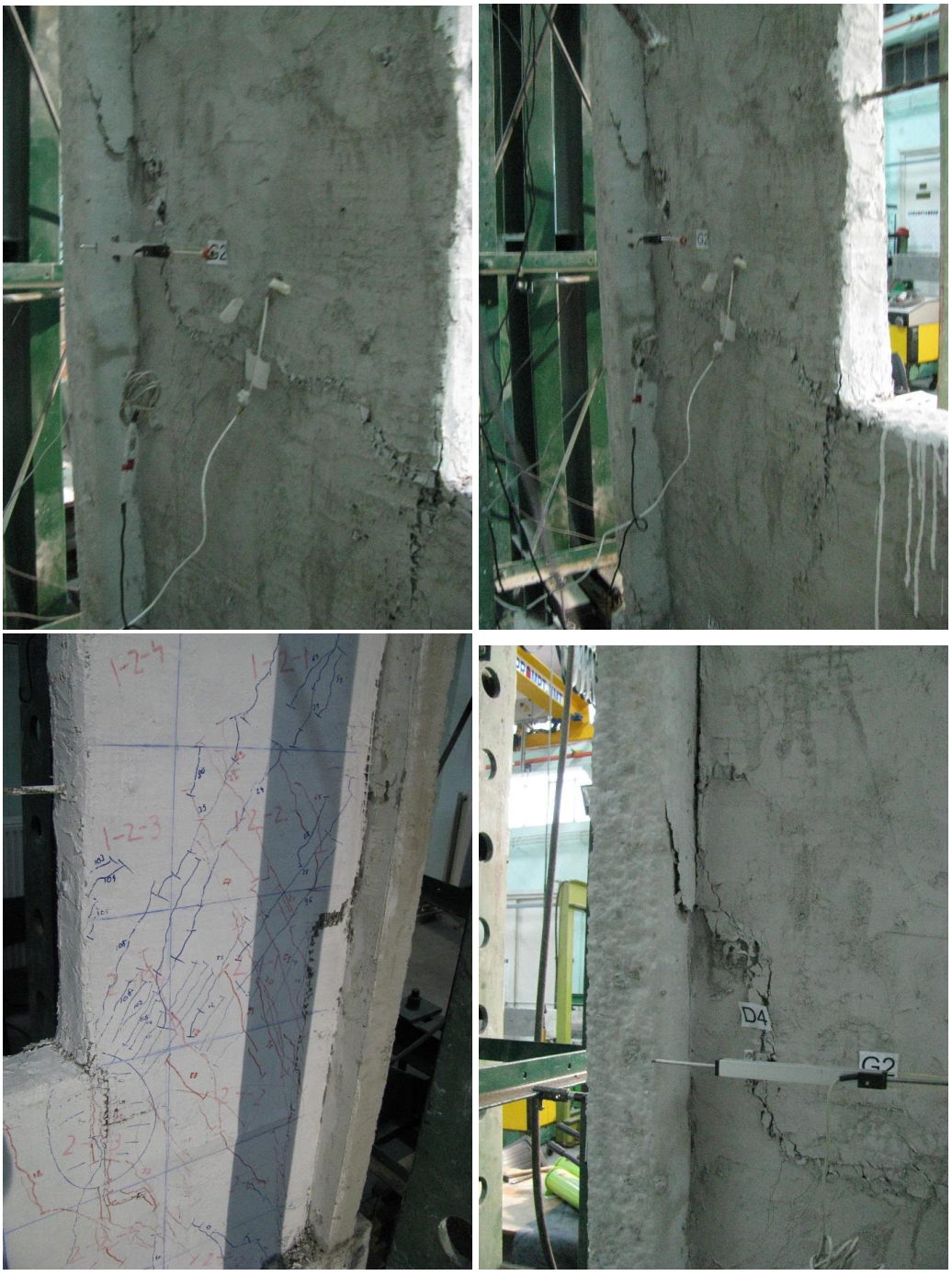
G2
D4
G2

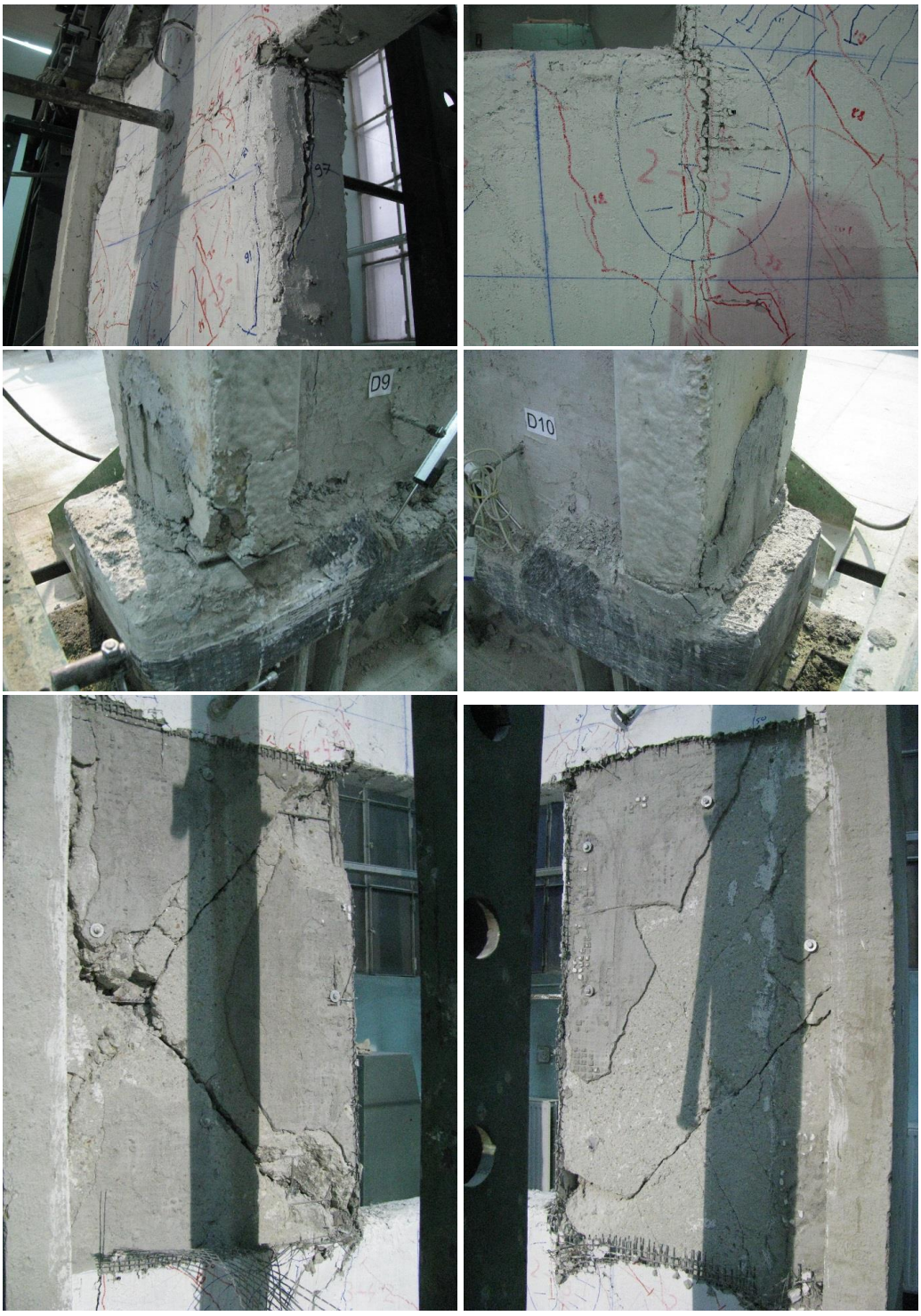
D9
D10

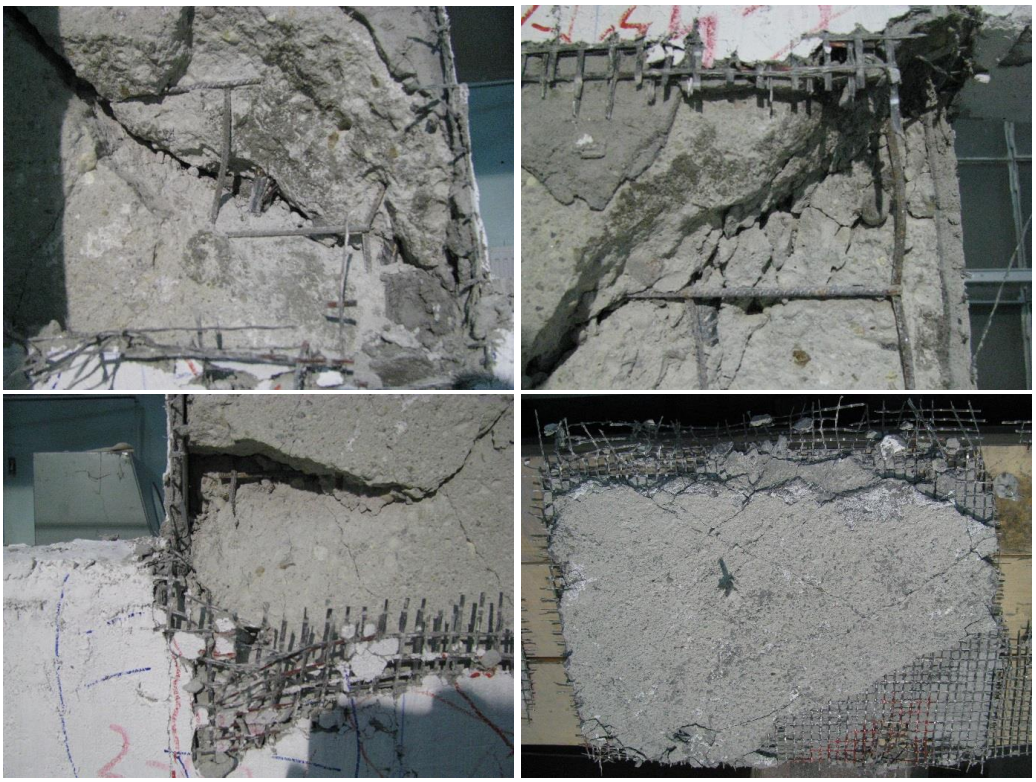

Figure 3.4 - Failure details of the PRCWP (10-L1/L3-T/R) specimen [109, 111-113, 116]

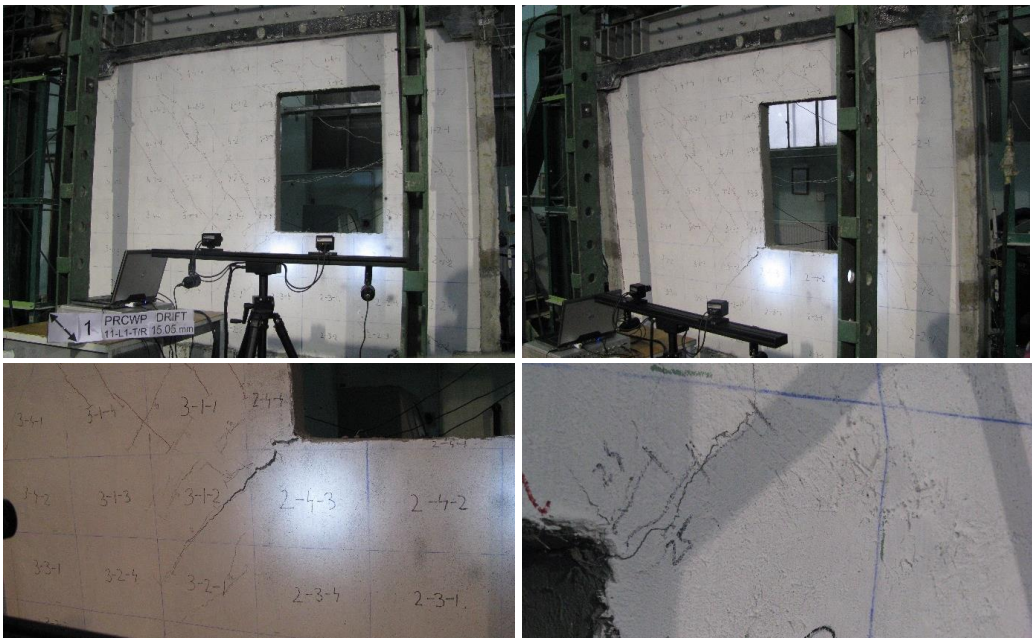


1-4-3
G2
G3

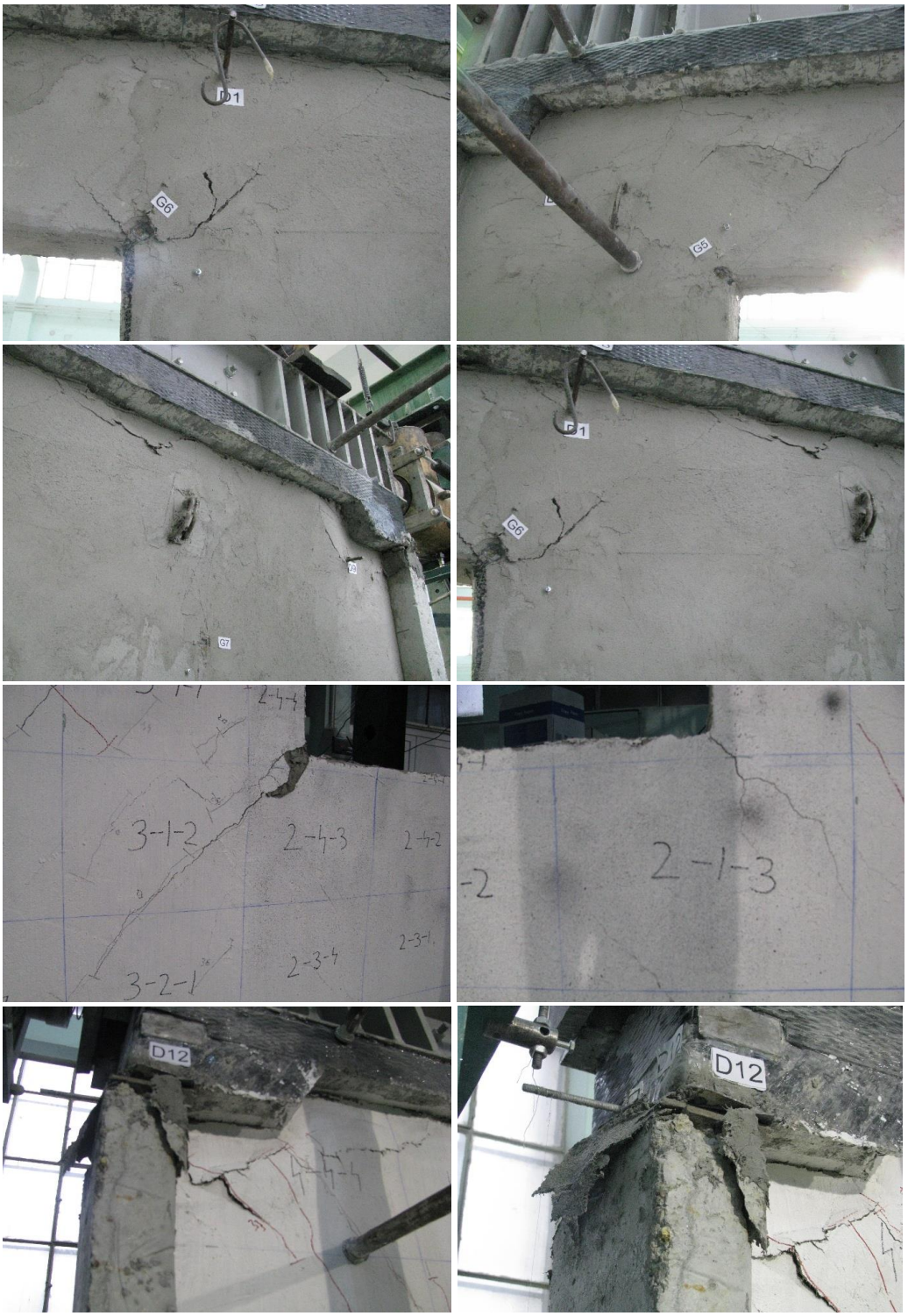
G6
G5
G7
C6
3-1-2
2-4-3
2-4-2
3-2-1
2-3-4
2-3-1
2-1-3
D12
D12

Figure 3.5 - Failure details of the PRCWP (11-L1-T/R) specimen [109, 113-114]

Figure 3.6 - Failure details of the PRCWP (12-E1-T/R) specimen [109, 120]

As the experimental research program presented here continued a previous phase, investigated and reported by Demeter [8], in which strengthening of the specimens with narrow/wide door cut-out opening was performed by means of EBR-CFRP, it is worth taking into account and comparing the failure details obtained. Among the reported failure observations in the case of the strengthened specimens were: snapping sounds of the FRP composites, opening of pre-existing inclined cracks, appearance of new cracks, fracture of vertical FRPs in the spandrel – pier connection region, horizontal FRP debonding at the intersection with inclined cracks, concrete crushing at the outside toe of right pier, FRP confinement fracture, FRP bulging (buckling) in compression. Demeter [8] concluded that the confinement strips showed the most stable response, the shear strips debond in the vicinity of the inclined cracks, whereas the flexural strips subjected to alternating load reversals, parallel to the fibre direction are likely to fail prematurely.

Similar failure aspects were observed for the strengthened specimens used in the current experimental program, presented in detail in Section 3.1.

3.2 Force–drift ratio response and observations

The basic results of the tested wall specimens are presented in Table 3.1. Examination of the strengthened and reference specimens during the experimental tests revealed a significant number of cracks in all the regions of the panel, a number of inclined cracks in the piers, concrete crushing, reinforcement yielding, FRP debonding and FRP fracture. The failure details of the tested specimens are presented in Fig. 2.21-2.25 for the reference specimens, and in Fig. 3.1-3.6 for the strengthened ones. The load bearing capacity results are presented in Table 3.2, showing a variation in the positive loading cycles between 54–111 % and between 93–132 % in the negative loading cycles, whereas for the drift at failure it was found a variation between 101-151 % in the positive loading cycles and between 105-137 % in the negative loading cycles. The drift at failure for PRCWP (11-L1-T/R) and PRCWP (12-E1-T/R) was not recorded during the experimental tests due to the constraints of the testing facility, however a higher performance was observed in terms of load and displacement capacity compared to the reference specimens. Table 3.3 summarizes the results depending on the peak force attained by PRCWP (11-L1-T/R) and PRCWP (12-E1-T/R) specimens, showing that on the negative loading cycle, the load bearing capacity was increased with 162 % for PRCWP (11) and with 132 % for PRCWP (12), compared at the same displacement level.

Table 3.1 - Primary results of the tested wall specimens

Specimen notation	Peak force (kN)		Drift at yielding (%)		Drift at peak force (%)		Drift at failure (%)		μ = Δu/Δy		Average $\mu_{0.85}$
	+	-	+	-	+	-	+	-	+	-	
PRCWP (7-E1-T)	858	723	0,59	0,48	0,70	0,70	0,73	0,79	1,24	1,66	1,45
PRCWP (7-E1-T/R)	669,5	698	0,55	0,63	0,70	0,80	0,97	1,08	1,76	1,71	1,74
PRCWP (8-E3-T)	207,5	247,5	0,60	0,78	0,78	1,00	1,17	1,08	1,94	1,39	1,67
PRCWP (8-E3-T/R)	229,5	249,5	0,80	1,00	1,00	1,06	1,18	1,13	1,48	1,13	1,31
PRCWP (9-E1/E3-R/T)	360,5	385,5	0,60	0,57	0,89	0,94	1,12	1,01	1,87	1,77	1,82
PRCWP (10-L1/L3-T)	323	344	0,38	0,37	0,57	0,60	0,59	0,65	1,53	1,77	1,65
PRCWP (10-L1/L3-T/R)	291	320	0,48	0,55	0,80	0,70	0,89	0,88	1,85	1,60	1,73
PRCWP (11-L1-T)	550,5	793,5	0,37	0,37	0,68	0,60	0,73	0,65	1,95	1,78	1,87
PRCWP (11-L1-T/R)	462,5	1005	0,27	0,32	0,38	0,36	-	-	-	-	-
PRCWP (12-E1-T)	656	763,5	0,49	0,35	0,70	0,48	0,76	0,70	1,55	2,01	1,78
PRCWP (12-E1-T/R)	355	1008	0,38	0,39	0,49	0,49	-	-	-	-	-

Table 3.2 **-** Load bearing capacity and failure drift results.

Specimen notation	Peak force (kN)		Peak force (%)		Failure drift (%)		Failure drift (%)	
	+	-	+	-	+	-	+	-
PRCWP (7-E1-T)	858	723	100	100	0,73	0,79	100	100
PRCWP (7-E1-T/R)	669,5	698	78	96,5	0,97	1,08	133	137
PRCWP (8-E3-T)	207,5	247,5	100	100	1,17	1,08	100	100
PRCWP (8-E3-T/R)	229,5	249,5	111	101	1,18	1,13	101	105
PRCWP (9-E1/E3-R/T)	360,5	385,5	-	-	1,12	1,01	-	-
PRCWP (10-L1/L3-T)	323	344	100	100	0,59	0,65	100	100
PRCWP (10-L1/L3-T/R)	291	320	90	93	0,89	0,88	151	135
PRCWP (11-L1-T)	550,5	793,5	100	100	0,73	0,65	100	100
PRCWP (11-L1-T/R)	462,5	1005	84	127	-	-	-	-
PRCWP (12-E1-T)	656	763,5	100	100	0,70	0,76	100	100
PRCWP (12-E1-T/R)	355	1008	54	132	-	-	-	-

Table 3.3 – Results depending on the peak force attained by (11-12) strengthened walls

Specimen notation	Peak force (kN)		Peak force (%)		Drift at peak force (%)	
	+	-	+	-	+	-
PRCWP (11-L1-T)	446	619,5	100	100	0,38	0,36
PRCWP (11-L1-T/R)	462,5	1005	104	162	0,38	0,36
PRCWP (12-E1-T)	579	763,5	100	100	0,49	0,48
PRCWP (12-E1-T/R)	355	1008	61	132	0,49	0,49

3.2.1 Force-drift ratio hysteresis loops

The behaviour of the tested wall panels is shown as load–drift ratio hysteresis loops in Fig. 3.7 for the reference specimens, in Fig. 3.8 for the strengthened specimens and in Fig. 3.9 the comparison of them, by overlapping the curves. Each hysteresis loop was composed of four branches, namely loading, unloading, opposite direction loading and opposite direction unloading, whereas each branch was delimited by two points: curve-to-horizontal axis intersection point (reloading point) and peak loading point (corresponding to the target displacement). Based on the obtained results given in Figure 3.7, it can be reported a significant reduction in lateral resistance of the specimens having large opening dimensions, namely PRCWP (8-E3-T) and PRCWP (10-L1/L3-T). The same conclusion was found for the strengthened specimens (Figure 3.8) regardless the rehabilitation strategy, the specimens having large opening dimensions, namely PRCWP (8-E3-T/R), PRCWP

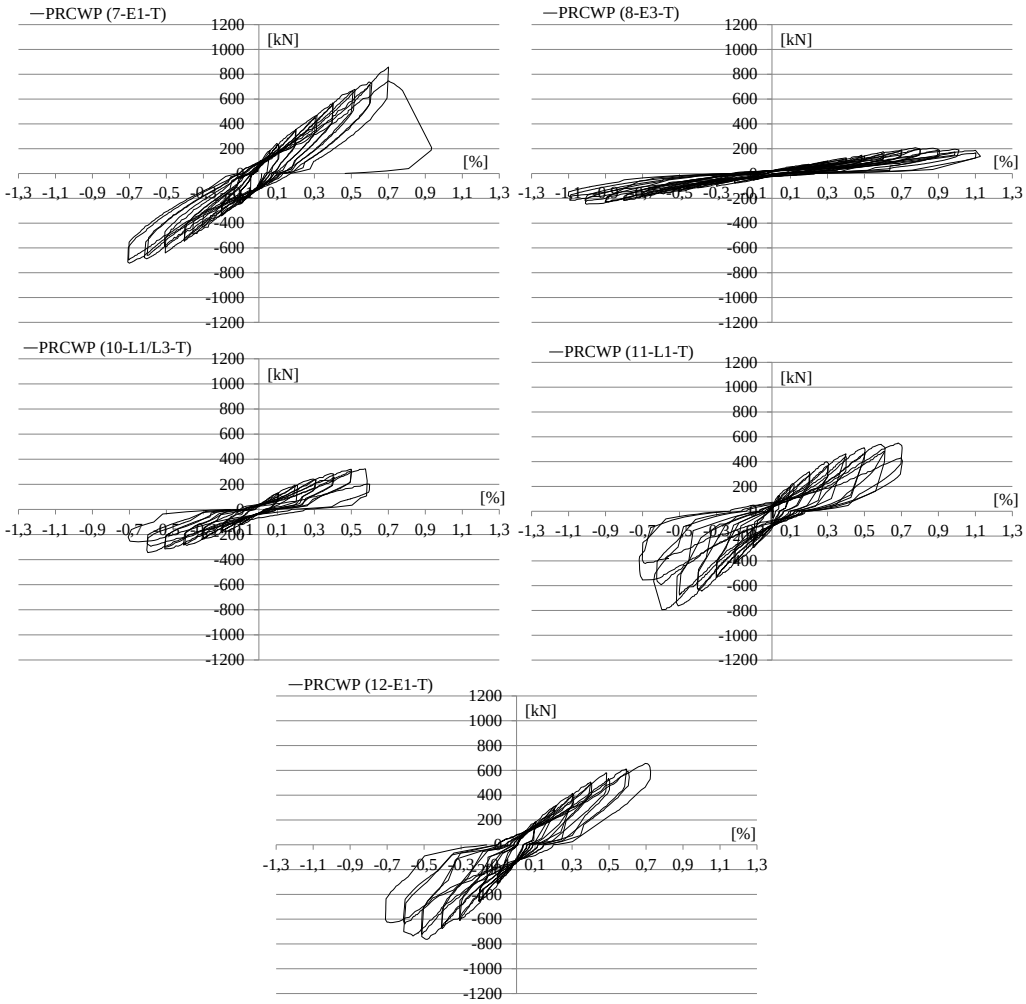

Figure 3.7 - Load-drift ratio hysteresis loops of the reference specimens

(9-E1/E3-R/T) and PRCWP (10-L1/L3-T/R) developed a lower lateral resistance. According to Figure 3.9, the load bearing capacity of the walls was restored through the rehabilitation strategies and increased in several cases, whereas the displacement capacity was higher for the strengthened specimens.

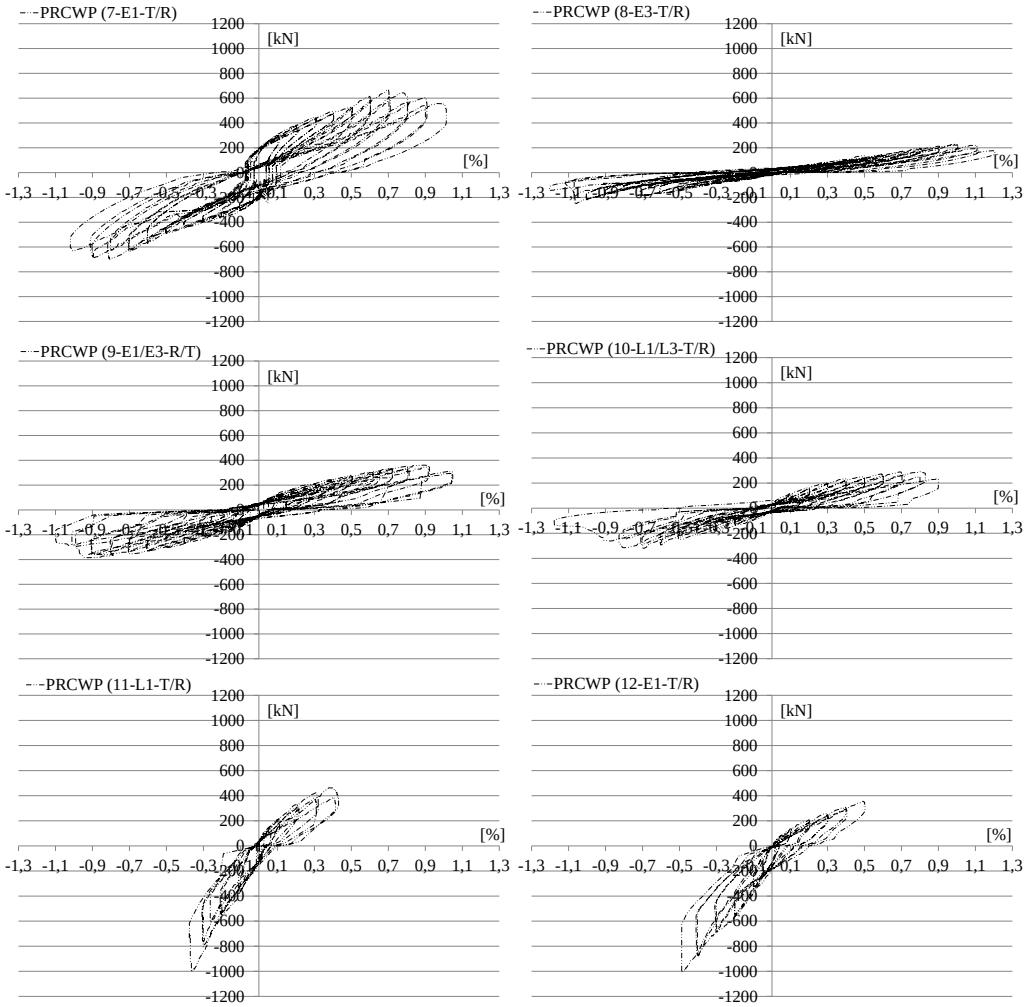

Figure 3.8 - Load-drift ratio hysteresis loops of the strengthened specimens

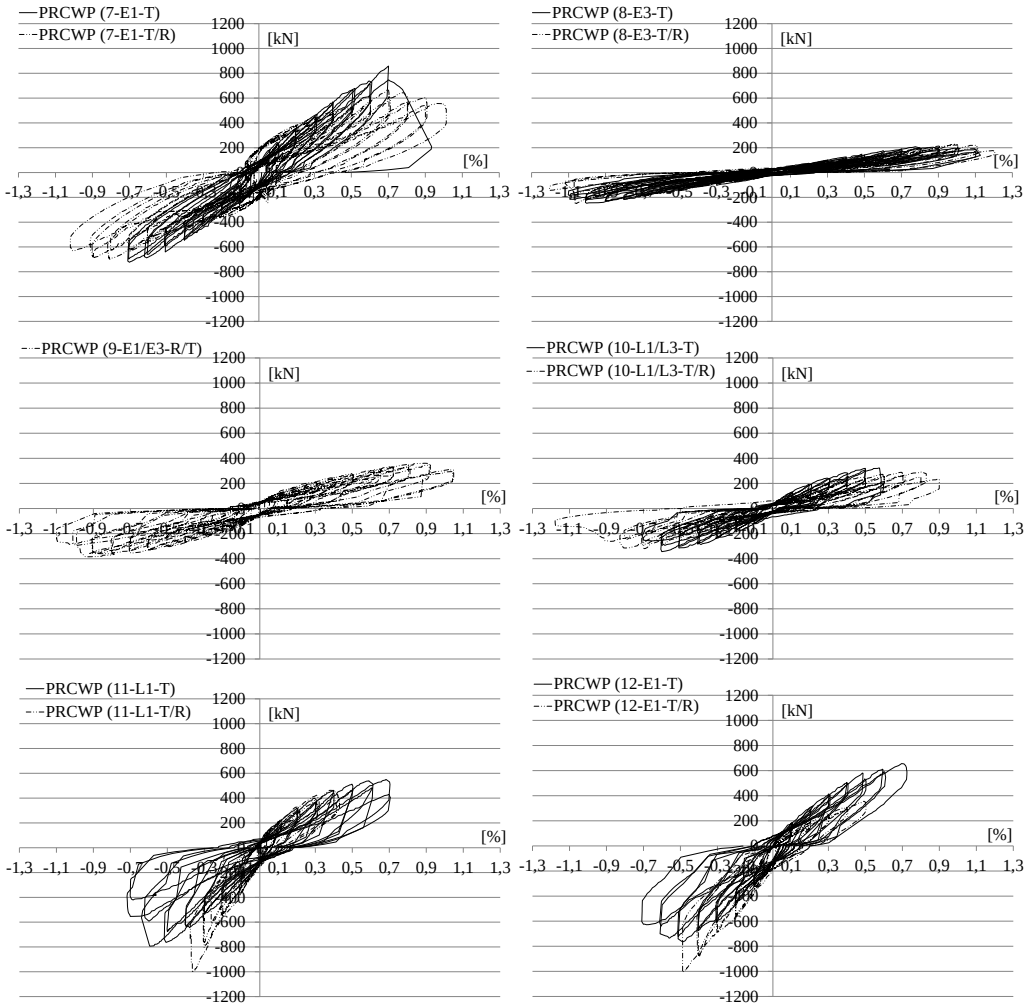

Figure 3.9 – Comparison of the load-drift ratio hysteresis loops for the tested walls

3.2.2 Force-drift ratio cyclic envelopes

During the experimental testing, for each drift level, two cycles were performed. Post-processing of the results in order to obtain the cyclic envelopes, requires the computation of the envelope curves in cycle 1 and 2.

These envelope curves were obtained by connecting the peak loading points through the consecutive drift levels. Then, the average cyclic envelope (denoted also "Envelope M2") can be obtained by calculating the arithmetic means between the two cycle envelope curves, by connecting the average peak loading points through each drift level.

The load–drift ratio cyclic envelopes are presented in Fig. 3.10 for the reference specimens, in Fig. 3.11 for the strengthened specimens and in Fig. 3.12 the comparison of them.

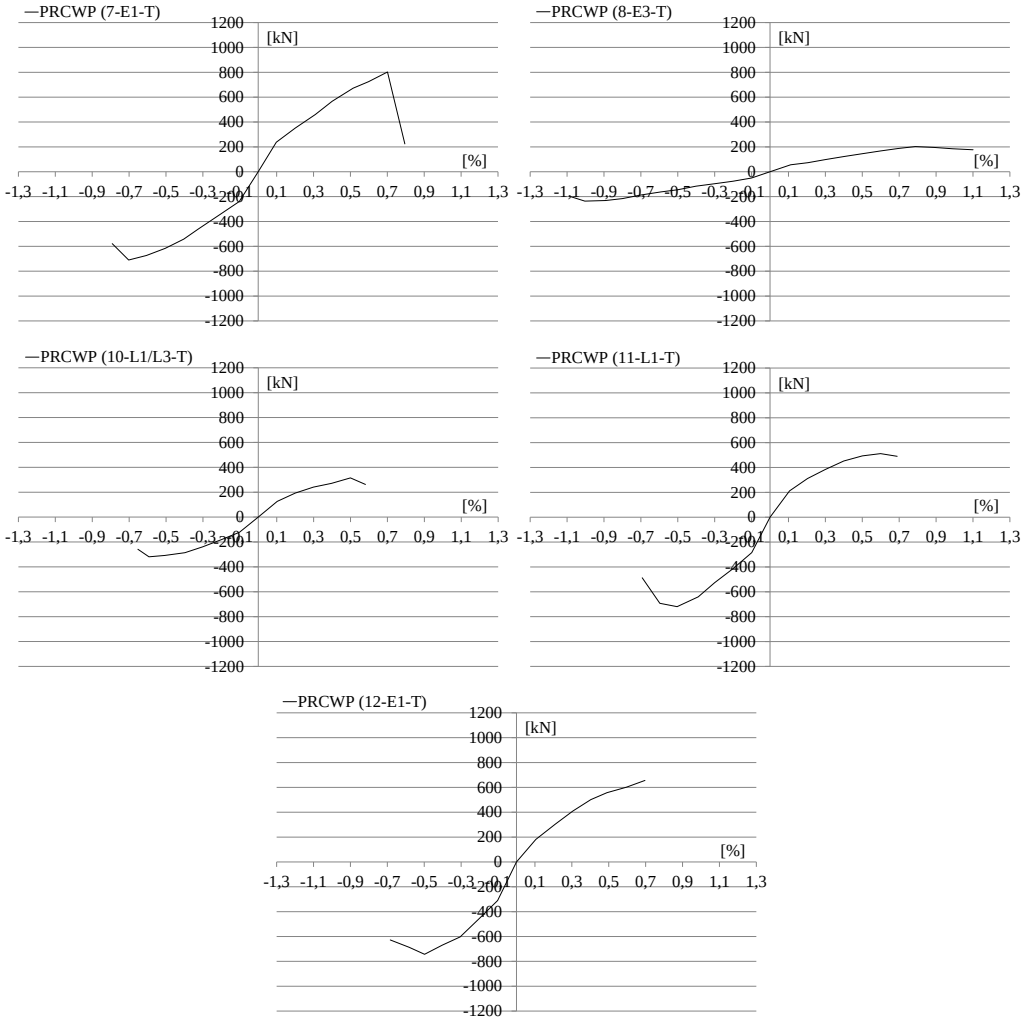

Figure 3.10 - Load-drift ratio cyclic envelopes of the reference specimens

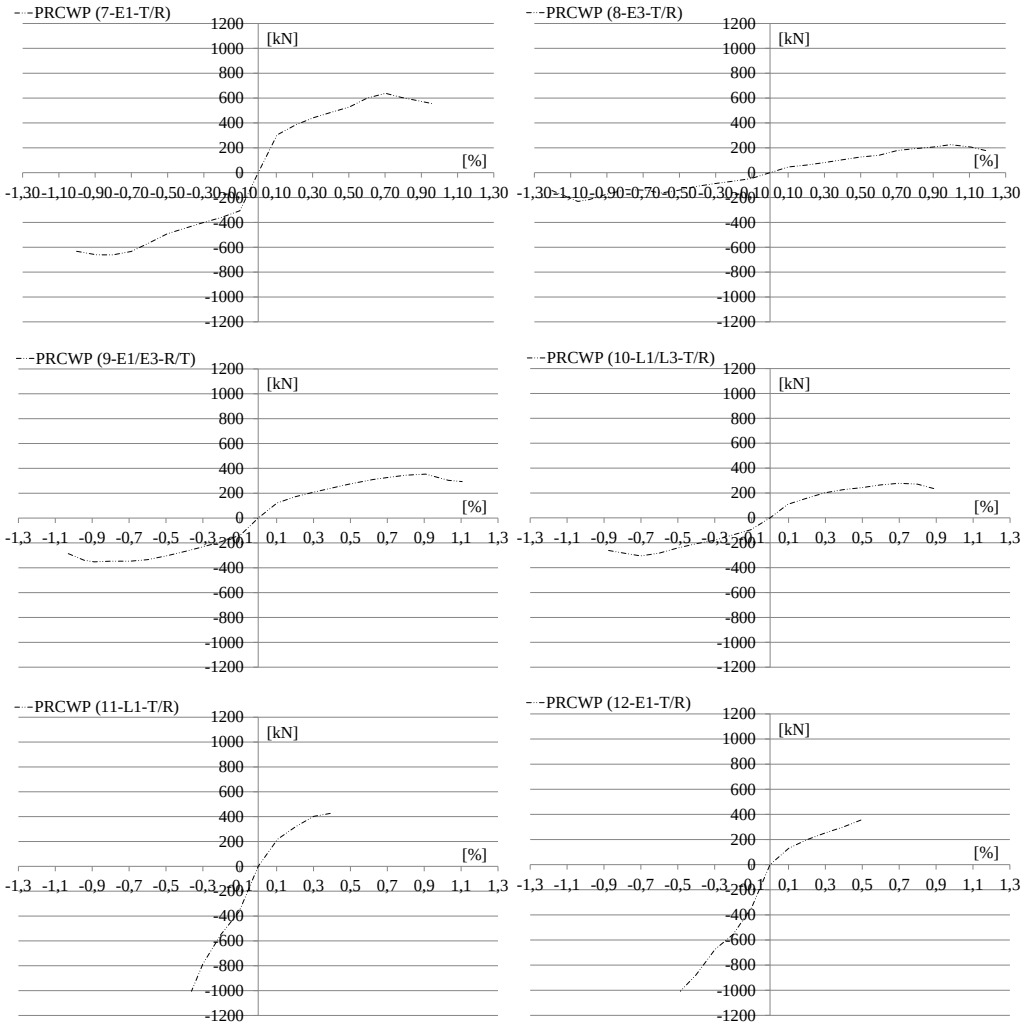

Figure 3.11 - Load-drift ratio cyclic envelopes of the strengthened specimens

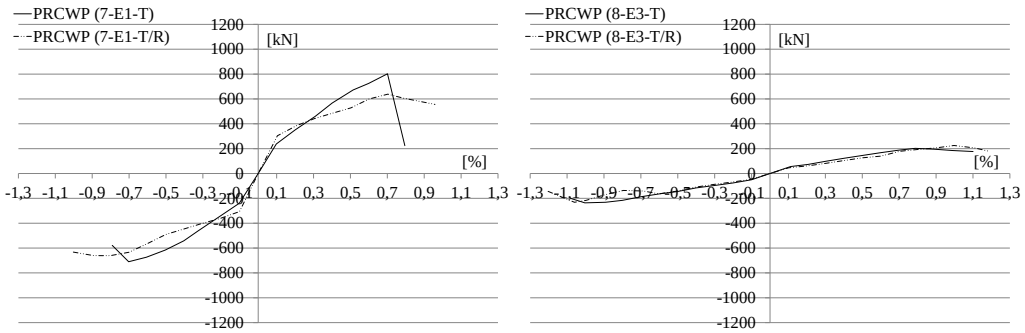

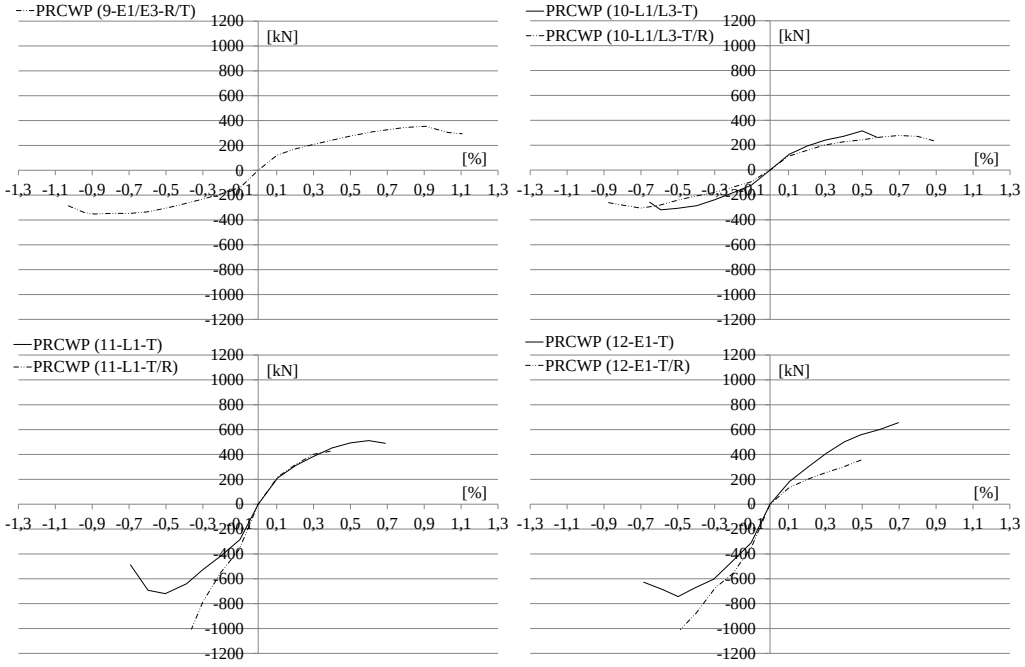

Figure 3.12 – Comparison of the load-drift ratio cyclic envelopes for the tested walls

3.2.3 Force-drift ratio monotonic envelopes

The monotonic force-drift envelope curves, denoted also „Envelope M1", were obtained from the average cyclic envelope (M2), by calculating the arithmetic means between the peak loading points (taken as absolute values) through each drift level. The load–drift ratio monotonic envelopes are presented in Fig. 3.13 for the reference specimens, in Fig. 3.14 for the strengthened specimens and in Fig. 3.15 the comparison of them.

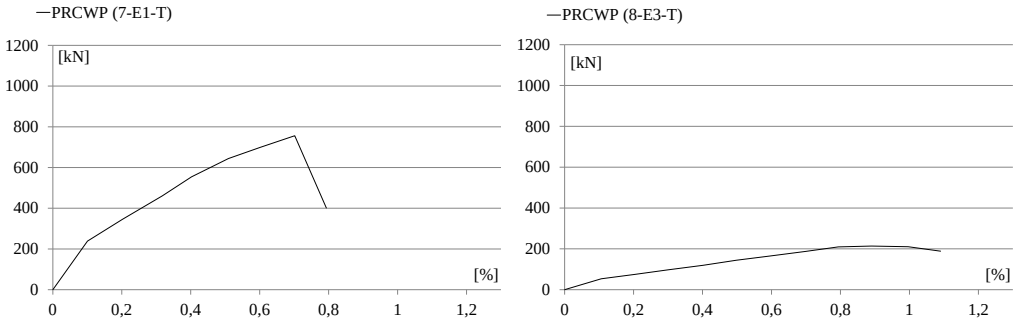

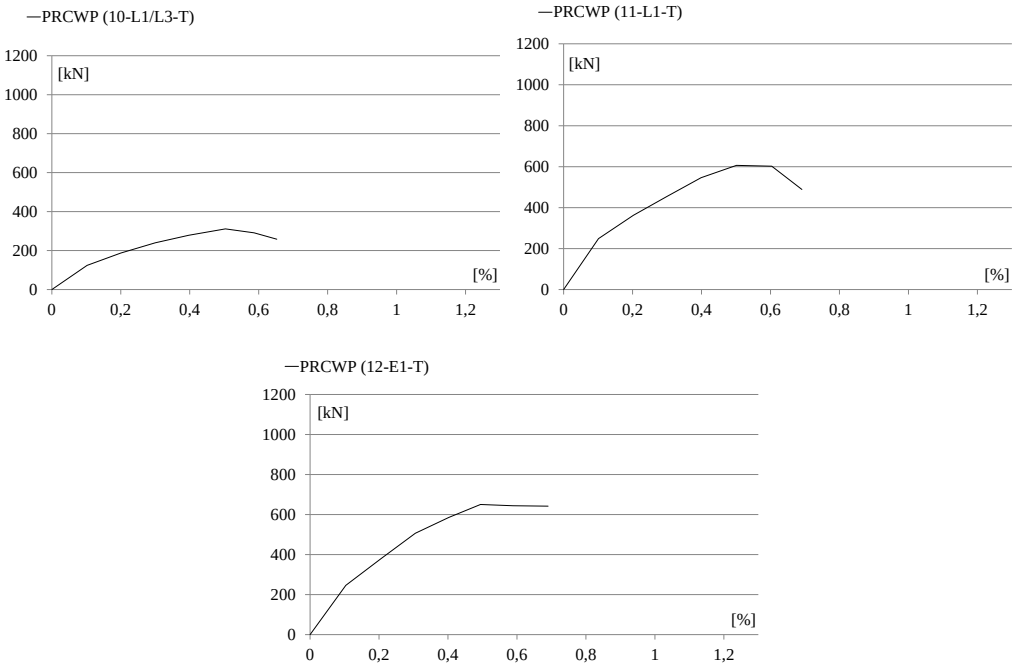

Figure 3.13 - Load-drift ratio monotonic envelopes of the reference specimens

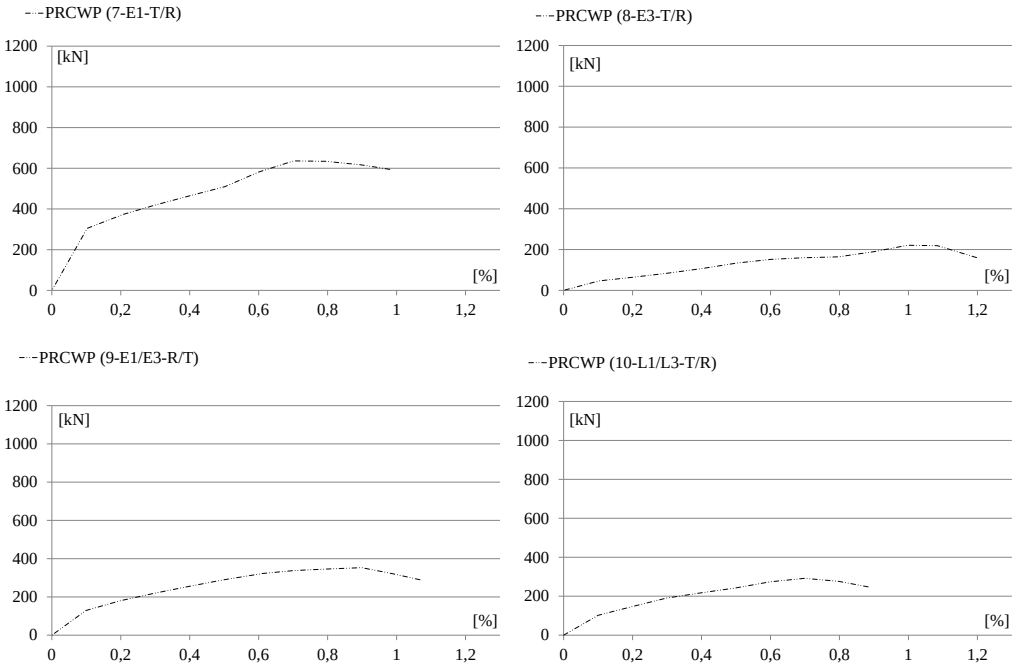

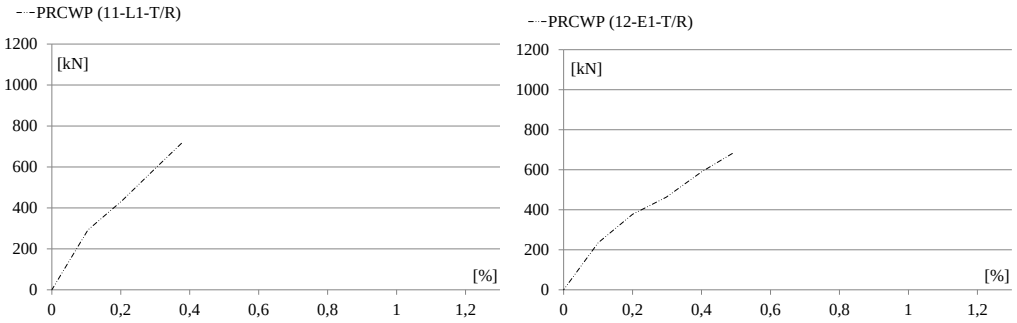

Figure 3.14 - Load-drift ratio monotonic envelopes of the strengthened specimens

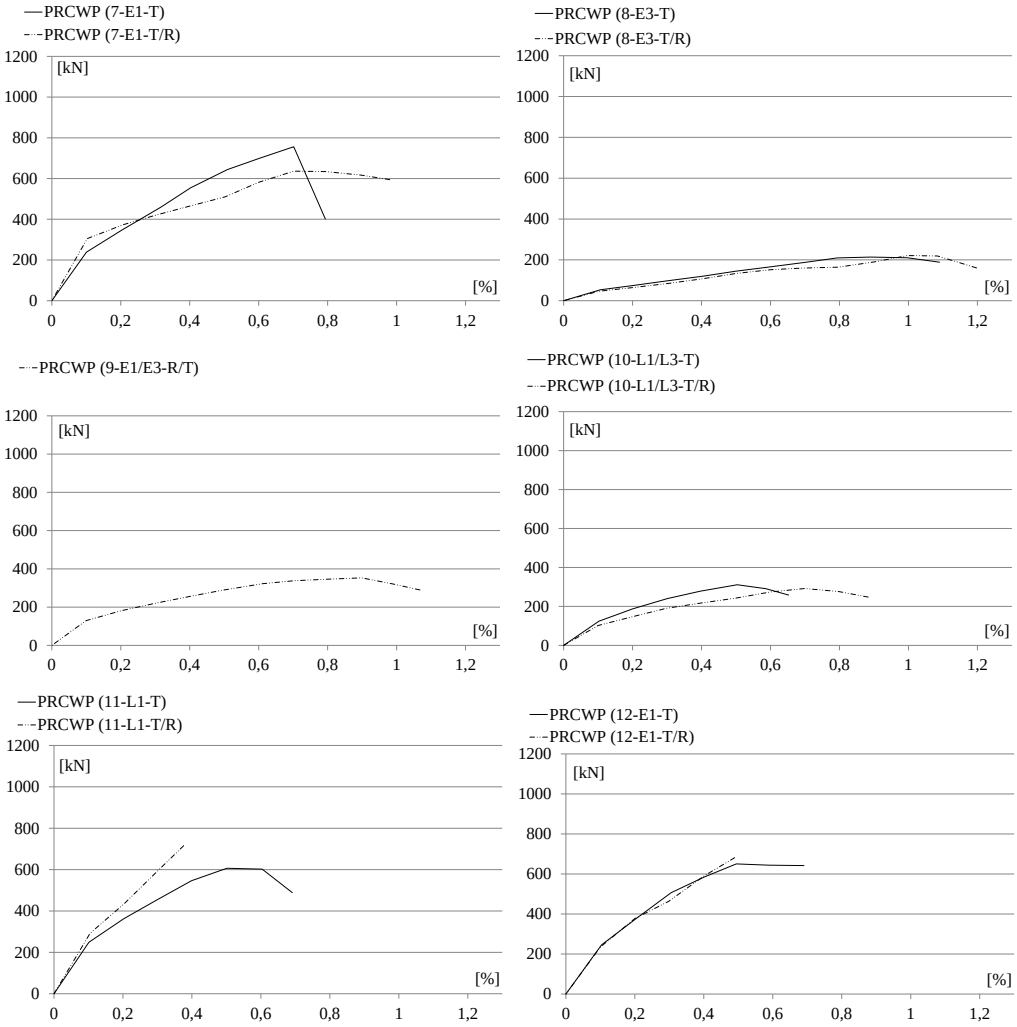

Figure 3.15 – Comparison of the load-drift ratio monotonic envelopes for the tested specimens

3.2.4 Force-drift ratio backbone envelopes

A number of two concept types of tri-linear backbone curves were adopted by the author in the current thesis, denoted backbone type 1 and backbone type 2. For the construction of the backbone type 1, three load-displacement points were selected, namely the cracking point (at the occurrence of the first inclined crack), the peak load point (corresponding to the maximum lateral force) and the failure point (when the specimen lost 20% of its load bearing capacity). For the construction of the backbone type 2, another set of three load-displacement points were considered, namely the yield point (at 0.85 of the maximum lateral load imposed), the peak load point (corresponding to the maximum lateral force) and the failure point (when the specimen lost 20% of its load bearing capacity). According to Figure 3.18, in most cases similar displacement values for the cracking point were found for the strengthened and reference specimens. Related to the yield point, considered at 0.85 of the maximum lateral load, also similar displacement values were found in most cases for the strengthened and reference walls.

The tri-linear backbone (type 1) curves are given in Fig. 3.16 for the reference specimens, in Fig. 3.17 for the strengthened specimens and in Fig. 3.18 the comparison of them, whereas the tri-linear backbone (type 2) curves are given in Fig. 3.19 for the reference specimens, in Fig. 3.20 for the strengthened specimens and in Fig. 3.21 the comparison of them.

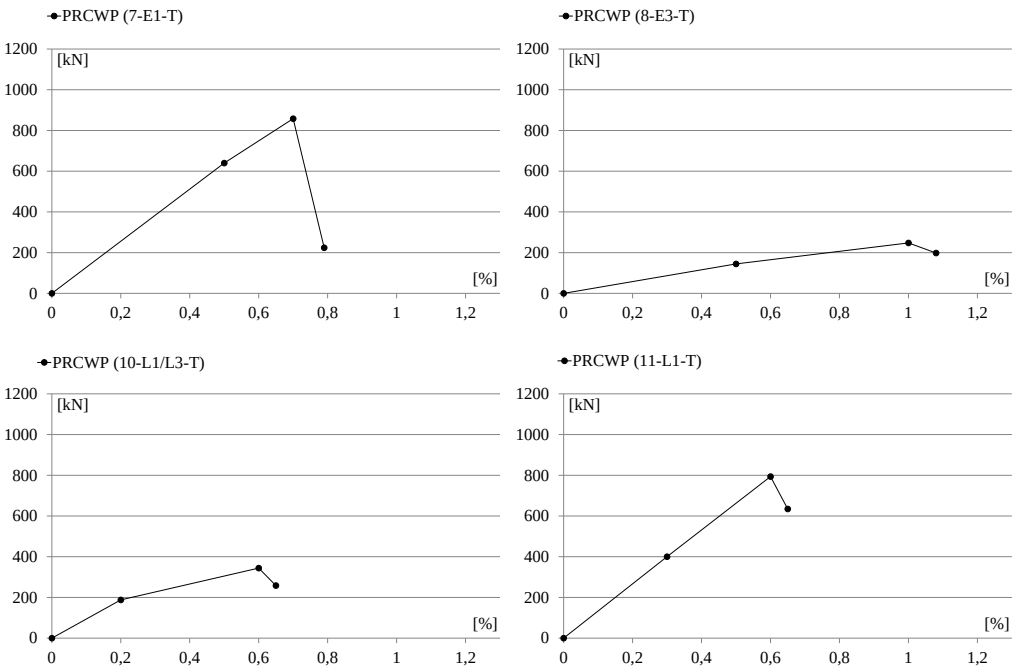

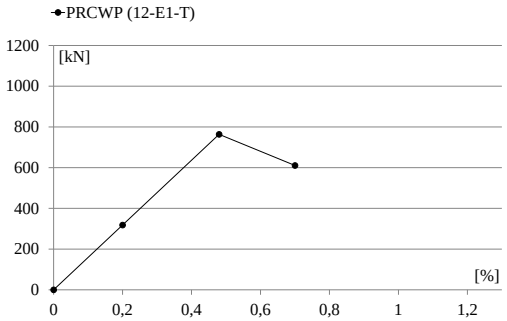

Figure 3.16 – Tri-linear backbone (type 1) curves of the reference specimens

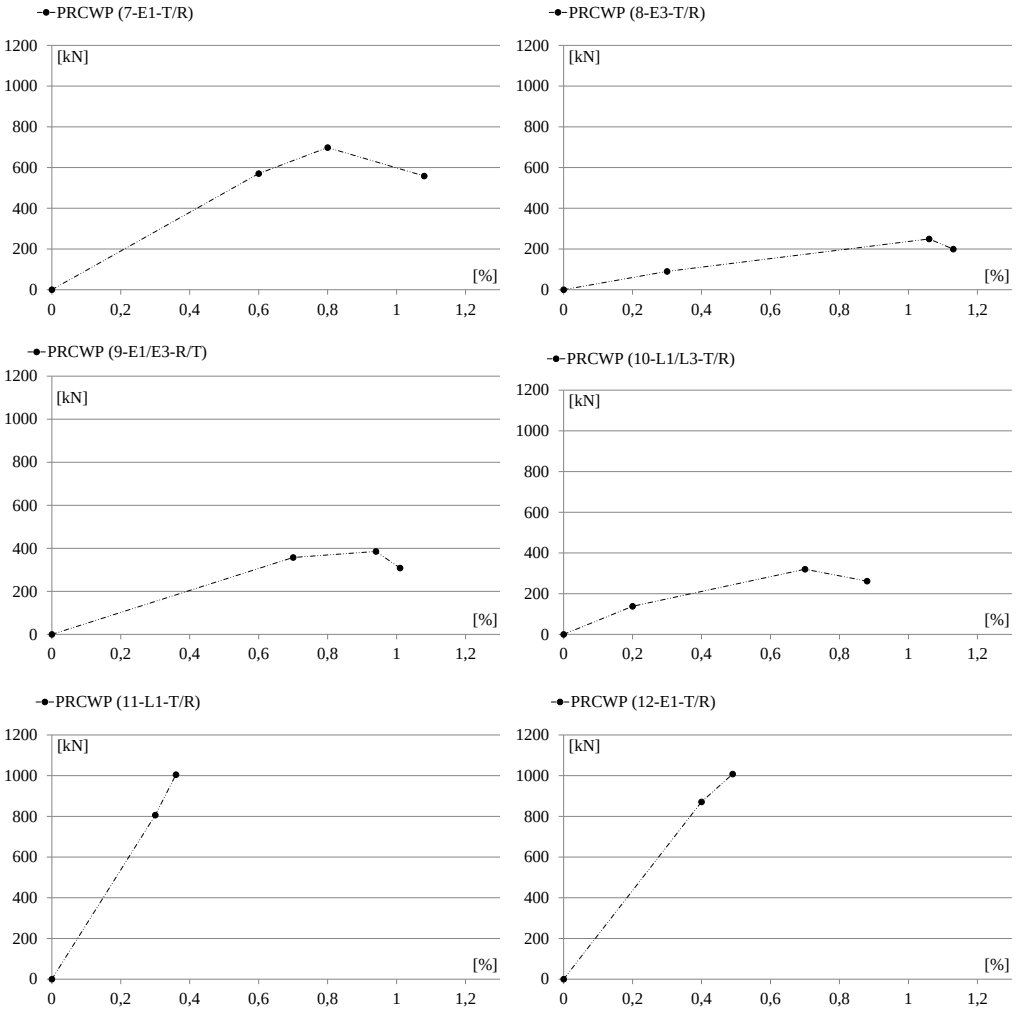

Figure 3.17 – Tri-linear backbone (type 1) curves of the strengthened specimens

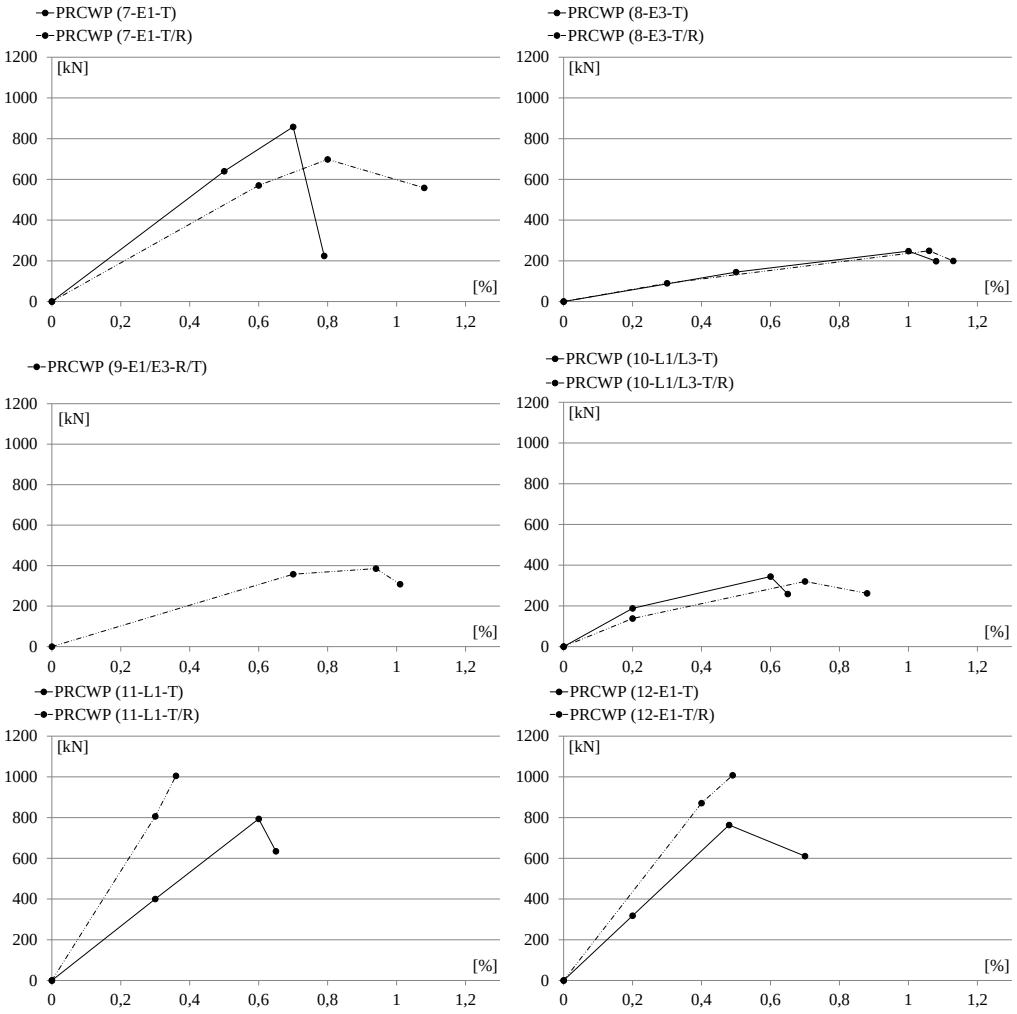

Figure 3.18 – Comparison of the tri-linear backbone (type 1) curves of the tested walls

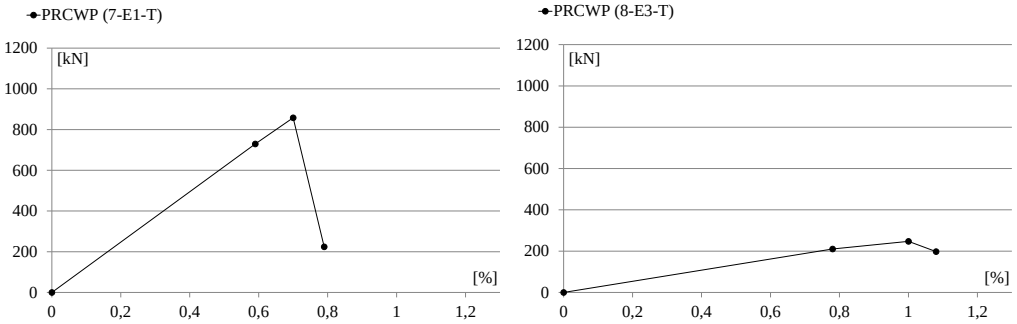

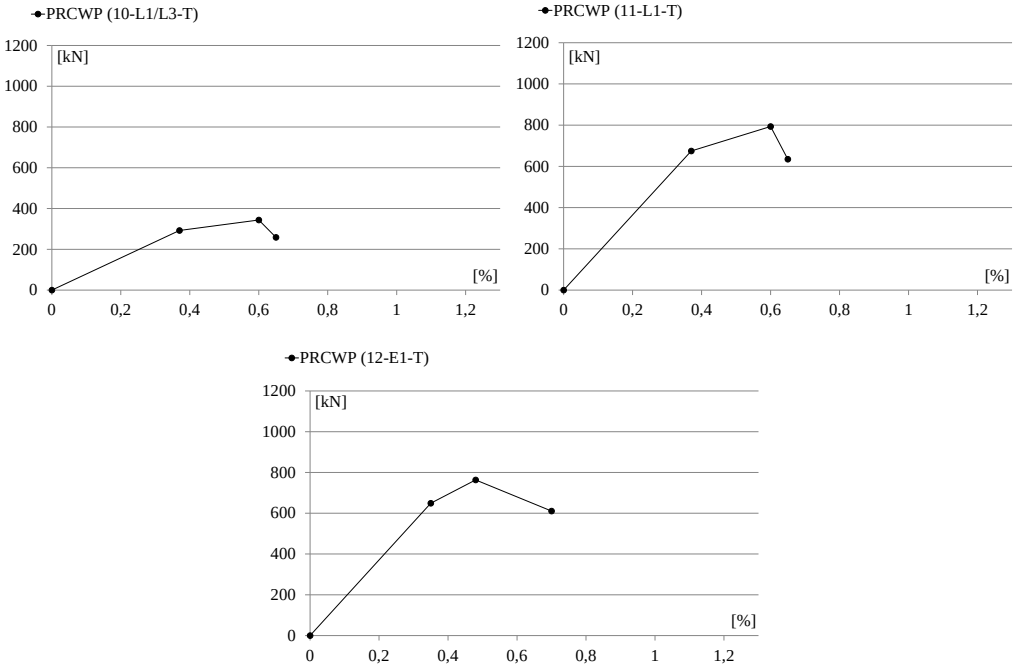

Figure 3.19 - Tri-linear backbone (type 2) curves of the reference specimens

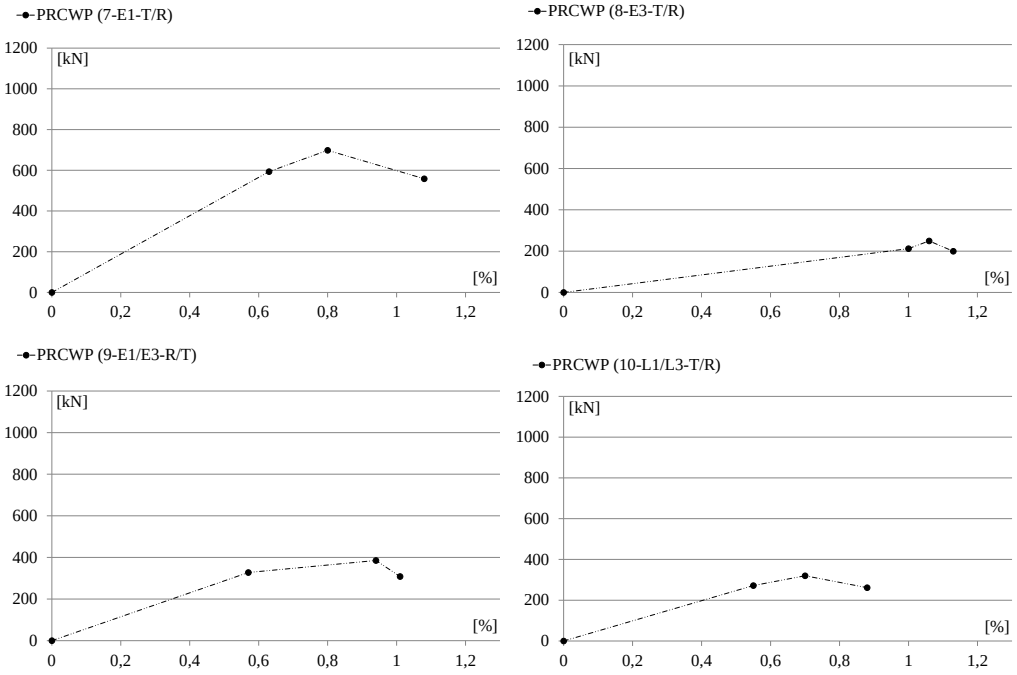

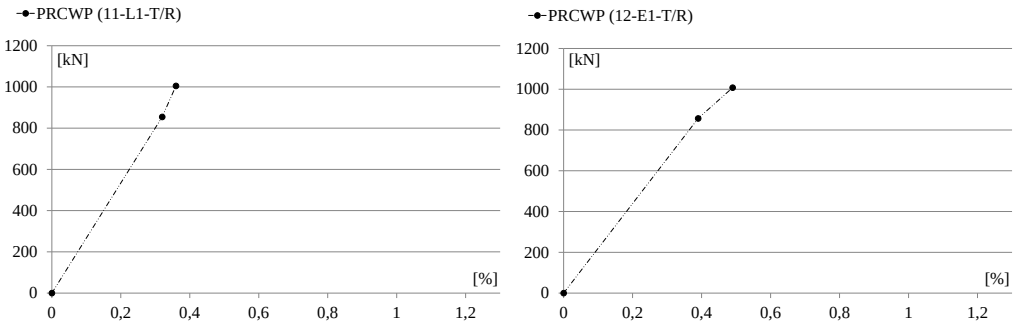

Figure 3.20 - Tri-linear backbone (type 2) curves of the strengthened specimens

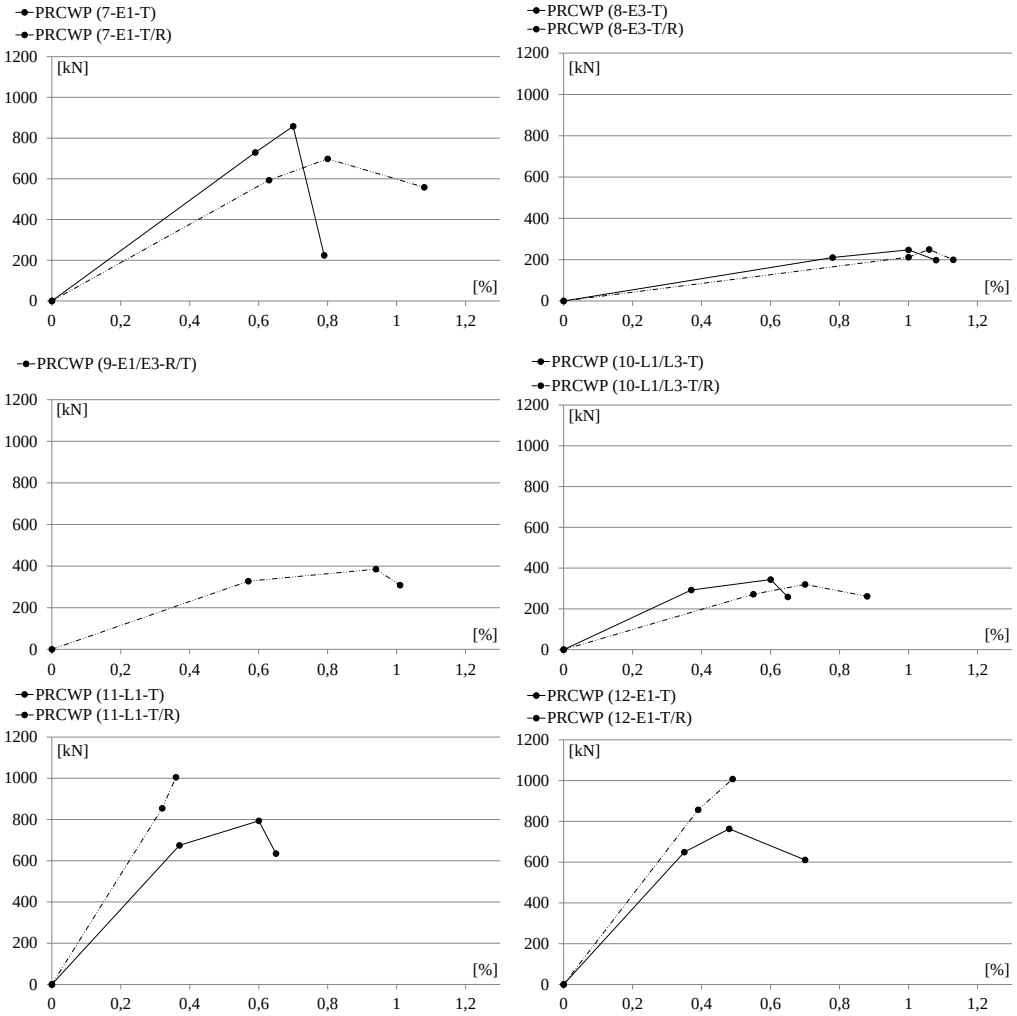

Figure 3.21 – Comparison of the tri-linear backbone (type 2) curves of the tested walls

3.2.5 Strength analysis

The shear strength of the five unstrengthened wall specimens is represented in Figure 3.22 a) as absolute values and in Figure 3.22 b) as normalized to the highest strength obtained, namely corresponding to PRCWP (7-E1-T). According to the shear strength histogram, the strength ranged from 247.5 kN to 858 kN. Based on the obtained results it is clear that the specimens having large opening dimensions developed lower lateral resistance. Comparing the shear strength results obtained for the specimens with narrow door opening and small window opening, similar values were found. Taking into account the different class of concrete used for the specimens with narrow door opening and small window opening, and the opening type which involves in the case of the window opening the use of the parapet, these two factors appear not to influence the maximum lateral load resisted by the wall specimen. The shear strength of the six strengthened wall specimens is shown in Figure 3.23 a) as absolute values and in Figure 3.23 b) as normalized to the highest strength obtained, namely corresponding to PRCWP (12-E1-T/R). According to the shear strength histogram, the strength ranged from 249.5 kN to 1008 kN. It is clear again, no matter the strengthening strategy used, that the specimens having large opening dimensions developed lower lateral resistance. Comparing the shear strength results obtained for the specimen with narrow door opening, namely PRCWP (12-E1-T/R) and small window opening, namely PRCWP (11-L1-T/R), similar values were found. Taking into account the different class of concrete, strengthening strategy used and the presence of the parapet in one case, these factors appear not to influence the maximum lateral load resisted by the specimen (with the mention that it is not the maximum lateral load resisted by the specimens (due to the encountered constraints), but the maximum lateral load that could be measured). Comparing the results obtained for PRCWP (7-E1-T/R) and PRCWP (12-E1-T/R), two factors are considered important for the difference in shear strength obtained, namely the contribution of NSM-CFRP strategy versus the contribution of EBR-CFRP strategy, and the high level of damage supported by PRCWP (7-E1-T). The shear strength of the eleven tested wall specimens is shown in Figure 3.24 a) as absolute values and in Figure 3.24 b) as normalized to the highest strength obtained. According to Figure 3.24, the load bearing capacity of the walls was restored through the rehabilitation strategies considered and increased in several cases.

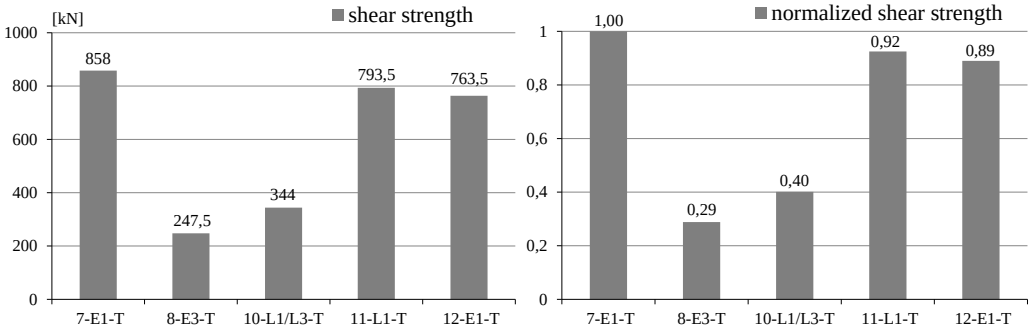

Figure 3.22 – The shear strength of the unstrengthened specimens

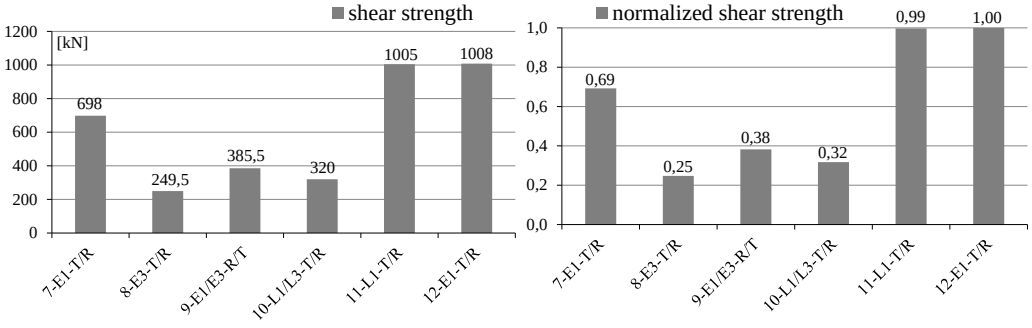

Figure 3.23 – The shear strength of the stregthened specimens

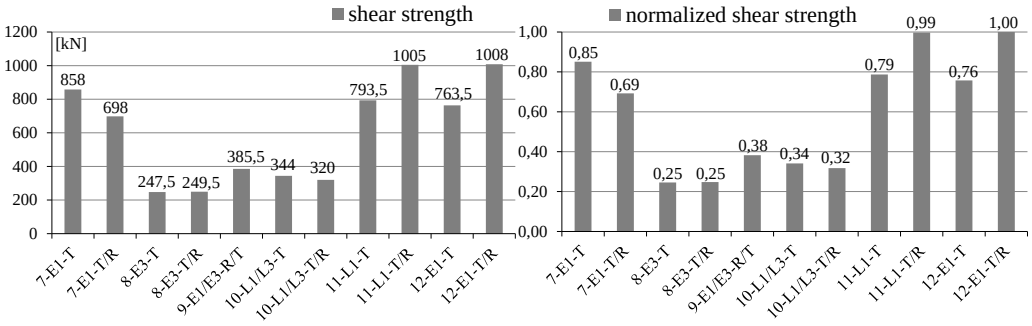

Figure 3.24 – The shear strength of the tested wall specimens

3.2.6 Displacement analysis

The drift at failure of the five unstrengthened wall specimens is represented in Figure 3.25 a) as absolute values and in Figure 3.25 b) as normalized to the highest drift at failure obtained, namely corresponding to PRCWP (8-E3-T). According to the drift at failure histogram, the drift ratio ranged from 0.65 % to 1.17 %. The drift at failure of six strengthened wall specimens is represented in Figure 3.26 a) as absolute values and in Figure 3.26 b) as normalized to the highest drift at failure obtained, namely corresponding to PRCWP (8-E3-T/R). According to the drift at failure histogram, the drift ratio ranged from *0.40 % to 1.18 %. In the case of PRCWP (11-L1-T/R) and PRCWP (12-E1-T/R), the symbol „*" was used in front of the value, meaning here that it is the maximum recorded drift (due to the already mentioned constraints). Similar drift at failure values were obtained for the unstrengthened specimens having narrow door openings, small window opening and wide window opening. Higher displacement value was obtained for the unstrengthened specimen having wide door opening.

Comparing the results obtained for the narrow door and small window opening, again the presence of the parapet does not influence much on the drift at failure. But, comparing the unstrengthened specimens having wide door opening and wide window opening, it appears that here the presence of parapet prevents the gain in displacement by not letting the specimen act like a frame. Related to the strengthened specimens, similar values of the drift at failure were obtained for

PRCWP (7-E1-T/R), PRCWP (8-E3-T/R) and PRCWP (9-E1-E3-R/T). It should be taken into account here the presence of multiple factors involved, and still similar drift at failure values obtained. These factors are considered the difference in concrete class, opening type, steel reinforcement, strengthening strategy, high level of damage taken by PRCWP (7-E1-T), recommended level of damage for PRCWP (8-E3-T/R), namely when the specimen lost 20% of its load bearing capacity, and no damage supported by PRCWP (9-E1-E3-R/T). In the case of PRCWP (10-L1/L3-T/R), the author considers the low value of drift at failure affected by the inefficient anchorage system used for the TRM strengthening.

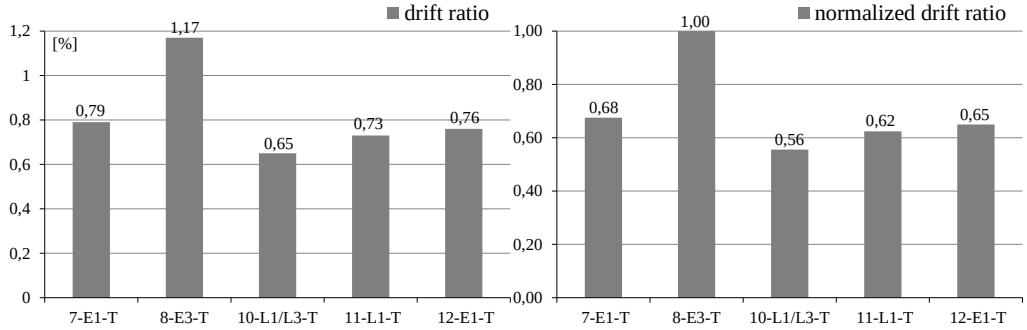

Figure 3.25 – The drift at failure of the unstrengthened wall specimens

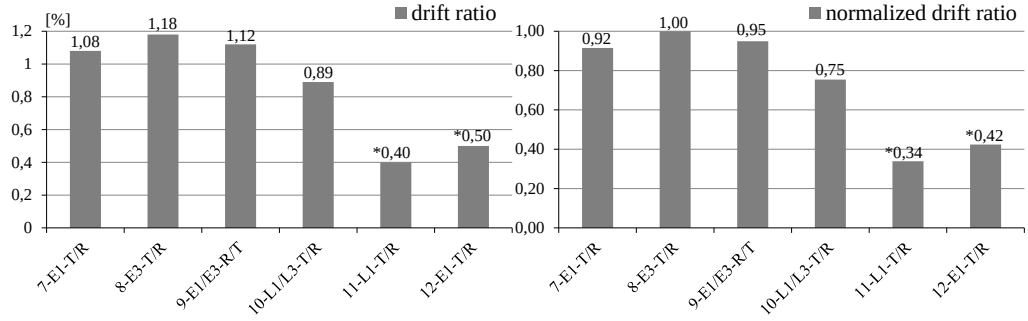

Figure 3.26 – The drift at failure of the strengthened wall specimens

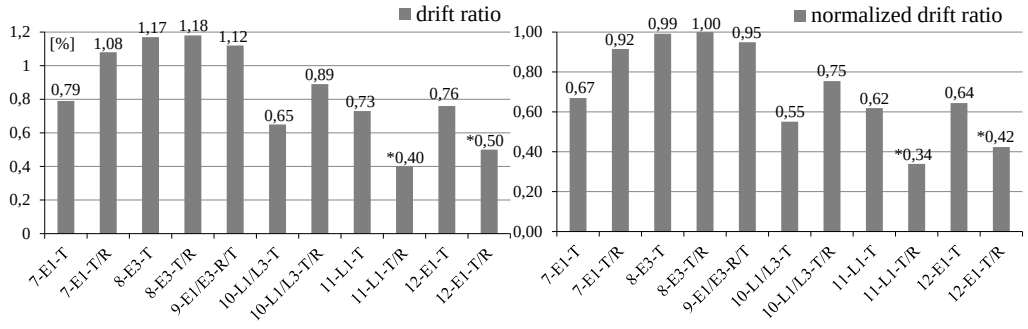

Figure 3.27 – The drift at failure of the tested wall specimens

3.2.7 Comparison

The load-drift ratio cyclic envelopes of the reference specimens are presented in Figure 3.28 a), whereas for the strengthened specimens are given in Figure 3.28 b). Figure 3.29 a) shows the monotonic load-drift ratio envelopes for the reference specimens, and Figure 3.29 b) for the strengthened specimens. In Figure 3.30 is represented the comparison of M2 and M1 envelopes for all the tested specimens involved in the current experimental program. The tri-linear backbone (type 1) curves of the reference specimens are shown in Figure 3.31 a), and in Figure 3.31 b) for the strengthened specimens.

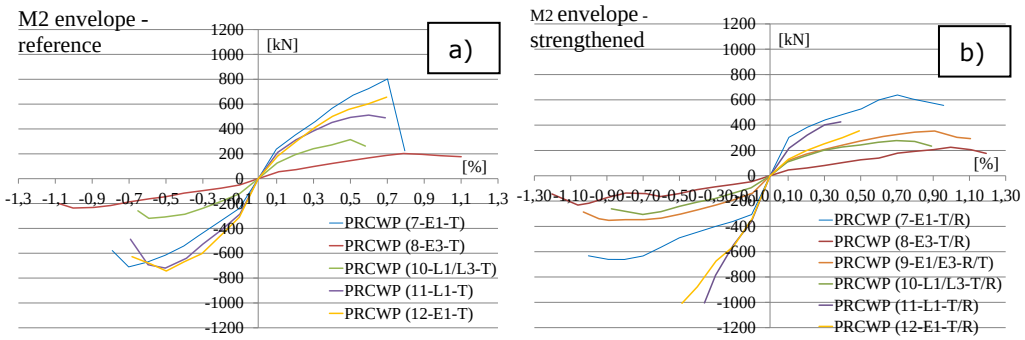

Figure 3.28 – Comparison of the M2 envelopes

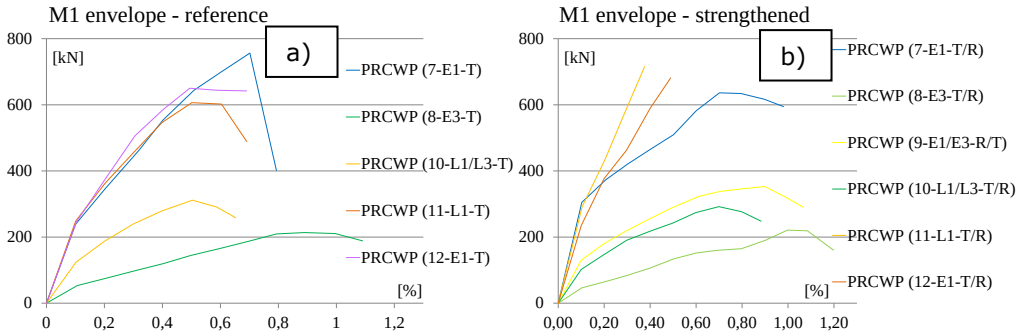

Figure 3.29 – Comparison of the M1 envelopes

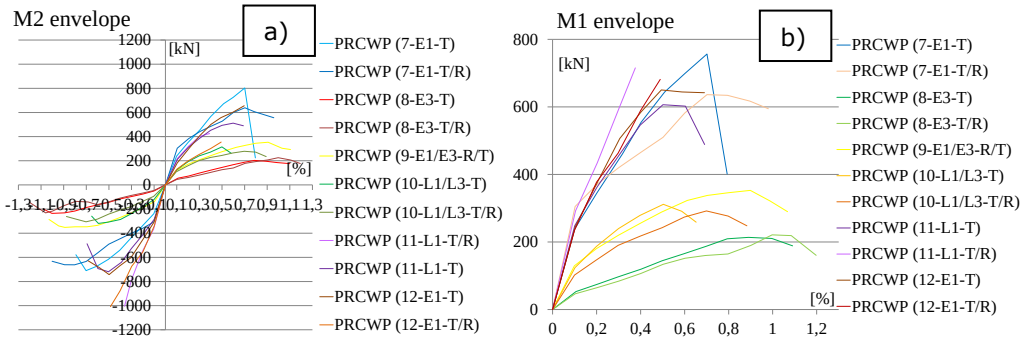

Figure 3.30 – Comparison of envelopes for the tested specimens

The tri-linear backbone (type 2) curves of the reference specimens are shown in Figure 3.32 a), and in Figure 3.32 b) for the strengthened specimens. In Figure 3.33 a) is represented the comparison of the backbone (type 1) curves and in Figure 3.33 b) the comparison of the backbone (type 2) curves for the tested specimens. The figures given in Section 3.2.7 are useful in order to rapidly depict important behavioural characteristics of the investigated wall specimens.

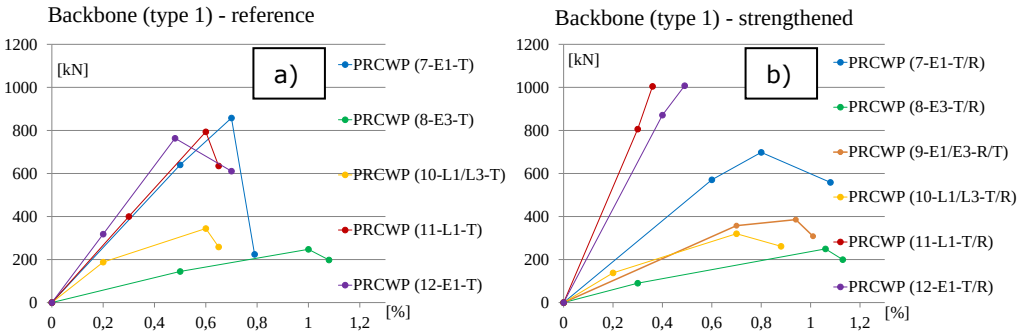

Figure 3.31 – Comparison of backbone (type 1) curves

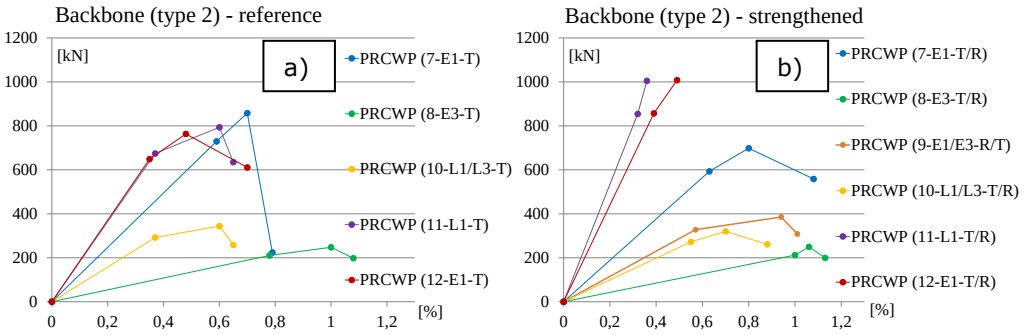

Figure 3.32 – Comparison of backbone (type 2) curves

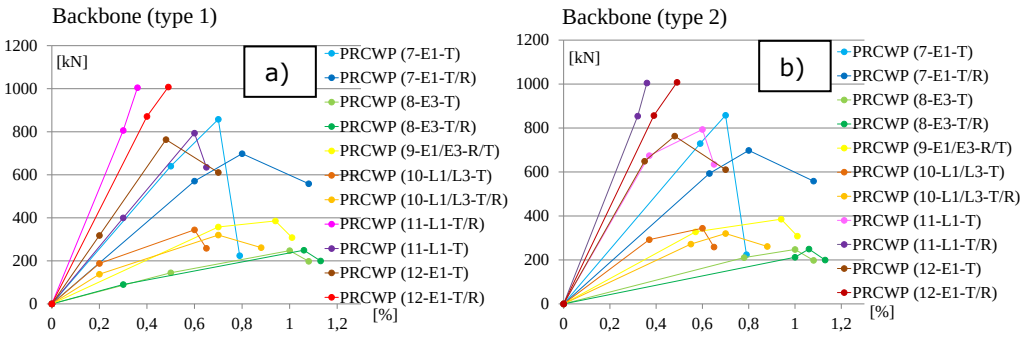

Figure 3.33 – Comparison of backbone curves

3.3 Energy dissipation

Based on the procedure used and reported in [8], the dissipated energy (E) was evaluated from the horizontal load versus lateral displacement hysteretic curves using the area bounded by hysteretic loop. Therefore, the cumulative energy dissipation was obtained by the continuous integration of the load–drift hysteretic response using the following equation:

$$CED_j = CED_{j-1} + \left(\delta_j - \delta_{j-1}\right) \cdot \left(\frac{V_j}{2} + \frac{V_{j-1}}{2}\right) \quad (3.1)$$

where CED is the cumulative energy dissipated; j is a point on the load–displacement curve; and δj and Vj are the corresponding drift and lateral load values.

The cumulative drift (CD) was calculated incrementally:

$$CD_j = CD_{j-1} + \left|\left(\delta_j - \delta_{j-1}\right)\right| \quad (3.2)$$

The cumulative drift ratio (CR) was obtained by:

$$CR_j\% = \left(\frac{CD_j}{2150}\right) \cdot 100 \quad (3.3)$$

Using the above mentioned relations, several representations for the dissipated energy of the specimens can now be computed. Figure 3.34 represents the cumulative energy dissipation versus drift ratio for the reference specimens, whereas in Figure 3.35 it is shown for the strengthened ones. The cumulative energy dissipation versus cumulative drift ratio is given in Figure 3.36 for the reference walls, and in Figure 3.37 for the strengthened specimens. It is clear according to the obtained results that the wall specimens having large opening dimensions dissipate less energy. In Figure 3.38 and Figure 3.39 is represented the energy dissipated by the specimens in each cycle. It can be noticed that in most cases the energy dissipation in the second cycle is lower compared to the first one.

In Figure 3.40 and Figure 3.41 are plotted the cumulative energy dissipation (per half-cycle), whereas in Figure 3.42 and Figure 3.43 are shown the cumulative energy dissipation (per cycle). Again, it can be noticed that the reference wall specimens with large openings developed the lowest contribution in energy dissipation, namely PRCWP (8-E3-T) and PRCWP (10-L1/L3-T). On the other hand, the specimens having large openings, exhibited an increased deformation capacity with respect to the panels with smaller openings, PRCWP (7-E1-T), (11-L1-T) and (12-E1-T). Higher energy dissipation was developed by the PRCWP (7, 10-11) strengthened specimens in comparison with their reference counterparts, whereas for PRCWP (8, 12) strengthened walls, the energy dissipation was similar with the reference ones. The PRCWP (9-E1/E3-R/T) wall specimen dissipated more energy with respect to PRCWP (8-E3-T/R), and less energy compared to PRCWP (7-E1-T/R) and (12-E1-T/R).

The average cumulative energy dissipation (among two cycles) is presented in Table 3.4. The cumulative energy dissipated ranged from (19,58 ÷ 53,94) for the reference specimens and from (14,69 ÷ 78,90) for the strengthened ones.

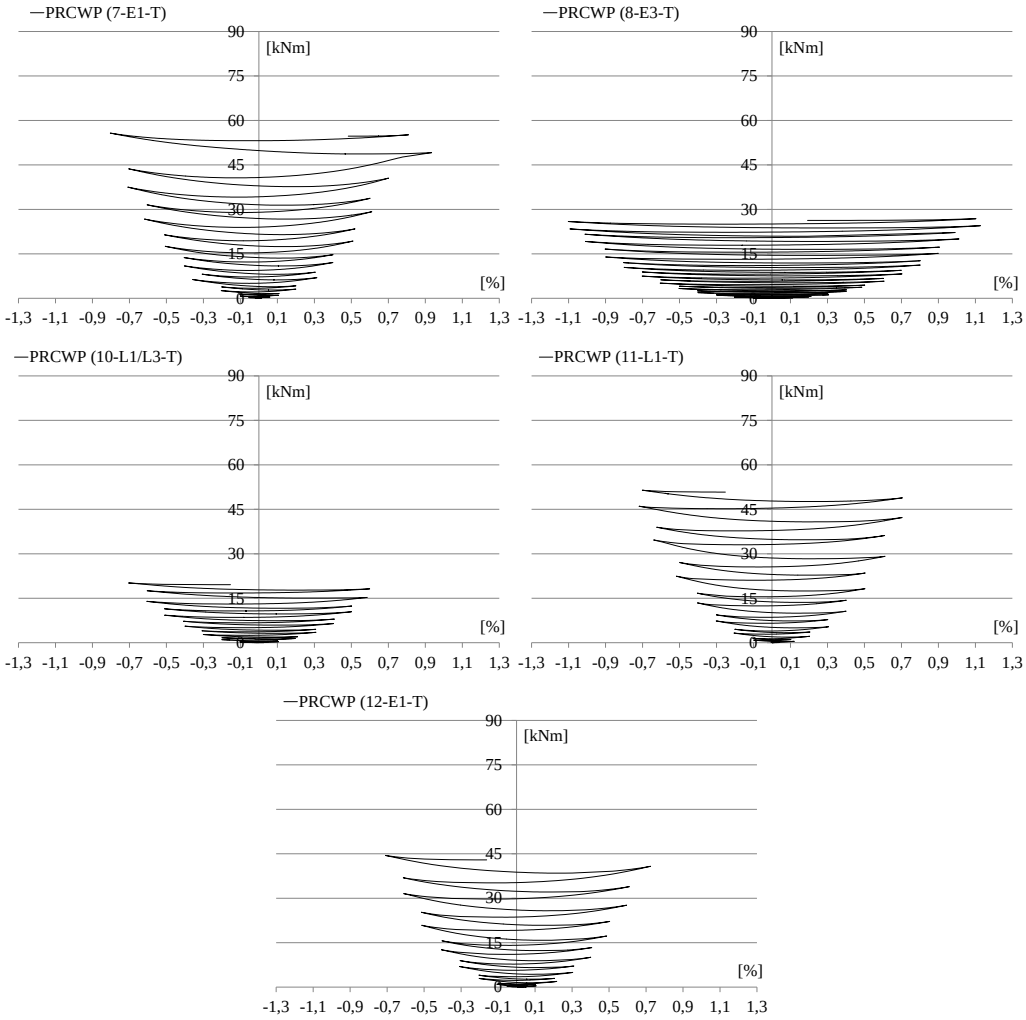

Figure 3.34 – Cumulative energy vs. drift ratio of the reference specimens

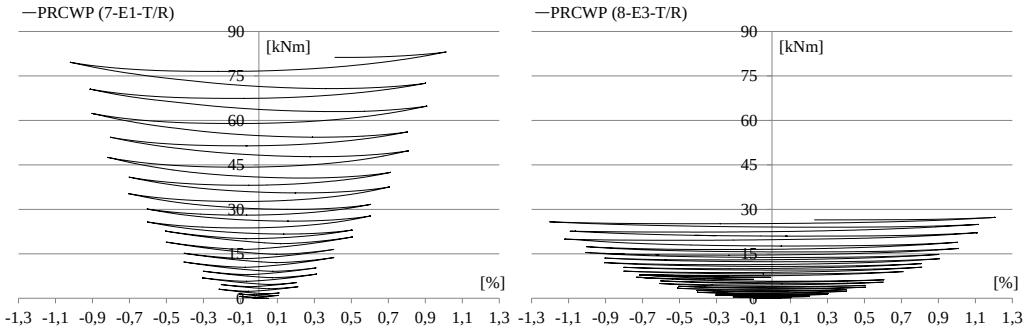

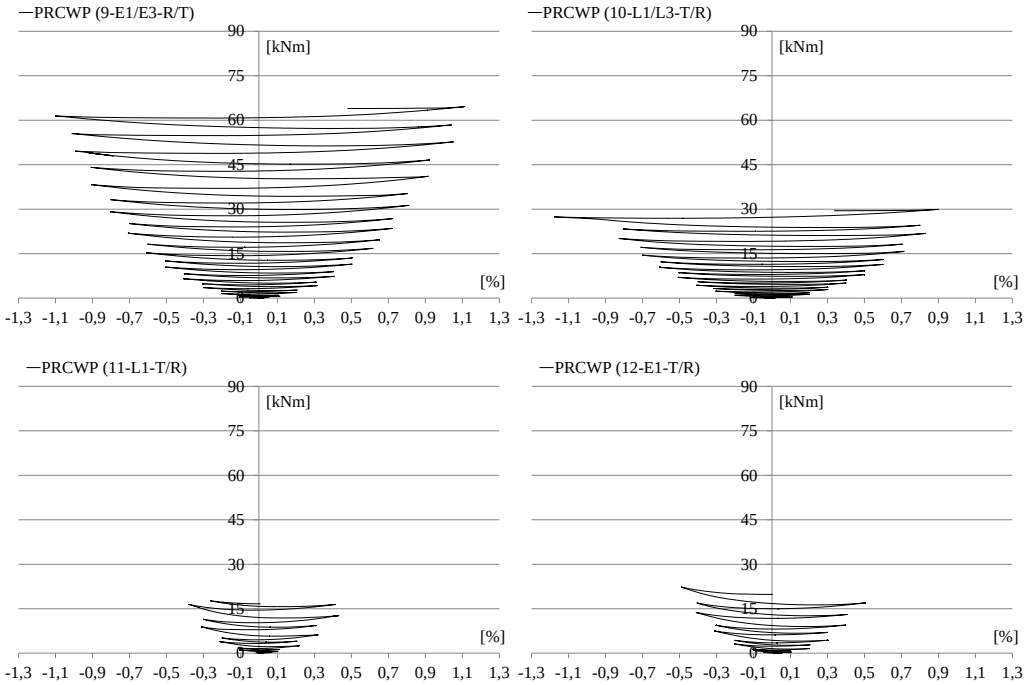

Figure 3.35 – Cumulative energy vs. drift ratio of the strengthened specimens

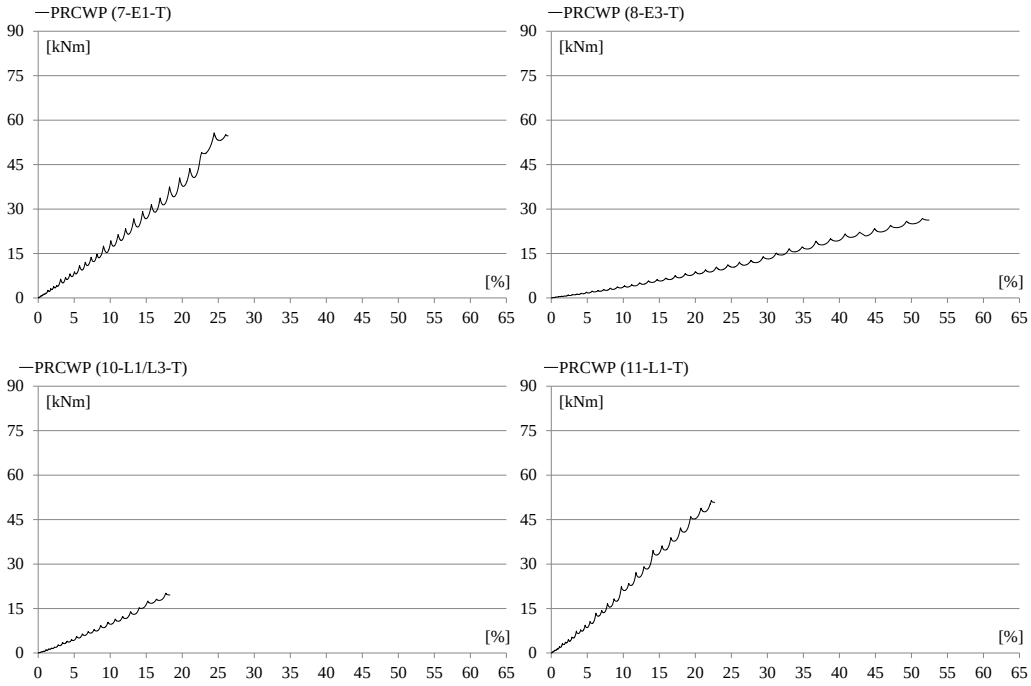

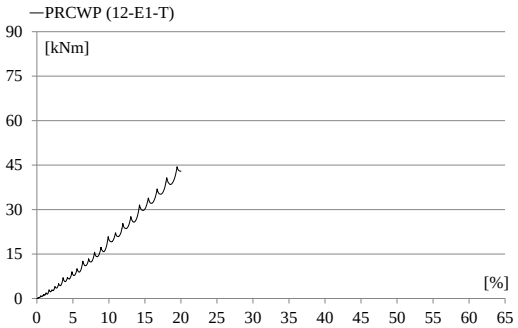

Figure 3.36 – Cumulative energy vs. cumulative drift ratio of the reference specimens

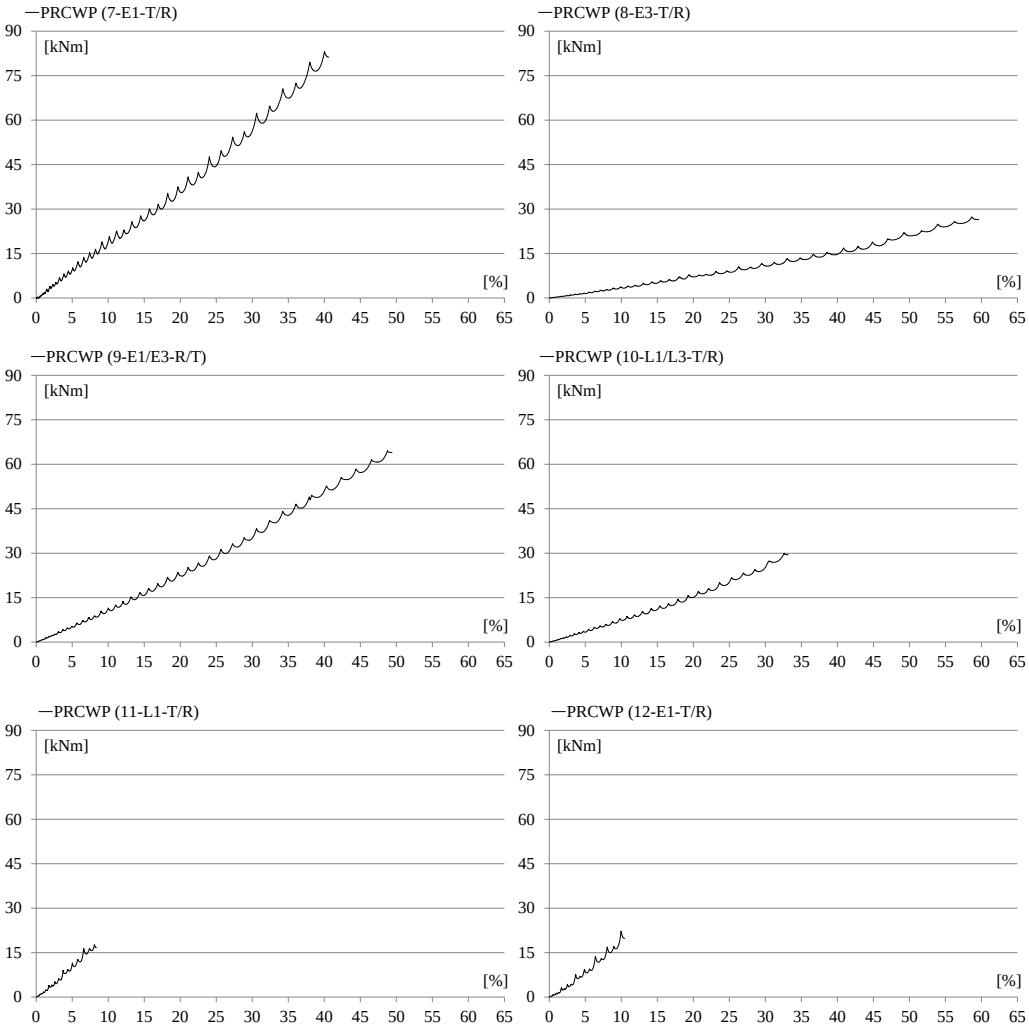

Figure 3.37 – Cumulative energy vs. cumulative drift ratio of the strengthened specimens

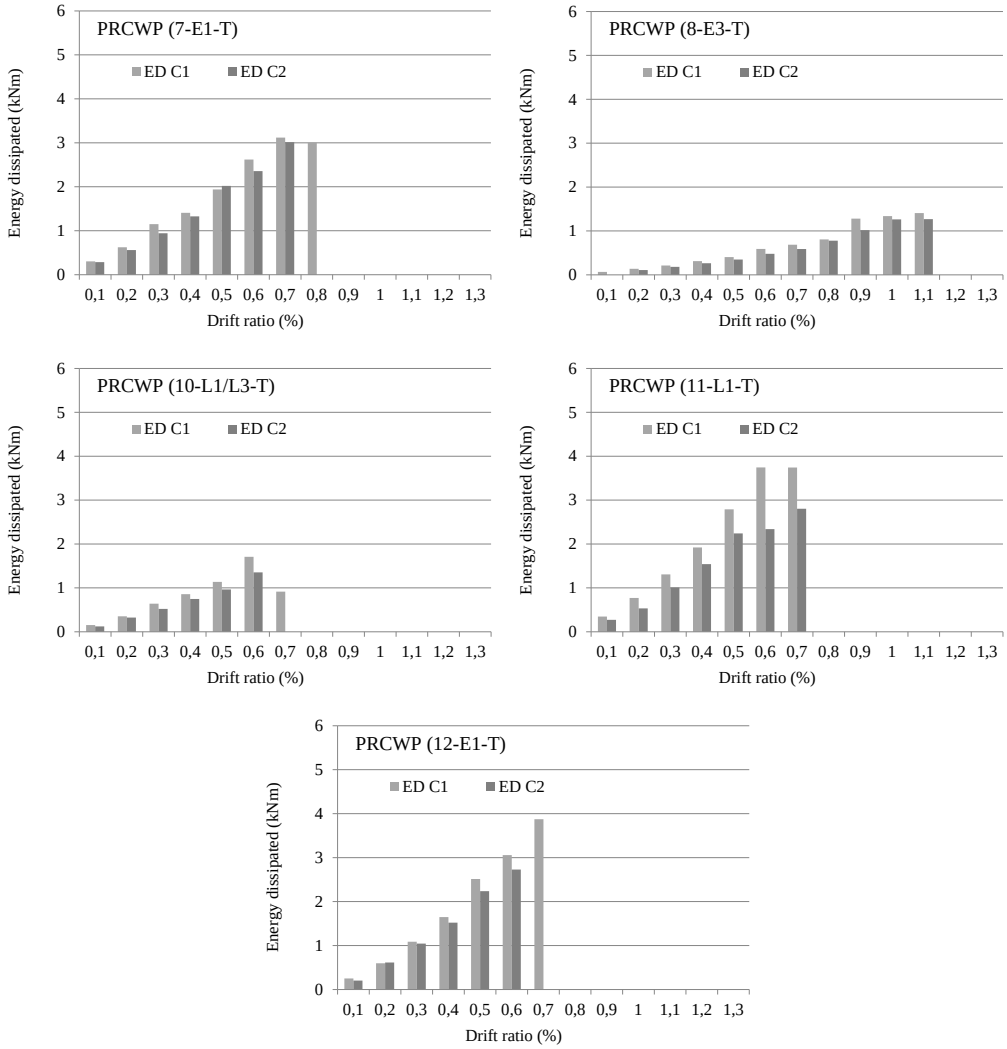

Figure 3.38 – Energy dissipation – reference specimens

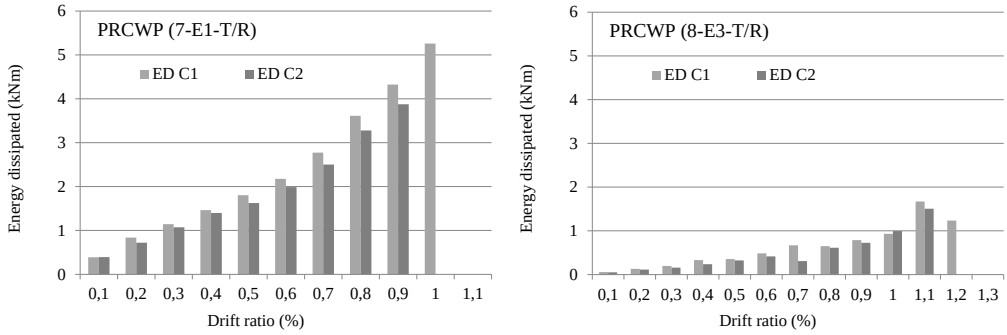

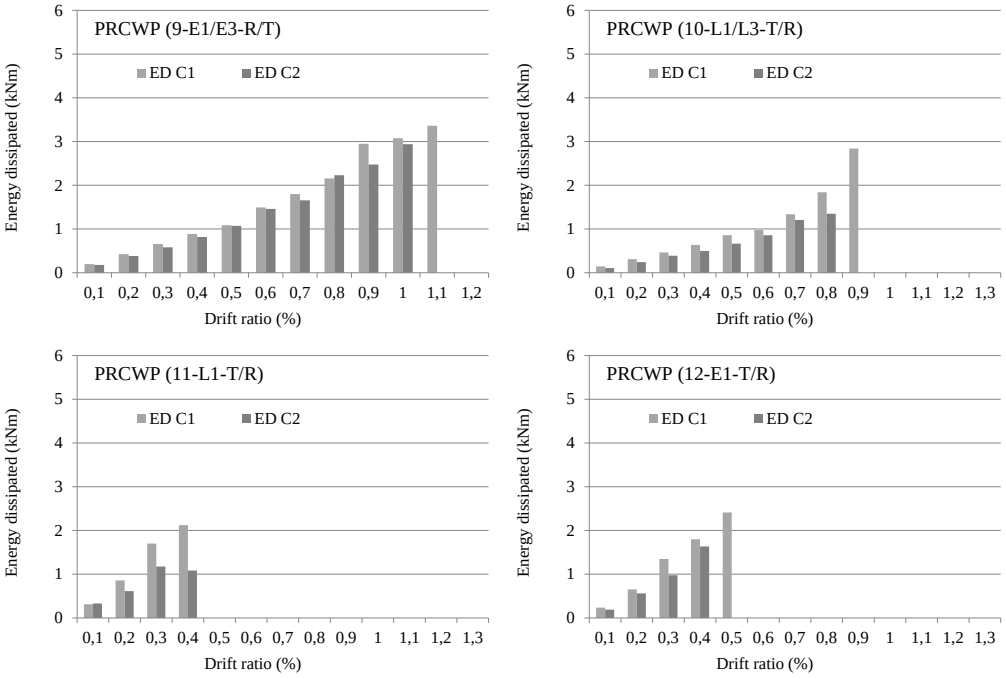

Figure 3.39 – Energy dissipation – strengthened specimens

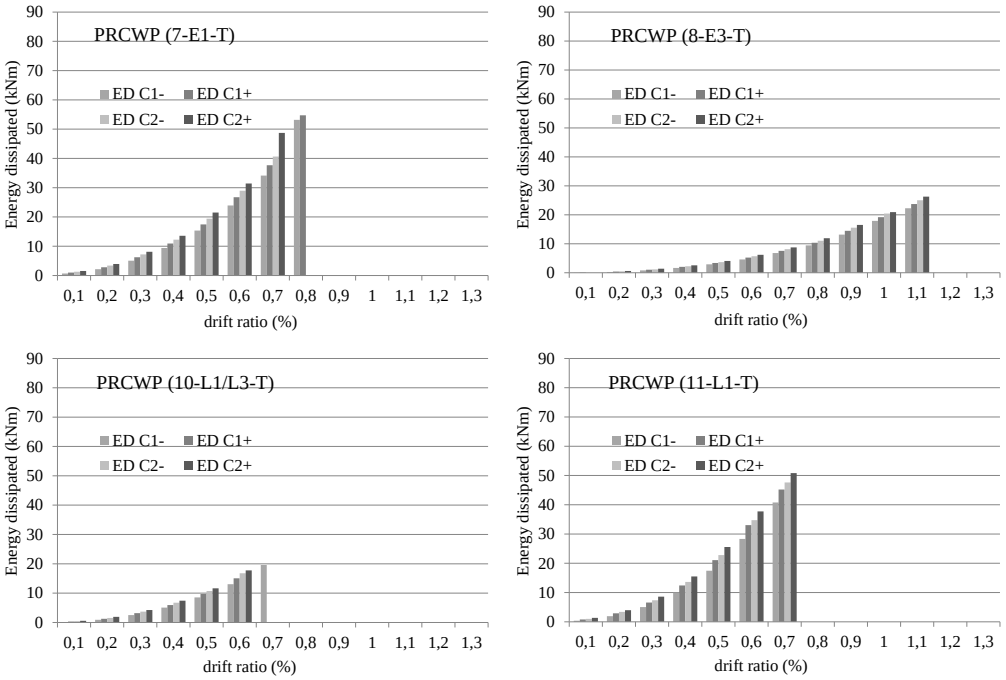

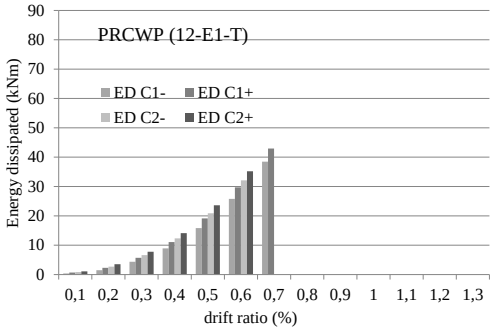

Figure 3.40 – Cumulative energy dissipation (per half-cycle) – reference specimens

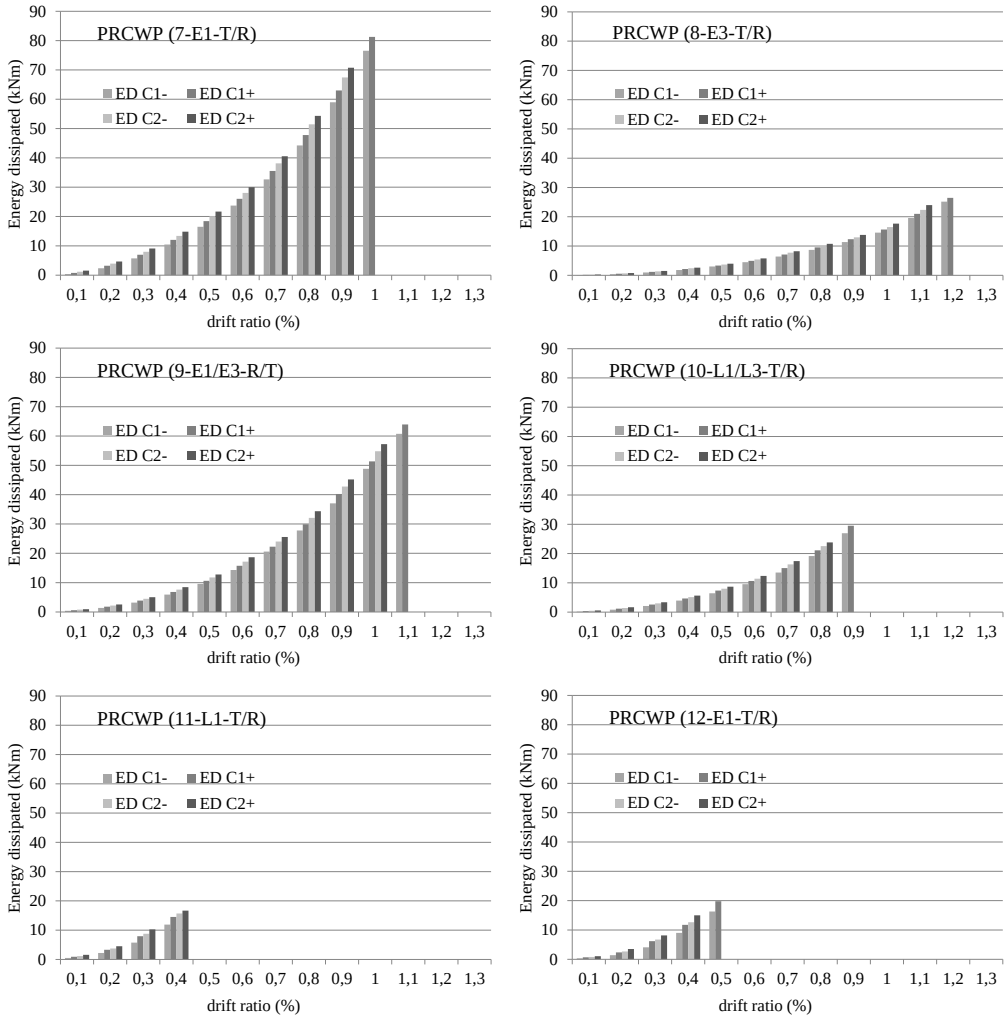

Figure 3.41 – Cumulative energy dissipation (per half-cycle) – strengthened walls

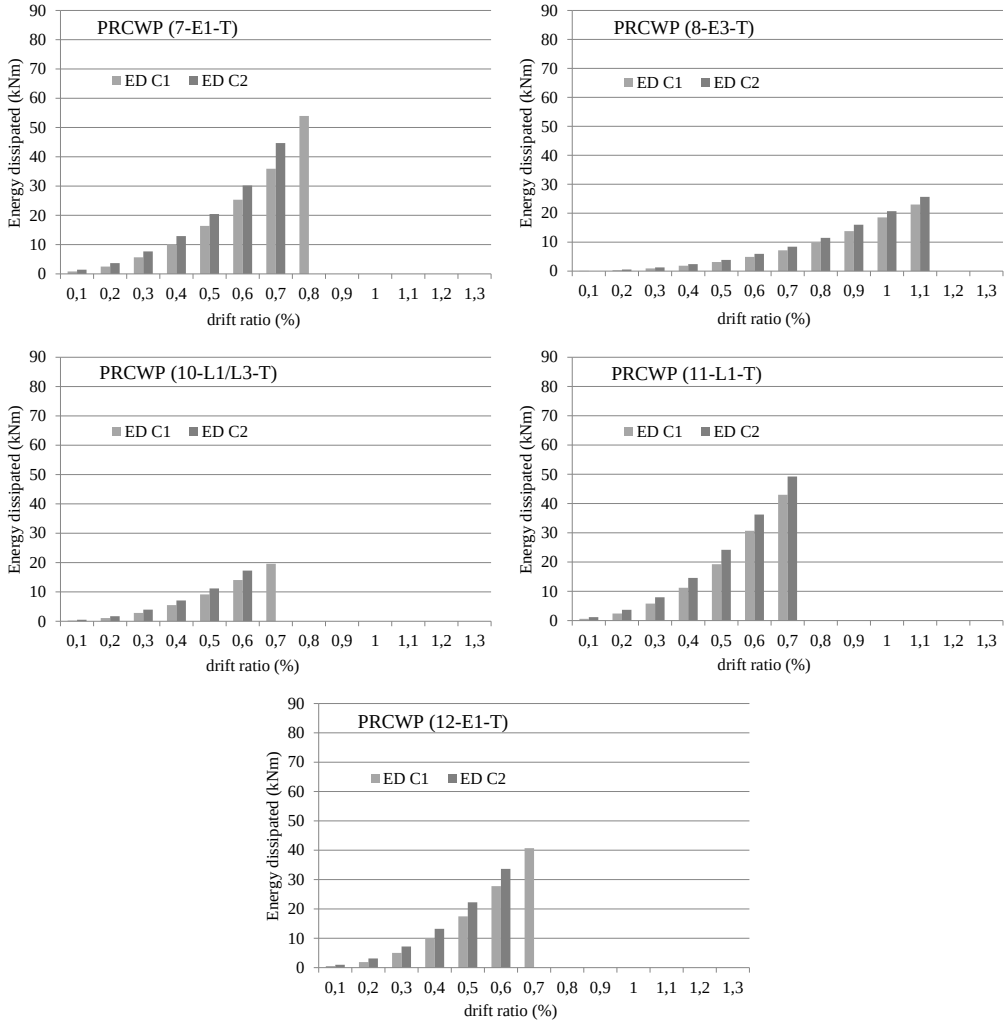

Figure 3.42 – Cumulative energy dissipation (per cycle) – reference specimens

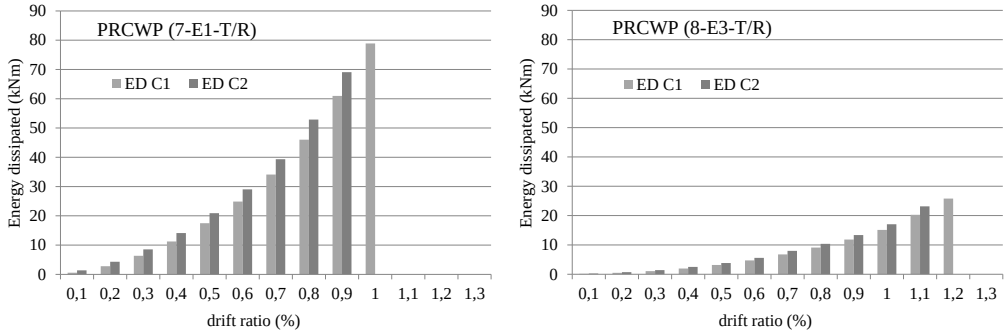

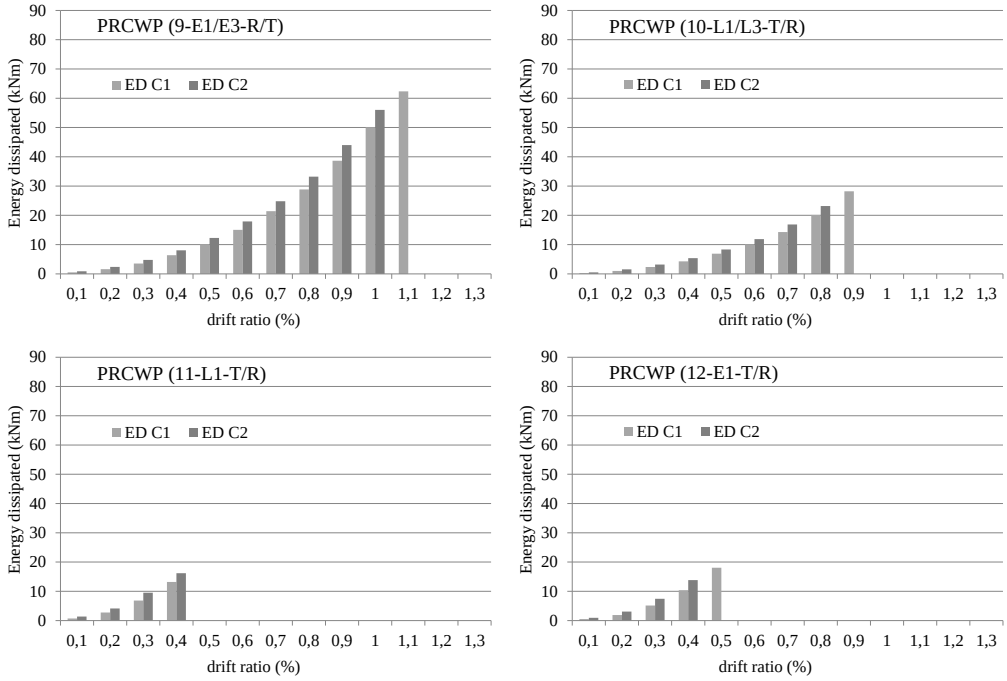

Figure 3.43 – Cumulative energy dissipation (per cycle) – strengthened specimens

Table 3.4 **–** Cumulative energy dissipation at each cycle

Element notation	Cumulative dissipated energy, CED (kNm)					
	Drift 0,10%	Drift 0,20%	Drift 0,30%	Drift 0,40%	Drift 0,50%	Drift 0,60%
PRCWP (7-E1-T)	1,13	3,07	6,65	11,54	18,42	27,76
PRCWP (7-E1-T/R)	0,96	3,54	7,44	12,67	19,18	26,95
PRCWP (8-E3-T)	0,09	0,45	1,11	2,13	3,50	5,44
PRCWP (8-E3-T/R)	0,19	0,59	1,23	2,23	3,49	5,14
PRCWP (9-E1/E3-R/T)	0,68	1,98	4,15	7,20	11,19	16,47
PRCWP (10-L1/L3-T)	0,36	1,40	3,40	6,29	10,15	15,66
PRCWP (10-L1/L3-T/R)	0,37	1,26	2,75	4,82	7,60	10,98
PRCWP (11-L1-T)	0,87	3,03	6,88	12,88	21,72	33,46
PRCWP (11-L1-T/R)	1,03	3,43	8,18	14,69	-	-
PRCWP (12-E1-T)	0,75	2,49	6,10	11,61	19,86	30,70
PRCWP (12-E1-T/R)	0,72	2,48	6,29	12,09	18,06	-

Element notation	Cumulative dissipated energy, CED (kNm)					
	Drift 0,70%	Drift 0,80%	Drift 0,90%	Drift 1,00%	Drift 1,10%	Drift 1,20%
PRCWP (7-E1-T)	40,29	53,94	-	-	-	-
PRCWP (7-E1-T/R)	36,72	49,45	65,03	78,90	-	-
PRCWP (8-E3-T)	7,82	10,70	14,93	19,62	24,33	-
PRCWP (8-E3-T/R)	7,36	9,74	12,60	16,08	21,72	25,80
PRCWP (9-E1/E3-R/T)	23,11	31,02	41,31	53,05	62,34	-
PRCWP (10-L1/L3-T)	19,58	-	-	-	-	-
PRCWP (10-L1/L3-T/R)	15,57	21,65	28,21	-	-	-
PRCWP (11-L1-T)	46,11	-	-	-	-	-
PRCWP (11-L1-T/R)	-	-	-	-	-	-
PRCWP (12-E1-T)	40,70	-	-	-	-	-
PRCWP (12-E1-T/R)	-	-	-	-	-	-

3.4 Ductility coefficient

Since the relation between strength and deformation may not have a well-defined yield point, the evaluation of the ductility of an element remains conventional. Estimations of the yield displacement have been performed also by Priestley (2000), Park (1988), Salonikios et al. (2000), Carrillo et al. (2014) [33]. In the current research, the author adopted for the evaluation of the ductility of the wall specimens the μ0.85 method. The μ0.85 method defines the ductility ($\mu = \Delta u/\Delta y$) as the ratio between the ultimate displacement (Δu – the corresponding drift ratio when the horizontal load value falls to 80% of the maximum lateral force) to the displacement corresponding to 0.85 of the peak load on the ascending branch (Δy – the drift ratio at yielding). The ductility coefficient μ0.85 for the strengthened specimens compared to the reference ones is presented in Fig. 3.44. It can be observed that the obtained ductility ranges from 1.31 to 1.87. In two cases the ductility of the strengthened specimens was higher compared to the reference ones, whereas for two strengthened specimens which did not reach failure during testing, based on the shape of the load-drift ratio hysteresis loops, the behaviour of the specimens looks rather rigid than ductile. In Figure 3.45 are represented several two considered relevant ductility comparisons between specimens. Specimen PRCWP (9-E1/E3-R/T) developed a higher ductility compared to the strengthened PRCWP (7, 8, 10), whereas specimen PRCWP (11-L1-T/R) developed a higher ductility compared to the strengthened PRCWP (7, 10, 12). Similar values of ductility coefficient were obtained for PRCWP (8-E3-T/R) and PRCWP (10-L1/L3-T/R). Comparison of the ductility coefficients for the reference specimens is given in Figure 3.46 a), and for the strengthened ones in Figure 3.46 b). On the condition of excluding from the comparison the ductility results of PRCWP (7-E1-T) due tot the obtained brittle failure, it can be observed that for the reference specimens having wide openings, e.g. PRCWP (8-E3-T) developed a lower ductility compared to a wall having a narrow door opening, PRCWP (12-E1-T), whereas a wall specimen having a wide window opening, PRCWP (10-L1/L3-T), developed a lower ductility compared to a wall having a narrow window opening, PRCWP (11-L1-T). According to the results presented in Figure 4.46 b), PRCWP (9-E1/E3-R/T) developed a higher ductility compared PRCWP (8-E3-T/R) and PRCWP (10-L1/L3-T/R), prooving the contribution of the considered strengthening. A general comparison of the ductility coefficients for the tested specimens is given in Figure 3.47 a), and of the normalized ductility coefficients in Figure 3.47 b).

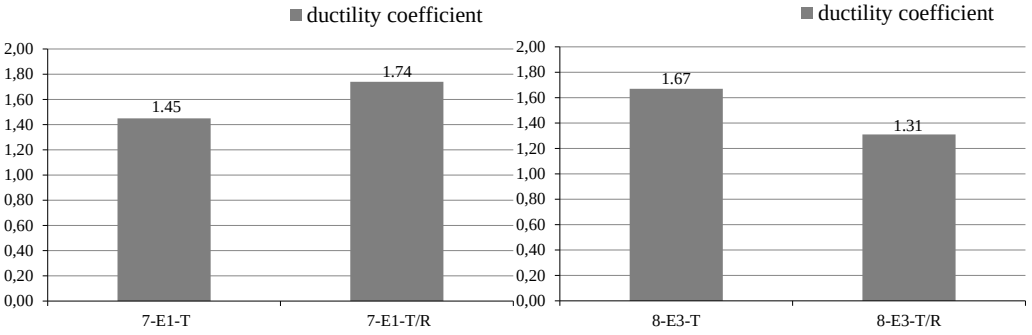

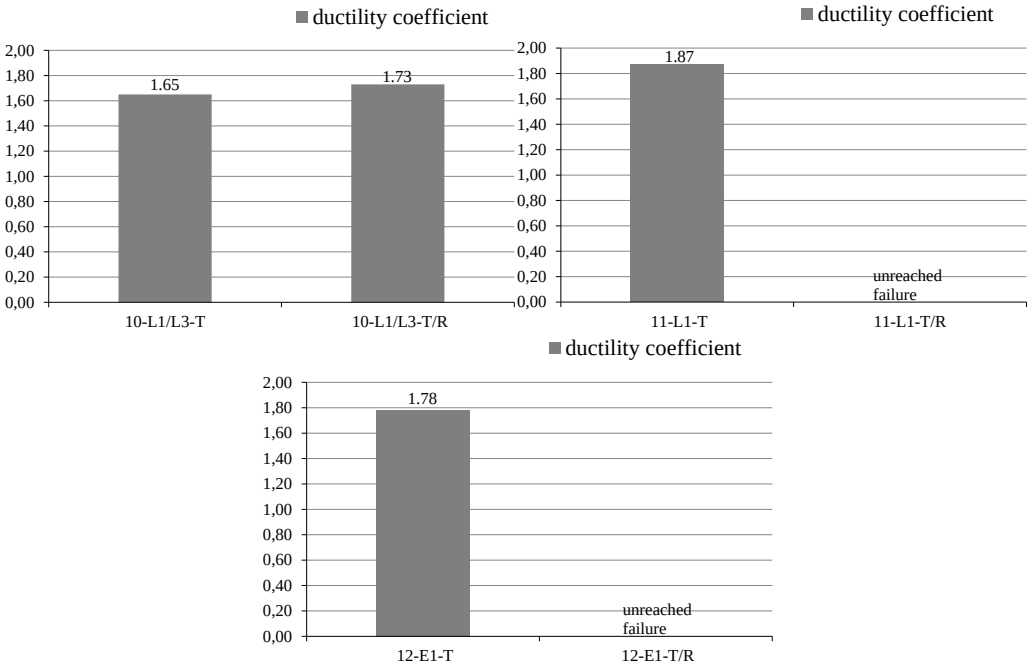

Figure 3.44 – The ductility coefficient of the tested specimens

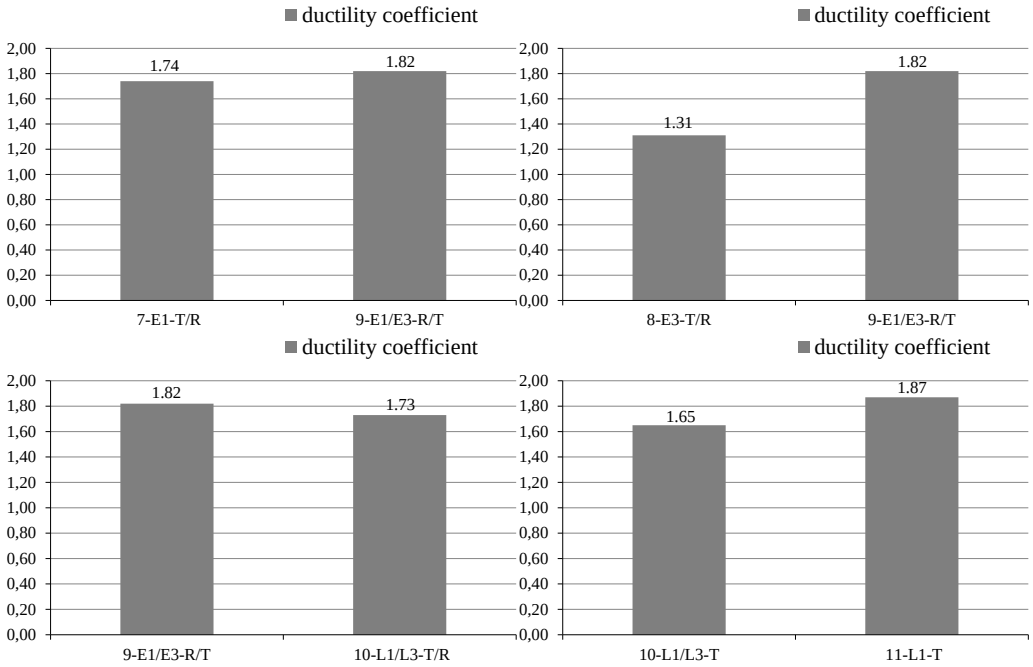

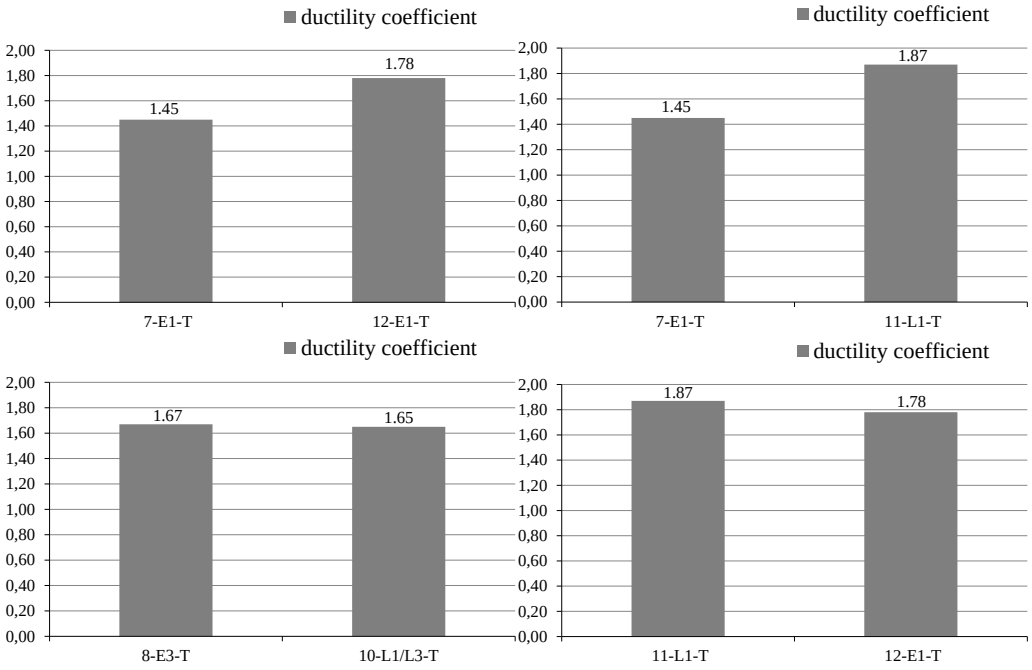

Figure 3.45 – Comparison of the ductility coefficients

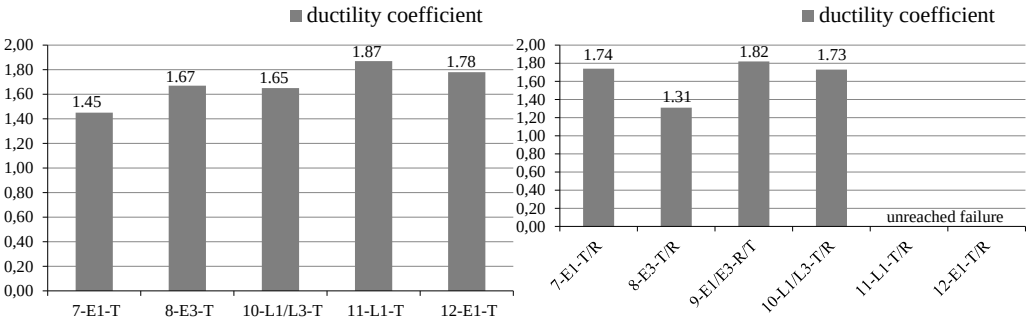

Figure 3.46 – Comparison of the ductility coefficients

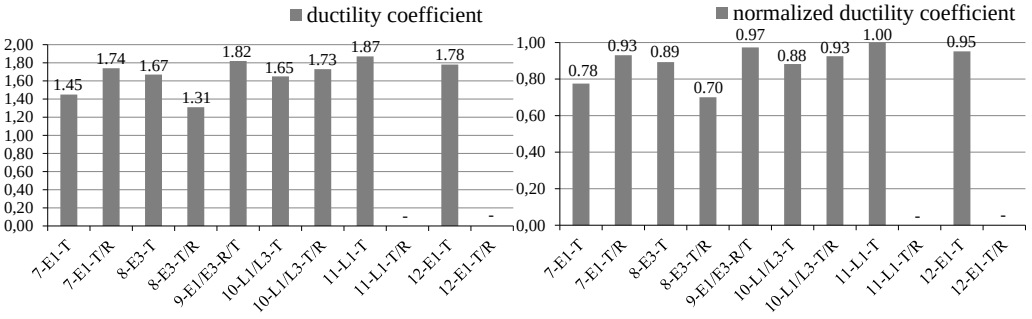

Figure 3.47 – Comparison of the ductility coefficients for the tested specimens

3.5 Strain analysis

Strain was measured on the vertical, horizontal and inclined reinforcing bars for the reference specimens, and on the vertical, horizontal and inclined FRPs for the strengthened specimens. The strain gauges position are given in Fig. 2.18, Section 2.6. The steel strain ε (‰) versus drift ratio for the tested wall specimens is represented in Figure 3.48. Steel reinforcement yielding was attained for almost all the reference wall panels in the critical regions, e.g., the top corners of the openings (spandrel-pier connection region), pier and parapet.

Strain gauges applied on FRPs did not indicate high strain values, but it is clear they were active during the experimental tests, mostly in the corners of the openings (spandrel-pier connection region) and piers.

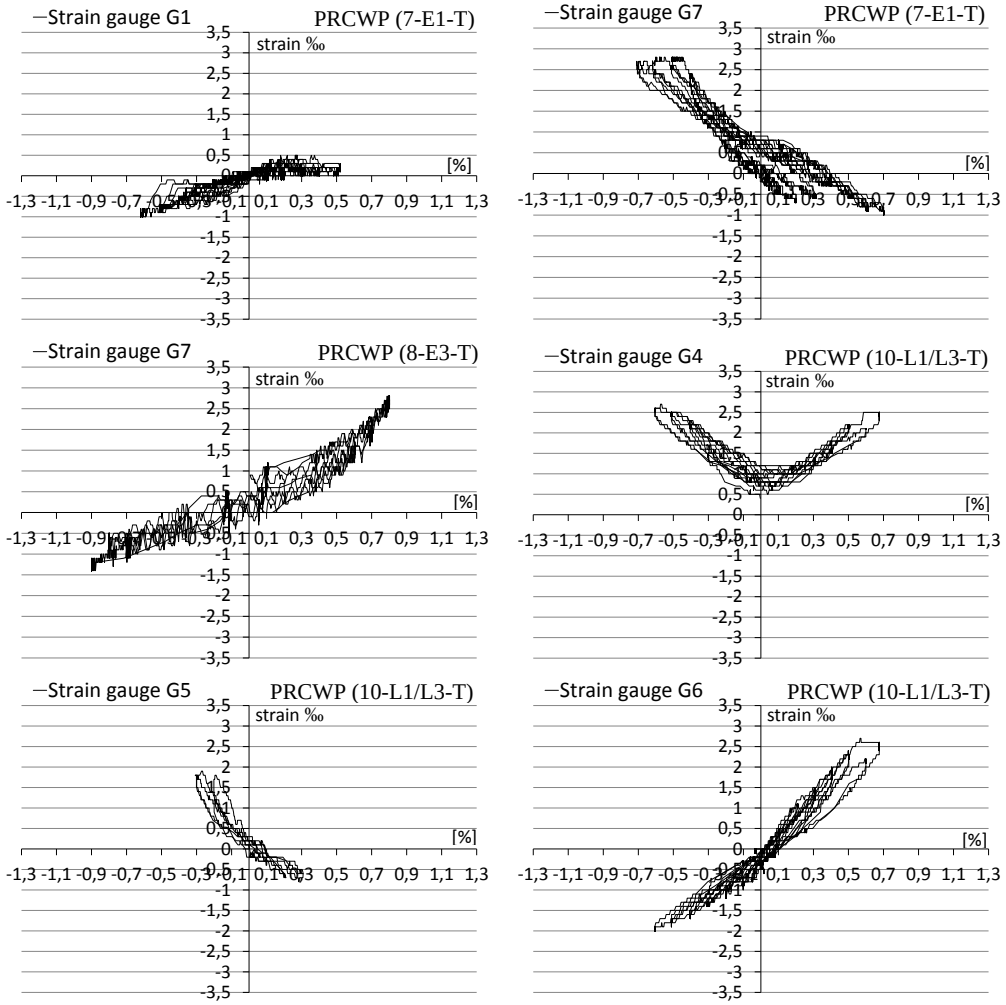

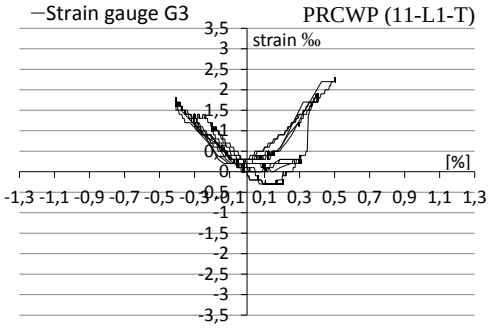
Strain gauge G3
PRCWP (11-L1-T)
strain ‰
[%]

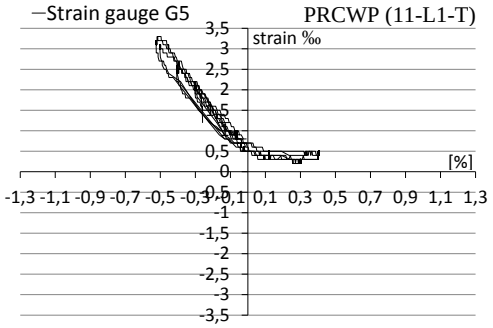
Strain gauge G5
PRCWP (11-L1-T)
strain ‰
[%]

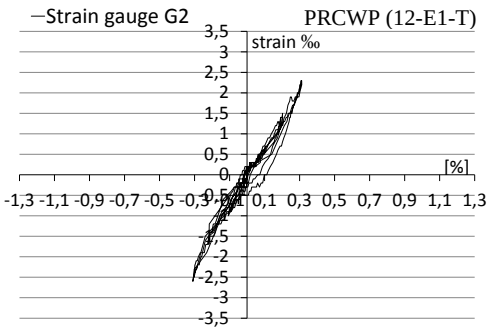
Strain gauge G2
PRCWP (12-E1-T)
strain ‰
[%]

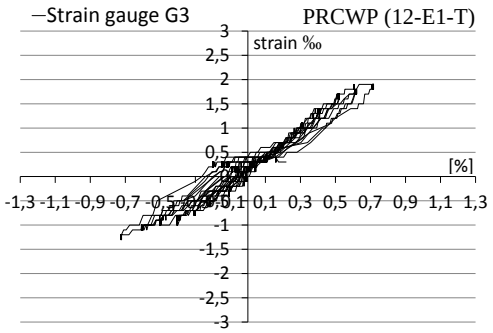
Strain gauge G3
PRCWP (12-E1-T)
strain ‰
[%]

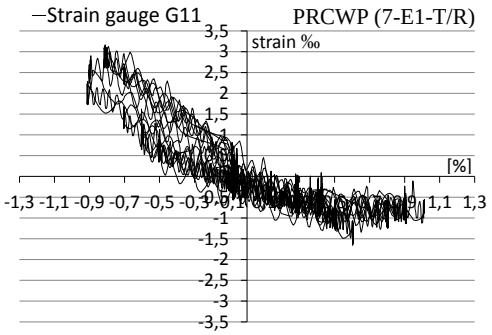
Strain gauge G11
PRCWP (7-E1-T/R)
strain ‰
[%]

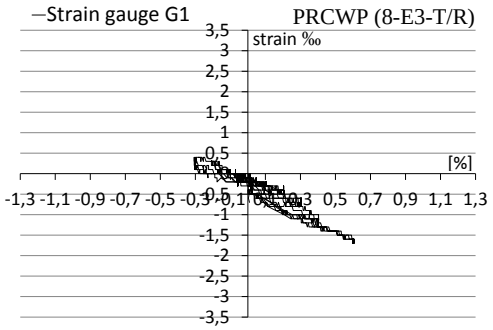
Strain gauge G1
PRCWP (8-E3-T/R)
strain ‰
[%]

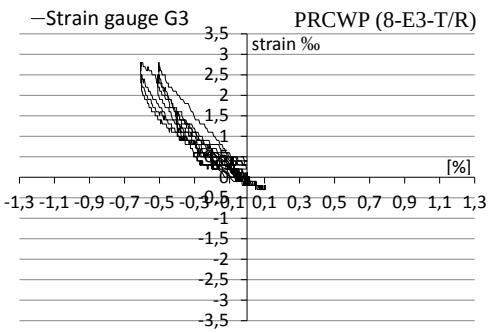
Strain gauge G3
PRCWP (8-E3-T/R)
strain ‰
[%]

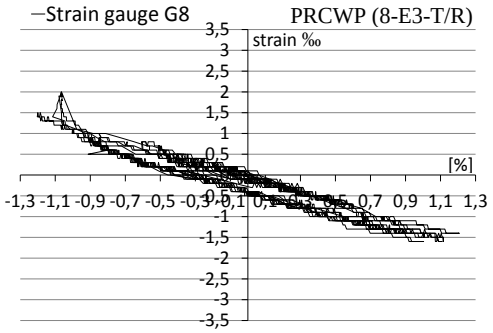
Strain gauge G8
PRCWP (8-E3-T/R)
strain ‰
[%]

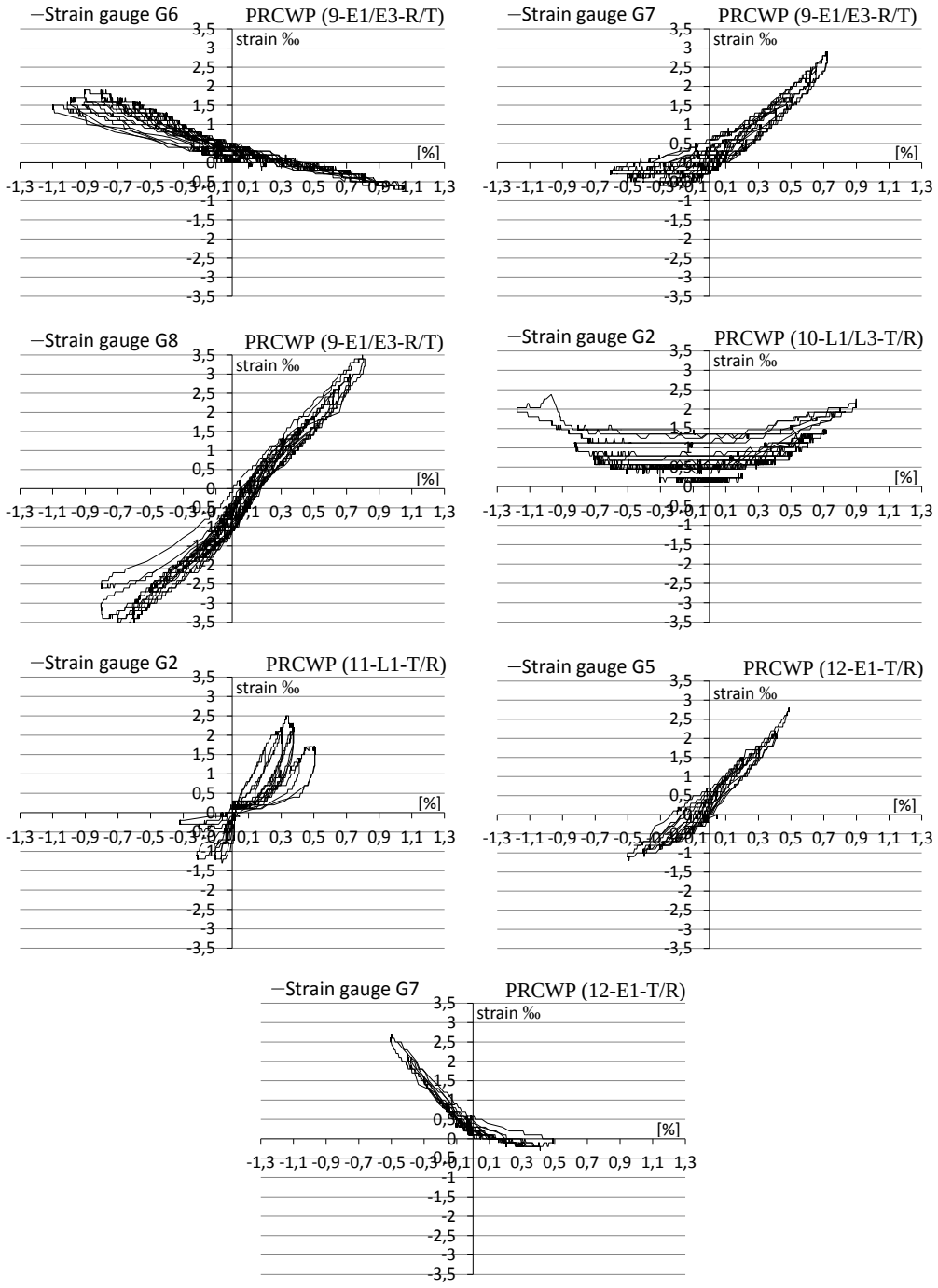

Figure 3.48 – Steel strain (ε) versus drift ratio of the tested specimens

Regardless of the strain activity, the author considers the strengthening efficient based on the general behaviour of the specimens, even with the development of premature FRP fracture or FRP debonding in several cases.

3.6 Stiffness degradation

The stiffness of an element, as defined in literature is the rigidity of the element, the extent to which it resists deformation in response to an applied load. Figure 3.49 presents several stiffness degradation comparisons between two specimens. In most cases, similar stiffness values were obtained for the strengthened specimens compared to the reference ones. The stiffness versus drift ratio diagram of the reference specimens is represented in Figure 3.50 a), showing that the walls with large opening dimensions (PRCWP 8-E3-T, 10-L1/L3-T) exhibit higher reductions in the initial stiffness compared to walls with smaller opening dimensions, namely (PRCWP 7-E1-T, 11-L1-T, 12-E1-T). According to Figure 3.50 b), again the walls with large opening dimensions (PRCWP 8-E3-T/R, 9-E1/E3-R/T, 10-L1/L3-T) exhibited higher reductions in the initial stiffness compared to the walls with smaller opening dimensions, namely (PRCWP 7-E1-T/R, 11-L1-T/R, 12-E1-T/R). The initial stiffness of the tested specimens is represented in the form of histograms in Figure 3.51. Analysing the results by computing the ratio between the measured initial stiffness of a wall having a large door opening (PRCWP 8-E3-T) and a wall having a narrow door opening (PRCWP 7-E1-T), a value of 1:4.75 was obtained, whereas the ratio between a wall with an initially small window opening enlarged to a large window opening (PRCWP 10-L1/L3-T) and a wall having a small window opening (PRCWP 11-L1-T) was 1:2. Several factors are considered important on the influence of the above comparisons, such as the concrete compressive strength, amount of initial steel reinforcement, value of constant axial load imposed in each case, opening dimensions and type. Related to the strengthened specimens, the initial stiffness of PRCWP (7-E1-T/R) was increased by 25% compared to the reference specimen, whereas PRCWP (9-E1/E3-R/T) developed a higher initial stiffness (2.88 times) than PRCWP (8-E3-T/R), a lower initial stiffness (2.28 times) compared to PRCWP (7-E1-T/R) and 1.80 times smaller compared to PRCWP (12-E1-T/R). The considered strengthening strategies and the level of damage sustained by the specimens can also be attributed to the above comparison. The stiffness degradation versus drift ratio diagram of all the specimens is presented in Figure 3.52 a), and the initial stiffness of all the tested specimens in Figure 3.52 b).

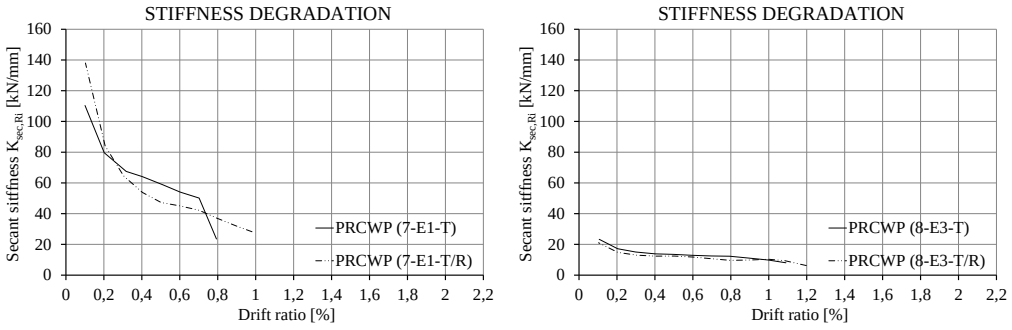

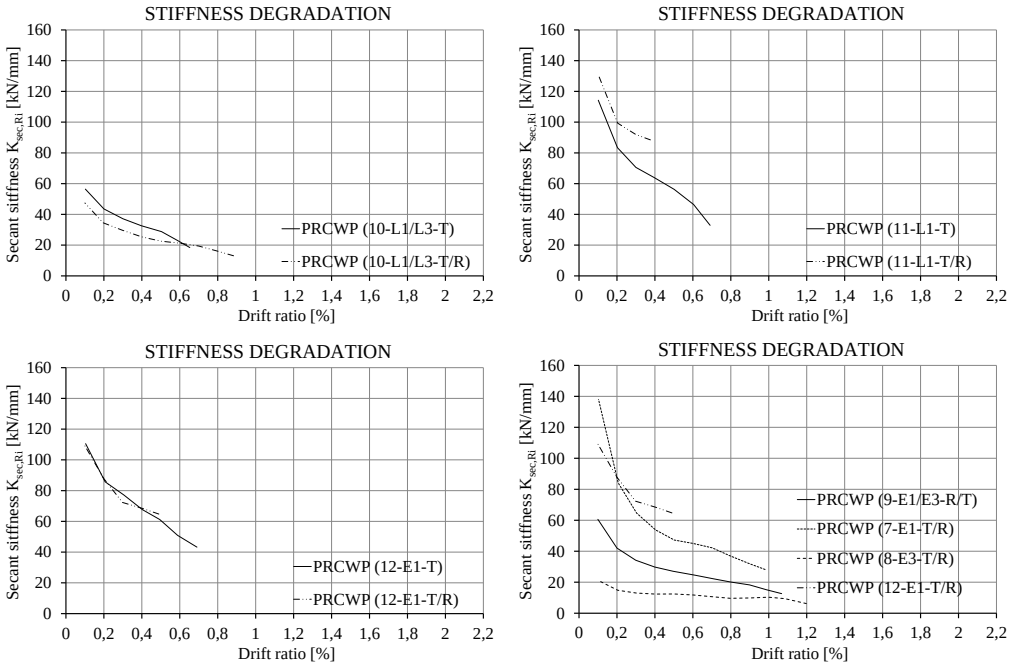

Figure 3.49 – Comparison of the stiffness degradation

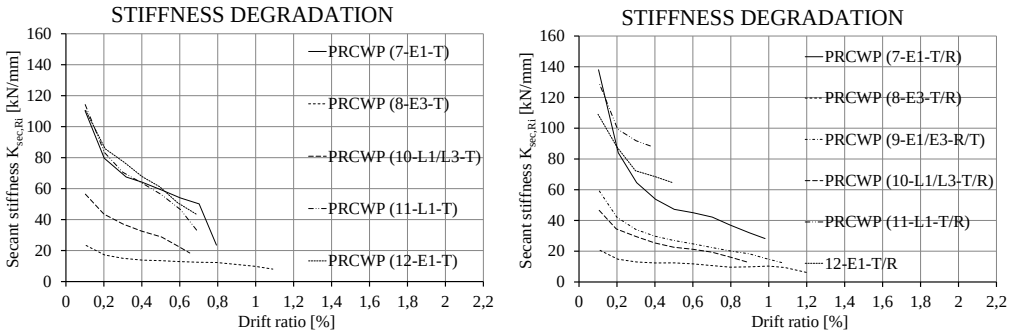

Figure 3.50 – The stiffness versus drift ratio diagram of the specimens

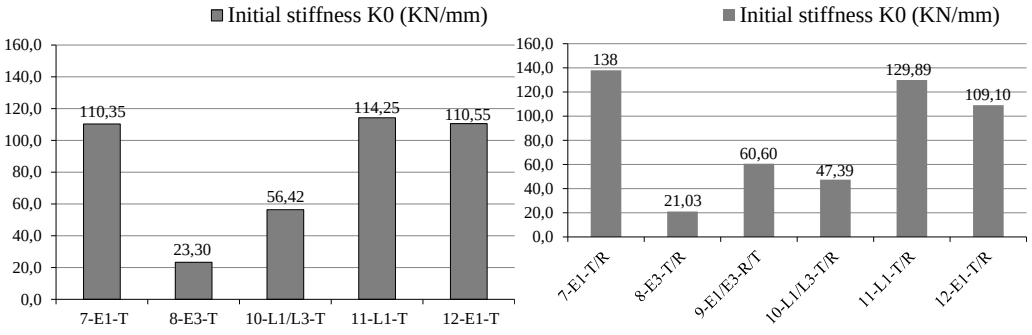

Figure 3.51 – Initial stiffness of the tested specimens

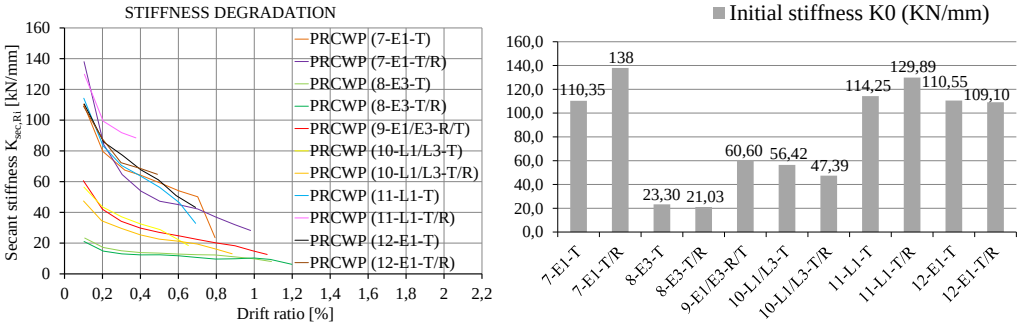

Figure 3.52 – The stiffness versus drift ratio diagram of the specimens

3.7 Numerical analysis for the prediction of the shear response

In order to predict the shear response of the experimental specimens, ATENA 2D software was chosen by the author. The used models integrate material characteristics and the behavioural response features, such as the occurrence of the first inclined crack, failure details, and nonlinear shear behaviour. The stress–strain law and failure criterion for the reinforcement and concrete are represented in Fig. 3.53. A bilinear stress–strain law for elastic–perfectly plastic was adopted for the reinforcement, whereas SBETA material model was used for concrete. The SBETA material includes the important behaviour aspects of concrete, like the nonlinear behaviour in compression, fracture of concrete in tension, biaxial strength failure criterion, reduction of compressive strength after cracking, tension stiffening effect, and reduction of the shear stiffness after cracking. The SBETA material parameters of concrete were determined according to Eurocode 2 [52]. In the case of the strengthened specimens, the EBR-CFRP strips and NSM-CFRP plates were modeled as independent reinforcement bars, and the TRM system was introduced as smeared reinforcement. A perfect connection was assumed for all strengthening systems used, therefore the anchorage systems were neglected in the numerical analysis.

Full connection between steel and concrete was used in the numerical analysis. In order to model the interface between the wall panel and the reaction beams, an interfacial failure and slip phenomena was considered in the model, having the properties given in Table 3.5. The values of the normal and tangential stiffness were calculated according to Atena Program Documentation – Part 1 (Theory) [121], while the cohesion and friction coefficient were calculated according to the Model Code 2010 [122]. As presented in Section 3.1, the vertical continuity steel rebars of the panel were welded in the experimental test to the continuity bars from the foundation beam. In the model, the welding was neglected, and continuous reinforcement bars were assumed for the connection of the foundation beam to the panel. Considering the experimental beams as having a complicated cross-section to model in a 2D version, a high reinforcing ratio was used for the two reaction beams in order to increase their stiffness and to direct the main response under loads to the wall panel. Approaching the experimental boundary conditions, in the model the foundation beam was fixed in both the horizontal and vertical directions.

Considering the recommendations of Atena software [123] and its users, the meshes used for modelling walls are in relation with the thickness of each element (wing, web panel, beams) and are close to the standard ones. Therefore, an element size of 0.10 m was used for the panel and reaction beams, and 0.05 m for the wings. Following further recommendations given in [123], CCIsoQuad finite elements were used for the upper beam and steel loading plates, and CCQ10SBeta for the web panel, wings and lower beam. The mentioned finite elements are of quadrilateral type. A general view of the mesh for the modelled specimens is represented in Fig. 3.54. In the model, the loading was applied from the left side to the right, by prescribing horizontal displacement in constant increments of 0.2 mm.

The constant axial loads were also applied in the model, having the same value as calculated and used in the experimental test, whereas for the variable axial loading, additional load was applied in each step performed by the analysis. According to the process in the ATENA Engineering Example Manual for Shear Wall with Opening [123], the Newton–Raphson solution method was used in the analysis. Two monitoring points were used in the analysis in order to record the drift and reaction force, one located in the vicinity of the loading point for the reaction force, and the other located in the middle of the upper edge of the panel for horizontal displacement. Analysing the numerical analysis results, it was found that the modeling approach can predict well the behaviour of the experimental specimens, except for drift at which the first diagonal cracks appear. In the numerical model the occurrence of the first inclined crack develops earlier compared to the experimental

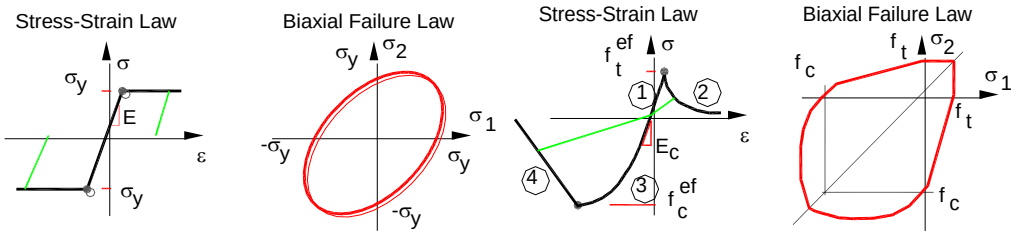

Figure 3.53 - Stress-strain and failure laws for materials [108-109]

Table 3.5 - Material properties of concrete-concrete interface (10 cm contact)

Element	Normal stiffness Knn	Tangential stiffness Ktt	Tensile strength ft	Cohesion c	Friction coefficient φ
	MN/m3	MN/m3	MPa	MPa	-
PRCWP (7-E1)	1.82 x E05	1.52 x E05	0	0.5	0.9
PRCWP (8-E3)	1.37 x E05	1.14 x E05	0	0.5	0.9
PRCWP (9-E1/E3)	1.81 x E05	1.52 x E05	0	0.5	0.9
PRCWP (10-L1/L3)	1.56 x E05	1.30 x E05	0	0.5	0.9
PRCWP (11-L1)	1.56 x E05	1.30 x E05	0	0.5	0.9
PRCWP (12-E1)	1.81 x E05	1.51 x E05	0	0.5	0.9

observations, and this might be due to the fact that very thin inclined cracks may not be easily seen by the eye. In Table 3.6 a and b are represented the comparison between the numerical analysis versus the experimental test results in terms of the first diagonal crack appearance, the maximum lateral load sustained by the members and the drift level corresponding to the maximum lateral load recorded.

The analytical and experimental load–drift ratio response of the analysed specimens is shown in Figure 3.55. Similar shapes of the experimental curves with those of the numerical model were obtained. However, the experimental specimens exhibit a brittle failure after the peak. As presented in Figure 3.56 (for unstrengthened wall specimens), cracking under the left-side loading was similar with the experimental ones. In Figure 3.56, pictures on the right side, is also presented the ultimate compressive strain state in the specimen. Based on the obtained results, it can be concluded that the numerical model is an efficient instrument tool for analysing the behaviour of precast reinforced concrete wall panels of different characteristics.

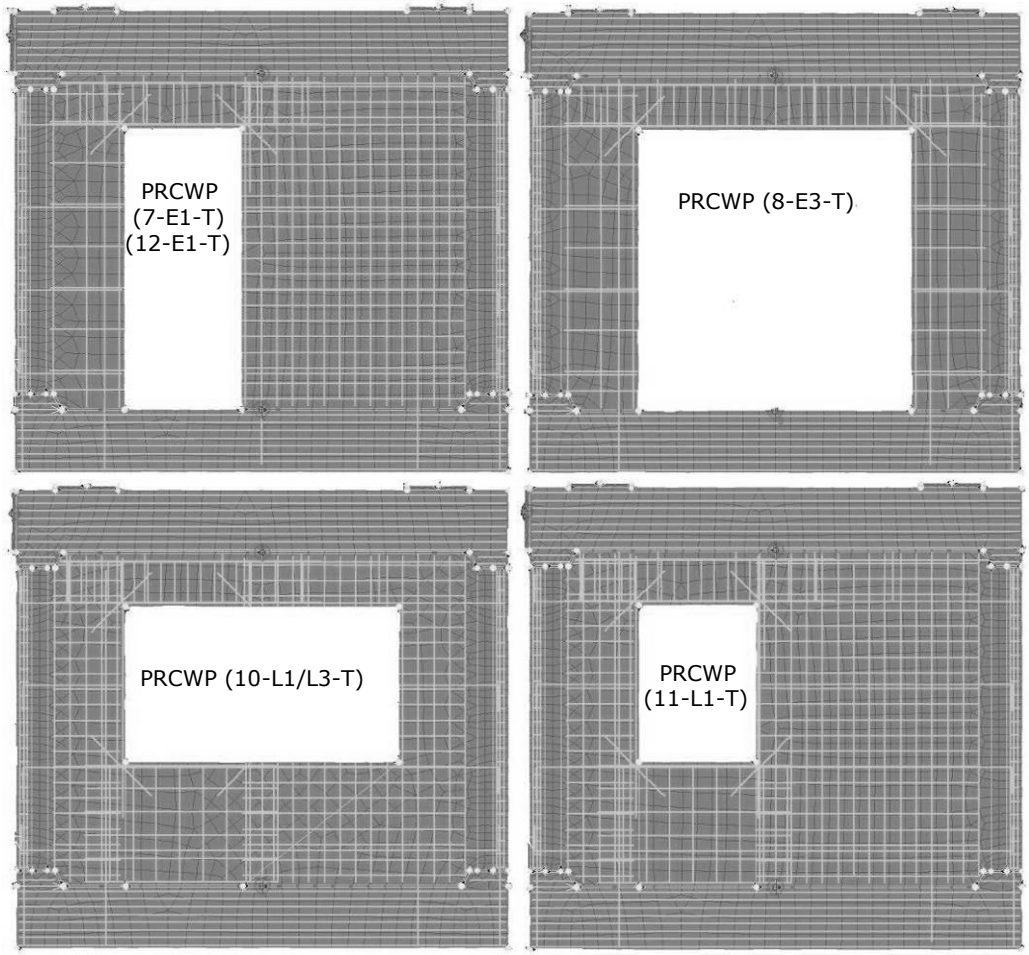

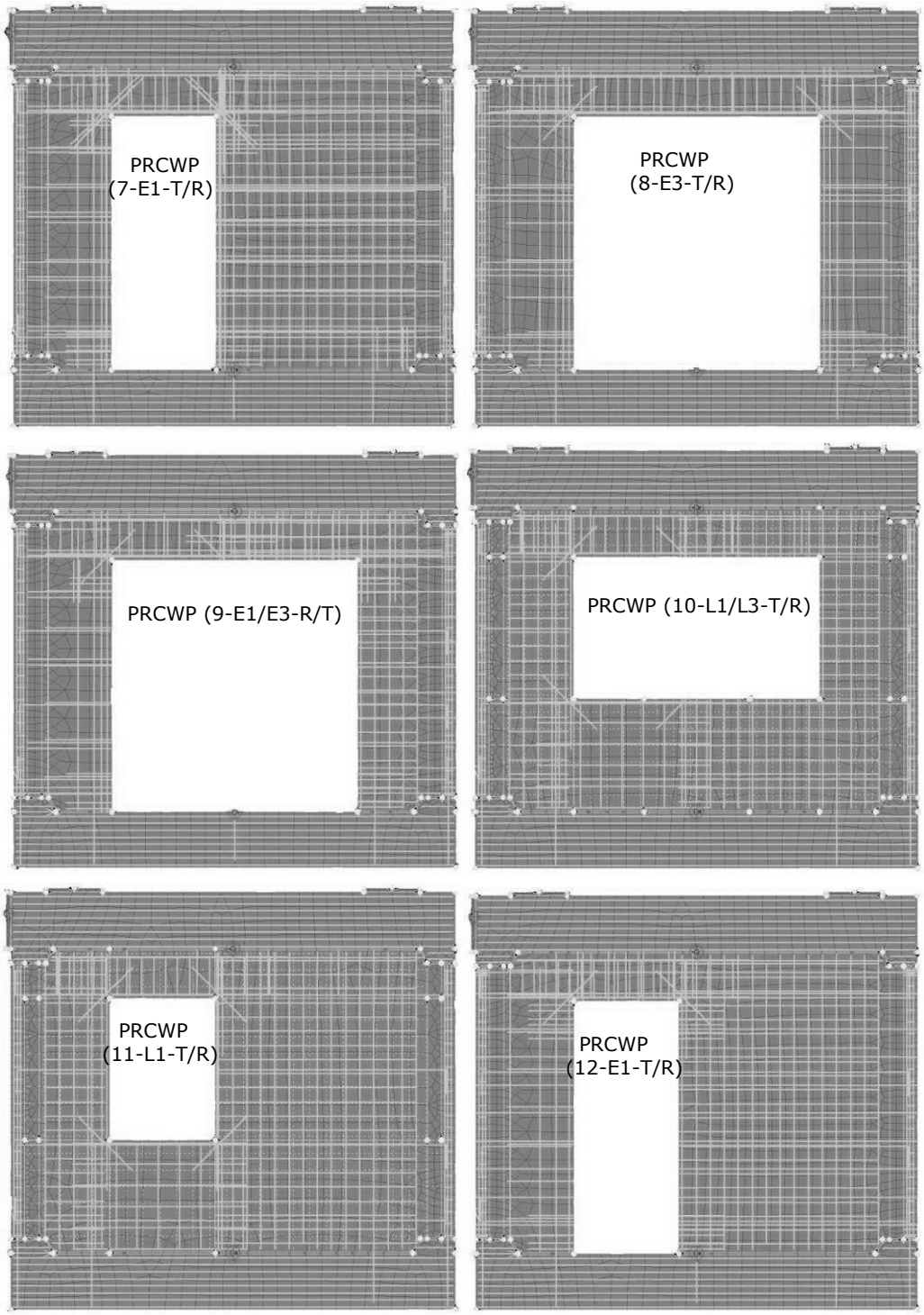

Figure 3.54 - The layout and meshes of the numerical specimens

Table 3.6a – Comparison of the analytical and experimental results

Element designation	First inclined crack [%]	Peak lateral load [kN]	Drift level corresponding to peak lateral load [%]
PRCWP (7-E1-T)			
Experimental	0,50	802,5	0,70
Numerical	0,14	620,3	0,86
PRCWP (7-E1-T/R)			
Experimental	0,60	638,8	0,70
Numerical	0,14	676,7	1,14
PRCWP (8-E3-T)			
Experimental	0,50	213,6	0,89
Numerical	0,21	205,3	1,19
PRCWP (8-E3-T/R)			
Experimental	0,30	221,0	1,00
Numerical	0,17	230,3	1,25
PRCWP (9-E1/E3-R/T)			
Experimental	0,70	352,8	0,90
Numerical	0,23	299,2	0,81
PRCWP (10-L1/L3-T)			
Experimental	0,20	311,5	0,50
Numerical	0,07	332,1	0,78
PRCWP (10-L1/L3-T/R)			
Experimental	0,20	291,9	0,70
Numerical	0,08	503,1	1,15
PRCWP (11-L1-T)			
Experimental	0,30	511,5	0,60
Numerical	0,11	510,2	0,55
PRCWP (11-L1-T/R)			
Experimental	0,30	425,8	0,39
Numerical	0,10	599,7	0,67
PRCWP (12-E1-T)			
Experimental	0,20	656	0,70
Numerical	0,15	606,4	0,66
PRCWP (12-E1-T/R)			
Experimental	0,40	355	0,49
Numerical	0,14	602,2	0,65

Table 3.6b – Comparison of the analytical and experimental results

Element designation	First inclined crack [%]	Peak lateral load [kN]	Drift level corresponding to peak lateral load [%]
PRCWP (7-E1-T)			
Experimental	0,50	858	0,70
Numerical	0,14	620,3	0,86
PRCWP (7-E1-T/R)			
Experimental	0,60	669,5	0,70
Numerical	0,14	676,7	1,14
PRCWP (8-E3-T)			
Experimental	0,50	247,5	1,00
Numerical	0,21	205,3	1,19
PRCWP (8-E3-T/R)			
Experimental	0,30	249,5	1,06
Numerical	0,17	230,3	1,25
PRCWP (9-E1/E3-R/T)			
Experimental	0,70	385,5	0,94
Numerical	0,23	299,2	0,81
PRCWP (10-L1/L3-T)			
Experimental	0,20	344,0	0,60
Numerical	0,07	332,1	0,78
PRCWP (10-L1/L3-T/R)			
Experimental	0,20	320	0,70
Numerical	0,08	503,1	1,15
PRCWP (11-L1-T)			
Experimental	0,30	550,5	0,68
Numerical	0,11	510,2	0,55
PRCWP (11-L1-T/R)			
Experimental	0,30	462,5	0,38
Numerical	0,10	599,7	0,67
PRCWP (12-E1-T)			
Experimental	0,20	656	0,70
Numerical	0,15	606,4	0,66
PRCWP (12-E1-T/R)			
Experimental	0,40	355	0,49
Numerical	0,14	602,2	0,65

As mentioned above, in Table 3.6 a and b are represented the comparison between the numerical analysis versus the experimental test results in terms of the first diagonal crack appearance, the maximum lateral load sustained by the members and the drift level corresponding to the maximum lateral load recorded. The difference between these two tables is that in Table 3.6a the author took the experimental values used for the computation of load-drift ratio curves presented in Figure 3.55, namely corresponding to the positive values of the M2 envelope curves (for unequal piers) and corresponding to M1 envelope curves (for equal piers), while in Table 3.6b the given experimental values correspond to the highest measured force in the positive direction (for unequal piers) and to the highest measured force among both directions (for equal piers). The author considers important the difference between these two considerations, as one corresponds to the real situation, and the other one considers the monotonic type of loading as performed in the numerical modeling.

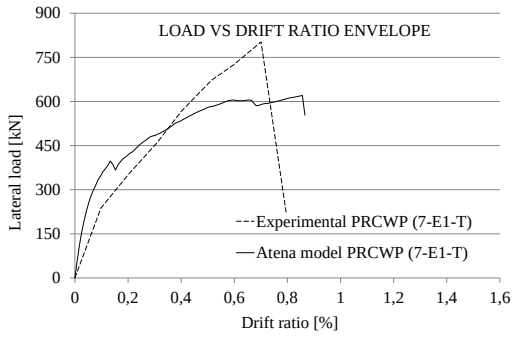

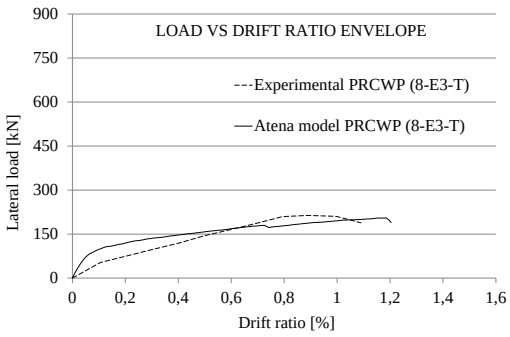

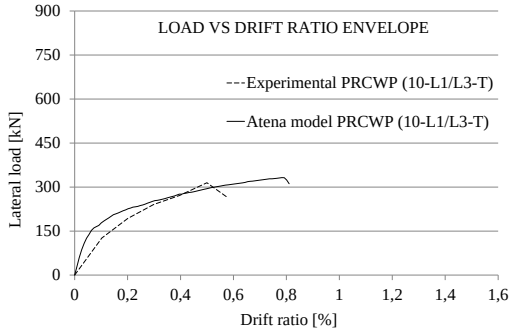

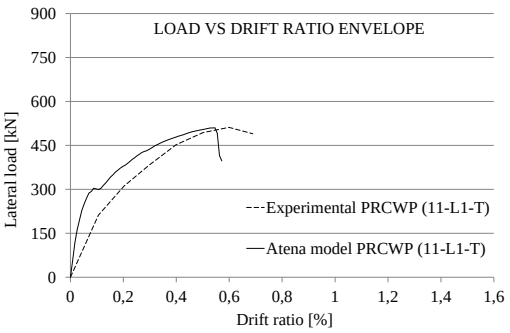

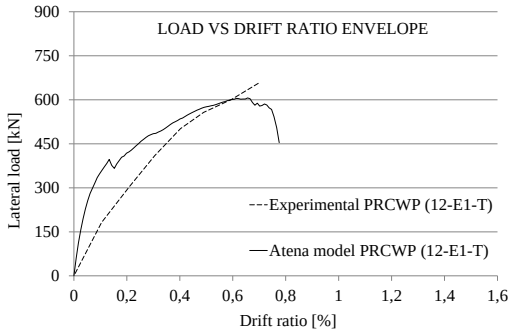

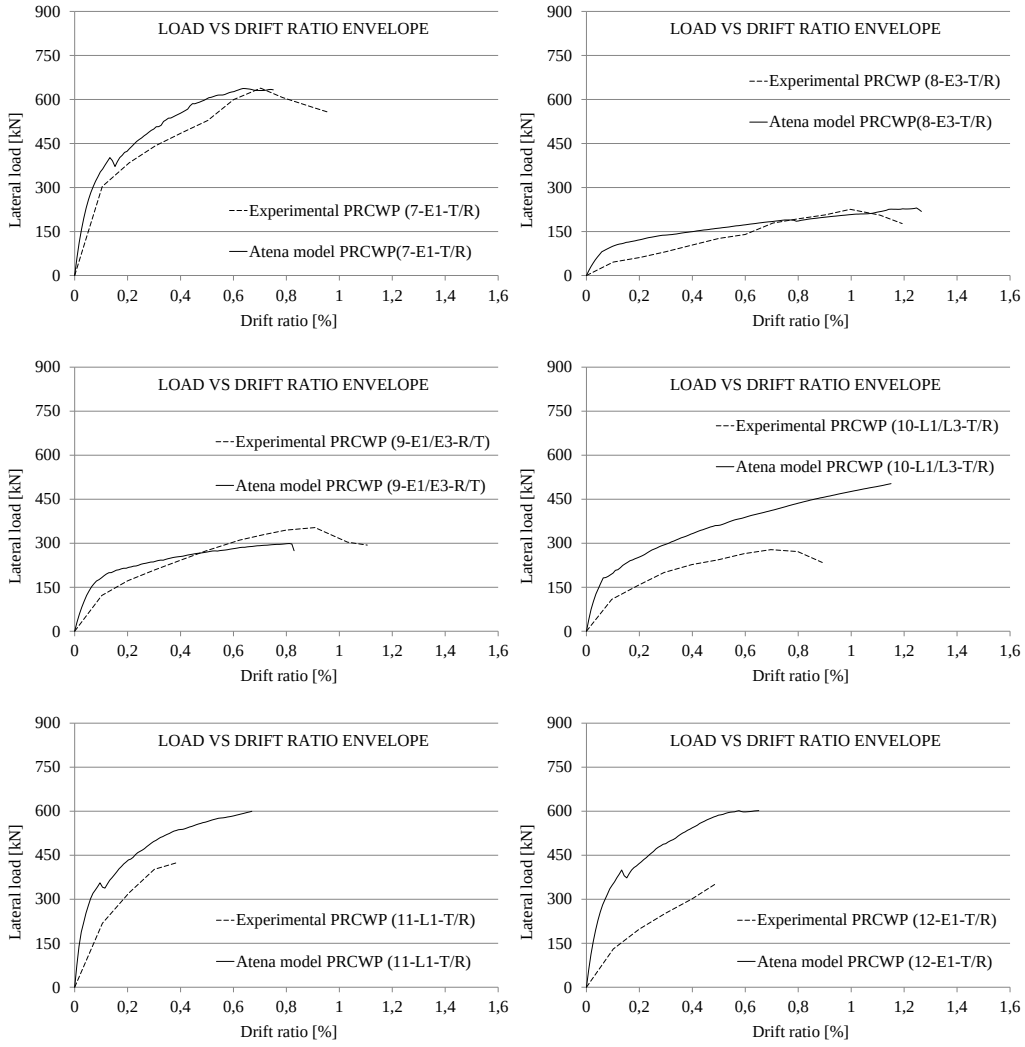

Figure 3.55 - Experimental versus numerical load-drift ratio curves

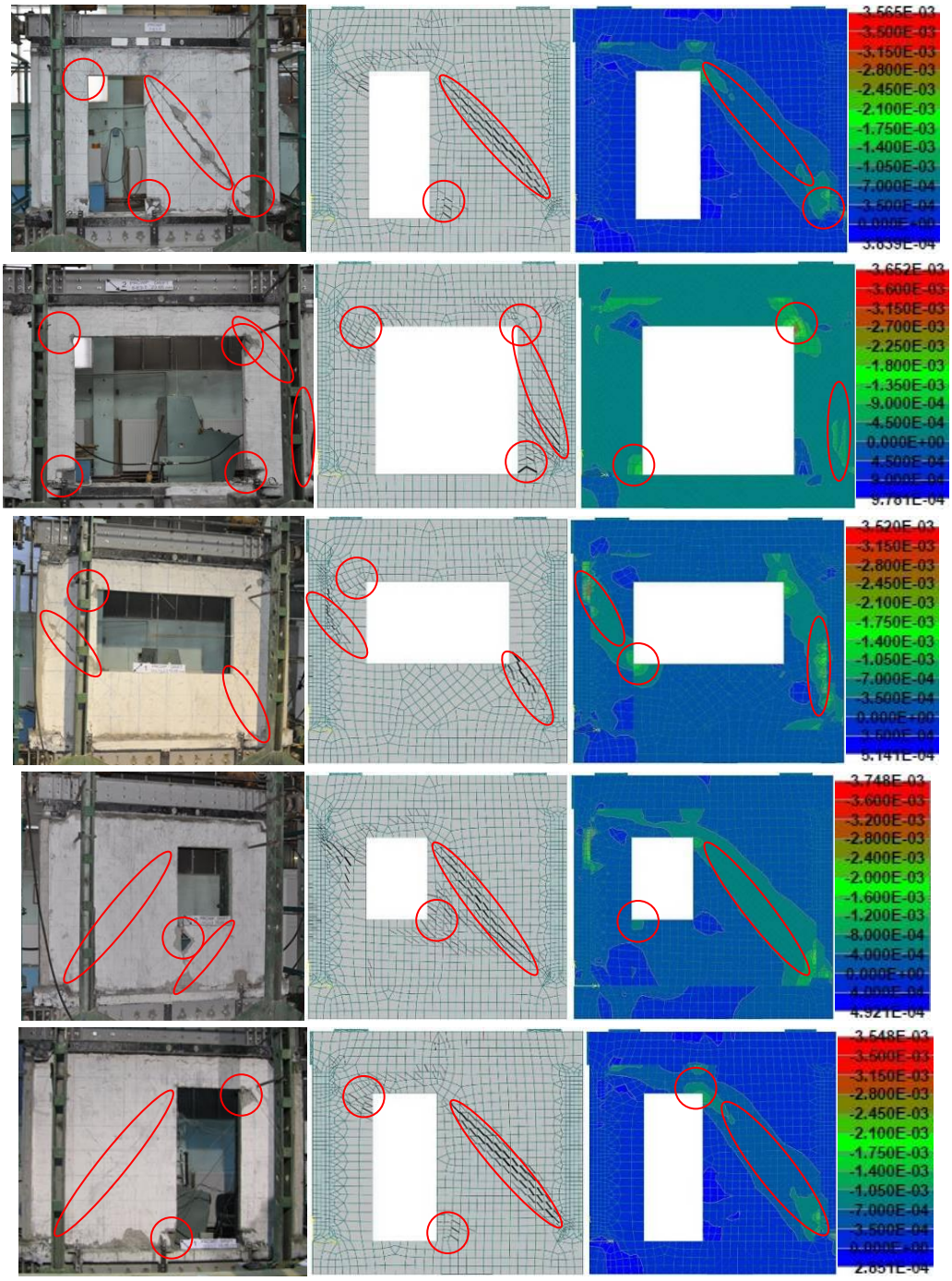

Figure 3.56 - Experimental versus numerical failure details

3.8 Theoretical study on the shear resistance of the specimens

3.8.1 Evaluation of the shear strength using design code provisions

In order to evaluate the shear resistance of the reference wall specimens, Eurocode 2 [52] (section 6) was used and the results are presented in Table 3.7 [108]. Considering the obtained results, the evaluated shear response appears to be limited by the yielding of the shear reinforcement. It can be observed that the experimental values obtained are significantly higher than those evaluated using formulas from EC2 [52]. Therefore, the code may be considered too conservative for the studied elements, probably due to the other effects not covered by the design formulas such as: the dowel effect, the redistribution of stresses, and rotation capacity.

Table 3.7 – Shear resistance of the reference walls evaluated using design code expressions

ELEMENT	PRCWP (7-E1-T)		PRCWP (10-L1/L3-T)		PRCWP (11-L1-T)		PRCWP (12-E1-T)	
	Pier 1	Pier 2	Pier 1	Pier 2	Pier 1	Pier 2	Pier 1	Pier 2
Reinforcement	ϕ10	ϕ10, ϕ4	ϕ10, ϕ4	ϕ10, ϕ4	ϕ10, ϕ4	ϕ10, ϕ4	ϕ10	ϕ10, ϕ4
A_{sw} [mm^2]	78,5	78.5; 12.6	78.5; 12.6	78.5; 12.6	78.5; 12.6	78.5; 12.6	78,5	78.5; 12.6
s [mm]	530	530; 100	530; 100	530; 100	530; 100	530; 100	530	530; 100
z [mm]	560	1360	560	560	560	1360	560	1360
f_y [N/mm^2]	450	450; 618	450; 618	450; 618	450; 618	450; 618	450	450; 618
θ [°]	45	36	30	28	34	37	33	35
α_{cw}	1	1	1	1	1	1	1	1
b_w [mm]	100	100	100	100	100	100	100	100
ν_1	0,53	0,53	0,55	0,55	0,55	0,55	0,53	0,53
f_{cm} [N/mm^2]	38	38	28	28	28	28	38	38
$V_{R,s}$ [kN]	37,32	270,45	140,17	152,23	120,02	260,82	57,48	280,67
$V_{R,s}$ (pier 1+2)	307,77		292,40		380,84		338,15	
$V_{R,max}$ [kN]	563,92	1302,44	373,50	357,40	399,63	1006,44	515,23	1287,14
$V_{R,max}$ (pier 1+2)	1866,36		730,89		1406,07		1802,37	
$0.4 \cdot V_{R,max}$ (1+2)	746,55		292,36		562,43		720,95	
$V_{exp,max}$ [kN]	858		344		793,5		763,5	

Following other recommendations available in literature, such as the ones of Biskinis et al. [124], the shear force which can be sustained by the concrete member, limited by crushing of the compression struts is overestimated in some cases, and for walls designed for high ductility class, $V_{Rd,max}$ should be taken as 0.4 of the value determined in other regions than the critical base one. Although a reduction factor for DCM walls is not provided in Eurocode, most probably due to the limited number of experimental tests performed on this type, the reduction factor 0.4 seems to be appropriate also for DCM walls. Postelnicu et al. [125] also reported

on the overestimation of the shear force which can be sustained by the concrete member and the 0.4 reduction factor.

3.8.2 Evaluation of the plastic mechanism model

According to the opening type, PRCWP (8-E3-T) specimen behaves like a frame under external loads. Considering the failure mechanism, where four plastic hinges appeared, on the top and bottom of the piers, the corresponding lateral load could be computed using the scheme presented in Figure 3.57.

$$M = A_{s1} \cdot f_{y1} \cdot z + N_c \cdot d_N = 47\ kNm$$

$$V_{th} = \frac{4 \cdot M}{H_w} + N_v \cdot (d_N + d_2) = 177\ kN < 207.5\ kN$$

As it can be observed, the evaluation based on the plastic mechanism model is reliable and can predict the shear resistance of shear wall specimens with wide openings.

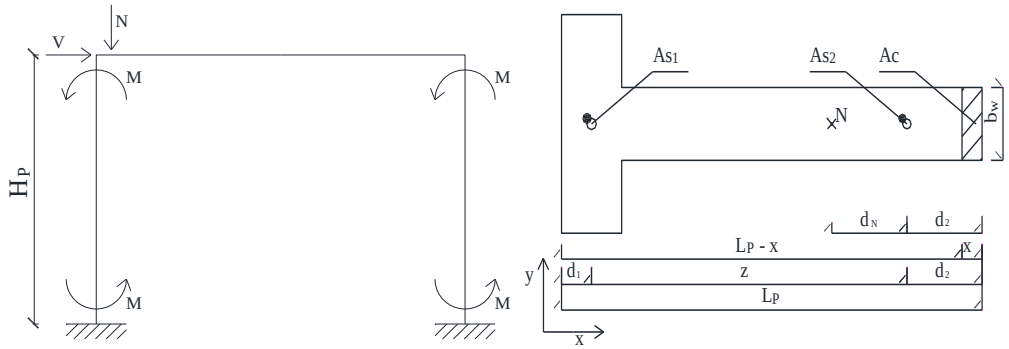

Figure 3.57 - Plastic mechanism considerations [108]

3.9 Weakening assessments

Among the main research interests investigated by the author is also the weakening assessment. The investigation is based on the assessment of door and window opening enlargement. Due to the fact that the current experimental program comprises only two such specimens, and because evaluation of several parameters would be necessary to be determined, the study needs to be completed with numerical data at the moment. Considering that good reliable data can be provided using numerical analysis, specimens having different characteristics can be further easily modeled and investigated. The experimental specimens selected for the investigation are PRCWP (10-L1/L3-T), PRCWP (11-L1-T) and PRCWP (12-E1-T).

The study was completed with a number of three additional numerical specimens for the evaluation of the weakening caused by cut-outs. As observed in Figure 3.58, the numerical specimens have intermediate door and window opening dimensions, and a wide door opening, whereas data related to the opening type and

dimensions are given in Table 3.8. The numerical analysis was performed also in ATENA 2D, following the same recommendations discussed in Section 3.7. The load-drift ratio envelope of the analysed specimens is shown in Figure 3.59, whereas the basic results are presented in table 3.9 showing a good agreement between the numerical results and the experimental tests of the wall specimens, and also a proportional reduction in the lateral resistance with the opening dimension increase. Since the experimental specimens were tested under quasi-static reversed cyclic lateral loading - displacement controlled, and the numerical models used a monotonic type of loading, for the comparison of the results it was taken the only positive cyclic M2 envelope curve of the experimental specimens.

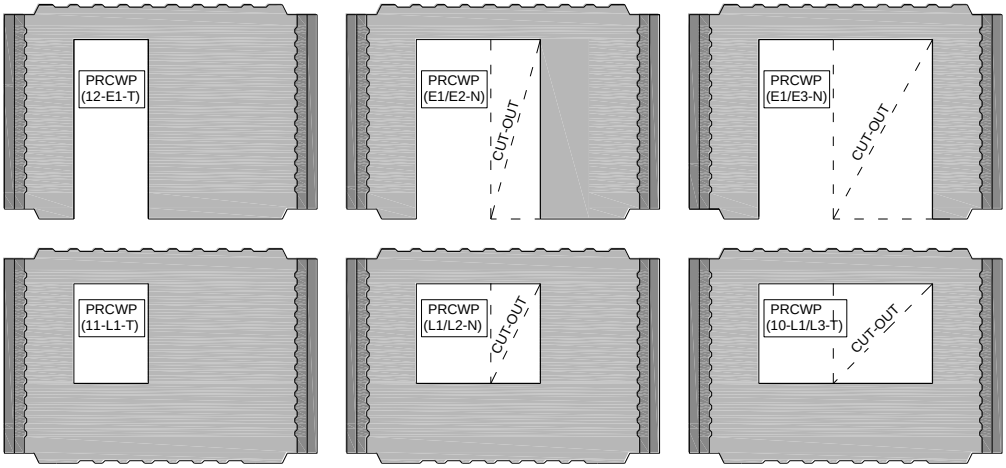

Figure 3.58 – Investigated wall specimen's layout.

Table 3.8 - Investigated wall specimens opening data

Element designation	As-built / cut-out opening type	Opening dimensions b x h [mm]	Experimental evidence
PRCWP (11-L1-T)	small window opening (L1)	750 x 1000	yes
PRCWP (L1/L2-N)	small window opening / medium window opening (L1/L2)	1250 x 1000	no
PRCWP (10-L1/L3-T)	small window opening / wide window opening (L1/L3)	1750 x 1000	yes
PRCWP (12-E1-T)	narrow door opening (E1)	750 x 1800	yes
PRCWP (E1/E2-N)	narrow door opening / medium door opening (E1/E2)	1250 x 1800	no
PRCWP (E1/E3-T)	narrow door opening / wide door opening (E1/E3)	1750 x 1800	no

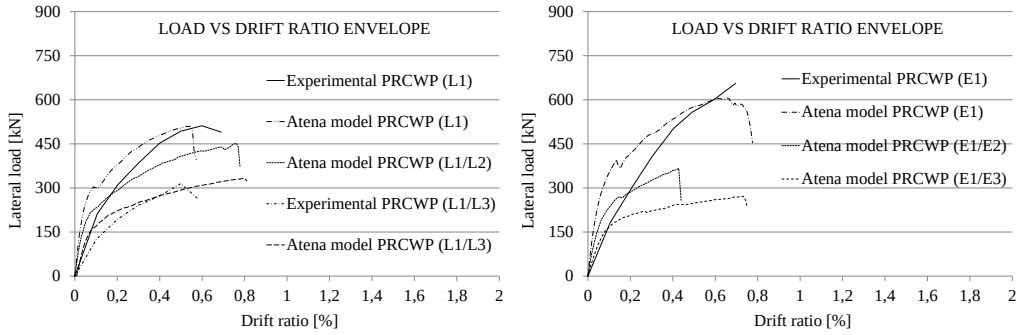

Figure 3.59 - Load – drift ratio curves

Table 3.9 Basic results of the investigated specimens

Element designation	Maximum lateral load [kN]	Drift ratio corresponding to maximum lateral load [mm]
Experimental PRCWP (L1)	511,50	0,60
Numerical PRCWP (L1)	510,20	0,55
Experimental PRCWP (L1/L2)	-	-
Numerical PRCWP (L1/L2)	451,30	0,76
Experimental PRCWP (L1/L3)	314,75	0,50
Numerical PRCWP (L1/L3)	332,10	0,78
Experimental PRCWP (E1)	656,00	0,70
Numerical PRCWP (E1)	606,40	0,66
Experimental PRCWP (E1/E2)	-	-
Numerical PRCWP (E1/E2)	366,70	0,43
Experimental PRCWP (E1/E3)	-	-
Numerical PRCWP (E1/E3)	271,46	0,72

The ultimate shear strength of a structural wall with opening can be estimated by multiplying the shear strength of the structural wall without opening with a reduction factor, according to the AIJ standards (AIJ 1999, AIJ 2010), on the condition that the opening ratio is less than 0.4 [126]. The shear strength of wall specimens having the opening ratio up to 0.46, can be estimated by combining the shear strength of structural walls without openings using truss and arch mechanism equation and Ono's reduction factor, according to Taleb et al. [127]. In current research, the following equations were derived from the AIJ 1999 [128] recommendation (quoted in [8, 126-127]):

$$(R)_{weak} = (R)_{sound} \cdot \alpha_p \tag{3.4}$$

where $(R)_{weak}$ is the response characteristic of the weakened structural member in terms of shear resistance, initial stiffness or energy dissipation rate; $(R)_{sound}$ is the response characteristic of the sound (solid) wall in terms of shear resistance, initial stiffness or energy dissipation rate; and α_p is the performance ratio, given by:

$$\alpha_p = 1 - \eta \tag{3.5}$$

The opening ratio η is given by the following relation:

$$\eta = P = \sqrt{A_o / A_w} \ \ for\ (R): shear\ resistance\ and\ stiffness \tag{3.6}$$

where P is the peripheral ratio, A_o and A_w is the in-plane area of the opening and the as-built wall member, respectively. The performance ratio indicates the response characteristic of the weakened element normalized to the corresponding characteristic of the as-built, reference one. In the present study, for the reference investigated wall specimens the above equations were verified for two peripheral ratios greater than the upper limit given in the AIJ standard, namely for 0.44 and 0.63 [129]. In Table 3.10 it is represented the response characteristic of the reference specimens, where R_r stands for response ratio. The experimental and numerical response ratio was determined by dividing the response of the weakened member to the response of the as-built wall. In Figure 3.60 are represented the experimental and numerical results regarding the weakening effect of the door and window cut-outs on the seismic response of the as-built reference wall, in terms of strength. The complementarity between the performance ratio and the cut-out ratio is represented with a dashed line, joining the unities of the two axes [8]. Based on the results given in Figure 3.60, one can remark the experimental evidence of complementarity between the strength performance and opening ratios.

According to the obtained results, it is obvious the reduction in lateral resistance proportional to the opening dimension increase. The estimated weakening effect of the cut-out openings was found to be in good agreement with the predictions provided by the AIJ equation, even if this was extended to higher peri-

Table 3.10 Response characteristic in terms of shear resistance

Element	$R_{sound,exp}$	$R_{sound,Atena}$	R_{atena}	$R_{exp.}$	$R_{weak,exp}$	$R_{weak,Atena}$	P	α_p	$R_{r,exp}$	$R_{r,Atena}$
	[kN]	[kN]	[kN]	[kN]	[kN]	[kN]	[%]	[%]	[%]	[%]
PRCWP (L1)	511,5	510,2	510,2	511,5	0,0	0,0	1,0	0,00	0,00	0,00
PRCWP (L1/L2)			451,3	-	352,9	352,0	0,31	0,69	-	0,88
PRCWP (L1/L3)			332,1	314,75	286,4	285,7	0,44	0,56	0,62	0,65
PRCWP (E1)	656	606,4	606,4	656	0,0	0,0	1,0	0,00	0,00	0,00
PRCWP (E1/E2)			366,7	-	367,4	339,6	0,44	0,56	-	0,60
PRCWP (E1/E3)			271,5	-	242,7	224,4	0,63	0,37	-	0,45

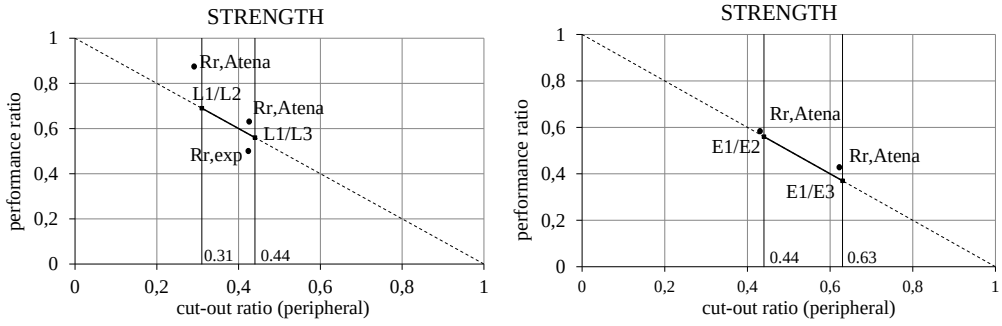

Figure 3.60 The weakening effect of the cut-outs on the seismic response. [129]

pheral ratio values here. The author considers that further investigations and tests related to the evaluation of the weakening are necessary, for the consideration of several parameters like the opening type, opening dimensions and strengthening strategies used.

3.10 Cracking pattern

Taking into account the importance of the cracking pattern, the front face of the wall specimens was monitored for crack occurrence and development during the experimental testing. Therefore, an orthogonal reference grid was drawn on the wall face, comprising a number of 64 rectangles (see Section 2.6), which were photographed and a photo-map was then assembled. Using AutoCAD Software, all the cracks were marked on the photo-map, and the final cracking pattern was computed and presented in Figure 3.61.

As observed in Figure 3.61, a significant number of flexural and shear cracks appeared during the experimental testing of the specimens. Flexural cracks appeared at the pier-to-reaction beams connection regions (mostly in the cast-in-place mortar). Few flexural cracks appeared along the piers' vertical edges (mostly between the web panel and unconfined wing) and in the spandrel beam. A significant number of inclined cracks can be seen in the piers, parapet and spandrel beam.

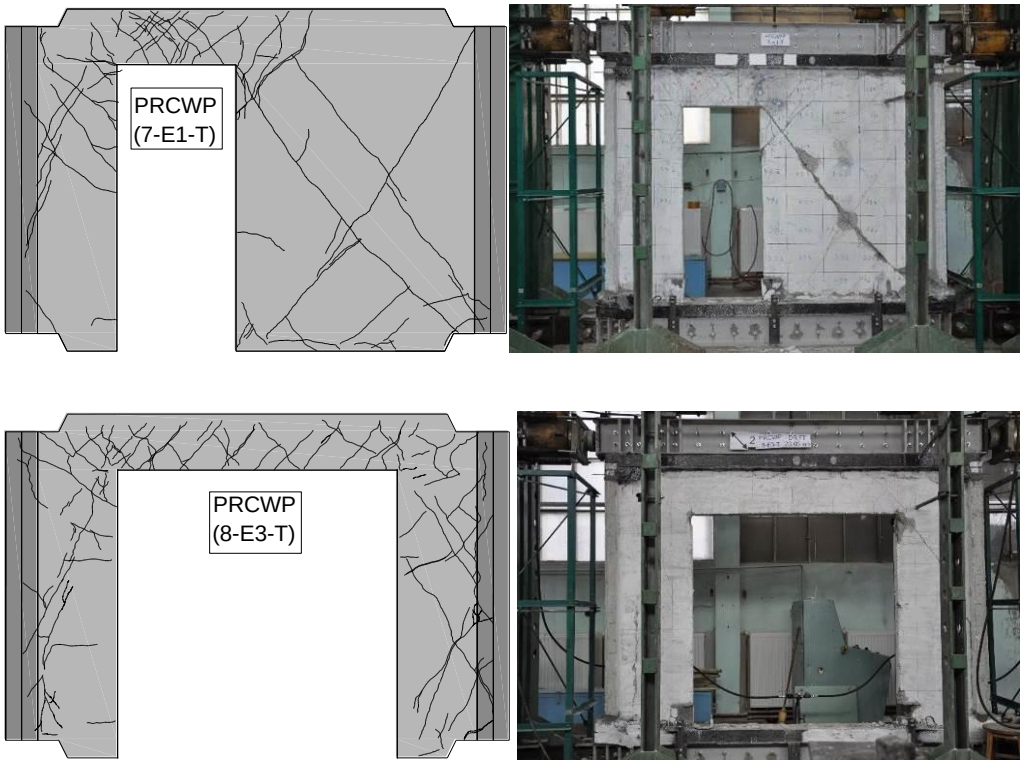

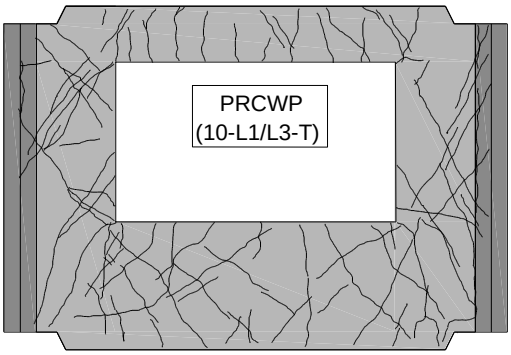
PRCWP
(10-L1/L3-T)

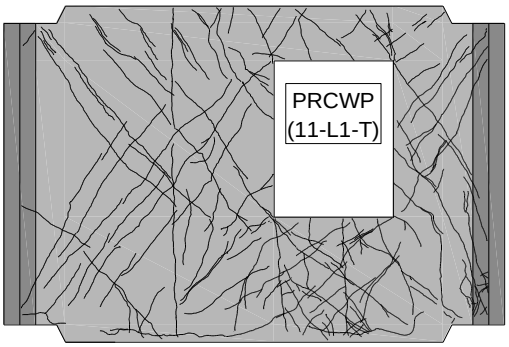
PRCWP
(11-L1-T)

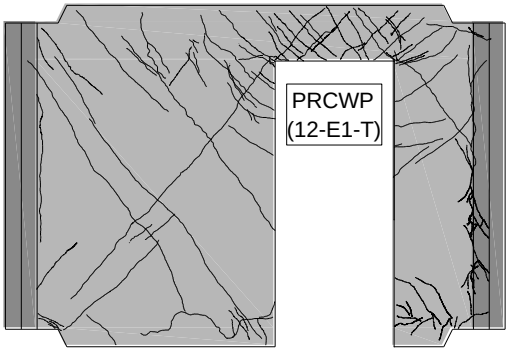
PRCWP
(12-E1-T)

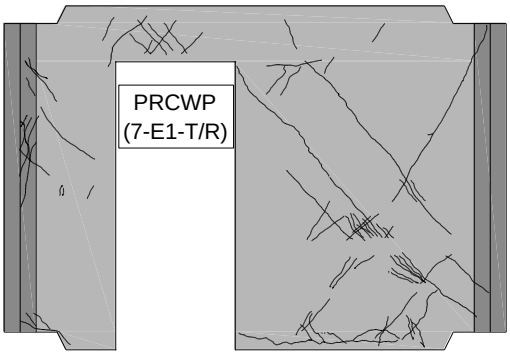
PRCWP
(7-E1-T/R)

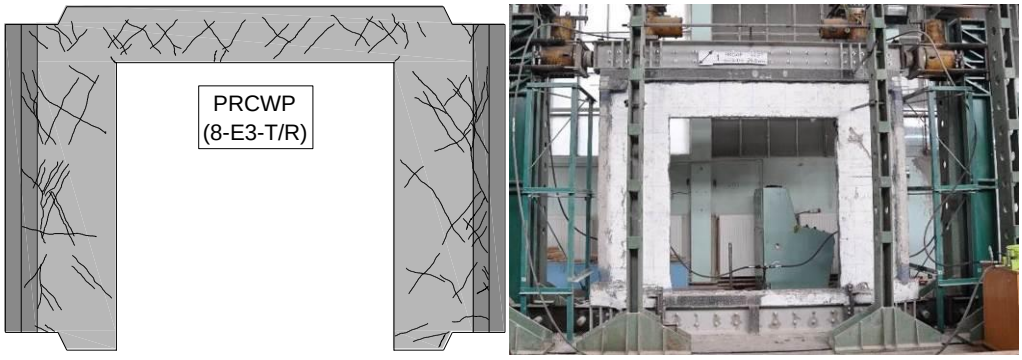
PRCWP
(8-E3-T/R)

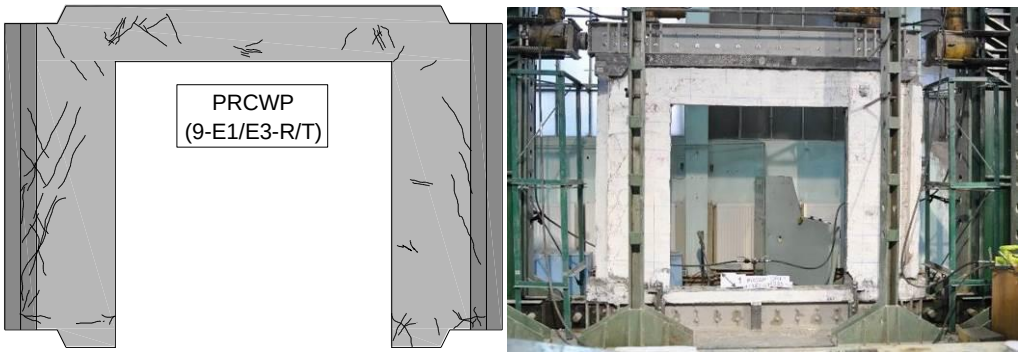
PRCWP
(9-E1/E3-R/T)

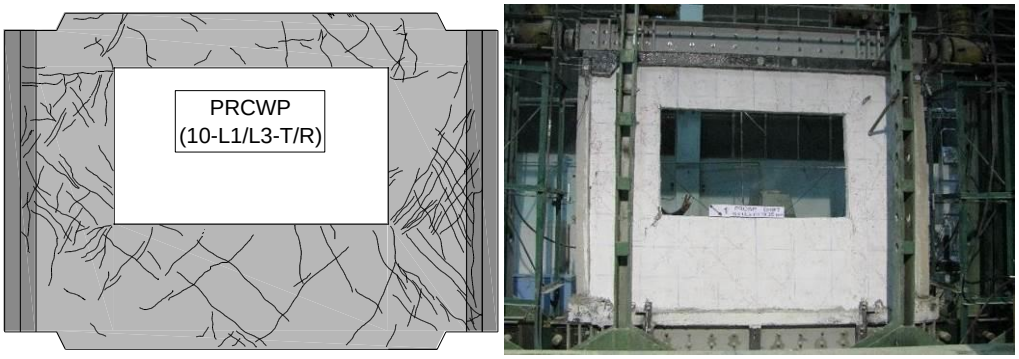
PRCWP
(10-L1/L3-T/R)

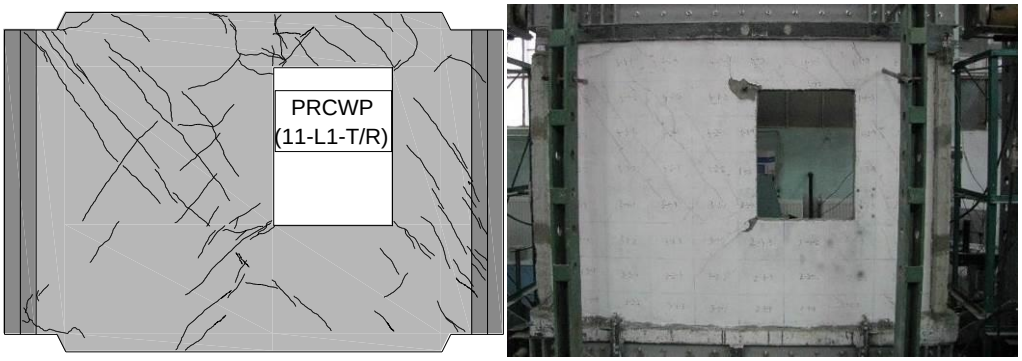
PRCWP
(11-L1-T/R)

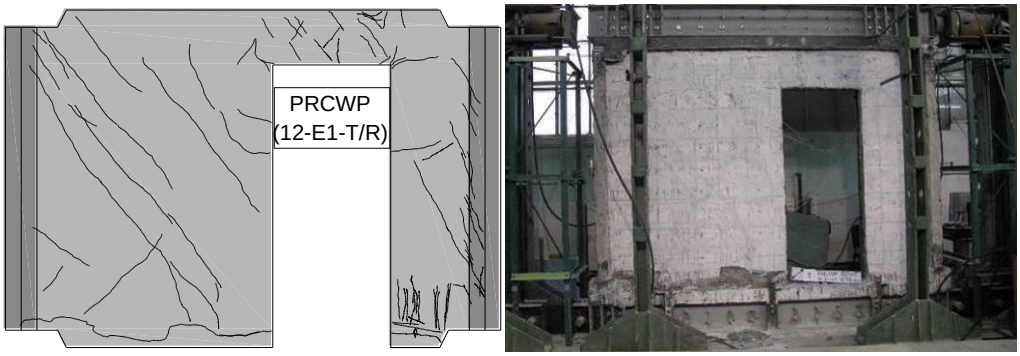

Figure 3.61 The final cracking pattern of the tested specimens

According to Appendix A, about 45 cracks were noticed during the experimental test of PRCWP (7-E1-T), 70 cracks for PRCWP (8-E3-T), 89 cracks for PRCWP (10-L1/L3-T), 79 for PRCWP (11-L1-T), 57 for PRCWP (12-E1-T), 16 for PRCWP (7-E1-T/R), 82 for PRCWP (8-E3-T/R), 57 for PRCWP (9-E1/E3-R/T), 115 for for PRCWP (10-L1/L3-T/R), 41 for for PRCWP (11-L1-T/R), and 49 for for PRCWP (12-E1-T/R).

4 Conclusions

This chapter summarizes the main conclusions which can be drawn within the limitations of the current research, performed on six near-full scale precast reinforced concrete wall panels. As the investigated wall specimens were 1:1.2 real scaled elements, the results nearly reflect the real behaviour.

– extensive cracking was observed in the case of the reference wall panels, together with reinforcement yielding, cast-in-place mortar crushing and concrete crushing developed at the extremities of the diagonal compressed struts, pier-spandrel connection region and bottom extremities of the piers –near the opening.

– related to the analysed strengthenings, horizontal and vertical FRP strips debonding were observed, confinement strips fracturing, TRM debonding when a punctual type of anchorage was used, diagonal cracks, cast in place mortar crushing and concrete crushing at the pier-spandrel connection regions. No failure was observed in the case of near-surface mounted CFRP plates.

– based on the obtained results, it can be seen that the load bearing capacity of the specimens was restored through the considered rehabilitation strategies and increased in some cases. A maximum load variation was found between 46.5% and 111% in the positive loading cycles and 93% and 154% in the negative loading cycles, whereas the displacement at failure was higher in the case of the strengthened elements.

– the energy dissipation analysis revealed that the wall panels with small openings, like PRCWP (7-E1-T, 11-L1-T, 12-E1-T) dissipate more energy compared to the specimens with large opening dimensions, namely PRCWP (8-E3-T, 10-L1/L3-T), whose the deformation capacity was found to be higher; also, a higher energy dissipation was found for the strengthened PRCWP (7, 10, 11) specimens, compared to the reference ones, whereas for PRCWP (8, 12) strengthened and reference specimens, a similar energy dissipation was obtained.

– the ductility considerations based on the μ0.85 method, showed that the wall specimens having large openings develop an inferior ductility compared to those having smaller openings, i.e., PRCWP (8-E3-T) compared to PRCWP (12-E1-T) and PRCWP (10-L1/L3-T) compared to PRCWP (11-L1-T); it was also found that the the ductility of PRCWP (7, 10) specimens was higher than for the reference specimens. Only in the case of the strengthened PRCWP 8, the ductility was lower compared to the reference specimen; related to PRCWP 9, a higher ductility was obtained compared to the strengthened PRCWP (7, 8) specimens.

– steel rebar yielding was attained for almost all the reference specimens in the critical regions, e.g., spandrel-pier connection regions, piers and parapet. Measurements on FRPs did not indicate high strain values, but they were certainly active during the experimental tests.

– significant reductions in stiffness were obtained for the specimens having large opening dimensions, like PRCWP (8-E3-T, 10-L1/L3-T) compared to the specimens having smaller openings, namely PRCWP (7-E1-T, 11-L1-T, 12-E1-T); a similar initial stiffness was found for most of the strengthened walls compared to their

reference counterparts, namely PRCWP (8, 10–12). For PRCWP 7 strengthened specimen, the initial stiffness increased (25%) compared to the reference one.

– The numerical analysis presented in this research proves that no sophisticated models are necessary to estimate the results in terms of peak lateral load and displacements. Based on the good agreement obtained between the numerical analysis and experimental tests of the wall specimens (reference or strengthened by different methods), it can be concluded that important response characteristics in terms of peak lateral load and displacement can be estimated for other walls having various parameters, like opening dimension and strengthening. In the case of PRCWP (10) strengthened specimen, the numerical model produced higher values compared to the experimental one where debonding of the TRM system occurred due to the used anchorage type. It is clearly that if a better connection between the panel and the TRM system would have been used, a higher load bearing capacity and displacement capacity could have been achieved.

– the evaluation of the shear strength using EC2 expressions showed that the shear force which can be sustained by the yielding shear reinforcement is too conservative compared to the obtained experimental values; whereas the shear force which can be sustained by the concrete member, limited by crushing of the compressed struts is overestimated. Considering the obtained results, the ‘‘0.4’’ reduction factor proposed by Biskinis et al. [28] seems to be more adequate for the prediction of the shear strength of the DCM walls, too. Further experimental tests on DCM walls have to be performed in order to confirm or calibrate the reduction factor.

– According to the opening type, PRCWP (8-E3-T) specimen behaves like a frame under external loads, therefore by using a simplified model based on plastic mechanism, the shear strength could be easily estimated for panels with wide openings too.

The author recommends further studies related to the ductility and strengthening of wall panels in order to establish the most convenient solutions for the seismic response. Also the behaviour of the wall panels with different cut-outs needs to be further investigated.

5 Personal contributions

The author considers the following contributions worth to notice:

1. Literature investigation on current similar research directions, such as: precast, reinforced concrete structures, reinforced concrete walls with/without openings, ductility estimations, strengthening using FRPs, numerical analysis. The database comprises 115 references.

2. Improving the initial experimental program by:

☐ testing 6 near-full scale specimens, conducting 11 quasi-static cyclic tests (more than 80 active hours);

☐ applying additional anchorage system in the span (between the wall panel and the foundation beam) composed of steel L channels;

☐ providing repair and strengthening materials from different sources;

☐ design and testing strengthening strategies of EBR-CFRP, NSM-CFRP and TRM (with glass fibre and carbon fibre grid), and also two types of anchorage systems;

☐ instrumentation scheme for each test.

3. processing of the observed and recorded results:

☐ more than 200.000 processed data lines;

☐ observations on the behaviour mode and failure details;

☐ computation of load versus displacement hysteresis loops;

☐ computation of cyclic load-drift envelopes, monotonic lateral load-drift envelopes, backbone lateral load-drift, strength and displacement histograms;

☐ energy dissipation (cumulative energy dissipated, cumulative drift, energy dissipation);

☐ ductility coefficient;

☐ strain analysis;

☐ stiffness (initial stiffness, secant stiffness degradation);

☐ computation of the numerical models;

☐ evaluation of the shear strength using design code provisions and plastic mechanism model;

☐ weakening assessment using design code provisions, numerical models and experimental tests;

☐ computation of the final cracking pattern based on photo-map;

4. synthesis of the results;

5. listing of the personal contributions;

6. further research directions.

During the doctoral studies the author published 18 papers (13 abroad and 5 in Romania) on the investigated theme and made contributions to a research program on integrated strategies and policy instruments for retrofitting buildings to reduce primary energy use and GHG emissions, and a strategic grant – Investing in People, within the Sectoral Operational Programme Human Resources Development 2007-2013. A selection of representative papers, and the contribution to the research grant is provided below.

Selected papers:

1. C. Toduț, D. Dan, V. Stoian, "Theoretical and experimental study on precast reinforced concrete wall panels subjected to shear force", Engineering Structures 80, pp. 323–338, 2014.

2. C. Toduț, D. Dan, V. Stoian, "Numerical and experimental investigation on seismically damaged reinforced concrete wall panels retrofitted with FRP composites", Composite Structures, 119 (2015) 648–665, (Available online 28 September 2014, In Press, Accepted Manuscript).

3. V. Stoian, C. Toduț, T. Nagy-György, I. Demeter, "Numerical Modeling of Reinforced Concrete Wall Panels Weakened by Cut-outs", Journal of Applied Engineering Sciences, Oradea, Romania, vol.2(15), issue 2, pp. 115-120, 2012.

4. C. Toduț, V. Stoian, I. Demeter, "Glass Fiber versus Carbon Fiber Grid used in Textile Reinforced Mortar Strengthening of Precast RC Walls", IACSIT International Journal of Engineering and Technology, vol.5, no.5, pp. 622-626, 2013.

5. C. Todut, D. Dan, V. Stoian, "TRM strengthening of precast reinforced concrete wall panel with cut-out opening - experimental investigation", Advances in Engineering Mechanics and Materials, ISBN: 978-1-61804-241-5, pp. 110-116, 2014.

6. C. Todut, V. Stoian, D. Dan, T. Nagy-György, "Seismic strengthening of a precast reinforced concrete wall panel using NSM-CFRP", Bulletin of the Transilvania University of Braşov, Vol. 7 (56) – 2014, Series I: Engineering Sciences.

7. C. Toduț, V. Stoian, D. Dan, "Experimental Assessment of FRP Strengthening Strategies for Precast RC Wall Panels", 12th International Conference on Steel, Space and Composite Structures, Prague, Czech Republic, pp. 379-386, May 2014.

8. C. Toduț, V. Stoian, I. Demeter, T. Nagy-György, V. Ungureanu, "Retrofitting of Earthquake Damaged Precast Concrete Wall Using FRP Composites", Fib Symposium "Engineering a Concrete Future: Technology, Modeling & Construction", Tel-Aviv, Israel, pp. 573-576, April 2013.

9. C. Toduț, V. Stoian, I. Demeter, T. Nagy-György, D. Dan, V. Ungureanu, "Seismic Strengthening of a Precast Reinforced Concrete Wall Panel Using Combined NSM and CFRP-EBR Method", 11th International Symposium on Fiber Reinforced Polymers for Reinforced Concrete Structures (FRPRCS11), Guimarães, Portugal, pp. 269-270, June 2013.

10. C. Todut, V. Stoian, D. Dan, T. Nagy-György, " Numerical Assessment of the Weakening Induced by Cut-outs Made in Precast Reinforced Concrete Wall Panels",

2nd Conference for PhD students in Civil Engineering CE-PhD 2014, 10-13 December 2014, Cluj-Napoca, Romania (to be published).

Contribution to research projects:

1. Grant no. 3-002/2011, INSPIRE – Integrated Strategies and Policy Instruments for Retrofitting buildings to reduce primary energy use and GHG emissions, Project type PN II ERA NET, financed by the Executive Agency for Higher Education, Research, Development and Innovation Funding (UEFISCDI), Romania.

2. Strategic grant POSDRU/159/1.5/S/137070 (2014) of the Ministry of National Education, Romania, co-financed by the European Social Fund – Investing in People, within the Sectoral Operational Programme Human Resources Development 2007-2013.

Acknowledgements

1. "Retrofit of RC walls and slabs with cut-out openings using FRP composites", financial support by the National University Research Council (CNCSIS), through grant No. 355/2006, CNCSIS, type A, coordinated by Prof. Stoian Valeriu, Politehnica University of Timisoara.

2. "Advanced strengthening systems of RC members, beams, columns, walls and slabs, using FRP composites", supported by the Ministry of Education and Research, Romania, through contract No. 1436/2006, CNCSIS, CEEX, type ET, coordinated by Dr. Nagy-György Tamás, Politehnica University of Timisoara.

3. Grant no. 3-002/2011, INSPIRE – Integrated Strategies and Policy Instruments for Retrofitting buildings to reduce primary energy use and GHG emissions, Project type PN II ERA NET, financed by the Executive Agency for Higher Education, Research, Development and Innovation Funding (UEFISCDI), Romania.

4. Strategic grant POSDRU/159/1.5/S/137070 (2014) of the Ministry of National Education, Romania, co-financed by the European Social Fund – Investing in People, within the Sectoral Operational Programme Human Resources Development 2007-2013.

6 Recommendations for further research

Since the current research is based on a limited number of experimental specimens, there is an obvious need for further investigations on experimental specimens.

The presented experimental investigations were made on nearly full-scale precast reinforced concrete shear walls, with as-built openings and/or opening enlargements. Although the test series comprised both door and window type of opening, further experimental research is needed to investigate on the following:

- influence of the type of opening and opening dimensions on the seismic response;
- assess several types of weakenings in walls;
- make further evaluation on the ductility of the specimens;
- evaluate the strengthening contribution to the shear strength of the walls;
- improve the numerical analysis in terms of strengthening modeling;
- further experimental tests on DCM walls have to be performed in order to confirm or calibrate the reduction factor for the evaluation of the shear strength using design code provisions.

This can be achieved by a large number of test series and would provide answers to the current research and would calibrate on the already concluded remarks.

Another important aspect of further research in the field is to study the behaviour of precast reinforced concrete large panel buildings having weakened structural walls and also investigate on the rehabilitation strategies.

BIBLIOGRAPHY

[1] Fintel M. Performance of Buildings with Structural Walls in Earthquakes of the Last Thirty Years. PCI Journal, 40(3), (1995), pp. 62–80.
[2] Fintel M. Shear Walls – An answer for Seismic Resistance? Concrete International, Vol. 13, No. 7, (1991), pp. 48–53.
[3] Alfred A. Yee. Structural and economic benefits of precast/prestressed concrete construction. PCI Journal, july-august (2001), pp. 34-42.
[4] Thomas D. J., Sritharan S. An evaluation of seismic design guidelines proposed for precast jointed wall systems. ISU-ERI-Ames Report ERI-04643; 2004.
[5] Park R. A perspective on the seismic design of precast concrete structures in New Zealand. PCI Journal, Vol. 40, No. 3, May-June 1995.
[6] Park R. The FIB state-of-the-art report on the seismic design of precast concrete building structures. 2003 Pacific Conference on Earthquake Engineering in Auckland, New Zealand, Paper number 11, Feb. 2003.
[7] Vernu S., Sritharan S. Section, member and system level analyses for precast concrete hybrid frames. ISU-ERI-Ames Report ERI-04635, Department of Civil, Construction and Environmental Engineering, Iowa State University, Ames, Iowa, June 2004.
[8] Demeter I. Seismic retrofit of precast RC walls by externally bonded CFRP composites. PhD thesis. Politehnica University of Timisoara; 2011.
[9] Dan D, Fabian A, Stoian V. Theoretical and experimental study on composite steel–concrete shear walls with vertical steel encased profiles. J Constr Steel Res 2011; 67:800–13.
[10] Greifenhagen C., Lestuzzi P. Static cyclic tests on lightly reinforced concrete shear walls. Eng Struct 2005; 27:1703–12.
[11] Parulekar Y. M., Reddy G. R., Vaze K. K., Pegon P., Wenzel H. Simulation of reinforced concrete short shear wall subjected tocyclic loading. Nuclear Engineering and Design, 270, (2014), pp. 344–350.
[12] Thomson E. D., Perdomo M. E., Picón R., Marante M. E., Flórez- López J. Simplified model for damage in squat RC shear walls. Eng Struct 2009; 31:2215–23.
[13] Sánchez-Alejandre A., Alcocer S. M. Shear strength of squat reinforced concrete walls subjected to earthquake loading trends and models. Eng Struct 2010; 32:2466–76.
[14] Pavese A., Bournas D. A. Experimental assessment of the seismic performance of a prefabricated concrete structural wall system. Eng Struct 2011; 33:2049–62.
[15] Jiang H., Kurama Y. C. An analytical investigation on the seismic retrofit of older medium-rise reinforced concrete shear walls under lateral loads. Eng Struct 2013; 46:459–70.
[16] Ganesan N., Indira P. V., Rajendra P. S. Ultimate strength of reinforced concrete wall panels. International Journal of Earth Sciences and Engineering. ISSN 0974-5904, Vol. 02, No. 04, August 2009, pp. 340-350.
[17] Kara I. F., Dundar C. Prediction of deflection of reinforced concrete shear walls. Advances in Engineering Software 2009; 40:777–785.
[18] Orakcal K., Massone L. M, Wallace J. W. Shear strength of lightly reinforced wall piers and spandrels. ACI Struct J 2009; July–August: 455–65.
[19] ACI Committee 318, Building Code Requirements for Structural Concrete (ACI 318-05) and Commentary (318R-05), American Concrete Institute, Farmington Hills, MI, 2005, 430 pp.
[20] Federal Emergency Management Agency, Prestandard and Commentary for the Seismic Rehabilitation of Buildings, Report No. FEMA-356/Nov.2000, Washington, DC, 2000, 518 pp.

[21] Guan H., Cooper C., Lee D. Ultimate strength analysis of normal and high strength concrete wall panels with varying opening configurations. Eng Struct 2010; 32:1341-55.
[22] Mosoarca M. Seismic behavior of reinforced concrete shear walls with regular and staggered openings after the strong earthquakes between 2009 and 2011. Eng Fail Anal 2013; 34:537–65.
[23] Wang J., Sakashita M., Kono S., Tanakah., Warashina M. A macro model for reinforced concrete structural walls having various opening ratios. The 14th World Conference on Earthquake Engineering October 12-17, 2008, Beijing, China.
[24] Takehara.M, Motitsuki, et al. (1993), Elasto-plastic analysis of framed shear walls with an opening using macro model. Summaries of Technical Papers of Annual Meeting Architectural Institute of Japan, Structures Ⅳ 303-304.
[25] Hara T., Doh J. Finite element investigation of R/C wall with openings. The 14th International Conference on Computing in Civil and Building Engineering. Moscow, Russia, 27-29 June, 2012.
[26] Li Bing, Chen Qin. Initial stiffness of reinforced concrete structural walls with irregular openings. Earthq Eng Struct Dyn 2010; 39:397–417 [Published online 10.08.09 in Wiley InterScience].
[27] Fragomeni S., Doh J. H., Lee D. J. Behavior of axially loaded concrete wall panels with openings: an experimental study. Adv Struct Eng 2012; 15(8):1345–58.
[28] Carrillo J., Alcocer S. Degradation Properties of Reinforced Concrete Walls with Openings. Dyna, ISSN 0012-7353 (2011), vol. 78, pp. 106-115.
[29] Wang J., Sakashita M., Kono S., Tanaka H., Lou W. Behavior of reinforced concrete structural walls with various opening locations: experiments and macro model. J Zhejiang Univ – Sci A (Appl Phys Eng) 2010; 11(3):202–11.
[30] Park R. Ductility evaluation from laboratory and analytical testing. Proceedings of 9th World Conference on Earthquake Engineering (9WCEE), Tokyo, Japan, (1988), 8:605-616.
[31] Priestley M. Performance based seismic design. Proceedings of 12th World Conference on Earthquake Engineering (12WCEE), Auckland, New Zealand, (2000), paper 2831.
[32] Salonikios T., Kappos A., Tegos I., Penelis G. Cyclic load behavior of low-slenderness reinforced concrete walls: failure modes, strength and deformation analysis, and design implications. ACI Structural Journal (2000); 97(1):132-142.
[33] Carrillo J., Gonzalez G., Rubiano A. Displacement ductility for seismic design of RC walls for low-rise housing. Lat Am J Solids Struct 2014; 11:725–37.
[34] Greifenhagen C. Seismic behavior of lightly reinforced concrete squat shear walls. PhD Thesis No. 3512. École Polytechnique Fédérale De Lausanne; 2006.
[35] Christidis K., Vougioukas E., Trezos K. Seismic assessment of existing RC shear walls non-compliant with current code provisions. Magazine of Concrete Research, 2013, 65(17), 1059-1072.
[36] Kuang J. S., Ho Y. B. Enhancing ductility of non-seismically designed RC shear walls. Proceedings of the Institution of Civil Engineers; Structures and Buildings 160, June 2007, Issue SB3, pp. 139-149.
[37] Bashar S. M., Ean L. W., Malek M. A. One way RC wall panels with openings strengthened with CFRP. Construction and Building Materials 2013; 40: 575–83.
[38] Saheb S. M., Desayi P. Ultimate strength of RC wall panels with openings. J Struct Eng 1990; 116(6):1565–78.
[39] Altin S., Anil Ö, Kopraman Y., Kara M. E. Hysteretic behavior of RC shear walls strengthened with CFRP strips. Composites: Part B, 2013; 44: 321–29.

[40] ACI Committee 440. Guide for the design and construction of externally bonded FRP systems for strengthening of concrete structures. Farmington Hills (MI, USA); 2002.
[41] Antoniades K. K, Salonikios T. N., Kappos A. J. Cyclic tests on seismically damaged reinforced concrete walls strengthened using fiber-reinforced polymer reinforcement. ACI Struct J 2003; July–August:510–8.
[42] Li Bing, Lim Chee Leong. Tests on seismically damaged reinforced concrete structural walls repaired using fiber-reinforced polymers. J Compos Constr ASCE 2010; September/ October: 597–608.
[43] Dan D. Experimental tests on seismically damaged composite steel concrete walls retrofitted with CFRP composites. Eng Struct 2012; 45:338–48.
[44] Kheyroddin A., Naderpour H., Hoseini Vaez S. R. Hysteretic evaluation of seismic behavior of RC shear walls strengthened with FRP sheets. The 14th World Conference on Earthquake Engineering October 12-17, 2008, Beijing, China.
[45] Meftah S.A., Yeghnem R., Tounsi A., Adda bedia E. A. Seismic behavior of RC coupled shear walls repaired with CFRP laminates having variable fibers spacing. Construction and Building Materials 2007; 21: 1661–71.
[46] Demeter I. , Nagy-György T., Stoian V., Dan D. Seismic retrofit of cut-out weakened precast RC walls by externally bonded CFRP composites. The 15th World Conference on Earthquake Engineering; 24-28 September, 2012, Lisbon, Portugal.
[47] AIJ (1999), "AIJ Standard for Structural Calculation of Reinforced Concrete Structures Based on Allowable Stress Concept", Architectural Institute of Japan.
[48] Warashina M., Kono S., Sakashita M., Tanaka H. Shear behavior of multi-story RC structural walls with eccentric openings. Proc., 14th World Conf. On Earthquake Engineering (14WCEE), Beijing, China (2008).
[49] Ghobarah A., Khalil A. A. Seismic rehabilitation of reinforced concrete walls using fibre composites. 13th World Conference on Earthquake Engineering Vancouver, B.C., Canada
August 1-6, 2004, Paper No. 3316.
[50] Antoniades K. K., Salonikios T. N., Kappos A. J. Evaluation of hysteretic response and strength of repaired R/C walls strengthened with FRPs. Eng Struct 2007; 29: 2158–71.
[51] Florut S-C., Sas G., Popescu C., Stoian V. Tests on reinforced concrete slabs with cut-out openings strengthened with fibre-reinforced polymers. Composites: Part B 2014; doi: http:// dx.doi.org/ 10.1016/j.compositesb.2014.06.008.
[52] EN 1992-1-1. Eurocode 2: Design of concrete structures - Part 1-1: General rules and rules for buildings. Brussels: COMITÉ EUROPÉEN DE NORMALISATION; 2004.
[53] Petersen RB. In-plane shear behaviour of unreinforced masonry panels strengthened with fibre reinforced polymer strips. PhD-thesis. The University of Newcastle; 2009.
[54] Konthesingha K.M.C., Masia M.J., Petersen R.B., Mojsilovic N., Simundic G., Page A.W. Static cyclic in-plane shear response of damaged masonry walls retrofitted with NSM FRP strips – An experimental evaluation. Eng Struct 2013; 50: 126–36.
[55] Sakar G., Hawileh R.A., Naser M. Z., Abdalla J. A., Tanarslan M. Nonlinear Behavior of Shear Deficient RC Beams Strengthened with Near Surface Mounted Glass Fiber Reinforcement under Cyclic Loading", Materials and Design (2014), doi:http://dx.doi.org/ 10.1016/j.matdes.2014.04.064.

[56] Griffith M. C., Kashyap J., Mohamed Ali M. S. Flexural displacement response of NSM FRP retrofitted masonry walls. Construction and Building Materials 2013; 49: 1032–40.
[57] Lee D., Cheng L. Bond of NSM systems in concrete strengthening – Examining design issues of strength, groove detailing and bond-dependent coefficient. Construction and Building Materials 2013; 47: 1512–22.
[58] Lee D., Cheng L., Hui J. Y. Bond characteristics of various NSM FRP reinforcements in concrete. J Compos Constr (ASCE) 2013; 17(1):117–29.
[59] American Concrete Institute Technical Committee 440. Guide for the design and construction of externally bonded FRP systems for strengthening concrete structures. ACI 440.2R-08, 2008.
[60] Breiman L., Friedman J. H., Olshen R. A., Stone C. G. Classification and regression trees. Belmont, CA, USA: Wadsworth International Group; 1984.
[61] Ripley B. D. Pattern recognition and neural networks. Cambridge, UK: Cambridge University Press; 1996.
[62] Bianco V., Barros J.A.O., Monti G. Three dimensional mechanical model for simulating the NSM FRP strips shear strength contribution to RC beams. Eng Struct 2009; 31: 815-26.
[63] Mohamed Ali M. S., Oehlers D. J., Griffith M.C., Seracino R. Interfacial stress transfer of near surface-mounted FRP-to-concrete joints. Eng Struct 2008; 30: 1861–68.
[64] De Lorenzis L., Lundgren K., Rizzo A. Anchorage length of near-surface mounted fiber-
reinforced polymer bars for concrete strengthening - experimental investigation and numerical modeling. ACI Structural Journal, March-April 2004; 269-278.
[65] Li T., Galati N., Tumialan J. G., Nanni A. Analysis of unreinforced masonry concrete walls
strengthened with glass fiber-reinforced polymer bars. ACI Structural Journal /July-August 2005, 569-577.
[66] Sas G. FRP shear strengthening of reinforced concrete beams. PhD Thesis. Luleå University of Technology; 2011.
[67] Bournas D.A., Triantafillou T.C. Innovative seismic retrofitting of old-type RC columns through jacketing: textile-reinforced mortars (TRM) versus fiber-reinforced polymers (FRP). The 14th World Conference on Earthquake Engineering October 12-17, 2008, Beijing, China.
[68] Ombres L. Debonding analysis of reinforced concrete beams strengthened with fibre reinforced cementitious mortar. Engineering Fracture Mechanics 2012; 81: 94–109.
[69] Papanicolaou C., Triantafillou T., Lekka M. Externally bonded grids as strengthening and seismic retrofitting materials of masonry panels. Construction and Building Materials 2011; 25: 504–514.
[70] Bernat-Maso E., Escrig C., Aranha C. A., Gil L. Experimental assessment of Textile Reinforced Sprayed Mortar strengthening system for brickwork wallettes. Construction and Building Materials 2014; 50: 226–36.
[71] Urban M., Stempniewski L. Evolution of a strengthening system for masonry buildings - from prototype to practical implementation "RÖFIX Sisma Calce". The International Conference "Skopje Earthquake - 50 Years of European Earthquake Engineering" (SE-50EEE), Skopje, Macedonia, 29-31 May 2013.
[72] Bernat E., Gil L., Roca P., Escrig C. Experimental and analytical study of TRM strengthened brickwork walls under eccentric compressive loading. Construction and Building Materials 2013; 44: 35-47.

[73] Papanicolaou C. G., Triantafillou T. C., Papathanasiou M., Karlos K. Textile reinforced mortar (TRM) versus FRP as strengthening material of URM walls: out-of-plane cyclic loading. Materials and Structures 2008; 41:143–157.
[74] Corradi M., Borri A., Castori G., Sisti R. Shear strengthening of wall panels through jacketing with cement mortar reinforced by GFRP grids. Composites: Part B, (2014), doi: http://dx.doi.org/10.1016/j.compositesb.2014.03.022.
[75] Triantafillou T. C., Papanicolaou C. G., Zissimopoulos P., Laourdekis T. Concrete confinement with textile-reinforced mortar jackets. ACI Structural Journal/ January-February 2006, pp. 28-37.
[76] San-José J.T., García D., El Hadid T., San-Mateos R., Al Far A., Marcos I. Novelty FRP and TRM strengthening systems applied to stone masonry walls: experimental programme presentation (I). Asia-Pacific Conference on FRP in Structures (APFIS 2007) S. T. Smith (ed)
© 2007 International Institute for FRP in Construction, pp. 271-276.
[77] Blanksvärd T. Strengthening of concrete structures by the use of mineral based composites. PhD Thesis. Luleå University of Technology; 2007.
[78] Eshwar N., Nanni A., Ibell T. J. Performance of two anchor systems of externally bonded fiber-reinforced polymer laminates. ACI Materials Journal/ January-February 2008, pp. 72-80.
[79] Zhang H. W., Smith S. T., Kim S. J. Optimisation of carbon and glass FRP anchor design. Construction and Building Materials 2012; 32: 1–12.
[80] Smith S. T., Hua S., Kima S. J., Seracino R. FRP-strengthened RC slabs anchored with FRP anchors. Eng Struct2011; 33: 1075–87.
[81] Khalifa A., Alkhrdaji T., Nanni A., Lansburg S. Anchorage of surface mounted FRP reinforcement. International: Design and Construction, Vol. 21, No.10, Oct. 1999, pp. 49-54.
[82] Huang X., Chen G. Bonding and anchorage characterization between FRP sheets, concrete, and viscoelastic layers under static and dynamic loading. Proceedings of International Symposium on Bond Behaviour of FRP in Structures (BBFS 2005) Chen and Teng (eds) © 2005 International Institute for FRP in Construction.
[83] Ko H., Matthys S., Palmieri A., Sato Y. Development of a simplified bond stress–slip model for bonded FRP–concrete interfaces. Construction and Building Materials 2014; 68: 142–57.
[84] Kotynia R. Bond between FRP and concrete in reinforced concrete beams strengthened with near surface mounted and externally bonded reinforcement. Construction and Building Materials, 32 (2012) 41–54.
[85] Kazaz I., Yakut A., Gu¨lkan P. Numerical simulation of dynamic shear wall tests: A benchmark study. Computers and Structures 2006; 84: 549–62.
[86] Belmouden Y., Lestuzzi P. Analytical model for predicting nonlinear reversed cyclic behaviour of reinforced concrete structural walls. Eng Struct 2007; 29: 1263–76.
[87] Jalali A., Dashti F. Nonlinear behavior of reinforced concrete shear walls using macroscopic and microscopic models. Eng Struct 2010; 32: 2959-68.
[88] Bilotta A., Di Ludovico M., Nigro E. FRP-to-concrete interface debonding: Experimental calibration of a capacity model. Composites: Part B 2011; 42: 1539–53.
[89] CNR-DT 200. Guide for the design and construction of externally bonded FRP systems for strengthening; 2004.

[90] fib Externally bonded FRP reinforcement for RC structures. fib Bulletin 14. Technical report prepared by the working party EBR of task group 9.3. International Federation for Structural Concrete; 2001.
[91] ACI 440.2R-08 Guide for the design and construction of externally bonded FRP systems for strengthening concrete structures. ACI440.2R-08, American Concrete Institute, Farmington Hills, MI; 2008. p. 76.
[92] Biscaia H. C., Chastre C., Silva M. A. G. Nonlinear numerical analysis of the debonding failure process of FRP-to-concrete interfaces. Composites: Part B 2013; 50: 210–23.
[93] Le Nguyen K., Brun M., Limam A., Ferrier E., Michel L. Pushover experiment and numerical analyses on CFRP-retrofit concrete shear walls with different aspect ratios. Composite Structures 2-014; 113: 403–18.
[94] Gebreyohaness A. S., Clifton G. C., Butterworth J. W. Finite element modeling of non-ductile RC walls. The 15th World Conference on Earthquake Engineering; 24-28 September, 2012, Lisbon, Portugal.
[95] Sas G., Da˘escu C., Popescu C., Nagy-György T. Numerical optimization of strengthening disturbed regions of dapped-end beams using NSM and EBR CFRP. Composites: Part B 2014; 67: 381–90.
[96] Gonzales H., López-Almansa F. Seismic performance of buildings with thin RC bearing walls. Eng Struct 2012; 34: 244–58.
[97] Tjhina T. N., Aschheim M. A., Wallace J. W. Yield displacement-based seismic design of RC wall buildings. Eng Struct 2007; 29: 2946–59.
[98] Bardakis V. G., Dritsos S. E. Evaluating assumptions for seismic assessment of existing buildings. Soil Dynamics and Earthquake Engineering 2007; 27: 223–33.
[99] American Society of Civil Engineers (ASCE). Pre-standard and commentary for the seismic rehabilitation of buildings. FEMA report 356. Washington, DC: ASCE for the Federal Emergency Management Agency; 2000.
[100] Greek Ministry for Environmental Planning and Public Works. GRECO (draft version)—Greek Retrofitting Code, Greek Organization for Seismic Planning and Protection, Athens, 2004 [in Greek].
[101] European Committee for Standardisation (CEN). European (draft) Standard EN 1998-1: Eurocode 8—design of structures for earthquake resistance—Part 1: general rules, seismic actions and rules for buildings. Brussels: CEN; 2003.
[102] Martinelli P., Filippou F. C. Simulation of the shaking table test of a seven-story shear wall building. Earthquake Engineering and Structural Dynamics 2009; 38: 587–607.
[103] Thermou G. E., Pantazopoulou S. J. Assessment indices for the seismic vulnerability of existing R.C. buildings. Earthquake Engng Struct. Dyn. 2011; 40: 293–313.
[104] IPCT: Cladiri de locuit P+4 din panourimari. Proiect 770-81, vol. C: Elemente prefabricate, Bucuresti, Romania; 1982. IPCT: precast reinforced concrete large panel buildings P+4. Project type 770-81, vol. C: Precast elements, Bucharest, Romania; 1982.
[105] IPCT: Cladiri de locuit P+4 din panourimari. Proiect 770-81, vol. D: Elemente prefabricate – Armari, Bucuresti, Romania; 1982. IPCT: precast reinforced concrete large panel buildings P+4. Project type 770-81, vol. D: precast elements – reinforcing, Bucharest, Romania; 1982.
[106] Demeter, I., Nagy-György, T. and Stoian, V. (2007), "Axial loading strategy for experimental tests on precast RC walls subjected to in-plane seismic actions", Scientific Bulletin of the "Politehnica" University of Timişoara, Vol. 52(66), No. 2, 11-16.

[107] Demeter, I., Nagy-György, T., Stoian, V. and Dan, D. (2008), "Quasi-static loading strategy for earthquake simulation on precast RC shear walls", Proc., 12th WSEAS International Conference on Systems, WSEAS Press, Vol. 2, pp. 813-819.
[108] C. Toduț, D. Dan, V. Stoian, "Theoretical and experimental study on precast reinforced concrete wall panels subjected to shear force", Engineering Structures 80, pp. 323–338, 2014.
[109] Todut C., D. Dan, Stoian V., "Numerical and experimental investigation on seismically damaged reinforced concrete wall panels retrofitted with FRP composites", Composite Structures, 119 (2015) 648–665, (Available online 28 September 2014).
[110] C. Toduț, V. Stoian, I. Demeter, T. Nagy-György, V. Ungureanu, "Seismic Performance of a Precast RC Wall Panel Retrofitted using CFRP Composites", 12th International Scientific Conference on Planning, design, construction and building renewal - iNDiS 2012", November 2012.
[111] C. Toduț, V. Stoian, I. Demeter, M. Fofiu, "Seismic Strengthening of a Precast Reinforced Concrete Wall Panel using Textile Reinforced Mortar", International Conference on Earthquake Engineering, Skopje, Macedonia, May 2013.
[112] V. Ungureanu, L. Fülöp. Romanian-Finnish Seminar on Opportunities in Sustainably Retrofitting the Large Panel Reinforced Concrete Building Stock. Editura Orizonturi Universitare, Timișoara (2013), pp. 49-66.
[113] C. Toduț, V. Stoian, I. Demeter, "Glass Fiber versus Carbon Fiber Grid used in Textile Reinforced Mortar Strengthening of Precast RC Walls", IACSIT International Journal of Engineering and Technology, vol.5, no.5, pp. 622-626, 2013.
[114] Todut C., Stoian V., Demeter I., Fofiu M., "Textile Reinforced Mortar Strengthening of a Precast Reinforced Concrete Wall Panel Using Carbon Fiber Grid", Symposium: Sustainable Construction: Efficient Solutions for the Design and Execution, and Building Rehabilitation, ZAT, Timisoara, Romania, pp. 56-62, 2013.
[115] C. Toduț, V. Stoian, D. Dan, "Experimental Assessment of FRP Strengthening Strategies for Precast RC Wall Panels", 12th International Conference on Steel, Space and Composite Structures, Prague, Czech Republic, pp. 379-386, May 2014.
[116] C. Todut, D. Dan, V. Stoian, "TRM strengthening of precast reinforced concrete wall panel with cut-out opening - experimental investigation", Advances in Engineering Mechanics and Materials, ISBN: 978-1-61804-241-5, pp. 110-116, 2014.
[117] C. Toduț, V. Stoian, I. Demeter, T. Nagy-György, V. Ungureanu, "Retrofitting of Earthquake Damaged Precast Concrete Wall Using FRP Composites", Fib Symposium "Engineering a Concrete Future: Technology, Modeling & Construction", Tel-Aviv, Israel, pp. 573-576, April 2013.
[118] C. Toduț, V. Stoian, I. Demeter, T. Nagy-György, D. Dan, V. Ungureanu, "Seismic Strengthening of a Precast Reinforced Concrete Wall Panel Using Combined NSM and CFRP-EBR Method", 11th International Symposium on Fiber Reinforced Polymers for Reinforced Concrete Structures (FRPRCS11), Guimarães, Portugal, pp. 269-270, June 2013.
[119] T. Nagy-Gyorgy, C. Florut, I. Demeter, C. Todut, V. Stoian, "Solutii de consolidarea a panourilor prefabricate din beton armat utilizand materiale compozite" (Rehabilitation solutions for precast reinforced concrete panels using composite materials), Conferinta AICSP, Bucuresti, Romania, 2014.
[120] C. Toduț, V. Stoian, D. Dan, T. Nagy-Gyorgy, "Seismic Strengthening of a Precast Reinforced Concrete Wall Panel Using NSM-CFRP", Proceedings of the

International Scientific Conference CIBv 2014, Brasov, Romania, (2014), pp. 437-442.
[121] Ceˇrvenka J, Jendele L. ATENA program documentation. Part 1: theory. Section 2.6; 2011.
[122] fib Bulletin 56: Model Code 2010. First complete draft – vol. 2. Published by the International Federation for Structural Concrete (fib); 2010. p. 41.
[123] Ceˇrvenka J, Jendele L. ATENA program documentation. Part 3–1: example manual. Section 2.10; 2010.
[124] Biskinis Dionysis, Roupakias George, Fardis Michael. Degradation of shear strength of reinforced concrete members with inelastic cyclic displacements. ACI Struct J 2004:773–81 [title no. 101-S76].
[125] Damian I, Morariu E, Buzaianu B, Postelnicu T, Zamfirescu D. In: Postelnicu T, editor. Proiectarea structurilor de beton armat in zone seismice (Design of reinforced concrete structures placed in seismic areas – in Romanian). Bucharest: MarLink; 2012.
[126] Warashina, M., Kono, S., Sakashita, M. and Tanaka, H. (2008), "Shear behavior of multi-story RC structural walls with eccentric openings", Proc., 14th World Conf. On Earthquake Engineering (14WCEE), Beijing, China.
[127] Taleb, R. and Kono, S. (2010), "Shear behavior of multi-story reinforced concrete walls with openings", Bulletin of IISEE, 45, 55-60.
[128] AIJ (1999), "AIJ Standard for Structural Calculation of Reinforced Concrete Structures Based on Allowable Stress Concept", Architectural Institute of Japan.
[129] C. Todut, V. Stoian, D. Dan, T. Nagy-György, "Numerical Assessment of the Weakening Induced by Cut-outs Made in Precast Reinforced Concrete Wall Panels", 2nd International Conference for PhD students in Civil Engineering CE-PhD 2014, 10-13 December 2014, Cluj-Napoca, Romania, pp. 163-169.

APPENDIX A

Behaviour of the specimens at each cycle peak

Table A.1 – Grid observations for PRCWP (7-E1-T)

SPECIMEN PRCWP (7-E1-T)

Cycle	Drift ratio (or force) level	Direction	Observations
1	10 kN	left	-
		right	-
1	50 kN	left	-
		right	-
1	100 kN	left	-
		right	-
1	150 kN	left	-
		right	-
1	1 mm	left	-
		right	9 cracks in the spandrel beam, grid number (4-4-2, 4-1-4, 4-1-1)
1	0.1 % (2.15 mm)	left	crack no. 13-15 in the spandrel beam
		right	crack no. 10-12 in the spandrel beam
2	0.1 % (2.15 mm)	left	crack no. 17 in the spandrel beam
		right	crack no. 16 and previous cracks extensions, namely 7 and 10
1	0.2 % (4.30 mm)	left	crack no. 2, 4, 19 extension
		right	crack no. 18 in spandrel, crack no. 19 in the cast-in-place mortar at the right pier-base beam connection region
2	0.2 % (4.30	left	crack no. 9 extension

	mm)	right	-
1	0.3 % (6.45 mm)	left	crack no. 8 and 17 extension, crack no. 22 in the left pier
		right	crack no. 20 and 21 in the cast-in-place mortar at the web-panel-loading beam region
2	0.3 % (6.45 mm)	left	crack no. 8 extension
		right	initial wall cracks development
1	0.4 % (8.60 mm)	left	crack no. 25 in the left pier, crack no. 19 extension
		right	crack no. 23 and 24 in the spandrel, crack no. 10 extension
2	0.4 % (8.60 mm)	left	crack no. 6, 14, 22 and 25 extension
		right	crack no. 24 extension, G2 strain gauge indicates steel rebar yielding
1	0.5 % (10.75 mm)	left	crack 27 - first inclined crack in the right pier (at 646 kN and 10.61 mm), crack no.13 extension
		right	crack no. 26 spandrel-right pier connection region, crack 5 and 7 extension, G7 indicates reinforcement yielding
2	0.5 % (10.75 mm)	left	crack no. 5, 17, 9 extension
		right	crack no. 28 - inclined in the right pier, cracks 29-32 in the left pier, G5 indicates yielding of reinforcement
1	0.6 % (12.90 mm)	left	crack no. 36 - 2nd inclined crack in the right pier, crack 37 in the spandrel, crack no. 14 extension
		right	crack no. 33-35 at the spandrel-right pier connection region, crack 29-30 extension, concrete crushing at the spandrel-right pier connection region
2	0.6 % (12.90 mm)	left	-
		right	crack no. 38 in the right wing
1	0.7 % (15.05	left	crack no 39 - inclined in the left pier, crack 8, 17 and 38 extension, crack no. 40

	mm)		in the right pier, crack no. 41 in the cast-in-place mortar at the pier-base beam region, cast-in-place mortar crushing at bottom corner of the opening
2	0.7 % (15.05 mm)	right	crack 30 and 35 extension
		left	crack 27 thickness increase, concrete exfoliation at the right pier-spandel region, crack no. 43 at the spandrel-right pier region, crack no. 44 in the left pier, concrete crushing at the bottom corner of the panel, crack no. 45 in the left pier
		right	crack no. 41 - inclined in the right pier, crack no. 42 in the spandrel
1	0.8 % (17.20 mm)	left	the panels lost more than 20 % of its load bearing capacity
		right	crack no. 28 and 31 thickness increase, crack no. 41 extension

Table A.2 - Grid observations for PRCWP (8-E3-T)

SPECIMEN PRCWP (8-E3-T)

Cycle	Drift ratio (or force) level	Direction	Observations
1	10 kN	left	-
		right	-
1	50 kN	left	-
		right	-
1	100 kN	left	-
		right	-
1	150 kN	left	-
		right	-
1	1 mm	left	-
		right	
1	0.1 % (2.15 mm)	left	-
		right	-
2	0.1 % (2.15 mm)	left	-
		right	-
1	0.2 % (4.30 mm)	left	cracks no. 1-4 in cast-in-place mortar at the bottom left corner of the opening, cracks no. 5-6 at the left pier-spandrel region
		right	-
2	0.2 % (4.30	left	crack no. 21 in the spandrel

	mm)	right	crack no. 7-20 in the spandrel and piers-spandrel connection region
1	0.3 % (6.45 mm)	left	crack no. 6, 8 and 26 extension, mortar exfoliation at the bottom left corner of the opening
		right	crack 22 in the spandrel, crack 23 at right pier-spandrel region, crack 24-25 in mortar at bottom right corner of the opening, crack 26 at the bottom region of the unconfined left wing
2	0.3 % (6.45 mm)	left	crack no. 31 in cast-in-place mortar at web panel-loading beam region, crack 29 at the top left corner of the panel, crack 30 in the spandrel
		right	crack no. 11 extension
1	0.4 % (8.60 mm)	left	cracks no. 7, 8, 9 and 28 extension, cracks 32-33 in the spandrel
		right	crack no. 23 extension
2	0.4 % (8.60 mm)	left	crack 35 in spandrel, crack 37 in cat-in-place mortar at the bottom left corner of the opening, crack no. 2 thickness increase
		right	crack no. 34 at the right pier-spandrel region, cracks no. 10, 13 and 14 extension
1	0.5 % (10.75 mm)	left	crack 14 extension, crack 38 - inclined in the right pier, crack 39 between right pier and wing, crack 40 in the right unconfined wing, crack 41 - inclined in the left pier, mortar crushing at the right pier-loading beam region
		right	crack 36 - inclined in the right pier, crack 23 extension
2	0.5 % (10.75 mm)	left	cracks 30, 32, 35 and 41 extension, crack 43 and 44 in the spandrel
		right	cracks 17 and 39 extension, crack 42 - inclined in the right pier, mortar crushing at the left pier-loading beam region
1	0.6 % (12.90 mm)	left	mortar crushing at the bottom left corner of the opening, crack 41 extension, crack 51 in the spandrel, crack 52 - inclined in the right pier
		right	crack 45 and 46 in the spandrel, crack 47 and 48 - inclined in the left pier, crack 49 in left unconfined wing, crack 50 - horizontal in the left pier
2	0.6 % (12.90	left	-

-	mm)	right	crack 53 - inclined in the right pier, crack 54 in the right unconfined wing, crack 55 - inclined, crack 42 and 49 extension
1	0.7 % (15.05 mm)	left	crack 48-49 extension
		right	crack 53 - inclined in the right pier, crack 54 in the left unconfined wing, crack 55 -horizontal in the left pier, cracks 25, 33, 38, 43, 44 and 52 extension
2	0.7 % (15.05 mm)	left	-
		right	cracks 36, 37, 47 and 48 extension
1	0.8 % (17.20 mm)	left	crack 56 in the spandrel, crack 57 in the left unconfined wing
		right	crack 53 extension, cracks 46 and 49 extension, mortar cracking at bottom right corner of the opening
2	0.8 % (17.20 mm)	left	-
		right	crack 58 - horizontal in the right pier, concrete exfoliation at the pier-spandrel region
1	0.9 % (19.35 mm)	left	cracks 38 and 52 thickness increase, crack 52 extension to the confined wing, crack 32 thickness increase, concrete crushing at the right pier-spandrel region
		right	crack 59 - inclined near the bottom right corner of the opening, cracks 38, 52, 55, 14, 15, 37, 47, 48 and 49 thickness increase
2	0.9 % (19.35 mm)	left	cracks 38 and 52 thickness increase, crack 40 extension to right confined wing, crack 61 and 62 - inclined in the right pier, crack 23 extension, crack 63 right pier-spandrel region ,cracks 44, 54 and 57 extension, crack 64 - inclined in the left pier
		right	crack 60 - inclined in the right pier, crack 25, 31, 36, 48 and 54 extension, concrete crushing at the right pier-spandrel region, crack 48 and 49 thickness increase
1	1.0 % (21.50 mm)	left	cracks 38 and 52 thickness increase, crack 25, 41 and 60 extension, crack 65 in the right confined wing
		right	cracks 60, 6, 10, 53, 49, 5, 37 extension, crack 61 in the right confined wing

2	1.0 % (21.50 mm)	left	crack 39 extension, crack 68 - inclined in the left unconfiend wing, concrete crushing at the right pier-spandrel region,
		right	crack 60 and 48 extension, crack 38 and 52 thickness increase, crack 66 at the bottom right ocrner of the panel, crack 67 in the spandrel
1	1.1 % (23.65 mm)	left	crack 38 and 52 thickness increase, crack 70 - incliend in the right pier
		right	mortar crushing at the bottom right corner of the right pier, crack 69 in the right pier-spandrel region, concrete crushing at the left pier-spandrelr egion
2	1.1 % (23.65 mm)	left	cracks 38 and 52 thickness increase, the specimen lost 20% of its load bearing capacity
		right	crack 49 and 66 thickness increase, concrete crushing at the left pier-spandrel region, mortar crushing at the bottom right corner of the opening

Table A.3 - Grid observations for PRCWP (10-L1/L3-T)

SPECIMEN PRCWP (10-L1/L3-T)

Cycle	Drift ratio (or force) level	Direction	Observations
1	10 kN	left	initial wall cracks at the pier-spandrel connection region
		right	-
1	50 kN	left	-
		right	-
1	100 kN	left	attained 1 mm displacement level
		right	-
1	150 kN	left	-
		right	-
1	1 mm	left	-
		right	
1	0.1 % (2.15 mm)	left	crack no. 1 and 2 at the parapet-right pier region, craxck no. 3 in the parapet, crack no. 4 in mortar at the left-pier-parapet bottom region, crack no. 5 at the left pier-parapet region
		right	-
2	0.1 % (2.15 mm)	left	-
		right	crack no. 5 extension
1	0.2 % (4.30 mm)	left	crack no. 14 in the right pier, crack 15 in the parapet, crack 16 - inclined in the left pier
		right	initial cracks and crack no. 1 and 5 extension, crack no 6 and 7 in the spandrel,

			crack 8 - inclined in the left pier, crack 9, 10 and 11 in the parapet, crack 12 - incliend in the left pier, crack 13 at spandrel-left pier region
2	0.2 % (4.30 mm)	left	crack no. 18 at the left pier-spandrel region
		right	crack 14 and 16 extension, crack no. 17 in theparapet
1	0.3 % (6.45 mm)	left	cracks 23 and 24 in the right pier, crack 25 - inclined in the right pier, crack 26 in parapet, carcks no. 2 and 16 extension, crack 27 and 28 (incliend) in the left pier, crack 29 in spandrel
		right	cracks 19 and 20 - incliend in the right pier, cracks no. 3 and 8 extension, crack 21 in parapet, crack 22 - inclined in the left pier, cracks in cast-in-place mortar at the web panel-loading beam region
2	0.3 % (6.45 mm)	left	cracks no. 1 and 16 extension, crack 31 in parapet, crack 32 in spandrel, mortar exfoliation at the left pier-parapet bottom region
		right	cracks no. 29 and 30 in the parapet, crack no. 10 extension
1	0.4 % (8.60 mm)	left	crack 37 at the bottom region of the right pier, cracks 1, 3 and 15 thickness increase, crack 25, 28 and 8 extension, crack 38 in spandrel, crack 39 in the left pier, crack 40 at the left pier-spandrelr egion
		right	cracks 33 and 34 - inclined in the right pier, crack 35 in spandrel, crack 36 at the bottom region of the parapet
2	0.4 % (8.60 mm)	left	crack 43 in spandrel, crack 44 in parapet, crack 45 in the left pier
		right	crack 41 in parapet, cracks 5, 8 and 11 extension, crack 42 - inclined int he left pier
1	0.5 % (10.75 mm)	left	cracks 43, 32, 39, 11 extension, crack 49, 50, 57 and 58 in spandrel, crack 51, 52, 53 and 54 in parapet, cracks 55 and 56 at parapet-right pier region
		right	carcks 17, 33, 34, 1, 9, 11, 22 extension, crack 45 in the right pier, crack 46 at spandrel-right pier region, crack 47 in parapet, crack 48 - inclined in the left pier
2	0.5 % (10.75 mm)	left	cracks 24, 14, 15, 29, 39 and 8 extension, carck 72 in the right pier, crack 73 and 74 in spandrel, crack 75 and 76 in the left pier, crack 77 in the left

-			
		right	unconfined wing, crack 79 at the parapet-left pier region, concrete crushing at the left pier-parapet region cracks 59 to 64 in parapet, crack 12 and 17 extension, carck 65 at the left pier-parapet region, crack 66 -inclined in the letf pier, crack 67 to 69 in spandrel, carck 70 at the right top corner of the panel, crack 71 at the right bottom region of the unconfined wing
1	0.6 % (12.90 mm)	left	crack 1 thickness increase, cracks 3, 24, 25 and 16 extension, carck 84 at parapet-right pier region, concrete crushing at the parapet-left pier region
		right	cracks no. 1, 20, 45, 34, 19, 47 and 48 extension, crack 80 - incliend in right pier, crack 81 in spandrel, cracks 82 and 83 in parapet
2	0.6 % (12.90 mm)	left	cracks 18 and 22 extension, cracks 9, 15 and 16 thickness icnrease, the specimens lost 20% of its load bearing capacity
		right	cracks 59, 48 and 66 extension, crack 85 at the top region of the right unconfiend wing, crack 86- horizontal in top region of the left pier, crack 87 in the left pier, crack 88 at parapet-left pier region
1	0.7 % (15.05 mm)	left	-
		right	crack 17 extension, crack 89 at the left pier-spandrel region, concrete crushing at spandrel-left pier region, failure of specimen

Table A.4 - Grid observations for PRCWP (11-L1-T)

SPECIMEN PRCWP (11-L1-T)

Cycle	Drift ratio (or force) level	Direction	Observations
1	10 kN	left	initial cracks in parapet, spandrel, left pier
		right	-
1	50 kN	left	-
		right	-
1	100 kN	left	-
		right	-
1	150 kN	left	-
		right	-
1	1 mm	left	-
		right	-
1	0.1 % (2.15 mm)	left	cracks 1 to 3 in parapet, carck 4 in the right pier, cracks 5 and 6 in spandrel, carck 7 at left pier-spandrel region, cracks 8 and 9 in parapet
		right	-
2	0.1 % (2.15 mm)	left	crack 15 in parapet, cracks 16 and 17 extension
		right	cracks 10 and 11 in parapet, crack 12 in the left pier, cracks 13 and 14 at right pier-spandrel region
1	0.2 % (4.30 mm)	left	cracks 2, 4, 5 and 10 extension, cracks 20 to 22 in parapet, carck 23 at spandrel-left pier region, crack 24 in left pier

		right	cracks 8, 10 and 12 extension, crack 18 in left pier, crack 19 in the left pier-parapet region
2	0.2 % (4.30 mm)	left	cracks 1, 3, 4, 7 and 20 extension
		right	cracks 11, 12 and 16 extension
1	0.3 % (6.45 mm)	left	carcks 34 to 37 parapet, crack 3 and 17 extension, cracks 38 to 40 - inclined in right pier, crack 41 in left pier
		right	cracks 25 and 26 - inclined in left pier, cracks 9, 10 and 28 extension, cracks 27, 28, 29 and 33 in parapet, crack 30 in right pier, cracks 31 and 32 in spandrel
2	0.3 % (6.45 mm)	left	crack 22 extension
		right	cracks 2, 11, 19 extension, crack 42 in parapet, crack 43 in left pier, carck 44 in spandrel, crack 45 in the right pier
1	0.4 % (8.60 mm)	left	crack 48 - inclined in left pier, carck 49 and 50 in left pier, crack 8 and 41extension, cracks 51 and 52 in right pier, crack 53 - incliend in right pier, crack 54 in right pier, crack 55 in spandrel, G5 indicates yielding of reinforcement, G3 and G6 close to indicating yielding of reinforcement
		right	crack 42 extension, crack 46 in parapet, crack 47 in left pier
2	0.4 % (8.60 mm)	left	cracks 63 and 64 in parapet, cracks 37, 4, 38, 6 and 41 extension, crack 65 in left pier, crack 67 - inclined in left pier
		right	cracks 56 to 59 in parapet, crack 42, 47, 12, 25 and 45 extension, cracks 61 and 62 in spandrel
1	0.5 % (10.75 mm)	left	cracks 23, 53, 65, 16, 36, 3 and 67 extension, crack 70 in left pier,carck 71 and 72 - incliend in left pier
		right	cracks 26 and 28 extension, carcks 68 and 69 -incliend in left pier, G3 indicates yielding of reinforcement
2	0.5 % (10.75	left	cracks 50 and 53 extension

	mm)		
		right	cracks 28, 43, 47, 69, 25, 61 and 30 extension, concrete exfoliation at the bottom region of parapet
1	0.6 % (12.90 mm)	left	concrete crushing at parapet-left pier region and parapet, crack 53, 47 and 16 thickness increase, crack 76 in spandrel, crack 7 extension, carck 77 in left pier, mortar crushing at the bottom region of parapet
		right	carcking and concrete crushing in the right wing, crack 73 inclined in right pier, cracks 30, 18 and 69 extension, crack 74 and 75 inclined in left pier
2	0.6 % (12.90 mm)	left	cracks 20, 6, 47, and 77 extension, concrete crushing at the top left corner of the panel and parapet
		right	carck 78 incliend in right pier
1	0.7 % (15.05 mm)	left	specimen lost over 20% of its load bearing capacity
		right	mortar crushing between panel and base beam, cracks 18, 25 and 75 extension, cracks 11, 42 and 46 thickness increase
2	0.7 % (15.05 mm)	left	-
		right	crack 79 in left pier

-

Table A.5 – Grid observations for PRCWP (12-E1-T)

SPECIMEN PRCWP (12-E1-T)

Cycle	Drift ratio (or force) level	Direction	Observations
1	10 kN	left	-
		right	-
1	50 kN	left	-
		right	-
1	100 kN	left	cracks 1 and 2 at the lft pier-spandrel region, cracks 3,4,6,7 and 8 at right pier-spandrelr egion, cracks 5, 9, 10, 11, 12 and 13 in spandrel, attained 1 mm displacement level
		right	-
1	150 kN	left	-
		right	-
1	1 mm	left	-
		right	-
1	0.1 % (2.15 mm)	left	carcks 17 to 21 in spandrel
		right	cracks 14 to 16 in spandrel
2	0.1 % (2.15 mm)	left	crack 22 in spandrel
		right	-
1	0.2 % (4.30	left	cracks 25 and 26 inclined in left pier

	mm)		
		right	crack 23 in spandrel, cracks 2, 5 and 8 extension, crack 24 at right pier-spandrel region
2	0.2 % (4.30 mm)	left	-
		right	crack 27 in spandrel
1	0.3 % (6.45 mm)	left	crack 39 inclined in left pier, cracks 31 and 32 inclined in right pier, crack 30 at left pier-spandrel region, carcks 33 to 38 in the right unconfined wing
		right	cracks 28 and 29 in spandrel, crack 16 extension, G2 indicates yielding of reinforcement
2	0.3 % (6.45 mm)	left	cracks in cast-in-place mortar between panel and loading beam
		right	-
1	0.4 % (8.60 mm)	left	crack 42 inclined in left pier, cracks 43 and 44 at spandrel-right pier region, mortar exfoliation between left pier and base beam
		right	crack 38 extension, cracks 40 and 41 inclined in right pier, crack 10 thickness increase, G1 indicates yielding of reinforcement
2	0.4 % (8.60 mm)	left	crack 45 and mortar crushing at bottom right corner of opening
		right	cracks 32, 33 and 41 extension, mortar exfoliation at bottom right corner of opening
1	0.5 % (10.75 mm)	left	crack 42 and 32thickness increase, crack 47 at the top left corner of the panel, cracks 30,18 and 31 extension, crack 48 between panel and left unconfined wing, cracks 49 and 50 in left pier, crack 51 at bottom right corner of opening
		right	crack 46 inclined in left pier, mortar crushing between base beam and left wing

2	0.5 % (10.75 mm)	left	cracks 31, 32 and 42 thickness increase
		right	crack 52 in right pier, cracks 38 and 41 extension
1	0.6 % (12.90 mm)	left	crack 57 inclined in left pier, mortar crushing at bottom left corner of opening
		right	crack 53 in spandrel, crack 54 inclined in left pier, cracks 55 and 56 in left pier
2	0.6 % (12.90 mm)	left	crack 43 extension, G5 indicates yielding of reinforcement, concrete crushing at spandrel-right pier region
		right	-
1	0.7 % (15.05 mm)	left	failure of specimen
		right	further mortar crushing between web panel and base beam

Table A.6 – Grid observations for PRCWP (7-E1-T/R)

SPECIMEN PRCWP (7-E1-T/R)

Cycle	Drift ratio (or force) level	Direction	Observations
1	10 kN	left	initial cracks at left pier-spandrel region and right pier
		right	-
1	50 kN	left	-
		right	-
1	100 kN	left	-
		right	-
1	150 kN	left	-
		right	-
1	1 mm	left	-
		right	-
1	0.1 % (2.15 mm)	left	-
		right	-
2	0.1 % (2.15 mm)	left	-
		right	-
1	0.2 % (4.30 mm)	left	crack no. 1 (inclined -previous test of reference specimen) reopening
		right	-
2	0.2 % (4.30 mm)	Left	-
		right	crack no. 2 (inclined -previous test of reference specimen) reopening

-

1	0.3 % (6.45 mm)	left	initial cracks extensionat spandrel-left pier region
		right	-
2	0.3 % (6.45 mm)	left	-
		right	CF fabric debonding in grid (4-3-2)
1	0.4 % (8.60 mm)	left	cracks in cast-in-place mortar between the left wing and base beam, inclined crack in right pier from previous test - thickness increase
		right	cracks in cast-in-place mortar between right pier-base beam
2	0.4 % (8.60 mm)	left	-
		right	inclined crack in right pier from previous test - thickness increase
1	0.5 % (10.75 mm)	left	G6 indicates yielding of reinforcement, carcks 5 and 6 in the right pier, CF strip debonding in grid (2-2-1)
		right	extension of initial cracks between the left pier and unconfined wing, c2 strip debonding at the bottom right corner of the opening
2	0.5 % (10.75 mm)	left	-
		right	-
1	0.6 % (12.90 mm)	left	crack 12 - inclined in right pier, cracks 13 to 15 in spandrel, shear strip debonding on rear face of the wall in grid (1-2-4)
		right	mortar exfoliation at bottom edge of left pier, cracks 8 to 10 in spandrel, crack 11 at spandrel-right pier connection region
2	0.6 % (12.90 mm)	left	G6 close to indicating yielding of reinforcement, crack 16 inclined in right pier, cracking at right pier-spandrel region, horizontal crack on rear face in right pier between the first two shear strips from bottom
		right	frist shear strip from bottom in the right pier debonding, mortar crushing under c2 right strip
1	0.7 % (15.05 mm)	left	snapping sounds from FRPs, shear strip no. 2 from bottom - debonding in right pier

		right	concrete and mortar crushing at the bottom region of the right wing
2	0.7 % (15.05 mm)	left	G8 indicates yielding of reinforcement, rear face -horizontal crack extension
		right	-
1	0.8 % (17.20 mm)	left	horizontal cracks at the right pier-spandrel region, rear face -horizontal crack extension
		right	
2	0.8 % (17.20 mm)	left	c1 confinement strip debonding at the right pier-spandrel region
		right	-
1	0.9 % (19.35 mm)	left	rear face -horizontal crack extension, c1 confinement strip debonding at the right pier-spandrel region
		right	rear face -horizontal crack extension
2	0.9 % (19.35 mm)	left	second shear strip from bottom in right pier - further debonding
		right	specimen lost 20% of its load bearing capacity
1	1.0 % (21.50 mm)	left	rear face -horizontal crack extension
		right	-

Table A.7 – Grid observations for PRCWP (8-E3-T/R)

SPECIMEN PRCWP (8-E3-T/R)

Cycle	Drift ratio (or force) level	Direction	Observations
1	10 kN	left	-
		right	-
1	50 kN	left	-
		right	-
1	100 kN	left	-
		right	-
1	150 kN	left	-
		right	-
1	1 mm	left	-
		right	-
1	0.1 % (2.15 mm)	left	crack no. 1 in the left pier, crack no.2 in the right pier
		right	carcks 3 and 4 in the right pier, cracks 5 and 6 in the left pier
2	0.1 % (2.15 mm)	left	crack 7 in the right pier
		right	crack 4 extension, crack 8 in spandrel, crack 9 in the left pier
1	0.2 % (4.30 mm)	left	cracks 1, 2 and 7 extension
		right	cracks 4 and 6 extension, crack 10 and 11 in spandrel, crack 12 in the left pier
2	0.2 % (4.30 mm)	left	-
		right	crack 13 in spandrel, crack 14 in the left pier

1	0.3 % (6.45 mm)	left	cracks 14 to 17 in spandrel, crack 18 - horizontal in the left pier
		right	cracks 19 and 20 in spandrel
2	0.3 % (6.45 mm)	left	crack no. 1 extension
		right	crack 21 in spandrel, crack 9 extension
1	0.4 % (8.60 mm)	left	cracks 22 to 24 in the right unconfined wing, cracks 25 to 27 in spandrel, crack 15 extension, snapping sounds of FRPs
		right	cracks 5 and 10 extension, cracks 28 and 29 in the right unconfined wing, cracks 30 and 31 in the right pier, crack 32 in the left unconfined wing, crack 33 in the left pier
2	0.4 % (8.60 mm)	left	crack 7 extension, crack 34 in the left unconfined wing, crack 35 in the right unconfined wing
		right	cracks 36 and 37 in the right unconfined wing, crack 5 extension
1	0.5 % (10.75 mm)	left	crack 38 between the left pier and unconfined wing
		right	cracks 31, 4, 14, 32, 5 extension
2	0.5 % (10.75 mm)	left	cracks 39 and 40 in the right pier, crack 1 extension, crack 41 in the left pier, vertical crack between the left pier and unconfined wing - thickness increase
		right	cracks 3, 31 and 14 extension, crack 42 in the spandrel
1	0.6 % (12.90 mm)	left	crack 43 in the right unconfined wing, cracks 17 and 26 extension, crack 44 in spandrel, crack 45 in the left pier, crack 46 bewteen left pier and unconfined wing
		right	cracks 37, 8, 13 extension, crack 47 in spandrel
2	0.6 % (12.90 mm)	left	cracks 2 and 16 extension, crack 48 at the left pier-spandrel region
		right	cracks 49 and 50 in the right pier, resin used to repair inclined cracks from previous test - cracking
1	0.7 % (15.05 mm)	left	cracks 51 and 52 - right pier, shear strip debonding in grid (1-2-2) -right pier, cracks 54 and 55 at the left pier-spandrel region

		right	first shear strip from bottom in the right pier - debonding, crack 53 in the right unconfined wing, inclined crack in the right pier- thickness increase
2	0.7 % (15.05 mm)	left	-
		right	-
1	0.8 % (17.20 mm)	left	flexural strip debonding in grid (1-1-3) and shear strip debonding in grid (1-1-2) and (3-3-3)
		right	concrete exfoliation between the unconfined wing and left pier, inclined crack in right pier extension to grid (1-1-3)
2	0.8 % (17.20 mm)	left	-
		right	-
1	0.9 % (19.35 mm)	left	cracks 16, 7 and 18 extension, crack 66 at top region of the left unconfined wing
		right	cracks 56 and 57 in mortar between right pier and base beam, crack 58 in the right pier, cracks 59 and 60 in sopandrel, cracks 61 to 65 in the left pier, crack 9 and 12 extension, crack 67 in the bottom region of the right unconfined wing
2	0.9 % (19.35 mm)	left	cracks 68 and 69 in spandrel, crack 70 in the left pier
		right	crack 71 and 72 in the right pier
1	1.0 % (21.50 mm)	left	inclined crack in right pier - thickness increase, shear strip in right pier further debonding
		right	cracks 71, 10, 21 and 14 extension, cracks in cast-in-place mortar between the left pier and loading beam
2	1.0 % (21.50 mm)	left	further shear strip debonding in grid (1-2-2) and further flexural strip debonding in grid (1-1-3), cracks 14 and 25 extension
		right	crack 72 in the right pier, further shear strip debonding in grid (3-4-3)
1	1.1 % (23.65 mm)	left	crack 73 in the right pier, further shear strip debonding in grid (1-2-2), crack 74 in the right pier, further flexural strip debonding in grid (1-1-3), crack 75 in spandrel, cracks 76 to 78 - inclined in the left pier

		right	crack 79 between the right unconfined and confined wing, crack 31 extension, shear strip debonding in grid (4-3-3)
2	1.1 % (23.65 mm)	left	crack 39 extension, shear strip rupture in grid (1-1-3) at right pier-spandrelr egion, mortar crushing at right pier-spandrel region
		right	crack 9 extension, crack 80 in the left pier, shear strip debonding in grid (3-3-3 and 3-3-2)
1	1.2 % (25.80 mm)	left	cracks 81 and 82 in the right unconfined wing, cracks 1 and 41 extension, specimen lost 20% of its load bearing capacity
		right	specimen lost 20% of its load bearing capacity

Table A.8 – Grid observations for PRCWP (9-E1/E3-R/T)

SPECIMEN PRCWP (9-E1/E3-R/T)

Cycle	Drift ratio (or force) level	Direction	Observations
1	10 kN	left	-
		right	-
1	50 kN	left	-
		right	-
1	100 kN	left	attained 1 mm displacement level
		right	-
1	150 kN	left	-
		right	-
1	1 mm	left	-
		right	-
1	0.1 % (2.15 mm)	left	-
		right	-
2	0.1 % (2.15 mm)	left	-
		right	-
1	0.2 % (4.30 mm)	left	snapping sounds of FRPs
		right	snapping sounds of FRPs
2	0.2 % (4.30 mm)	left	snapping sounds of FRPs, cracks 2-5 in spandrel
		right	snapping sounds of FRPs, crack 1 in spandrel

1	0.3 % (6.45 mm)	left	crack 6 at the right pier-spandrelr egion, f2 strip debonding, snapping sounds of FRPs
		right	crack 7 in spandrel, crack 8 at the left pier-spandrel region, crack 9 in mortar at base beam-left pier region
2	0.3 % (6.45 mm)	left	-
		right	-
1	0.4 % (8.60 mm)	left	cracks 8 and 10 extension
		right	crack 10 in mortar at bottom right corner of the opening, cracks 11 and 12 in spandrel
2	0.4 % (8.60 mm)	left	crack 14 in spandrel, cracks 15 and 16 in mortar at bottom left corner of the opening
		right	crack 13 in spandrel
1	0.5 % (10.75 mm)	left	crack 18 extension
		right	crack 17 in mortar at bottom region of left wing
2	0.5 % (10.75 mm)	left	crack 20 in spandrel
		right	crack 11 extension, crack 19 at right pier-spandrel region
1	0.6 % (12.90 mm)	left	crack 28 in mortar between base beam and right pier, mortar crushing at bottom region of the left wing
		right	crack 21 in spandrel, cracks 22 to 27 in left pier
2	0.6 % (12.90 mm)	left	crack 31 to 33 in spandrel
		right	crack 29 in (4-4-4), crack 30 in (3-3-2) and pull-out attempt of FRP anchorage in (3-3-2)
1	0.7 % (15.05 mm)	left	cracks 14 and 28 extension, snapping sounds of FRPs
		right	crack 34 inclined in left pier, crack 24 and 10 extension, f1 and f6 strips

			debonding
2	0.7 % (15.05 mm)	left	crack 32 extension, Hdr and f1 strips debonding at right pier-spandrel region
		right	cracks 24, 34 extension, crack 35 in spandrel, cracks 36 and 37 at right pier-spandrel region, crack 38 in mortar at bottom right corner of the opening
1	0.8 % (17.20 mm)	left	crack 25 extension, crack 39 in mortar at bottom right corner of the opening, further debonding in grid (1-1-3) and (4-4-2)
		right	-
2	0.8 % (17.20 mm)	left	cracks 43 and 44 in spandrel, mortar crushing at bottom right corner of the opening
		right	further debonding of Hdr strip, cracks 41 and 42 in left pier, crack 40 in right pier
1	0.9 % (19.35 mm)	left	cracks 25 and 34 extension, f2 debonding on the right side
		right	cracks 45 and 46 in spandrel, crack 47 in the left unconfiend wing
2	0.9 % (19.35 mm)	left	crack 53 in the left unconfiend wing, crack 42 extension, cracks 49 to 52 in the right pier, concrete crushing at left pier-spandrel region
		right	crack 34 extension, crack 48 in the left unconfined wing
1	1.0 % (21.50 mm)	left	crack 53 in spandrel, crack 54 and 55 in the left pier, crack 56 in left pier
		right	cracks 46, 48, 26, 47 extension, crack 22 - thickness increase, f2 further debonding, further debonding in (4-4-2 and 4-4-3) with Hst strip rupture
2	1.0 % (21.50 mm)	left	further debonding in grid (4-3-4 and 4-4-2), specimen lost 20% of its load bearing capacity
		right	crack 22 and 34 thickness increase
1	1.1 % (23.65 mm)	left	-
		right	crack 57 in the bottom region of the right wing, f1 further debonding, cracks 48, 22, 26 and 34 -thickness increase

Table A.9 – Grid observations for PRCWP (10-L1/L3-T/R)

SPECIMEN PRCWP (10-L1/L3-T/R)

Cycle	Drift ratio (or force) level	Direction	Observations
1	10 kN	left	-
		right	-
1	50 kN	left	-
		right	-
1	100 kN	left	attained 2.15 mm displacement level
		right	-
1	150 kN	left	-
		right	-
1	1 mm	left	-
		right	-
1	0.1 % (2.15 mm)	left	crack 1 in spandrel, cracks 2 and 3 in parapet, crack 4 in the left pier
		right	snapping sounds of FRPs
2	0.1 % (2.15 mm)	left	crack 6 at spandrel-left pier region
		right	crack 5 in parapet
1	0.2 % (4.30 mm)	left	crack 15 at parapet - left pier region, cracks 16 to 18 in parapet, cracks 19 to 22 in the right pier, crack 23 in the left pier, crack 4 extension
		right	cracks 7 to 12 at parapet-left pier region, crack 13 in the left unconfined wing, crack 14 in spandrel

2	0.2 % (4.30 mm)	left	crack 2 extension
		right	crack 24 in the right pier, cracks 25 to 27 in parapet
1	0.3 % (6.45 mm)	left	cracks 16, 3, 18, 20, 21 extension, crack 2 thickness increase, crack 33 in the right pier, crack 34 in spandrel, crack 35 at left pier-spandrel region, crack 36 in the left pier, crack 37 and 38 in parapet
		right	cracks 28 and 29 in the right pier, cracks 30 to 32 at bottom right corner of the panel, crack 14 extension, crack 13 thickness increase
2	0.3 % (6.45 mm)	left	crack 2 and 4 extension, crack 47 in parapet
		right	crack 39 in the right pier, crack 28, 26 and 19 extension, cracks 40 to 43 in parapet, crack 44 in the left pier, crack 45 and 46 in parapet, mortar exfoliation in the left pier
1	0.4 % (8.60 mm)	left	crack 55 in the right pier, cracks 2, 18, 30, 20, 34 and 15 extension, cracks 56 to 58 in spandrel, cracks 59 and 60 in the left pier, crack 61 in parapet
		right	crack 48 in parapet, crack 49 to 51 in the right pier, crack 52 in spandrel, cracks 28, 10, 25, 5, 7, 46 and 41 extension, crack 53 and 54 in parapet
2	0.4 % (8.60 mm)	left	crack 63 in the left pier, crack 2 and 7 - thickness increase, exfoliation and debonding of TRM system at parapet-left pier region
		right	crack 62 in spandrel, cracks 39, 14 and 43 extension
1	0.5 % (10.75 mm)	left	cracks 17, 37, 2, 19, 20, 36 and 37 extension, crack 65 in the right pier, debonding in grid (4-3-4) and at the parapet-left pier region
		right	crack 64 at the bottom right corner of the panel, crack 43, 8 and 39 extension
2	0.5 % (10.75 mm)	left	crack 67 in the right pier, crack 24 extension
		right	crack 25 extension, crack 66 in the left pier, debonding in (4-3-3)
1	0.6 % (12.90 mm)	left	cracks 20, 55, 67, 65, 18 and 16 extension, TRM debonding at the right pier-spandrel region, crack 74 at the right pier-spandrel region, crack 75 at the left pier-spandrel region, crack 76 and 77 in the left pier, crack 78 - vertical in the left unconfined wing, crack 79 in the left pier

		right	crack 68 and 69 in the right pier, crack 51, 28, 24, 29 and 62 extension, cracks 70 to 73 in the left pier
2	0.6 % (12.90 mm)	left	crack 4 and 15 extension, cracks 82 to 86 in the left pier, crack 87 in parapet
		right	crack 39 extension, crack 80 in the right pier, crack 81 at the right pier-spandrel region
1	0.7 % (15.05 mm)	left	crack 88 in the right pier, crack 2 thickness increase, crack 37, 23, 85 and 86 extension, crack 89 - vertical in the left unconfined wing, crack 90 in the left pier, mortar crushing at the parapet - left pier region, TRM debonding in (4-3-3 and 3-4-4)
		right	cracks 64 and 32 extension
2	0.7 % (15.05 mm)	left	cracks 94 and 95 in the right pier, crack 22, 5 and 7 extension, debonding at the right pier-spandrel region and left pier-spandrel region
		right	cracks 39, 30 and 52 extension, crack 91 at the right pier-spandrel region, debonding in (3-4-3), cracks 92 and 93 in the left pier
1	0.8 % (17.20 mm)	left	thickness increase of the vertical crack at the right pier-parapet region, cracks 20, 65 and 89 extension
		right	crack 40 extension, further debonding at parapet-right pier region (3-3.5 cm from wall surface), crack 96 in the right pier, crack 97 at the left pier-spandrel region,
2	0.8 % (17.20 mm)	left	crack 100 in parapet, crack 64, 88 and 95 extension, crack 101 in the right pier, crack 102 in the left pier
		right	crack 98 at the right pier-spandrel region, crack 99 in spandrel, specimen lost 20% of its load bearing capacity
1	0.9 % (19.35 mm)	left	debonding in (2-1-2)
		right	cracks 103 to 105 in the right pier, cracks 24, 39 extension, cracks 106 to 115 in the right pier, mortar crush at the right wing-base beam region

Table A.10 – Grid observations for PRCWP (11-L1-T/R)

SPECIMEN PRCWP (11-L1-T/R)

Cycle	Drift ratio (or force) level	Direction	Observations
1	10 kN	left	-
		right	-
1	50 kN	left	-
		right	-
1	100 kN	left	-
		right	-
1	150 kN	left	-
		right	-
1	1 mm	left	-
		right	-
1	0.1 % (2.15 mm)	left	-
		right	-
2	0.1 % (2.15 mm)	left	-
		right	-
1	0.2 % (4.30 mm)	left	crack 1 at the left pier-spandrel region, crack 2 at the right pier-parapet region
		right	-
2	0.2 % (4.30 mm)	left	-
		right	-

1	0.3 % (6.45 mm)	left	crack 7 - inclined in the left pier, crack 8-12 in the left pier, crack 13 at the left pier-spandrel region, crack 14 in spandrel, cracks 15 and 16 inclined in the right pier, crack 17 in parapet, crack 18 at the bottom right corner of the opening
		right	crack 3 - inclined in the left pier, crack 4 and 5 in the left pier, snapping sounds, crack 6 at the parapet-left pier region
2	0.3 % (6.45 mm)	left	crack 7, 8 and 9 extension, crack 21 in the right pier, crack 22 in the left wing
		right	cracks 19 and 20 in the right pier, crack 3 extension
1	0.4 % (8.60 mm)	left	cracks 22, 5, 10 extension, crack 27 in the left pier, cracks 28 and 29 in spandrel, specimen attains 1003 kN at 7.85 mm displacement level
		right	crack 23 in the left pier, cracks 24 and 25 at the right pier-spandrel region, crack 26 at the left pier-parapet region
2	0.4 % (8.60 mm)	left	crack 30 in the right pier, crack 31 in spandrel, crack 32 in the right pier, specimen attains 1000 kN lateral load
		right	-
1	0.5 % (10.75 mm)	left	crack 7 extension, crack 35 in the right pier, crack 34 in spandrel, crack 33 at the top left corner of the panel
		right	-
2	0.5 % (10.75 mm)	left	-
		right	crack 36 in the left pier, mortar crushing at the left pier-parapet region
1	0.6 % (12.90 mm)	left	crack 39 in spandrel, cracks 7 and 11 extension, cracks in parapet
		right	cracks 20 and 23 extension, cracks 37 and 38 in spandrel
1	0.7 % (15.05 mm)	left	cracks in the left pier - grids (3-1-3, 3-1-2, 3-4-2, 3-2-2, 4-1-2, 4-1-1, 4-1-2, 4-1-3, 1-4-4), debonding in (4-1-1, 1-4-3, 1-1-3, 2-1-2, 2-2-1, 2-2-2, 2-1-1, 1-2-2)
		right	cracks 40 and 41 in the left pier

Table A.11 – Grid observations for PRCWP (12-E1-T/R)

SPECIMEN PRCWP (12-E1-T/R)

Cycle	Drift ratio (or force) level	Direction	Observations
1	10 kN	left	-
		right	-
1	50 kN	left	-
		right	-
1	100 kN	left	specimen attains 1 mm displacement, initial cracks 1-5 in the right pier opening
		right	-
1	150 kN	left	-
		right	-
1	1 mm	left	-
		right	-
1	0.1 % (2.15 mm)	left	crack 5 extension, crack 7 to 9 - initial cracks reopening
		right	crack 6 in the right pier
2	0.1 % (2.15 mm)	left	-
		right	-
1	0.2 % (4.30 mm)	left	cracks 8 and 9 extension, cracks 10 to 12 in mortar at the bottom left corner of the opening, cracks 13 to 18 in spandrel, cracks 19 and 20 in the right pier
		right	snapping sounds
2	0.2 % (4.30	left	-

	mm)	right	crack 21 in spandrel
1	0.3 % (6.45 mm)	left	cracsk 22 and 23 at the left pier-spandrel region, mortar exfoliation at the bottom elft corner of the opening, and c1 strip debonding
		right	G7 close to indicating yielding of reinforcement
2	0.3 % (6.45 mm)	left	crack 27 - horizontal in mortar at the bottom right corner of the opening, crack 28 in the right unconfined wing, crack 19 extension, crack 29 in the right pier, cracks 30 to 33 in spandrel, crack 34 in the left pier
		right	cracks 24 and 26 at the right pier-spandrelr egion, crack 25 in spandrel
1	0.4 % (8.60 mm)	left	c1 strip debondings at the bottom left corner of the opening, crack 35 and 36 in the left pier, crack 37 inclined in the left pier, crack 38 in the left pier
		right	-
2	0.4 % (8.60 mm)	left	crack 34 extension, crack 39 between the right unconfined wing and the right pier, crack 45 in the right pier, crack 46 in spandrel, crack 47 at the left pier-spandrel region, crack 48 inclined in the left pier
		right	crack 2 extension, crack 40 in the right pier
1	0.5 % (10.75 mm)	left	specimens attains 1000 kN at 10.50 mm displacement level, G5 indicates yielding of reinforcement, crack 51 inclined in theleft pier, crack 50 in the right unconfined wing
		right	crack 49 in spandrel
2	0.5 % (10.75 mm)	left	-
		right	G7 indicates yielding of reinforcement, concrete crushing at the bottom left corner of the panel

APPENDIX B

Sensor list of the specimens

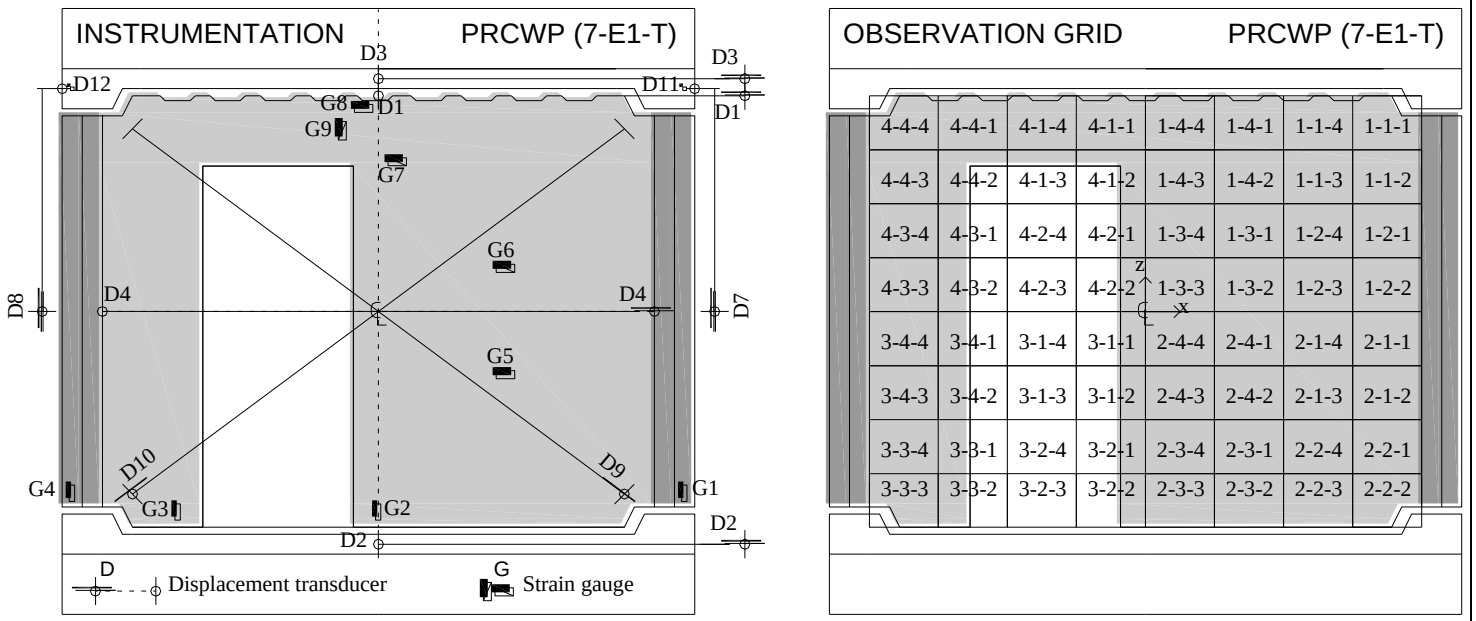

Table B.1 – Sensor list for PRCWP (7-E1-T) specimen

ID	Type	Location	x (mm)	y (mm)	z (mm)
D1	Displacement, top horizontal	(1-4-4); (4-1-1)	0	50	1075
D2	Displacement, bottom horizontal	Base beam	0	150	-1160
D3	Displacement, top horizontal	Loading beam	0	150	1160
D4 start	Displacement, mid horizontal	(1-2-2); (2-1-1)	1375	50	0
D4 end		(4-3-3); (3-4-4)	-1375	50	0

D7	Displacement, vertical	Loading beam	1575	0	1110
D8	Displacement, vertical	Loading beam	-1575	0	1110
D9 start	Displacement, diagonal	(2-2-2)	1225	50	-910
D9 end		(4-4-4)	-1225	50	910
D10 start	Displacement, diagonal	(3-3-3)	-1225	50	-910
D10 end		(1-1-1)	1225	50	910
D11	Displacement, out-of-plane	Loading beam	1525	-150	1110
D12	Displacement, out-of-plane	Loading beam	-1525	-150	1110
G1	Strain gauge, vertical steel rebar	wing base	1525	0	-990
G2	Strain gauge, vertical steel rebar	(2-3-3); (3-2-2)	0	0	-990
G3	Strain gauge, vertical steel rebar	(3-3-2)	-1005	0	-990
G4	Strain gauge, vertical steel rebar	wing base	-1525	0	-990
G5	Strain gauge, horizontal steel rebar	(2-4-2)	635	0	-315
G6	Strain gauge, horizontal steel rebar	(1-3-2)	635	0	215
G7	Strain gauge, horizontal steel rebar	(1-4-3)	95	0	745
G8	Strain gauge, horizontal steel rebar	(4-1-1)	-75	0	1010
G9	Strain gauge, vertical steel rebar	(4-1-1)	-180	0	855
P1	Pressure, lateral load V	Hydraulic line	-	-	-
P2	Pressure, axial load N1	Hydraulic line	-	-	-
P3	Pressure, axial load N2	Hydraulic line	-	-	-

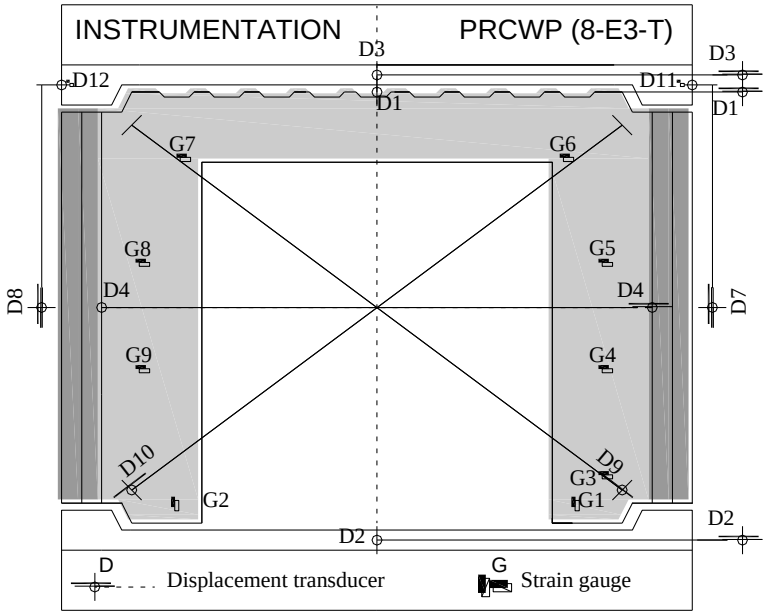

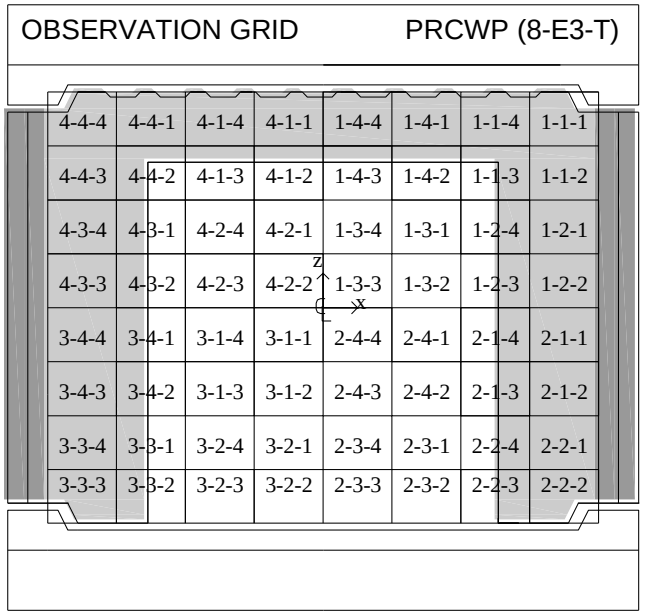

Table B.2 – Sensor list for PRCWP (8-E3-T) specimen

ID	Type	Location	x (mm)	y (mm)	z (mm)
D1	Displacement, top horizontal	(1-4-4); (4-1-1)	0	50	1075
D2	Displacement, bottom horizontal	Base beam	0	150	-1160
D3	Displacement, top horizontal	Loading beam	0	150	1160
D4 start	Displacement, mid horizontal	(1-2-2); (2-1-1)	1375	50	0
D4 end		(4-3-3); (3-4-4)	-1375	50	0

D7	Displacement, vertical	Loading beam	1575	0	1110
D8	Displacement, vertical	Loading beam	-1575	0	1110
D9 start	Displacement, diagonal	(2-2-2)	1225	50	-910
D9 end		(4-4-4)	-1225	50	910
D10 start	Displacement, diagonal	(3-3-3)	-1225	50	-910
D10 end		(1-1-1)	1225	50	910
D11	Displacement, out-of-plane	Loading beam	1525	-150	1110
D12	Displacement, out-of-plane	Loading beam	-1525	-150	1110
G1	Strain gauge, vertical steel rebar	(2-2-3)	1000	0	-985
G2	Strain gauge, vertical steel rebar	(3-3-2)	-1000	0	-985
G3	Strain gauge, horizontal steel rebar	(2-2-2)	1150	0	-845
G4	Strain gauge, horizontal steel rebar	(2-1-2)	1150	0	-315
G5	Strain gauge, horizontal steel rebar	(1-2-2)	1150	0	215
G6	Strain gauge, horizontal steel rebar	(1-1-3)	955	0	740
G7	Strain gauge, horizontal steel rebar	(4-4-2)	-955	0	740
G8	Strain gauge, horizontal steel rebar	(4-3-3)	-1150	0	215
G9	Strain gauge, vertical steel rebar	(3-4-3)	-1150	0	-315
P1	Pressure, lateral load V	Hydraulic line	-	-	-
P2	Pressure, axial load N1	Hydraulic line	-	-	-
P3	Pressure, axial load N2	Hydraulic line	-	-	-

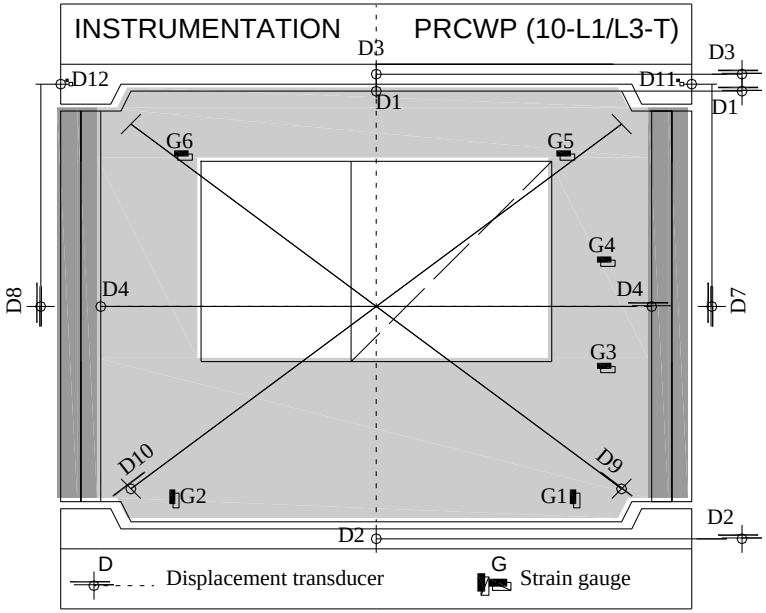

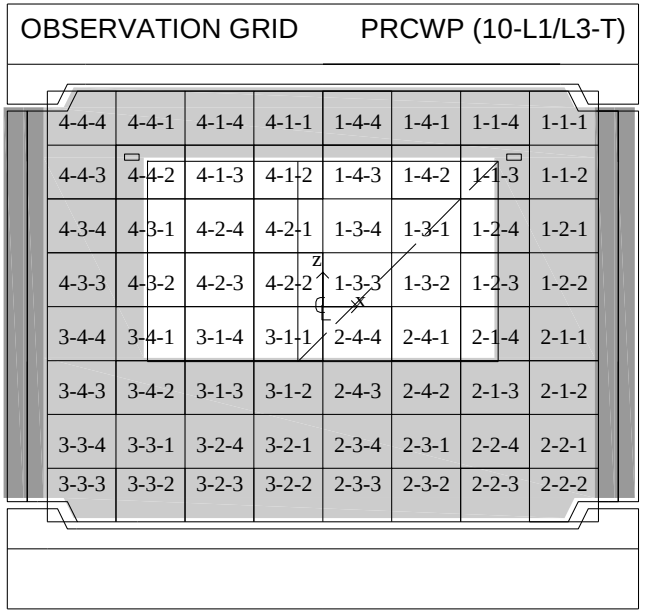

Table B.3 – Sensor list for PRCWP (10-L1/L3-T) specimen

ID	Type	Location	x (mm)	y (mm)	z (mm)
D1	Displacement, top horizontal	(1-4-4); (4-1-1)	0	50	1075
D2	Displacement, bottom horizontal	Base beam	0	150	-1160
D3	Displacement, top horizontal	Loading beam	0	150	1160
D4 start	Displacement, mid horizontal	(1-2-2); (2-1-1)	1375	50	0
D4 end		(4-3-3); (3-4-4)	-1375	50	0

D7	Displacement, vertical	Loading beam	1575	0	1110
D8	Displacement, vertical	Loading beam	-1575	0	1110
D9 start	Displacement, diagonal	(2-2-2)	1225	50	-910
D9 end		(4-4-4)	-1225	50	910
D10 start	Displacement, diagonal	(3-3-3)	-1225	50	-910
D10 end		(1-1-1)	1225	50	910
D11	Displacement, out-of-plane	Loading beam	1525	-150	1110
D12	Displacement, out-of-plane	Loading beam	-1525	-150	1110
G1	Strain gauge, vertical steel rebar	(2-2-3)	1000	0	-985
G2	Strain gauge, vertical steel rebar	(3-3-2)	-1000	0	-985
G3	Strain gauge, horizontal steel rebar	(2-1-2)	1155	0	-315
G4	Strain gauge, horizontal steel rebar	(1-2-2)	1155	0	215
G5	Strain gauge, horizontal steel rebar	(1-1-3)	955	0	745
G6	Strain gauge, horizontal steel rebar	(4-4-2)	-955	0	745
P1	Pressure, lateral load V	Hydraulic line	-	-	-
P2	Pressure, axial load N1	Hydraulic line	-	-	-
P3	Pressure, axial load N2	Hydraulic line	-	-	-

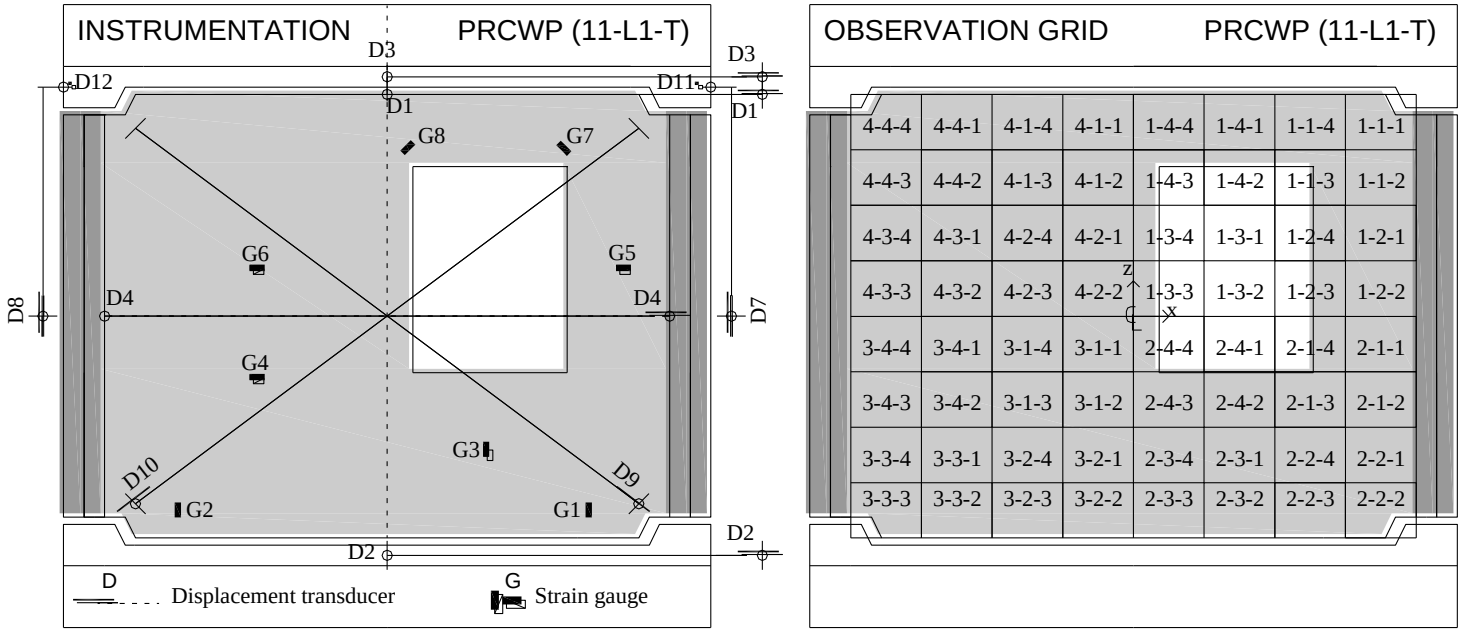

Table B.4 – Sensor list for PRCWP (11-L1-T) specimen

ID	Type	Location	x (mm)	y (mm)	z (mm)
D1	Displacement, top horizontal	(1-4-4); (4-1-1)	0	50	1075
D2	Displacement, bottom horizontal	Base beam	0	150	-1160
D3	Displacement, top horizontal	Loading beam	0	150	1160
D4 start	Displacement, mid horizontal	(1-2-2); (2-1-1)	1375	50	0

D4 end		(4-3-3); (3-4-4)	-1375	50	0
D7	Displacement, vertical	Loading beam	1575	0	1110
D8	Displacement, vertical	Loading beam	-1575	0	1110
D9 start	Displacement, diagonal	(2-2-2)	1225	50	-910
D9 end		(4-4-4)	-1225	50	910
D10 start	Displacement, diagonal	(3-3-3)	-1225	50	-910
D10 end		(1-1-1)	1225	50	910
D11	Displacement, out-of-plane	Loading beam	1525	-150	1110
D12	Displacement, out-of-plane	Loading beam	-1525	-150	1110
G1	Strain gauge, vertical steel rebar	(2-2-3)	1000	0	-985
G2	Strain gauge, vertical steel rebar	(3-3-2)	-1000	0	-985
G3	Strain gauge, vertical steel rebar	(2-3-1)	500	0	-675
G4	Strain gauge, horizontal steel rebar	(3-1-3)	-615	0	-315
G5	Strain gauge, horizontal steel rebar	(1-2-2)	1160	0	215
G6	Strain gauge, horizontal steel rebar	(4-2-3)	-615	0	215
G7	Strain gauge, inclined steel rebar	(1-1-3)	880	0	790
G8	Strain gauge, inclined steel rebar	(1-4-3)	125	0	790
P1	Pressure, lateral load V	Hydraulic line	-	-	-
P2	Pressure, axial load N1	Hydraulic line	-	-	-
P3	Pressure, axial load N2	Hydraulic line	-	-	-

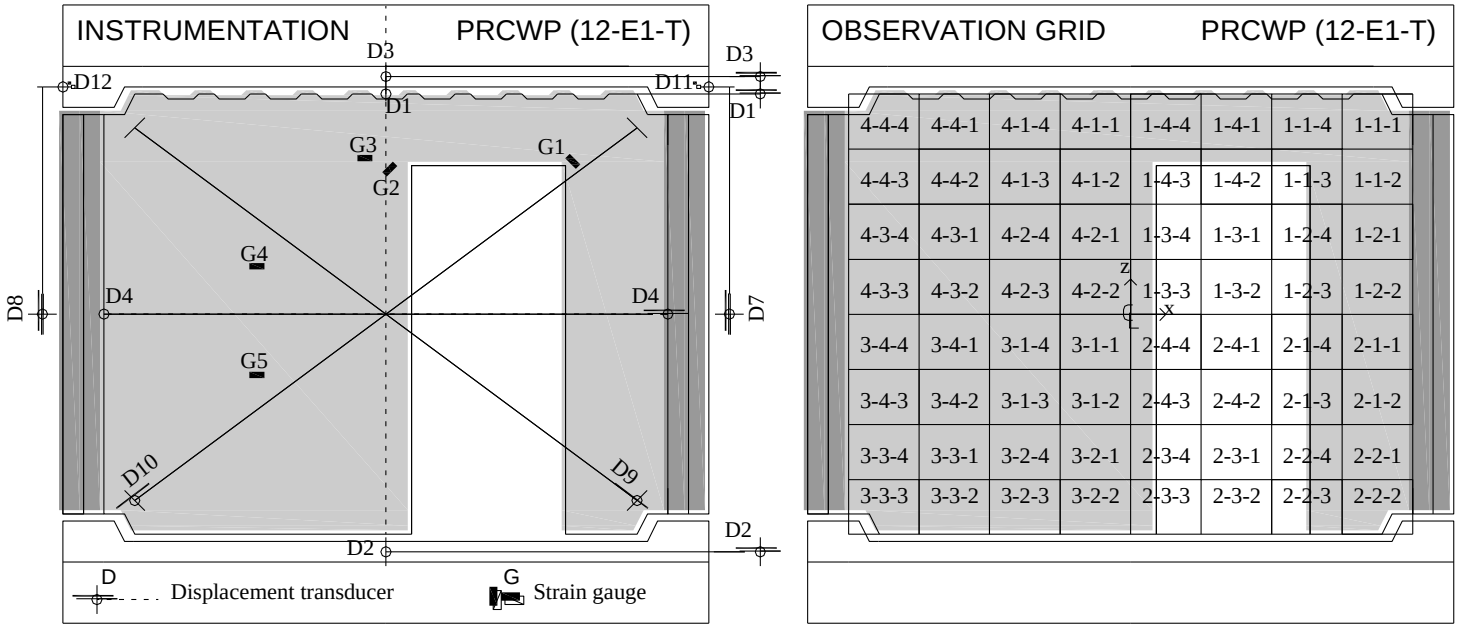

Table B.5 – Sensor list for PRCWP (12-E1-T) specimen

ID	Type	Location	x (mm)	y (mm)	z (mm)
D1	Displacement, top horizontal	(1-4-4); (4-1-1)	0	50	1075
D2	Displacement, bottom horizontal	Base beam	0	150	-1160
D3	Displacement, top horizontal	Loading beam	0	150	1160
D4 start	Displacement, mid horizontal	(1-2-2); (2-1-1)	1375	50	0

D4 end		(4-3-3); (3-4-4)	-1375	50	0
D7	Displacement, vertical	Loading beam	1575	0	1110
D8	Displacement, vertical	Loading beam	-1575	0	1110
D9 start	Displacement, diagonal	(2-2-2)	1225	50	-910
D9 end		(4-4-4)	-1225	50	910
D10 start	Displacement, diagonal	(3-3-3)	-1225	50	-910
D10 end		(1-1-1)	1225	50	910
D11	Displacement, out-of-plane	Loading beam	1525	-150	1110
D12	Displacement, out-of-plane	Loading beam	-1525	-150	1110
G1	Strain gauge, inclined steel rebar	(1-1-3)	930	0	730
G2	Strain gauge,inclined steel rebar	(1-4-3)	45	0	690
G3	Strain gauge, horizontal steel rebar	(4-1-2)	-85	0	745
G4	Strain gauge, horizontal steel rebar	(4-2-3)	-610	0	215
G5	Strain gauge, horizontal steel rebar	(3-1-3)	-610	0	-315
P1	Pressure, lateral load V	Hydraulic line	-	-	-
P2	Pressure, axial load N1	Hydraulic line	-	-	-
P3	Pressure, axial load N2	Hydraulic line	-	-	-

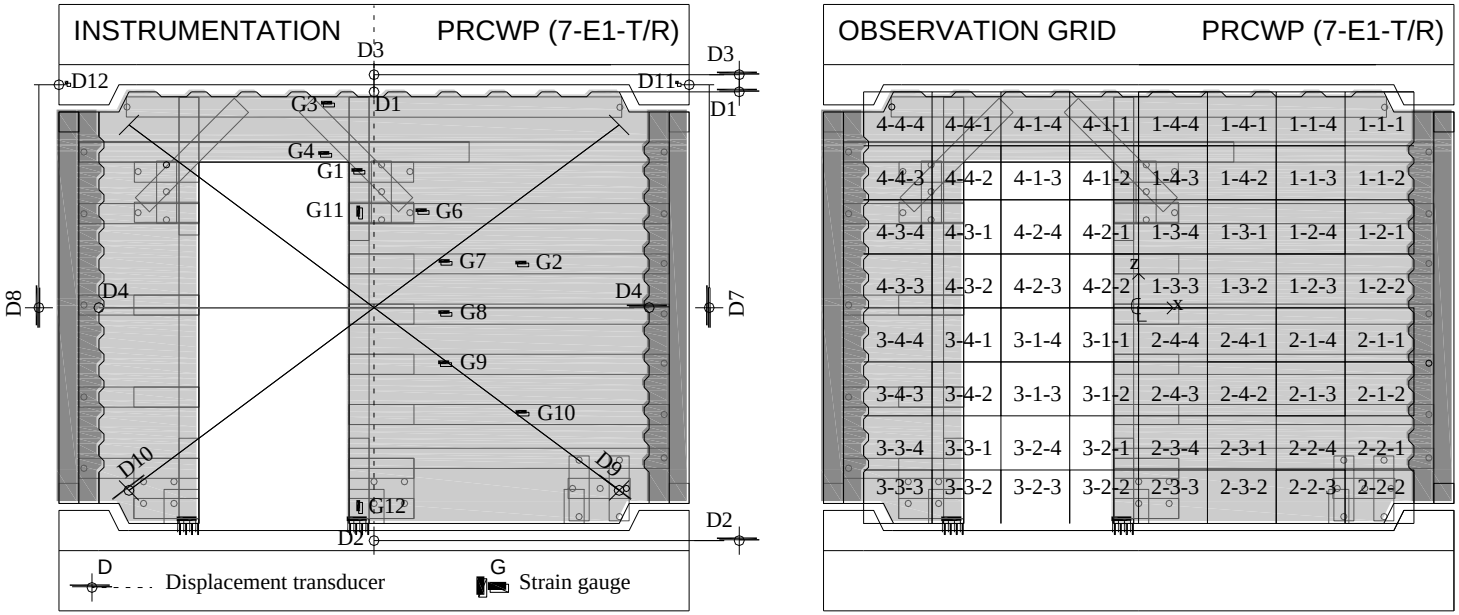

Table B.6 – Sensor list for PRCWP (7-E1-T/R) specimen

ID	Type	Location	x (mm)	y (mm)	z (mm)
D1	Displacement, top horizontal	(1-4-4); (4-1-1)	0	50	1075
D2	Displacement, bottom horizontal	Base beam	0	150	-1160
D3	Displacement, top horizontal	Loading beam	0	150	1160
D4 start	Displacement, mid horizontal	(1-2-2); (2-1-1)	1375	50	0
D4 end		(4-3-3); (3-4-4)	-1375	50	0

D7	Displacement, vertical	Loading beam	1575	0	1110
D8	Displacement, vertical	Loading beam	-1575	0	1110
D9 start	Displacement, diagonal	(2-2-2)	1225	50	-910
D9 end		(4-4-4)	-1225	50	910
D10 start	Displacement, diagonal	(3-3-3)	-1225	50	-910
D10 end		(1-1-1)	1225	50	910
D11	Displacement, out-of-plane	Loading beam	1525	-150	1110
D12	Displacement, out-of-plane	Loading beam	-1525	-150	1110
G1	Strain gauge, horizontal FRP strip	(4-1-2)	-75	0	675
G2	Strain gauge, horizontal FRP strip	(1-2-3)	745		215
G3	Strain gauge, horizontal FRP strip	(4-1-1)	-225	0	1010
G4	Strain gauge, horizontal FRP strip	(4-1-2)	-240	0	760
G6	Strain gauge, horizontal FRP strip	(1-3-4)	245	0	475
G7	Strain gauge, horizontal FRP strip	(1-3-2)	365	0	215
G8	Strain gauge, horizontal FRP strip	(2-4-1)	365	0	-35
G9	Strain gauge, horizontal FRP strip	(2-4-2)	365	0	-285
G10	Strain gauge, horizontal FRP strip	(2-1-3)	745	0	-530
G11	Strain gauge, vertical FRP strip	(4-2-1)	-65		470
G12	Strain gauge, vertical FRP strip	(3-2-2)	-75	0	-995
P1	Pressure, lateral load V	Hydraulic line	-	-	-
P2	Pressure, axial load N1	Hydraulic line	-	-	-
P3	Pressure, axial load N2	Hydraulic line	-	-	-

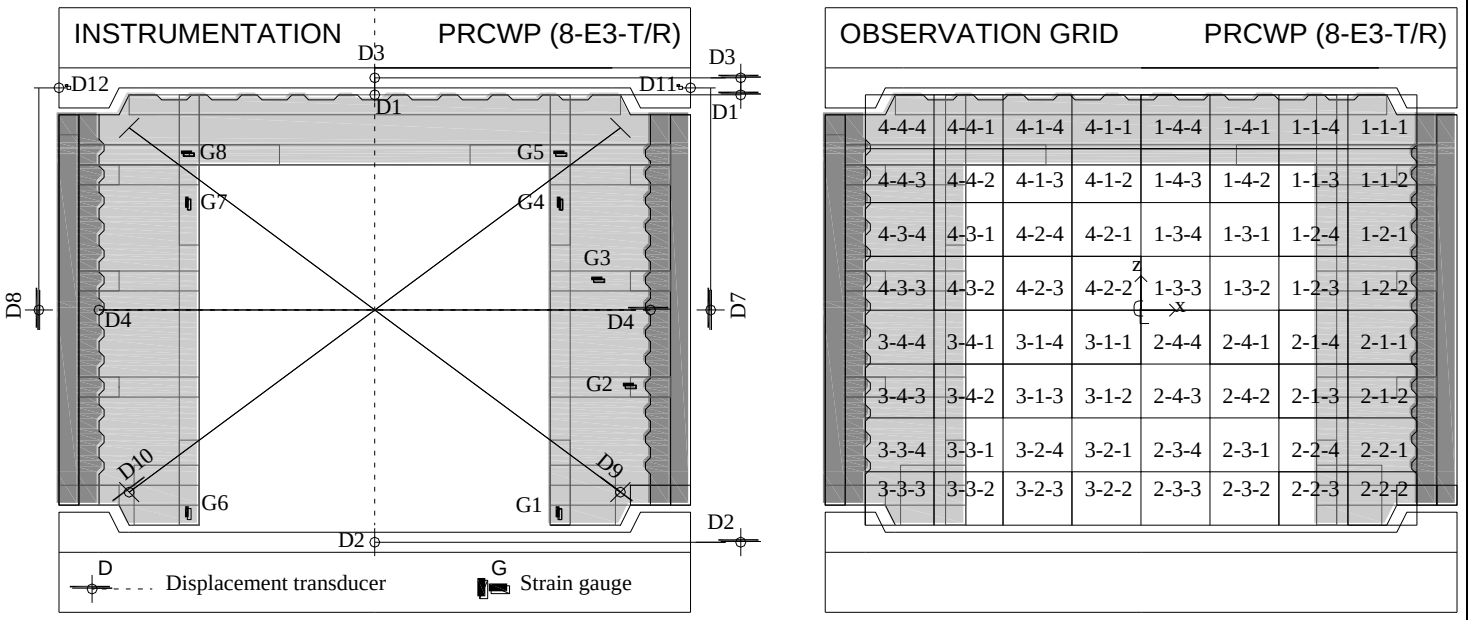

Table B.7 – Sensor list for PRCWP (8-E3-T/R) specimen

ID	Type	Location	x (mm)	y (mm)	z (mm)
D1	Displacement, top horizontal	(1-4-4); (4-1-1)	0	50	1075
D2	Displacement, bottom horizontal	Base beam	0	150	-1160
D3	Displacement, top horizontal	Loading beam	0	150	1160
D4 start	Displacement, mid horizontal	(1-2-2); (2-1-1)	1375	50	0
D4 end		(4-3-3); (3-4-4)	-1375	50	0

D7	Displacement, vertical	Loading beam	1575	0	1110
D8	Displacement, vertical	Loading beam	-1575	0	1110
D9 start	Displacement, diagonal	(2-2-2)	1225	50	-910
D9 end		(4-4-4)	-1225	50	910
D10 start	Displacement, diagonal	(3-3-3)	-1225	50	-910
D10 end		(1-1-1)	1225	50	910
D11	Displacement, out-of-plane	Loading beam	1525	-150	1110
D12	Displacement, out-of-plane	Loading beam	-1525	-150	1110
G1	Strain gauge, vertical FRP strip	(2-2-3)	1010	0	-990
G2	Strain gauge, horizontal FRP strip	(2-1-2)	1275	0	-385
G3	Strain gauge, horizontal FRP strip	(1-2-3)	1120	0	145
G4	Strain gauge, vertical FRP strip	(1-2-4)	925	0	525
G5	Strain gauge, horizontal FRP strip	(1-1-3)	930	0	775
G6	Strain gauge, vertical FRP strip	(3-3-2)	-1010	0	-990
G7	Strain gauge, vertical FRP strip	(4-3-1)	-925	0	525
G8	Strain gauge, horizontal FRP strip	(4-4-2)	-930	0	775
P1	Pressure, lateral load V	Hydraulic line	-	-	-
P2	Pressure, axial load N1	Hydraulic line	-	-	-
P3	Pressure, axial load N2	Hydraulic line	-	-	-

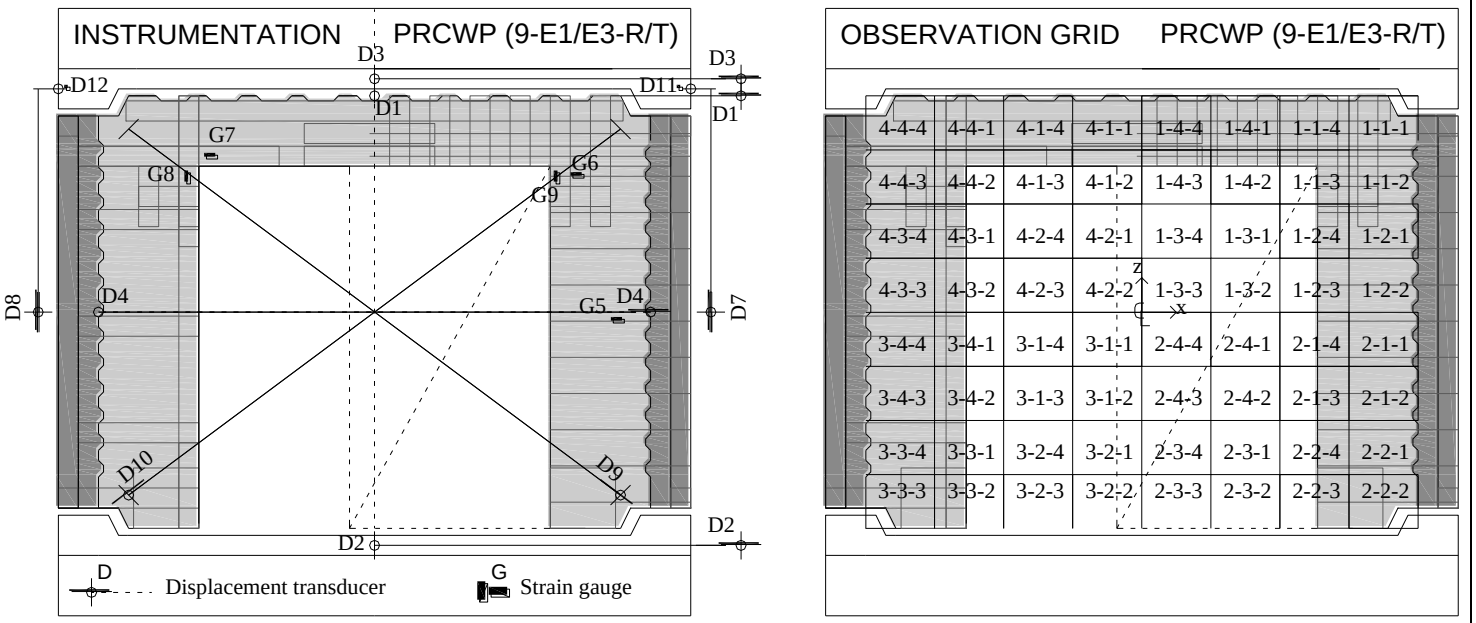

Table B.8 – Sensor list for PRCWP (9-E1/E3-R/T) specimen

ID	Type	Location	x (mm)	y (mm)	z (mm)
D1	Displacement, top horizontal	(1-4-4); (4-1-1)	0	50	1075
D2	Displacement, bottom horizontal	Base beam	0	150	-1160
D3	Displacement, top horizontal	Loading beam	0	150	1160
D4 start	Displacement, mid horizontal	(1-2-2); (2-1-1)	1375	50	0

D4 end		(4-3-3); (3-4-4)	-1375	50	0
D7	Displacement, vertical	Loading beam	1575	0	1110
D8	Displacement, vertical	Loading beam	-1575	0	1110
D9 start	Displacement, diagonal	(2-2-2)	1225	50	-910
D9 end		(4-4-4)	-1225	50	910
D10 start	Displacement, diagonal	(3-3-3)	-1225	50	-910
D10 end		(1-1-1)	1225	50	910
D11	Displacement, out-of-plane	Loading beam	1525	-150	1110
D12	Displacement, out-of-plane	Loading beam	-1525	-150	1110
G5	Strain gauge, horizontal FRP strip	(1-2-2), (2-1-1)	1215	0	-45
G6	Strain gauge, horizontal FRP strip	(1-1-3)	1015	0	675
G7	Strain gauge, horizontal FRP strip	(4-4-2)	-810	0	770
G8	Strain gauge, vertical FRP strip	(4-4-2)	-925	0	665
G9	Strain gauge, vertical FRP strip	(1-1-3)	925	0	665
P1	Pressure, lateral load V	Hydraulic line	-	-	-
P2	Pressure, axial load N1	Hydraulic line	-	-	-
P3	Pressure, axial load N2	Hydraulic line	-	-	-

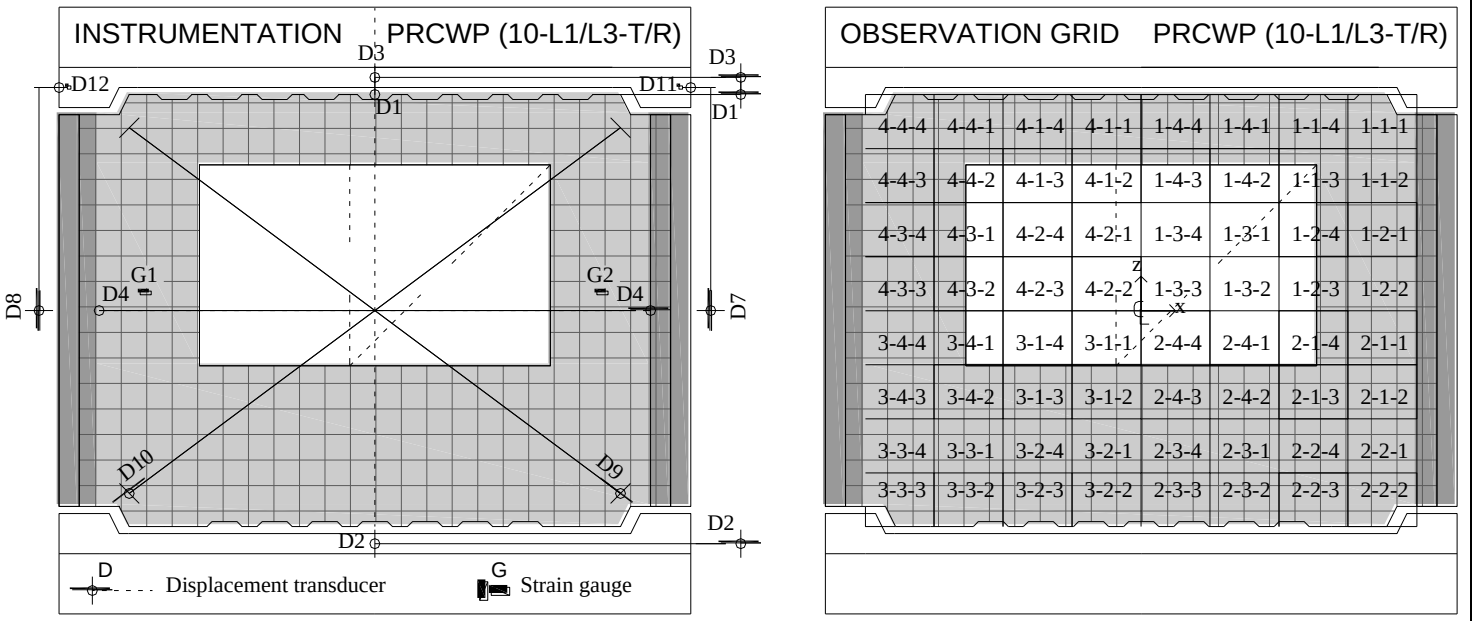

Table B.9 – Sensor list for PRCWP (10-L1/L3-T/R) specimen

ID	Type	Location	x (mm)	y (mm)	z (mm)
D1	Displacement, top horizontal	(1-4-4); (4-1-1)	0	50	1075
D2	Displacement, bottom horizontal	Base beam	0	150	-1160
D3	Displacement, top horizontal	Loading beam	0	150	1160
D4 start	Displacement, mid horizontal	(1-2-2); (2-1-1)	1375	50	0

D4 end		(4-3-3); (3-4-4)	-1375	50	0
D7	Displacement, vertical	Loading beam	1575	0	1110
D8	Displacement, vertical	Loading beam	-1575	0	1110
D9 start	Displacement, diagonal	(2-2-2)	1225	50	-910
D9 end		(4-4-4)	-1225	50	910
D10 start	Displacement, diagonal	(3-3-3)	-1225	50	-910
D10 end		(1-1-1)	1225	50	910
D11	Displacement, out-of-plane	Loading beam	1525	-150	1110
D12	Displacement, out-of-plane	Loading beam	-1525	-150	1110
G1	Strain gauge, horizontal FRP grid	(4-3-3)	-1145	0	85
G2	Strain gauge, horizontal FRP grid	(1-2-2)	1135	0	85
P1	Pressure, lateral load V	Hydraulic line	-	-	-
P2	Pressure, axial load N1	Hydraulic line	-	-	-
P3	Pressure, axial load N2	Hydraulic line	-	-	-

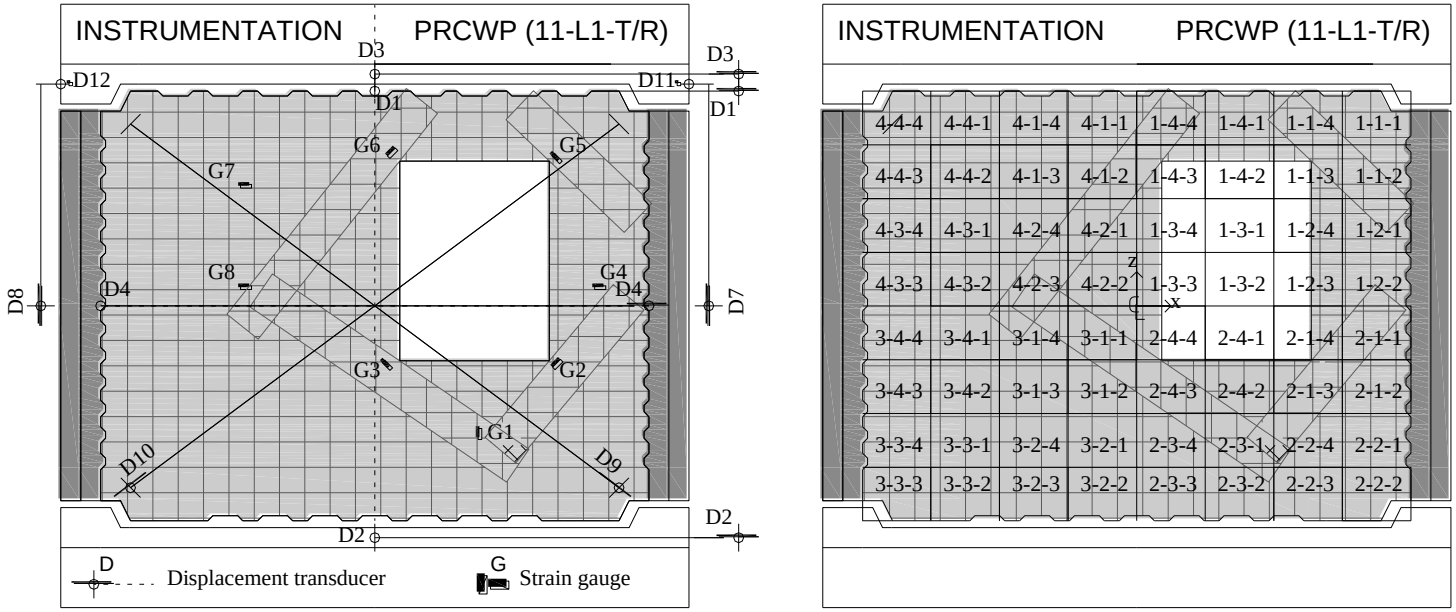

Table B.10 – Sensor list for PRCWP (11-L1-T/R) specimen

ID	Type	Location	x (mm)	y (mm)	z (mm)
D1	Displacement, top horizontal	(1-4-4); (4-1-1)	0	50	1075
D2	Displacement, bottom horizontal	Base beam	0	150	-1160
D3	Displacement, top horizontal	Loading beam	0	150	1160
D4 start	Displacement, mid horizontal	(1-2-2); (2-1-1)	1375	50	0
D4 end		(4-3-3); (3-4-4)	-1375	50	0

D7	Displacement, vertical	Loading beam	1575	0	1110
D8	Displacement, vertical	Loading beam	-1575	0	1110
D9 start	Displacement, diagonal	(2-2-2)	1225	50	-910
D9 end		(4-4-4)	-1225	50	910
D10 start	Displacement, diagonal	(3-3-3)	-1225	50	-910
D10 end		(1-1-1)	1225	50	910
D11	Displacement, out-of-plane	Loading beam	1525	-150	1110
D12	Displacement, out-of-plane	Loading beam	-1525	-150	1110
G1	Strain gauge,vertictal FRP grid	(2-3-1)	530	0	-640
G2	Strain gauge, inclined FRP grid	(2-1-3)	925	0	-300
G3	Strain gauge, inclined FRP grid	(2-4-3)	55	0	-300
G4	Strain gauge, horizontal FRP grid	(1-2-2)	1130	0	90
G5	Strain gauge, inclined FRP grid	(1-1-3)	910	0	755
G6	Strain gauge, inclined FRP grid	(1-4-3)	90	0	755
G7	Strain gauge, horizontal FRP grid	(4-1-3)	-645	0	600
G8	Strain gauge, horizontal FRP grid	(4-2-3)	-645	0	90
P1	Pressure, lateral load V	Hydraulic line	-	-	-
P2	Pressure, axial load N1	Hydraulic line	-	-	-
P3	Pressure, axial load N2	Hydraulic line	-	-	-

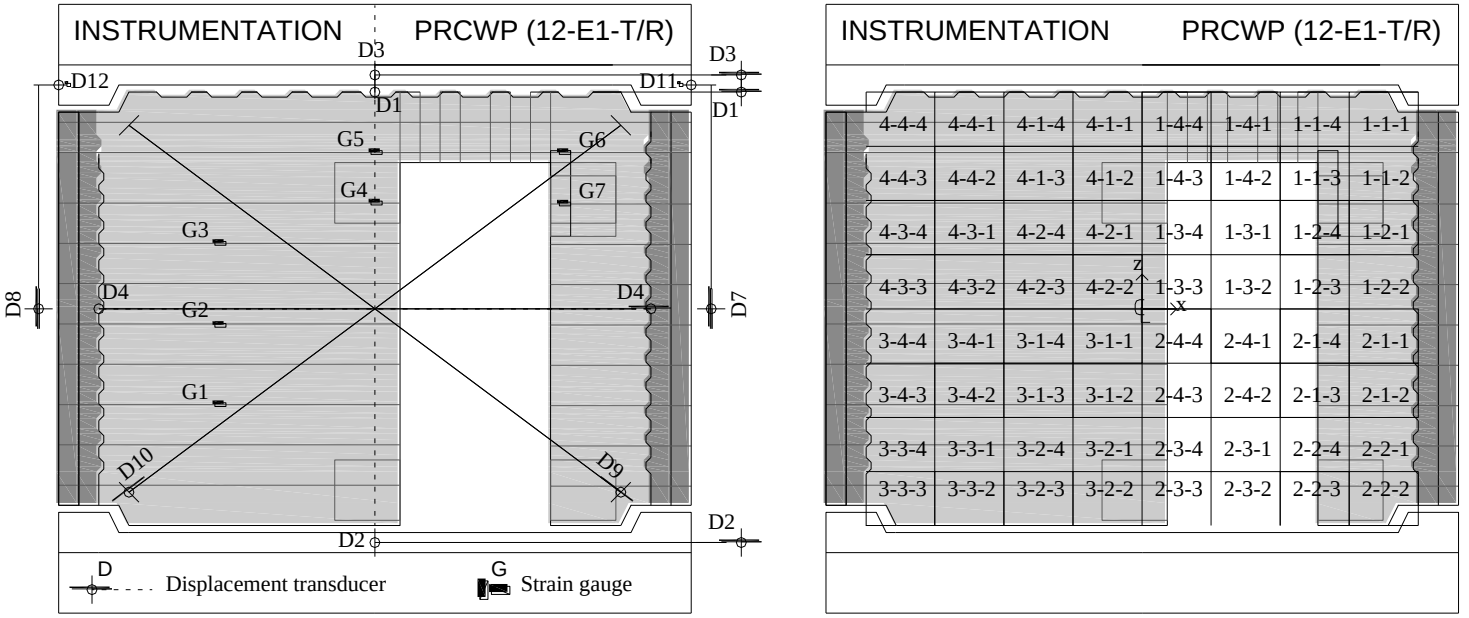

Table B.11 – Sensor list for PRCWP (12-E1-T/R) specimen

ID	Type	Location	x (mm)	y (mm)	z (mm)
D1	Displacement, top horizontal	(1-4-4); (4-1-1)	0	50	1075
D2	Displacement, bottom horizontal	Base beam	0	150	-1160
D3	Displacement, top horizontal	Loading beam	0	150	1160
D4 start	Displacement, mid horizontal	(1-2-2); (2-1-1)	1375	50	0

D4 end		(4-3-3); (3-4-4)	-1375	50	0
D7	Displacement, vertical	Loading beam	1575	0	1110
D8	Displacement, vertical	Loading beam	-1575	0	1110
D9 start	Displacement, diagonal	(2-2-2)	1225	50	-910
D9 end		(4-4-4)	-1225	50	910
D10 start	Displacement, diagonal	(3-3-3)	-1225	50	-910
D10 end		(1-1-1)	1225	50	910
D11	Displacement, out-of-plane	Loading beam	1525	-150	1110
D12	Displacement, out-of-plane	Loading beam	-1525	-150	1110
G1	Strain gauge,horizontal FRP plate	(3-4-2)	770	0	-475
G2	Strain gauge, horizontal FRP plate	(3-4-1)	770	0	-75
G3	Strain gauge, horizontal FRP plate	(4-3-1)	770	0	325
G4	Strain gauge, horizontal FRP plate	(1-3-4)	10	0	525
G5	Strain gauge, horizontal FRP plate	(1-4-3)	10	0	775
G6	Strain gauge, horizontal FRP plate	(1-1-3)	945	0	775
G7	Strain gauge, horizontal FRP plate	(1-2-4)	945	0	525
P1	Pressure, lateral load V	Hydraulic line	-	-	-
P2	Pressure, axial load N1	Hydraulic line	-	-	-
P3	Pressure, axial load N2	Hydraulic line	-	-	-

APPENDIX C

Strengthening cost evaluation

Table C.1 – Repair and strengthening costs for PRCWP (7-E1-T/R) specimen

SURFACE PREPARATION							
MATERIAL	DETAILING	UM	PRICE [EUR]	QUANTITY	VALUE [EUR]	TVA [EUR]	PRICE [EUR]
Wood formwork	for wall repair	sqm	3,00	2,00	6,00	1,44	7,44
Builder tools	for wall repair	pieces	10,00	0,50	5,00	1,20	6,20
Diamond grinding head	concrete surface polish	pieces	200	0,30	60,00	14,40	74,40
Hammer drill	transverse anchorage	pieces	10,00	0,50	5,00	1,20	6,20
Vacuum bag	concrete surface cleaning	pieces	5,00	0,50	2,50	0,60	3,10
Sika Monotop 614 (25 kg)	repair mortar	kg	0,94	25	23,47	5,63	29,10
					Surface preparation material price		**126,44**
LABOR	DETAILING	UM	PRICE [EUR]	QUANTITY	VALUE [EUR]	TVA [EUR]	PRICE [EUR]
Wall structural repair	cracks, crushed concrete	hours	5,00	3,00	15,00	3,60	18,60
Wall surface grinding	EBR surface preparation	sqm	10,00	10,42	104,0	25,01	129,21

Concrete hole drilling	FRP anchorage	hours	5,00	1,00	5,00	1,20	6,20
Wall surface blowing by compressed air	surface preparation	hours	5,00	0,50	2,50	0,60	3,10
Wall surface vacuum-cleaning	surface preparation	hours	5,00	0,50	2,50	0,60	3,10
					Surface preparation labor price		**160,21**

EQUIPMENT	DETAILING	UM	PRICE [EUR]	QUANTITY	VALUE [EUR]	TVA [EUR]	PRICE [EUR]
Percussion drill	drilling, crushed concrete removal, mortar prepare	hours	10	2,00	20,00	4,80	24,80
Grinder	concrete surface polish	hours	10,00	2,00	20,00	4,80	24,80
Dust extraction system (vacuum-cleaner)	concrete surface cleaning	hours	10,00	0,50	5,00	1,20	6,20
Air compressor	concrete surface cleaning	hours	10,00	0,50	5,00	1,20	6,20
					Surface preparation equipment price		**62,00**
					Surface preparation total price		**348,65**

STRENGTHENING APPLICATION							
MATERIAL	DETAILING	UM	PRICE [EUR]	QUANTITY	VALUE [EUR]	TVA [EUR]	PRICE [EUR]
Sika wrap hex 230C (0.6 m x 50 m)	carbon fibre fabric	sqm	32,55	8,40	273,45	65,63	339,08
Sika sikadur 330 (5kg)	resin for carbon fibre fabric	kg	14,65	10,00	146,47	35,15	181,62
Colma cleaner (25 kg)	fabric and tools cleaning	kg	5,20	3,00	15,60	3,74	19,34
Protection foil	dust protection	roll	5,00	1,00	5,00	1,20	6,20
Plastic spatules	resin application	pieces	0,50	4,00	2,00	0,48	2,48
Scissors	fabric cut	pieces	10,00	0,20	2,00	0,48	2,48
Gloves	resin application	pieces	2,50	2,00	5,00	1,20	6,20
Safety glasses	working protection	pieces	5,00	0,50	2,50	0,60	3,10
Plastic roll	EBR application	pieces	27,00	0,20	5,40	1,30	6,70
					Strengthening application material price		**567,20**

LABOR	DETAILING	UM	PRICE [EUR]	QUANTITY	VALUE [EUR]	TVA [EUR]	PRICE [EUR]
CF fabric cleaning	fabric preparation	hours	5,00	1,50	7,50	1,80	9,30
CF fabric cut	using scissors	hours	5,00	2,00	10,00	2,40	12,40
Resin application	mixing and application	sqm	5,00	8,40	42,00	10,08	52,08
CF fabric application	EBR application	sqm	5,00	8,40	42,00	10,08	52,08
FRP anchorage application	anchorage application	pieces	1,00	49,00	49,00	11,76	60,76
					Strengthening application labor price		**186,62**
EQUIPMENT	DETAILING	UM	PRICE [EUR]	QUANTITY	VALUE [EUR]	TVA [EUR]	PRICE [EUR]
Percussion drill	resin mixing	hours	10,00	0,50	5,00	1,20	6,20
Electronic scale	resin weighting	hours	10,00	0,50	5,00	1,20	6,20
					Strengthening application equipment price		**12,40**
					Strengthening application total price		**766,22**

REHABILITATION TOTAL PRICE	**1114,9**

REHABILITATION TOTAL PRICE / SQM	**106,99**

Table C.2 – Repair and strengthening costs for PRCWP (8-E3-T/R) specimen

SURFACE PREPARATION							
MATERIAL	DETAILING	UM	PRICE [EUR]	QUANTITY	VALUE [EUR]	TVA [EUR]	PRICE [EUR]
Wood formwork	for wall repair	sqm	3,00	1,00	3,00	0,72	3,72
Builder tools	for wall repair	pieces	10,00	0,50	5,00	1,20	6,20
Diamond grinding head	concrete surface polish	pieces	200	0,20	40,00	9,60	49,60
Hammer drill	transverse anchorage	pieces	10,00	0,50	5,00	1,20	6,20
Vacuum bag	concrete surface cleaning	pieces	5,00	0,50	2,50	0,60	3,10
Sika Monotop 614 (25 kg)	repair mortar	kg	0,94	10,00	9,39	2,25	11,64
						Surface preparation material price	**80,46**

LABOR	DETAILING	UM	PRICE [EUR]	QUANTITY	VALUE [EUR]	TVA [EUR]	PRICE [EUR]
Wall structural repair	cracks, crushed concrete	hours	5,00	1,5	7,50	1,80	9,30
Wall surface grinding	EBR surface preparation	sqm	10,00	6,82	68,20	16,37	84,57
Concrete hole drilling	FRP anchorage	hours	5,00	2,00	10,00	2,40	12,40
Wall surface blowing by compressed air	surface preparation	hours	5,00	0,30	1,50	0,36	1,86
Wall surface vacuum-cleaning	surface preparation	hours	5,00	0,30	1,50	0,36	1,86
					Surface preparation labor price		**109,99**

EQUIPMENT	DETAILING	UM	PRICE [EUR]	QUANTITY	VALUE [EUR]	TVA [EUR]	PRICE [EUR]
Percussion drill	drilling, crushed concrete removal, mortar prepare	hours	10,00	2,00	20,00	4,80	24,80
Grinder	concrete surface polish	hours	10,00	1,50	15,00	3,60	18,60
Dust extraction system (vacuum-cleaner)	concrete surface cleaning	hours	10,00	0,30	3,00	0,72	3,72

Air compressor	concrete surface cleaning	hours	10,00	0,30	3,00	0,72	3,72
					Surface preparation equipment price		**50,84**
					Surface preparation total price		**241,29**

STRENGTHENING APPLICATION							
MATERIAL	DETAILING	UM	PRICE [EUR]	QUANTITY	VALUE [EUR]	TVA [EUR]	PRICE [EUR]
Sika wrap hex 230C (0.6 m x 50 m)	carbon fibre fabric	sqm	32,55	4,42	143,9	34,53	178,42
Sika sikadur 330 (5kg)	resin for carbon fibre fabric	kg	14,65	8,00	117,2	28,12	145,30
Colma cleaner (25 kg)	fabric and tools cleaning	kg	5,20	2,00	10,40	2,50	12,90
Protection foil	dust protection	roll	5,00	1,00	5,00	1,20	6,20
Plastic spatules	resin application	pieces	0,50	4,00	2,00	0,48	2,48
Scissors	fabric cut	pieces	10,00	0,20	2,00	0,48	2,48
loves	resin application	pieces	2,50	2,00	5,00	1,20	6,20

Safety glasses	working protection	pieces	5,00	0,50	2,50	0,60	3,10
Plastic roll	EBR application	pieces	22,00	0,20	4,40	1,06	5,46
					Strengthening application material price		**362,53**
LABOR	DETAILING	UM	PRICE [EUR]	QUANTITY	VALUE [EUR]	TVA [EUR]	PRICE [EUR]
CF fabric cleaning	fabric preparation	hours	5,00	1,00	5,00	1,20	6,20
CF fabric cut	using scissors	hours	5,00	1,50	7,50	1,80	9,30
Resin application	mixing and application	sqm	5,00	4,42	22,10	5,30	27,40
CF fabric application	EBR application	sqm	5,00	4,42	22,10	5,30	27,40
FRP anchorage application	anchorage application	pieces	1,00	38,00	38,00	9,12	47,12
					Strengthening application labor price		**117,43**
EQUIPMENT	DETAILING	UM	PRICE [EUR]	QUANTITY	VALUE [EUR]	TVA [EUR]	PRICE [EUR]
Percussion drill	resin mixing	hours	10,00	0,30	3,00	0,72	3,72
Electronic scale	resin weighting	hours	10,00	0,30	3,00	0,72	3,72

Strengthening application equipment price	**7,44**
Strengthening application total price	**487,40**
REHABILITATION TOTAL PRICE	**728,69**
REHABILITATION TOTAL PRICE / SQM	**106,85**

Table C.3 – Strengthening costs for PRCWP (9-E1/E3-R/T) specimen

SURFACE PREPARATION							
MATERIAL	DETAILING	UM	PRICE [EUR]	QUANTITY	VALUE [EUR]	TVA [EUR]	PRICE [EUR]
Diamond grinding head	concrete surface polish	pieces	200	0,20	40,00	9,60	49,60
Hammer drill	transverse anchorage	pieces	10,00	0,50	5,00	1,20	6,20
Diamond cutting discs	NSM channel cut	pieces	200	0,50	100,00	24,00	124,00
Steel profile	channel cut guiding	pieces	10,00	0,20	2,00	0,48	2,48

	system						
Vacuum bag	concrete surface cleaning	pieces	5,00	0,50	2,50	0,60	3,10
					Surface preparation material price		**185,38**

LABOR	DETAILING	UM	PRICE [EUR]	QUANTITY	VALUE [EUR]	TVA [EUR]	PRICE [EUR]
Wall surface grinding	EBR surface preparation	sqm	10,00	6,82	68,20	16,37	84,57
Concrete hole drilling	FRP anchorage	hours	5,00	2,00	10,00	2,40	12,40
Guiding system	for channels cut	hours	5,00	1,50	7,50	1,80	9,30
Channels cut	for NSM-CFRP	hours	5,00	3,00	15,00	3,60	18,60
Wall surface blowing by compressed air	surface preparation	hours	5,00	0,30	1,50	0,36	1,86
Wall surface vacuum-cleaning	surface preparation	hours	5,00	0,30	1,50	0,36	1,86
					Surface preparation labor price		**128,59**

EQUIPMENT	DETAILING	UM	PRICE [EUR]	QUANTITY	VALUE [EUR]	TVA [EUR]	PRICE [EUR]
Percussion drill	drilling, crushed concrete removal,	hours	10,00	2,00	20,00	4,80	24,80

	mortar prepare						
Grinder	concrete surface polish	hours	10,00	1,50	15,00	3,60	18,60
Double disc grinder	channels cut	hours	10,00	3,00	30,00	7,20	37,20
Dust extraction system (vacuum-cleaner)	concrete surface cleaning	hours	10,00	0,30	3,00	0,72	3,72
Air compressor	concrete surface cleaning	hours	10,00	0,30	3,00	0,72	3,72
					Surface preparation equipment price		**88,04**
					Surface preparation total price		**402,01**

STRENGTHENING APPLICATION							
MATERIAL	DETAILING	UM	PRICE [EUR]	QUANTITY	VALUE [EUR]	TVA [EUR]	PRICE [EUR]
Sika wrap hex 230C (0.6 m x 50 m)	carbon fibre fabric	sqm	32,55	4,80	156,26	37,50	193,76
Sika sikadur 330 (5kg)	resin for carbon fibre fabric	kg	14,65	7,00	102,53	24,61	127,14
Colma cleaner (25 kg)	fabric and tools cleaning	kg	5,20	2,00	10,40	2,50	12,90

Sika carbodur S512	carbon fibre plates	m	21,54	5,10	109,85	26,36	136,22
Sika sikadur 30 (6kg)	resin for carbon fibre plates	kg	8,01	9,00	72,09	17,30	89,39
Protection foil	dust protection	roll	5,00	1,00	5,00	1,20	6,20
Plastic spatules	resin application	pieces	0,50	4,00	2,00	0,48	2,48
Scissors	fabric cut	pieces	10,00	0,20	2,00	0,48	2,48
Cutter	plates cut	pieces	10,00	0,20	2,00	0,48	2,48
Gloves	resin application	pieces	2,50	2,00	5,00	1,20	6,20
Safety glasses	working protection	pieces	5,00	0,50	2,50	0,60	3,10
Plastic roll	EBR application	pieces	22,00	0,20	4,40	1,06	5,46
				Strengthening application material price			**587,80**

LABOR	DETAILING	UM	PRICE [EUR]	QUANTITY	VALUE [EUR]	TVA [EUR]	PRICE [EUR]
CF fabric and plates cleaning	fabric preparation	hours	5,00	2,00	10,00	2,40	12,40
CF fabric and plates cut	using scissors and	hours	5,00	3,00	15,00	3,60	18,60

	cutter						
Resin application for fabric	mixing and application	sqm	5,00	4,80	24,00	5,76	29,76
Resin application for plates	mixing and application	m	2,50	20,00	50,00	12,00	62,00
CF fabric application	EBR application	sqm	5,00	4,42	22,10	5,30	27,40
CF plates application	NSM application	m	2,50	20,00	50,00	12,00	62,00
FRP anchorage application	anchorage application	pieces	1,00	16,00	16,00	3,84	19,84
					Strengthening application labor price		**232,00**
EQUIPMENT	DETAILING	UM	PRICE [EUR]	QUANTITY	VALUE [EUR]	TVA [EUR]	PRICE [EUR]
Percussion drill	resin mixing	hours	10,00	0,30	3,00	0,72	3,72
Electronic scale	resin weighting	hours	10,00	0,30	3,00	0,72	3,72
					Strengthening application equipment price		**7,44**
					Strengthening application total price		**827,24**
					REHABILITATION TOTAL PRICE		**1229,25**
					REHABILITATION TOTAL PRICE / SQM		**180,24**

Table C.4 – Repair and strengthening costs for PRCWP (10-L1/L3-T/R) specimen

SURFACE PREPARATION							
MATERIAL	DETAILING	UM	PRICE [EUR]	QUANTITY	VALUE [EUR]	TVA [EUR]	PRICE [EUR]
Wood formwork	for wall repair	sqm	3,00	2,00	6,00	1,44	7,44
Builder tools	for wall repair	pieces	10,00	0,50	5,00	1,20	6,20
Diamond grinding head	concrete surface polish	pieces	200	0,50	100,00	24,00	124,00
Hammer drill	transverse anchorage	pieces	10,00	0,70	7,00	1,68	8,68
Vacuum bag	concrete surface cleaning	pieces	5,00	0,50	2,50	0,60	3,10
Sika Monotop 614 (25 kg)	repair mortar	kg	0,96	35	33,60	8,06	41,66
						Surface preparation material price	**191,08**
LABOR	DETAILING	UM	PRICE [EUR]	QUANTITY	VALUE [EUR]	TVA [EUR]	PRICE [EUR]
Wall structural repair	cracks, crushed concrete	hours	5,00	2,00	10,00	2,40	12,40

Wall surface grinding	TRM surface preparation	sqm	10,00	9,62	96,20	23,09	119,29
Concrete hole drilling	mechanical anchorage	hours	5,00	2,00	10,00	2,40	12,40
Wall surface blowing by compressed air	surface preparation	hours	5,00	0,50	2,50	0,60	3,10
Wall surface vacuum-cleaning	surface preparation	hours	5,00	0,50	2,50	0,60	3,10
						Surface preparation labor price	**150,29**

EQUIPMENT	DETAILING	UM	PRICE [EUR]	QUANTITY	VALUE [EUR]	TVA [EUR]	PRICE [EUR]
Percussion drill	drilling, crushed concrete removal, mortar prepare	hours	10,00	2,50	25,00	6,00	31,00
Grinder	concrete surface polish	hours	10,00	2,00	20,00	4,80	24,80
Dust extraction system (vacuum-cleaner)	concrete surface cleaning	hours	10,00	0,50	5,00	1,20	6,20
Air compressor	concrete surface cleaning	hours	10,00	0,50	5,00	1,20	6,20
						Surface preparation equipment price	**68,20**
						Surface preparation total price	**409,57**

STRENGTHENING APPLICATION							
MATERIAL	DETAILING	UM	PRICE [EUR]	QUANTITY	VALUE [EUR]	TVA [EUR]	PRICE [EUR]
Sika wrap 350G (1m x 50 m)	glass fibre grid	sqm	8,60	18,00	154,80	37,15	191,95
Sika Monotop 722 Mur (25kg)	mortar for TRM	kg	1,12	175	196,00	47,04	243,04
Sika Monotop 910 N (25 kg)	bonding primer for TRM	kg	1,10	35	38,50	9,24	47,74
Sika sikadur 30 (6kg)	resin for rods	kg	8,00	1,00	8,00	1,92	9,92
Colma cleaner (25 kg)	tools cleaning	kg	5,20	1,00	5,20	1,25	6,45
Threaded rod, nut, washer	anchorage for TRM	pieces	0,15	98,00	14,70	3,53	18,23
Protection foil	dust protection	roll	5,00	1,00	5,00	1,20	6,20
Plastic spatules	resin application	pieces	0,50	4,00	2,00	0,48	2,48
Scissors	fabric cut	pieces	10,00	0,20	2,00	0,48	2,48
Gloves	resin application	pieces	2,50	2,00	5,00	1,20	6,20

Safety glasses	working protection	pieces	5,00	0,50	2,50	0,60	3,10

Strengthening application material price **537,79**

LABOR	DETAILING	UM	PRICE [EUR]	QUANTITY	VALUE [EUR]	TVA [EUR]	PRICE [EUR]
GF grid cut	using scissors	hours	5,00	2,00	10,00	2,40	12,40
Resin application	mixing and application	hours	5,00	2,00	10,00	2,40	12,40
GF grid application	TRM application	sqm	5,00	18,00	90,00	21,60	111,60
mortar application	TRM application	sqm	5,00	9,62	48,10	11,54	59,64
anchorage application	anchorage application	pieces	0,50	98,00	49,00	11,76	60,76

Strengthening application labor price **256,80**

EQUIPMENT	DETAILING	UM	PRICE [EUR]	QUANTITY	VALUE [EUR]	TVA [EUR]	PRICE [EUR]
Percussion drill	resin mixing	hours	10,00	2,00	20,00	4,80	24,80
Electronic scale	resin weighting	hours	10,00	0,50	5,00	1,20	6,20

Strengthening application equipment price	**31,00**
Strengthening application total price	**825,59**
REHABILITATION TOTAL PRICE	**1235,16**
REHABILITATION TOTAL PRICE / SQM	**128,40**

Table C.5 – Repair and strengthening costs for PRCWP (11-L1-T/R) specimen

SURFACE PREPARATION							
MATERIAL	DETAILING	UM	PRICE [EUR]	QUANTITY	VALUE [EUR]	TVA [EUR]	PRICE [EUR]
Wood formwork	for wall repair	sqm	3,00	3,00	9,00	2,16	11,16
Builder tools	for wall repair	pieces	10,00	0,50	5,00	1,20	6,20
Diamond grinding head	concrete surface polish	pieces	200	0,50	100,00	24,00	124,00
Hammer drill	transverse anchorage	pieces	10,00	0,50	5,00	1,20	6,20

Vacuum bag	concrete surface cleaning	pieces	5,00	0,50	2,50	0,60	3,10
Mapegrout easy flow GF (25 kg)	repair mortar	kg	0,95	50	47,50	11,40	58,90
					Surface preparation material price		**209,56**

LABOR	DETAILING	UM	PRICE [EUR]	QUANTITY	VALUE [EUR]	TVA [EUR]	PRICE [EUR]
Wall structural repair	cracks, crushed concrete	hours	5,00	4,00	20,00	4,80	24,80
Wall surface grinding	TRM surface preparation	sqm	10,00	11,62	116,20	27,89	144,09
Concrete hole drilling	mechanical anchorage	hours	5,00	2,00	10,00	2,40	12,40
Wall surface blowing by compressed air	surface preparation	hours	5,00	0,50	2,50	0,60	3,10
Wall surface vacuum-cleaning	surface preparation	hours	5,00	0,50	2,50	0,60	3,10
					Surface preparation labor price		**187,49**

EQUIPMENT	DETAILING	UM	PRICE [EUR]	QUANTITY	VALUE [EUR]	TVA [EUR]	PRICE [EUR]
Percussion drill	drilling, crushed concrete removal, mortar prepare	hours	10,00	2,50	25,00	6,00	31,00

Grinder	concrete surface polish	hours	10,00	2,00	20,00	4,80	24,80
Dust extraction system (vacuum-cleaner)	concrete surface cleaning	hours	10,00	0,50	5,00	1,20	6,20
Air compressor	concrete surface cleaning	hours	10,00	0,50	5,00	1,20	6,20
					Surface preparation equipment price		**68,20**
					Surface preparation total price		**465,25**

STRENGTHENING APPLICATION

MATERIAL	DETAILING	UM	PRICE [EUR]	QUANTITY	VALUE [EUR]	TVA [EUR]	PRICE [EUR]
Mapegrid C170 (1 m x 50 m)	carbon fibre grid	sqm	60,00	23,50	1410,00	338,40	1748,40
Planitop HDM (30.5kg)	mortar for TRM	kg	1,40	396,5	555,10	133,22	688,32
Colma cleaner (25 kg)	tools cleaning	kg	5,20	1,00	5,20	1,25	6,45
Epojet (4kg)	resin for crack injection	kg	21,70	2,50	54,25	13,02	67,27
Adesilex PG2 (6kg)	cord preimpregnation	kg	11,20	6,00	67,20	16,13	83,33

	resin						
Mapewrap 11 (6kg)	resin for cord fixing	kg	10,70	6,00	64,20	15,41	79,61
Mapewrap S fiocco (25 m)	steel fibre cord	m	24,00	8,00	192,00	46,08	238,08
Sika mechanical packers (MPS)	packers for crack injection	pieces	2,28	15,00	34,20	8,21	42,41
Protection foil	dust protection	roll	5,00	1,00	5,00	1,20	6,20
Plastic spatules	resin application	pieces	0,50	4,00	2,00	0,48	2,48
Scissors	fabric cut	pieces	10,00	0,20	2,00	0,48	2,48
Gloves	resin application	pieces	2,50	2,00	5,00	1,20	6,20
Safety glasses	working protection	pieces	5,00	0,50	2,50	0,60	3,10
					Strengthening application material price		**2974,33**

LABOR	DETAILING	UM	PRICE [EUR]	QUANTITY	VALUE [EUR]	TVA [EUR]	PRICE [EUR]
CF grid impregnation	grid preparation	hours	5,00	0,50	2,50	0,60	3,10
CF grid cut	using scissors	hours	5,00	2,50	12,50	3,00	15,50

Resin application	mixing and application	hours	5,00	2,00	10,00	2,40	12,40
Anchorage preparation	preimpregnation	hours	5,00	2,00	10,00	2,40	12,40
CF grid application	TRM application	sqm	5,00	23,50	117,50	28,20	145,70
mortar application	TRM application	sqm	5,00	11,62	58,10	13,94	72,04
surface anchorage application	anchorage application	pieces	1,00	23,00	23,00	5,52	28,52
						Strengthening application labor price	**289,66**

EQUIPMENT	DETAILING	UM	PRICE [EUR]	QUANTITY	VALUE [EUR]	TVA [EUR]	PRICE [EUR]
Percussion drill	resin mixing	hours	10,00	2,00	20,00	4,80	24,80
Hand pump	crack injection	pieces	60,00	0,30	18,00	4,32	22,32
Electronic scale	resin weighting	hours	10,00	0,50	5,00	1,20	6,20
						Strengthening application equipment price	**53,32**
						Strengthening application total price	**3317,31**

REHABILITATION TOTAL PRICE	**3782,56**

REHABILITATION TOTAL PRICE / SQM	**325,52**

Table C.6 – Repair and strengthening costs for PRCWP (12-E1-T/R) specimen

SURFACE PREPARATION							
MATERIAL	DETAILING	UM	PRICE [EUR]	QUANTITY	VALUE [EUR]	TVA [EUR]	PRICE [EUR]
Wood formwork	for wall repair	sqm	3,00	2,00	6,00	1,44	7,44
Builder tools	for wall repair	pieces	10,00	0,50	5,00	1,20	6,20
Diamond grinding head	concrete surface polish	pieces	200	0,10	20,00	4,80	24,80
Hammer drill	transverse anchorage	pieces	10,00	0,70	7,00	1,68	8,68
Diamond cutting discs	NSM channel cut	pieces	200	0,70	140,00	33,60	173,60
Steel profile	channel cut guiding system	pieces	10,00	0,20	2,00	0,48	2,48
Vacuum bag	concrete surface	pieces	5,00	1,00	5,00	1,20	6,20

	cleaning						
Mapegrout easy flow GF (25 kg)	repair mortar	kg	0,95	15	14,25	3,42	17,67
					Surface preparation material price		**247,07**
LABOR	DETAILING	UM	PRICE [EUR]	QUANTITY	VALUE [EUR]	TVA [EUR]	PRICE [EUR]
Wall structural repair	cracks, crushed concrete	hours	5,00	2,00	10,00	2,40	12,40
Wall surface grinding	EBR surface preparation	sqm	10,00	2,00	20,00	4,80	24,80
Concrete hole drilling	FRP anchorage	hours	5,00	4,00	20,00	4,80	24,80
Guiding system	for channels cut	hours	5,00	3,00	15,00	3,60	18,60
Channels cut	for NSM-CFRP	hours	5,00	6,00	30,00	7,20	37,20
Wall surface blowing by compressed air	surface preparation	hours	5,00	0,5,	2,50	0,60	3,10
Wall surface vacuum-cleaning	surface preparation	hours	5,00	0,50	2,50	0,60	3,10
					Surface preparation labor price		**124,00**
EQUIPMENT	DETAILING	UM	PRICE [EUR]	QUANTITY	VALUE [EUR]	TVA [EUR]	PRICE [EUR]

Percussion drill	drilling, crushed concrete removal, mortar prepare	hours	10,00	4,50	45,00	10,80	55,80
Grinder	concrete surface polish	hours	10,00	1,00	10,00	2,40	12,40
Double disc grinder	channels cut	hours	10,00	6,00	60,00	14,40	74,40
Dust extraction system (vacuum-cleaner)	concrete surface cleaning	hours	10,00	0,50	5,00	1,20	6,20
Air compressor	concrete surface cleaning	hours	10,00	0,50	5,00	1,20	6,20
					Surface preparation equipment price		**155,00**
					Surface preparation total price		**526,07**

STRENGTHENING APPLICATION							
MATERIAL	DETAILING	UM	PRICE [EUR]	QUANTITY	VALUE [EUR]	TVA [EUR]	PRICE [EUR]
MapeWrap C UNI-AX 300/40 (1m x 50m)	carbon fibre fabric	sqm	40,00	1,50	60,00	14,40	74,40
Mapewrap 31 (5kg)	resin for carbon fibre fabric	kg	20,80	1,5	31,20	7,49	38,69

Colma cleaner (25 kg)	fabric and tools cleaning	kg	5,20	1,00	5,20	1,25	6,45
Carboplate E170/100/1.4 (25 m)	carbon fibre plates	m	85,00	6,25	531,25	127,50	658,75
Adesilex PG1 (6kg)	resin for carbon fibre plates	kg	11,20	5,00	56,00	13,44	69,44
Protection foil	dust protection	roll	5,00	1,00	5,00	1,20	6,20
Plastic spatules	resin application	pieces	0,50	4,00	2,00	0,48	2,48
Scissors	fabric cut	pieces	10,00	0,20	2,00	0,48	2,48
Cutter	plates cut	pieces	10,00	0,70	7,00	1,68	8,68
Gloves	resin application	pieces	2,50	2,00	5,00	1,20	6,20
Safety glasses	working protection	pieces	5,00	0,50	2,50	0,60	3,10
Plastic roll	EBR application	pieces	22,00	0,20	4,40	1,06	5,46
					Strengthening application material price		**882,32**

LABOR	DETAILING	UM	PRICE [EUR]	QUANTITY	VALUE [EUR]	TVA [EUR]	PRICE [EUR]
CF fabric and plates cleaning	fabric preparation	hours	5,00	1,00	5,00	1,20	6,20

CF fabric and plates cut	using scissors and cutter	hours	5,00	3,00	15,00	3,60	18,60
Resin application for fabric	mixing and application	sqm	5,00	1,50	7,50	1,80	9,30
Resin application for plates	mixing and application	m	2,50	51,00	127,50	30,60	158,10
CF fabric application	EBR application	sqm	5,00	1,50	7,50	1,80	9,30
CF plates application	NSM application	m	2,50	51,00	127,50	30,60	158,10
FRP anchorage application	anchorage application	pieces	1,00	20,00	20,00	4,80	24,80
					Strengthening application labor price		**384,40**

EQUIPMENT	DETAILING	UM	PRICE [EUR]	QUANTITY	VALUE [EUR]	TVA [EUR]	PRICE [EUR]
Percussion drill	resin mixing	hours	10,00	0,50	5,00	1,20	6,20
Electronic scale	resin weighting	hours	10,00	0,50	5,00	1,20	6,20
					Strengthening application equipment price		**12,40**
					Strengthening application total price		**1279,12**

REHABILITATION TOTAL PRICE	**1805,19**
REHABILITATION TOTAL PRICE / SQM	**173,24**

Table C.7 – Economical evaluation summary

PRCWP (7-E1-T/R) – REHABILITATION (EBR-CFRP) TOTAL PRICE (EUR/SQM)	**106,99**
PRCWP (8-E3-T/R) – REHABILITATION (EBR-CFRP) TOTAL PRICE (EUR/SQM)	**106,85**
PRCWP (9-E1/E3-R/T) – REHABILITATION (EBR-CFRP + NSM-CFRP) TOTAL PRICE (EUR/SQM)	**180,24**
PRCWP (10-L1/L3-T/R) – REHABILITATION (TRM – GF GRID) TOTAL PRICE (EUR/SQM)	**128,40**
PRCWP (11-L1-T/R) – REHABILITATION (TRM – CF GRID) TOTAL PRICE (EUR/SQM)	**325,52**
PRCWP (12-E1-T/R) – REHABILITATION (NSM-CFRP + EBR-CFRP) TOTAL PRICE (EUR/SQM)	**173,24**

Titluri recent publicate în colecţia „TEZE DE DOCTORAT” seria 5: Inginerie Civilă

1. **Árpad Ladislau Jancsó** - *Tehnologii tradiţionale şi moderne la construcţia podurilor din Banat, ISBN: (10) 973-625-383-X, (13) 978-973-625-383-6*, (2006);

2. **Ionel Mircea Cristuţiu** – *Studiul stabilităţii şi ductilităţii halelor metalice uşoare cu structuri în cadre cu secţiuni variabile de clasă 3 şi 4, ISBN: (10) 973-625-388-0, (13) 978-973-625-388-1*, (2006);

……
……

122. **Monica Dorina Isacu** – *Consideraţii cu privire la eficientizarea staţiilor de epurare orăşeneşti, ISBN:978-606-554-835-0*, (2014);

123. **Marius Adam** - *Optimizarea instalaţiilor de ventilare/ climatizare în regim de răcire în scopul asigurării eficienţei energetice şi a con-fortului în clădiri de birouri, ISBN:978-606-554-863-3*, (2014);

124. **Paul Molnar** - *Lucrări hidrotehnice pentru asigurarea continuităţii ecohidraulice a râurilor interioare şi a fluviului Dunărea, ISBN:978-606-554-865-7*, (2014);

125. **Marius Hârţa** - *Impactul structurilor metalice în arhitectura modernă, ISBN:978-606-554-867-1*, (2014);

126. **Mirela-Adriana Szitar** - *Locuinţa colectivă versus locuinţa individuală urbană prin prisma dezvoltării durabile în Câmpia Banatului, ISBN:978-606-554-886-2*, (2014);

127. **Izabella Ştefania Szigyarto** - *Consideraţii cu privire la implementarea sistemelor vacuumate de canalizare - Studii de caz comuna Borş, judeţul Bihor comuna Pericei, judeţul Sălaj, ISBN:978-606-554-891-6*, (2014);

128. **Vergina Popescu** – *Consideraţii privind managementul apelor meteorice din centrele populate, ISBN:978-606-554-903-6*, (2015);

129. **Carla Toduţ** - *Seismic strengthening of precast RC wall panels using FRP composites, ISBN:978-606-554-919-7*, (2015).

EDITURA POLITEHNICA

Lista completă a tezelor publicate sub sigla Editurii Politehnica poate fi consultată la adresa: **http://www.editurapolitehnica.upt.ro**